The Intramolecular Photoredox Behaviour of Substituted Benzophenones and Related Compounds

by

Devin Paul Mitchell
B.Sc., McGill University, 1997
M.Sc., University of British Columbia, 2000

A Thesis Submitted in Partial Fulfillment of the
Requirements for the Degree of

DOCTOR OF PHILOSOPHY

in the Department of Chemistry

The Intramolecular Photoredox Behaviour of Substituted Benzophenones and Related Compounds

by

Devin Paul Mitchell
B.Sc., McGill University, 1997
M.Sc., University of British Columbia, 2000

Supervisory Committee

Dr. P. Wan, (Department of Chemistry)
Supervisor

Dr. R. Mitchell, (Department of Chemistry)
Departmental Member

Dr. A.G. Briggs, (Department of Chemistry)
Departmental Member

Dr. R. K. Keeler, (Department of Physics and Astronomy)
Outside Member

Dr. M. S. Workentin, (University of Western Ontario; London, ON)
External Member

Supervisory Committee

Dr. P. Wan, (Department of Chemistry
Supervisor

Dr. R. Mitchell, (Department of Chemistry)
Departmental Member

Dr. A.G. Briggs, (Department of Chemistry)
Departmental Member

Dr. R. K. Keeler, (Department of Physics and Astronomy)
Outside Member

Dr. M. S. Workentin, (University of Western Ontario; London, ON)
External Member

Abstract

The discovery and mechanistic investigation of a new class of photochemical reactions of benzophenones and related compounds is documented in this Thesis. Their photobehaviour in aqueous solvent media varied dramatically from their well-known behaviour in organic solvents and suggests unique and unprecedented mechanistic pathways. The aqueous photoredox chemistry of various substituted benzophenones was initially explored. Particular attention was paid to 3-(hydroxymethyl)benzophenone (**47**), which upon photolysis in acidic aqueous media undergoes an intramolecular photoredox reaction to produce 3-formylbenzhydrol (**61**). Extensive investigation into the mechanistic behaviour of 3-(hydroxymethyl)benzophenone (**47**) produced evidence of a unique solvent-mediated, acid catalysed photoreaction. A mechanism has been proposed for the intramolecular photoredox reaction that proceeds via the protonated triplet state. This protonated triplet state subsequently promotes the deprotonation of the benzylic carbon before rearranging to form the redox product. The modification of the benzylic

carbon with an alkyl group or with a phenyl group resulted in only slight changes in the photobehaviour. In both cases intramolecular photoredox reactions were observed although significantly more oligomeric side products were observed in some cases.

To more fully elucidate the photobehaviour and to test the generality of the photoredox reaction, a variety of structurally related hydroxyalkyl aromatic carbonyls were synthesized and studied. Alternative chromophores were explored using xanthone and fluorenone derivatives. Both types of derivative compounds underwent an intramolecular photoredox reaction, supporting the assertion that the intramolecular photoredox reaction could be considered a general feature of aromatic carbonyls under aqueous conditions. However, significant differences in photoreactivity were also observed. It was found that 2-(hydroxymethyl)xanthone (**53**) exhibited sufficient photoactivity that the intramolecular photoredox reaction was observable even under neutral conditions whereas 2-(hydroxymethyl)fluorenone (**54**) was nearly photoinert.

The last topic focuses on the extension of the electronic transmission from the carbonyl functional group to the benzylic alcohol by insertion of an additional phenyl group. The addition of the phenyl group also provided a bichromophoric molecule, rather than the monochromophoric substrates studied to this point. The substituent's position played an important role in the photobehaviour, in that both of the *meta*- and *ortho*-substituted compounds underwent intramolecular photoredox reaction, while the *para*-substituted compound primarily exhibited photobehaviour indicative of hydrogen abstraction.

Table of Contents

2 Chapter 2

Intramolecular Photoredox Reactions of Benzophenones and Simple Derivatives

List of Tables

List of Figures

List of Abbreviations

ACN	Acetonitrile
AM1	Austin Model 1 (semi-empirical computational method)
Conc.	Concentrated
CT	Charge Transfer
EA	Electron Affinity
EI	Electron Impact
F	Fluorescence
Φ	Quantum Yield
hν	Photons
HOMO	Highest Occupied Molecular Orbital
HPLC	High Performance Liquid Chromatography
HRMS	High Resolution Mass Spectrometry
Hz	Hertz (s^{-1})

IC	Internal Conversion
IE	Ionization Energy
i-PrOH	Isopropanol
IR	Infrared
ISC	Intersystem Crossing
λ_{ex}	Wavelength of Excitation
LFP	Laser Flash Photolysis
Lit.	Literature Value
LSIMS	Liquid Secondary Ion Mass Spectrometry
LUMO	Lowest Unoccupied Molecular Orbital
MeOH	Methanol
mp	Melting Point
MS	Mass Spectrometry / Mass Spectrometer
NBS	N-bromosuccinimide
NMR	Nuclear Magnetic Resonance
OD	Optical Density
OP	Oligomeric Sideproduct
ppm	Parts Per Million
P	Phosphorescence
$\mathbf{S_0}$	Ground State
$\mathbf{S_1}$	First Singlet Excited State
SET	Single Electron Transfer
$\mathbf{T_1}$	First Triplet Excited State
Tf	Trifluoromethanesulfonyl
THF	Tetrahydrofuran
TLC	Thin Layer Chromatography
UV-Vis	Ultraviolet-Visible
YAG	Yttrium Aluminum Garnet

List of Key Numbered Compounds – Names

26 3-Benzoylphenylacetic acid

28 3-Methylbenzophenone

42 2-(Hydroxymethyl)anthraquinone

47 3-(Hydroxymethyl)benzophenone

48 3-(1-Hydroxyethyl)benzophenone

49 3-(Benzoyl)benzhydrol

50 3-(Methoxymethyl)benzophenone

51 2-(Hydroxymethyl)benzophenone

52 4-(Hydroxymethyl)benzophenone

53 2-(Hydroxymethyl)xanthone

54 2-(Hydroxymethyl)fluorenone

55 3-(2'-Hydroxymethyl)phenyl)benzophenone

56 3-(3'-Hydroxymethyl)phenyl)benzophenone

57 3-(4'-Hydroxymethyl)phenyl)benzophenone

59 3-Formylbenzophenone (oxidized product of **47**)

60 3-Benzoylbenzophenone (oxidized product of **49**)

61 3-Formylbenzhydrol (redox product of **47**)

62 3-Benzoylbenzoic acid (fully oxidized product of **47**, **59** or **61**)

63 4-Formylbenzhydrol (redox product of **52**)

64 4-Formylbenzophenone (oxidized product of **52**)

67 2-Formylbenzhydrol (redox product of **51**)

68 2-Formylbenzophenone (oxidized product of **51**)

72 3-Acetylbenzhydrol (redox product of **48**)

73 3-Acetylbenzophenone (oxidized product of **48**)

74 3-[(3-Benzoyl-benzyloxy)-phenyl-methyl]-benzaldehyde (condensation product of **47** and **61**)

75 (condensation dimer of **61**)

76 3-Benzoyl-4’-methylbenzhydrol

77 3-Benzoyl-4’-methoxybenzhydrol

78 3-Benzoyl-3’-methoxybenzhydrol

79 3-Benzoyl-3’-(hydroxymethyl)benzhydrol

80 3-Benzoyl-3’-formylbenzhydrol

81 3-(Hydroxy-phenyl-methyl)-4’-methylbenzophenone (redox product of **76**)

82 3-Benzoyl-4’-methylbenzophenone (oxidized product of **76**)

83 3-(Hydroxy-phenyl-methyl)-4’-methoxybenzophenone (redox product of **77**)

84 3-Benzoyl-4’-methoxybenzophenone (oxidized product of **77**)

85 3-(Hydroxy-phenyl-methyl)-3’-(hydroxymethyl)benzophenone (redox product of **79**)

86 3-Formyl-3’-(hydroxy-phenyl-methyl)benzhydrol (redox product of **85**)

97 2-Formylxanthen-9-ol (redox product of **53**)

98 2-Formylxanthone (oxidized product of **53**)

99 9-(9-Oxo-9H-xanthen-2-ylmethoxy)-9H-xanthene-2-carbaldehyde (condensation product of **97** and **53**)

108 9-Fluorenone-2-carboxylic acid

109 2-Formylfluorenol (redox product of **54**)

110 2-Formylfluorenone (oxidized product of **54**)

130 3-(2'-Formyl)phenyl)benzophenone (oxidized product of **55**)

131 4-Benzoylfluorenol (cyclized redox product of **55**)

132 3-(2'-Formylphenyl)benzhydrol (redox product of **56**)

133 3-(3'-Formylphenyl)benzophenone (oxidized product of **56**)

134 3-(4'-Formylphenyl)benzophenone (oxidized product of **57**)

135 3-(4'-Formylphenyl)benzhydrol (redox product of **57**)

List of Key Numbered Compounds – Structures

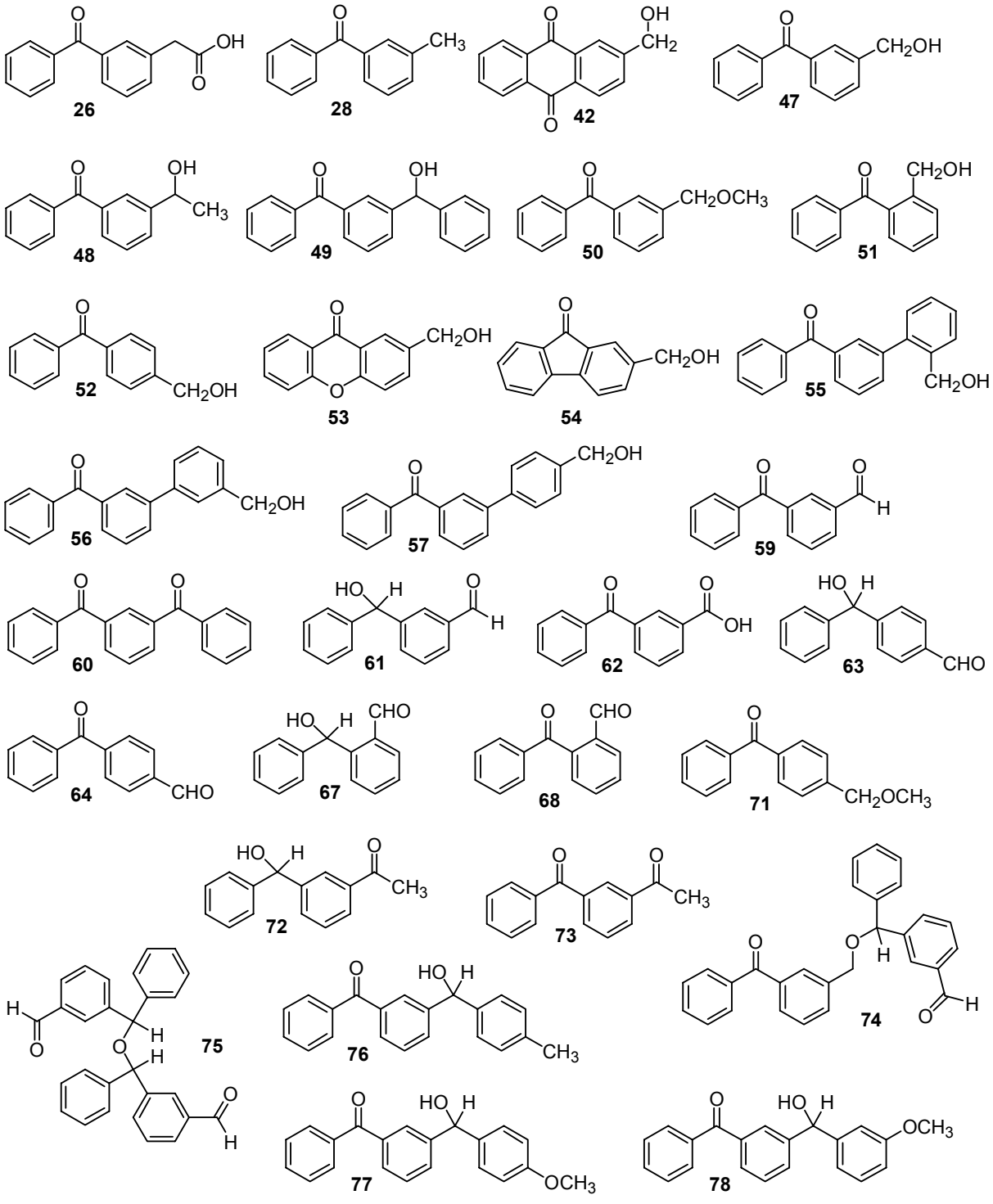

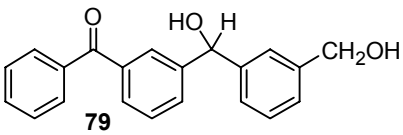

79

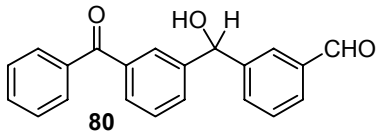

80

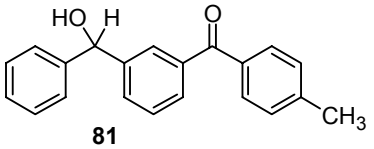

81

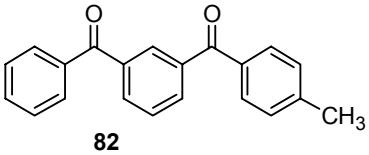

82

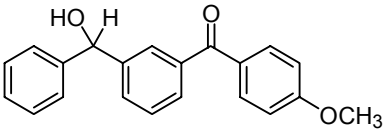

83

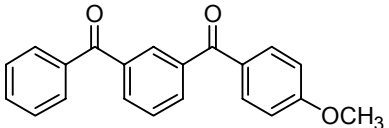

84

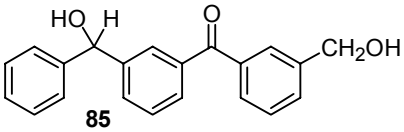

85

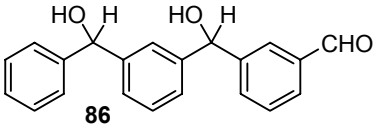

86

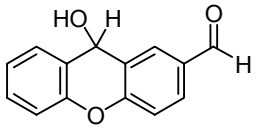

97

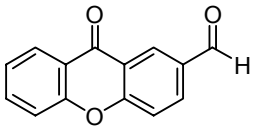

98

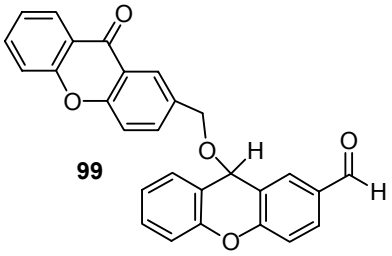

99

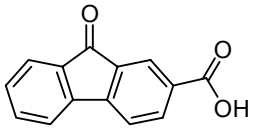

108

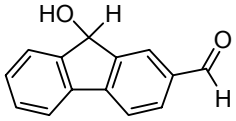

109

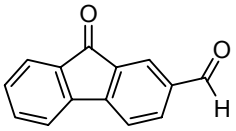

110

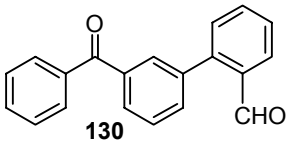

130

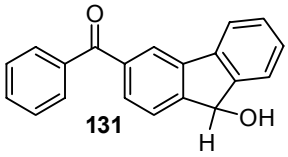

131

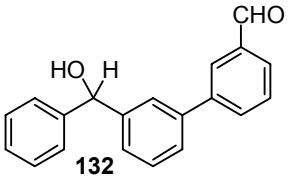

132

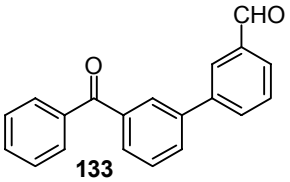

133

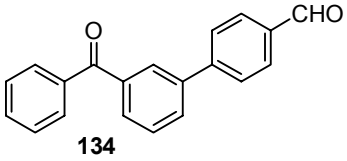

134

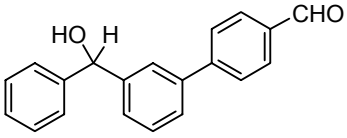

135

Acknowledgements

I would like to thank Dr. Peter Wan for his assistance, guidance and support in the experiments conducted at the University of Victoria. I would also like to thank the Wan Group members both past and present. Their kindness, humour and friendship are most appreciated.

The office and technical staff were invaluable to the success of my project and I would like to express my appreciation of their efforts. Special attention must be given to Chris Greenwood and Dr. David McGillivray for performing NMR and MS experiments for me. I would also like to thank Dr. Cornelia Bohne and Tamara Pace for all of their help with the LFP system. Funding of my research from the University of Victoria and NSERC is gratefully acknowledged.

Dedication

I would like to dedicate this Thesis to my wife, Karycia, my son Teagan and the rest of my family for their love and support. Thank you for standing by me.

Chapter 1
Introduction

1.1 Basic Photophysical and Photochemical Processes

Photochemistry is the study of the chemical reactions arising from the absorption of photons. Absorption of a photon produces an electronically excited state which, in addition to adding significant energy, also leads to profound changes in a molecule's electronic and nuclear configurations. An electronically excited state is not stable and there exist several deactivation pathways. These are graphically illustrated in the simplified Jablonski diagram in Figure 1.1. Pathways from the excited singlet state (S_1) include fluorescence (F, spin-allowed emission of a photon), internal conversion (IC, radiationless deactivation) and intersystem crossing (ISC, change in multiplicity). Typically, deactivation of excited singlet states occurs at rates in the 10^8-10^{12} s^{-1} range. Pathways from the excited triplet state (T_1) include phosphorescence (P, spin-forbidden emission of a photon) and ISC. Deactivation of triplet excited states tends to occur more slowly than that of excited singlet states (lifetimes of several microseconds or longer are not uncommon) as the intersystem crossing from the T_1 state to the singlet ground state (S_0) is spin-forbidden.

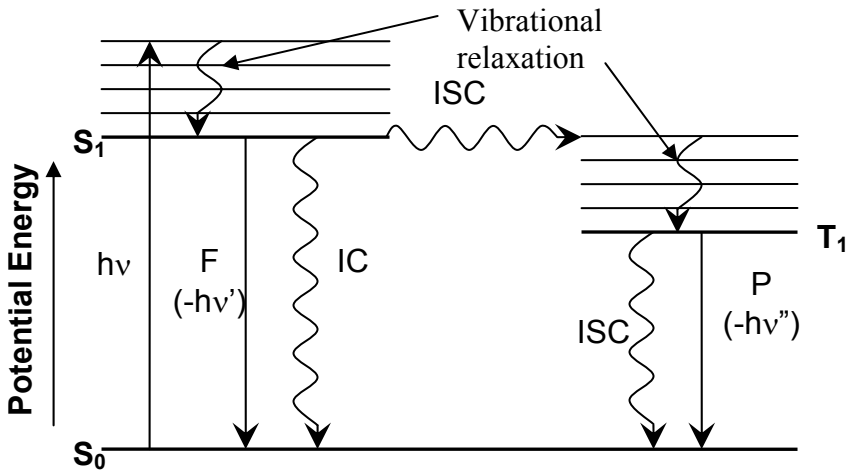

Figure 1.1 Simplified Jablonski Diagram Showing Photophysical Decay Pathways of Electronically Excited States

In addition to the photophysical deactivation pathways, photochemical reactions are also possible. However, in order for photochemical reactions to compete successfully with the photophysical deactivation pathways, the rates of reaction must be of a similar magnitude as photophysical deactivation. Consequently, although chemical reactions may proceed from either the singlet or the triplet excited state, not all reactions are possible. The singlet excited state is especially limited due to its relatively short lifetime. Reactions that proceed via triplet states do not present the same problem because triplet excited states are much longer lived.

Photochemical reactions may be studied through indirect or direct methods. Standard characterization methods like NMR, IR, and UV-vis spectroscopy and Mass Spectrometry may be used to determine the identity of the photoproducts but offer no direct information on the identity of the reactive excited state. The reaction pathway may be inferred from the photoproducts but direct observation of the reactive excited states and short-lived intermediates is often necessary to fully elucidate the mechanism. Nanosecond laser flash photolysis (LFP) allows direct detection of short-lived transients

(~20 ns $\leq \tau \leq$ 1 s), by obtaining their UV-vis absorption spectra, and is the most useful method for the detection of triplet excited states. More information about triplet state reactions may also be gathered using triplet quenching and sensitization techniques.

1.2 Photochemical Reduction-Oxidation Reactions

Photoreduction, photooxidation, and photoredox reactions all require electrons to formally move from one moiety to another. This Thesis shall primarily focus on intramolecular photoredox reactions. Consequently, we will not be discussing photoreduction and photooxidation processes a great deal as they are necessarily bimolecular in nature. However these reactions may occur as minor side-products to the main photoredox products in the systems explored in this Thesis.

Photoredox reactions differ from their equivalent ground state reactions in that the excited states produced by absorption of a photon can always be considered to be potential powerful redox reagents relative to their ground state. By examining the different electronic configurations between the ground and excited states of a molecule, shown in Figure 1.2, it becomes evident that electronic excitation makes the molecule both a stronger oxidizing agent, due to the hole produced, and a stronger reducing agent, as an electron is in a higher energy level.[1] The promoted electron, being in a higher energy level than the equivalent electron in the ground state, has a lower ionization energy (IE) and thus the excited molecule is more easily oxidized. Similarly, the production of a hole following excitation of that electron creates a void into which an electron may be placed. This hole is at a lower energy than the equivalent empty position

in the ground state molecule and consequently has a larger electron affinity (EA). Thus the electronically excited molecule is also more easily reduced.

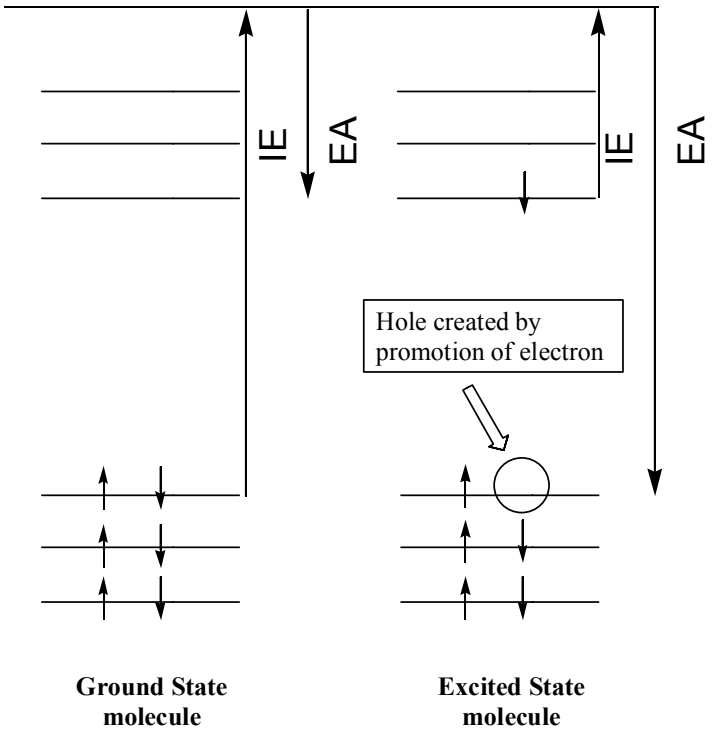

Figure 1.2 Comparative Redox Potentials for Ground and Excited States

1.3 Photoredox Chemistry of Nitroaromatic Compounds

Nitroaromatic compounds have been a focus for study in the photochemical community since the first paper appeared in 1886;[2] their photoactivity has been explored in detail since the 1960s.[3] Although nitro compound photochemistry is often compared with carbonyl photochemistry, it differs in several important ways. The nitro group may be photochemically transformed into a larger variety of functional groups than carbonyl groups. In addition the C-N bond is easier to break than the C-O bond. Additionally, the

carbonyl group may be incorporated into the carbon skeleton of the molecule as a ketone. By contrast, the nitro group must always be "external" to the framework.

Many of the photoinduced reactions of nitro compounds originate from the triplet state because the nitro group provides low-lying triplet states, by enhancing the singlet-triplet transition rate without appreciably changing the triplet to ground state transition rate. Three excited state configurations are important for nitro compounds; n,π*; π,π* and charge transfer (CT).

In order for a formal photoredox reaction to occur intramolecularly, two different moieties must be involved. Photoredox reactions involving nitro groups typically involve the oxidation of another functional group, concomitant with the reduction of the nitro group, as the nitro group is already highly oxidized. One such functional group is the amino group.[3] If a nitrophenyl group and an alkyl amino group are linked by a length of oligomethylene chain, photoredox chemistry may be observed depending on the length of the methylene chain. The effect of chain length is illustrated in Eqn [1.1] for compound **1**.[4]

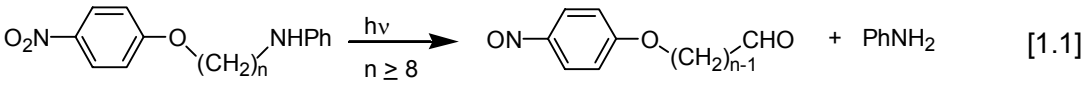

1 **2** [1.1]

A photoredox reaction is observed only if the chain length has n ≥ 8. The nitro group is reduced to a nitroso group and the carbon attached to the amino group is oxidized to produce an aldehyde (compound **2)**. The oxidation of the methylene chain releases aniline. No such reaction occurs if the chain length has n < 8. Biradical intermediates are suggested because the photoredox reaction is noticeably influenced by a magnetic field.[5] The dependence of the reaction upon chain length illustrates the necessity of direct

contact between the two moieties; with n < 8, the two moieties cannot approach each other to a sufficient distance for reaction as illustrated by simple molecular models. The reaction mechanism proposed, and shown in Eqn [1.2], proceeds via the triplet excited state and involves hydrogen abstraction by the nitro group of the hydrogen of the methylene next to the amino to form the biradical **3**. Formation of the redox product **2** requires an electron transfer to occur intramolecularly to form the zwitterion **4**, followed by conventional ground state chemistry via the cyclic intermediate **5**.

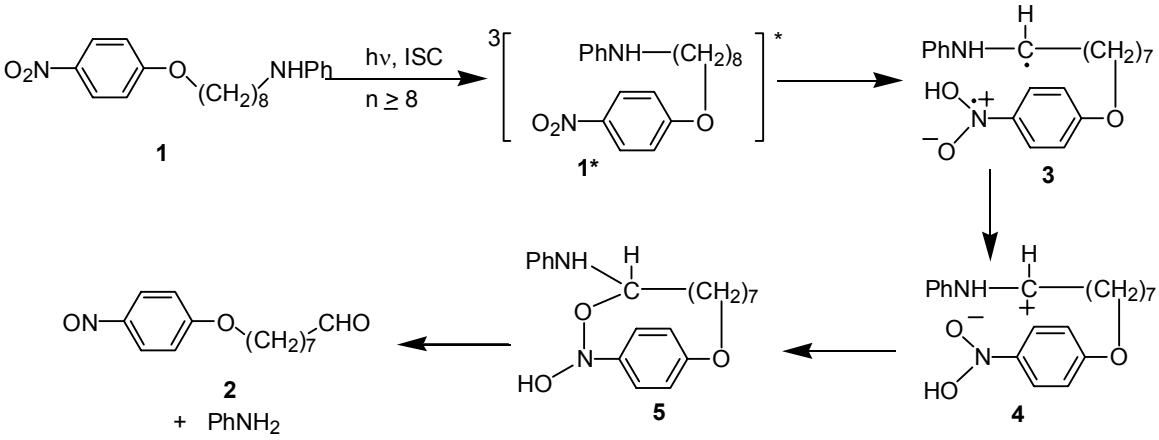

[1.2]

The most commonly reported formal intramolecular redox reactions involve *ortho*-substituted nitrobenzenes,[6,7,8] primarily because hydrogen abstraction is very easily accomplished by the excited nitro group. This results in a biradical that subsequently undergoes a transformation that results in an overall reduction of the nitro group and oxidation of the other group. Yip *et al*[8,9] examined the photoreactions of *ortho*-substituted alkyl nitrobenzenes and found that the reaction proceeds to give the nitroso alcohol redox product through both a singlet state pathway and a triplet state pathway with approximately 40% of product originating from the singlet. Electron-donating substituents at the benzylic carbon were found to enhance the intramolecular photoredox reaction towards the quinoid type intermediate present during the photoreaction.

The intramolecular hydrogen-abstraction pathway is not available for the *para* and *meta* isomers of nitrobenzyl alcohol (**6** and **7** respectively), as the distances are too great. Despite this obstacle these isomers also exhibited photoredox chemistry. There is however a distinct difference in the behaviour. The *ortho* isomer, **8**, reacts according to the standard hydrogen abstraction pathway with no discernable difference in efficiency of photoreaction regardless of solvent. However, photochemistry was observed for the *meta* and *para* isomers only when photolysis was performed in aqueous solution.[10] *Para*- and *meta*-nitrobenzyl alcohols were discovered to be base and acid catalysed, respectively.

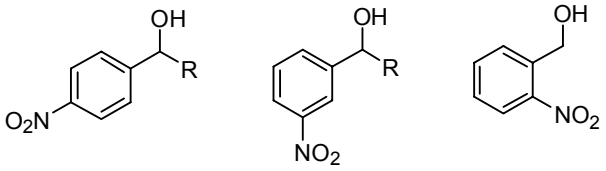

6 a R = H
b R = CH_3

7 a R = H
b R = CH_3
c R = Ph

8

The *para*-substituted nitrobenzyl alcohols (**6a,b**) when photolysed in aqueous CH_3CN at a pH > 11 gave nitrosocarbonyl compounds (**9a,b** isolated as dimers) exclusively with conversions of up to 40% (Eqn. [1.3]).

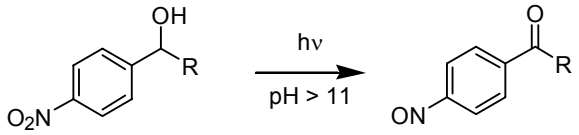

[1.3]

6 a R = H
b R = CH_3

9 a R = H
b R = CH_3

Photolysis of **6** in solvent media that is insufficiently alkaline (pH < 11) resulted in complete recovery of the substrate after photolysis. The *meta*-substituted nitrobenzyl alcohols (**7a-c**) have similar but not identical photochemistry. When the *meta*-substituted alcohols are photolysed in aqueous medium, be it basic, neutral or acidic, nitrocarbonyl

(**10a-c**) and azoxycarbonyl compounds (**11a-c**) are formed (Eqn. [1.4]) with a total yield of ~50%.

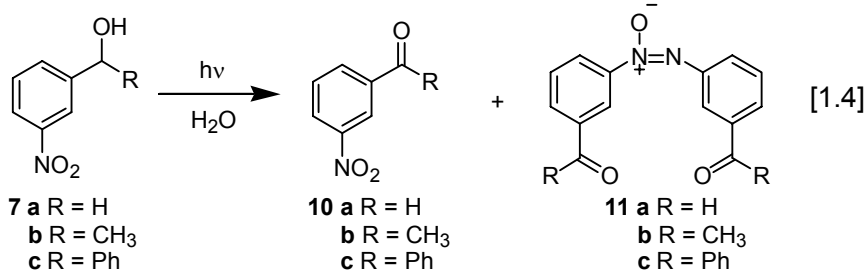

When photolysed in organic solvents, no reaction was observed and only substrate was recovered. Upon photolysis in aqueous media two products are formed, the oxidized nitrocarbonyl compounds **10,** and the azoxycarbonyl compound **11**. Both the oxidized nitro compounds **10**, and the azoxycarbonyl compounds **11**, are proposed to be derived from an intermediate via a thermal reaction. The two types of products are formed in approximately the same ratios for wide ranges of conversion suggesting that both come either from primary photochemistry or are formed via rapid dark reactions subsequent to the primary photochemical step. The mechanisms were presented[10] as follows: *p*-nitrobenzyl alcohol mechanism (Eqn. [1.5]), *m*-nitrobenzyl alcohol mechanism (Eqn. [1.6]).

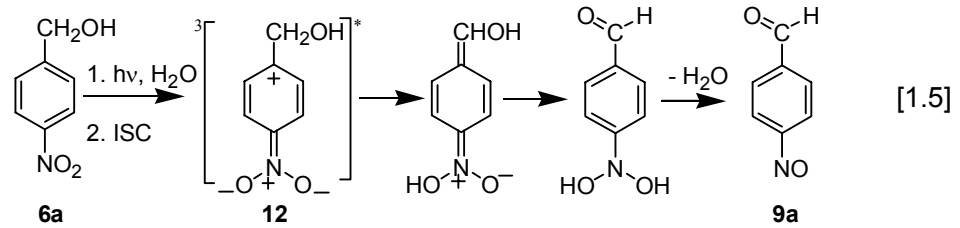

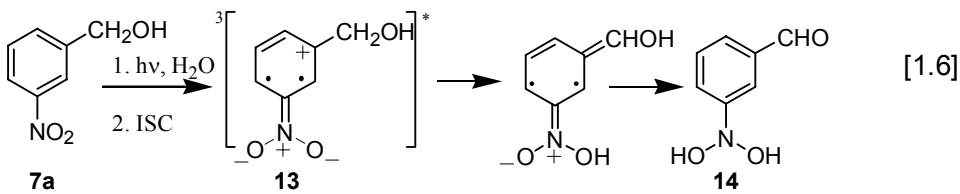

Notice that in both cases a highly polarized triplet excited state (**12** and **13** for the *para* and *meta* compounds, respectively) is proposed that subsequently results in the deprotonation of a benzylic proton. This is consistent with the base catalysis observed for the *para*- isomer whereas water is sufficient as a base for the *meta*- isomer. Due to the highly polarized nature of the triplet the acidity of the benzyl proton is expected to be much higher than in the ground state and in the case of the *meta* isomers the increase in acidity could be greater than 20 log units since even water will deprotonate the benzylic protons. The production of the two products of the photolysis of the *meta* compound proceeds from the hydrated nitroso product **14**, via a disproportionation, to give hydroxylamine **15**, and *m*-nitrobenzaldehyde (**10a**) as shown in Eqn [1.7]. Subsequent coupling of **14** and **15** gives the observed azoxy product **11a**.

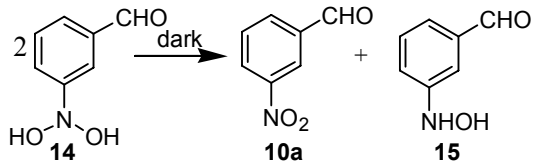

[1.7]

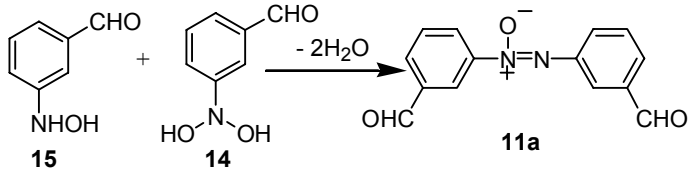

[1.8]

Although simple nitrobenzenes are believed to have (n,π*) triplets as their lowest energy excited state, the compounds in this reaction were proposed to have a (π,π*) triplet state as molecules that have (n,π*) lowest triplet states are not known to achieve the benzene ring activation necessary for this reaction. One possible explanation of why the π,π* would be the lowest triplet state[10] is that solvents of high dielectric constants stabilize (π,π*) and destabilize (n,π*) configurations. Thus, in water ($\varepsilon = 80$) the two configurations must either be inverted or else are very close in energy to allow the

observed reaction. This explanation is also consistent with the lack of reaction in organic solvents as they tend to have $\varepsilon < 40$ and therefore would not stabilize the (π,π^*) excited state significantly.

More recently it has been shown[11] that the electronic effects discussed above may be transferred through a biphenyl ring. Under acidic conditions (pH 2) in aqueous acetonitrile *p*-(*p*'-nitrophenyl)benzyl alcohol, (**16**), undergoes photoredox cleanly to *p*-(*p*'-nitrosophenyl)benzaldehyde (**17**) (Eqn [1.9]).

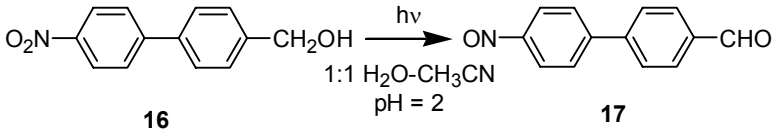

16 **17** [1.9]

Under neutral conditions however, the photoredox product is not formed and instead two products are formed, an oxidized (**18**) and a reduced product (Eqn [1.10]). This reduction product does not arise from secondary photolysis of the nitro- compound and it was suggested that the reduction product arose via an external electron source. This electron source was proposed to be a "reducing" carbanion formed as an intermediate on the way to the nitro compound. The azoxy compound **19**, is formally obtained by condensing a hydrated nitroso with a hydroxylamine compound in a manner analogous to Eqn [1.8].

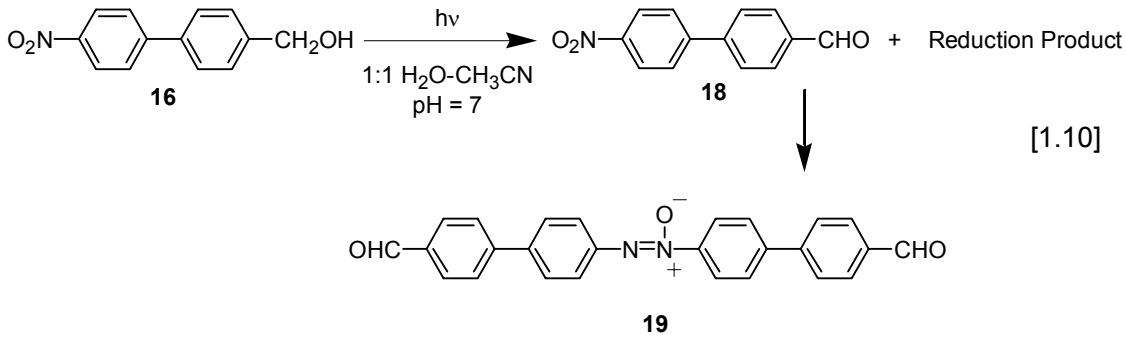

16 **18** [1.10]

19

1.4 Photochemistry of the Carbonyl Chromophore

As this Thesis deals primarily with aromatic ketones, an examination of the carbonyl chromophore is appropriate. Like the aromatic nitro compounds examined in section 1.3, ketones are heavily represented in the photochemical literature.[12]

Aliphatic ketones differ from aromatic ketones in the types of pathways that are open to them. Some of the reactions possible to aliphatic ketones include: α-cleavage reactions (Norrish Type I), free-radical decarbonylation, intramolecular elimination, intermolecular and intramolecular hydrogen abstraction, Norrish Type II cleavages, photocycloaddition to olefins, and photorearrangements.

The alkoxy radical is a suitable model[13,14,15,16,17,18,19,20] when examining the (n,π*) triplet state's behaviour because the (n,π*) triplet state has electrons with parallel spins that are as far removed from one another as possible. Observation of α-cleavage reactions, attack on carbon-carbon double bonds, and especially the (n,π*) triplet state's ability to abstract a hydrogen atom are all consistent with behaviour associated with alkoxy radicals.

The α-cleavage of ketones, generally known as the Norrish Type I process, was first described in 1907 by Ciamician and Silber.[21] As previously mentioned, (n,π*) triplet state behaves in a manner analogous to an alkoxy radical and this observation is supported by the fact that both undergo cleavage at the α bond. The process, which can be understood in terms of the weakening of the α bond by overlap with the vacant non-bonding orbital, yields alkyl and acyl radicals for acyclic aliphatic ketones and an acyl radical for aliphatic aldehydes as the C-H bond preferentially cleaves. The resulting

radicals may undergo further fragmentation, decarbonylation, disproportionation and result in a multitude of products expected from radical reactions. The photodecarbonylation is only observed in solution when the acyl radical has an adjacent stabilizing substituent present to promote the second α cleavage.

Aromatic ketones, by contrast to aliphatic ketones, have fewer pathways available to them and are most known for their involvement in hydrogen abstraction.

1.4.1 Hydrogen Atom Abstraction by the Carbonyl Group

Hydrogen abstraction is the most common bimolecular reaction in solution and generates alkyl radicals and semi-pinacol radicals. This generally results in the reduction of the carbonyl group, which may mean either an overall reduction of the molecule if the hydrogen abstraction was intermolecular or an intramolecular redox reaction if the hydrogen abstraction was intramolecular (assuming fragmentation does not occur). Although this reaction has been studied for over a hundred years, controversy reigned for many years[22] on whether singlet or triplet (n,π*) excited states were more reactive in hydrogen abstractions and has only been resolved in the last 10 years.[23]

One of the earliest reported photochemical reactions was the photoreduction of benzophenone in 2-propanol described by Ciamician and Silber in 1900.[24] Since then secondary alcohols have become a favorite hydrogen donor solvent but photoreduction of the ketone triplet can occur in any solvent containing reactive C-H bonds. As compared to the *tert*-butoxy radical, the benzophenone triplet shows a rather close similarity with regards to the absolute rate of reaction and selectivity,[18,25] with the ketone triplet being more selective and electrophilic than the alkoxy radical.[26] This supports the concept that

the triplet excited state has n,π* configuration in which an electron deficiency is created at the carbonyl oxygen by promoting a non-bonding electron (n) into an antibonding orbital (π*).

Although aliphatic ketones undergo photoreduction[27,28] aromatic ketones are more associated with photoreduction because the phenyl-carbonyl bond is not as susceptible towards Type I cleavage. Aromatic methyl ketones are also not susceptible towards Type II cleavage. This reaction, illustrated in Eqn [1.11], involves the intramolecular abstraction of a hydrogen atom from the γ position of the aliphatic chain. Subsequently, this can lead to Norrish Type II photoelimination in aliphatic ketones and results in an olefin and an enol that tautomerizes to another ketone. The equivalent for aromatic ketones would be hydrogen abstraction from an *ortho*-substituted alkyl group. However this does not result in photoelimination because that would require fragmentation of the aromatic ring.

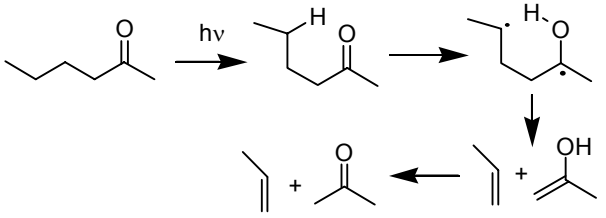

[1.11]

1.4.2 Acid-Base Properties of Aromatic Ketones

Just as the redox behaviour of an excited state molecule may vary significantly from that of its ground state, so too can the acid-base properties vary, and for many of the same reasons. The increased polarization of molecules in their excited states causes the electron density to shift affecting the strength of their acid-base properties. These properties were first explored by Förster[29] and Weller[30] and have been reviewed many times.[31,32]

Phenols are considerably more acidic in their S_1 state than in their ground states, while aromatic ketones have been shown to be much stronger bases.[33] The effect of polarization is so significant that even hydrogens attached to carbons may be deprotonated if there are other stabilizing features. This stabilization may arise from strong electron withdrawing groups on an aromatic ring in the case of benzylic C-Hs. The deprotonation of the benzylic proton of nitrobenzyl alcohols to yield a carbanion is an example of this and was presented in Section 1.3. Another mechanism of stabilization is the energy derived from aromatization. If the loss of a proton results in the formation of an aromatic ring upon excitation the proton becomes acidic in the excited state, such as suberene (**20**).[34] Upon photolysis (see Eqn [1.12]) suberene undergoes deprotonation to form an aromatic carbanion (4nπ electrons in the excited state) which upon relaxation to the ground state is reprotonated (deuterated to form **20D^1** if in D_2O).

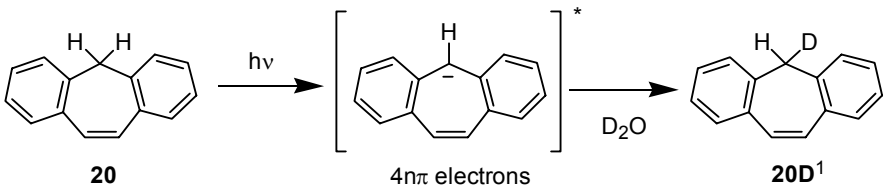

20 4nπ electrons **20D^1** [1.12]

Aromatic ketones also undergo a change in their acid-base properties upon excitation due to the increased polarization. Unlike phenols however, aromatic ketones become more basic. The increased base strength of aromatic ketones may be understood by examining the energy levels of the different states of the protonated and unprotonated ketone.[35] The pK_as shown in Figure 1.3 illustrate the relative positions between the different energy levels for protonated and deprotonated benzophenone. Protonated benzophenone (BH^+) has a $S_1 - T_1$ splitting greater than the (n,π*) transition and a lower energy for the $S_1 \leftarrow S_0$ transition than for unprotonated benzophenone (B). Therefore benzophenone becomes a stronger base upon excitation to S_1 and an even stronger base in the T_1 state. The relative pK_as are p$K(T_1)$> p$K(S_1)$> p$K(S_0)$. Note that for the protonated benzophenone the S_1 and T_1 excited states are (π,π*) rather than (n,π*) as observed for benzophenone.

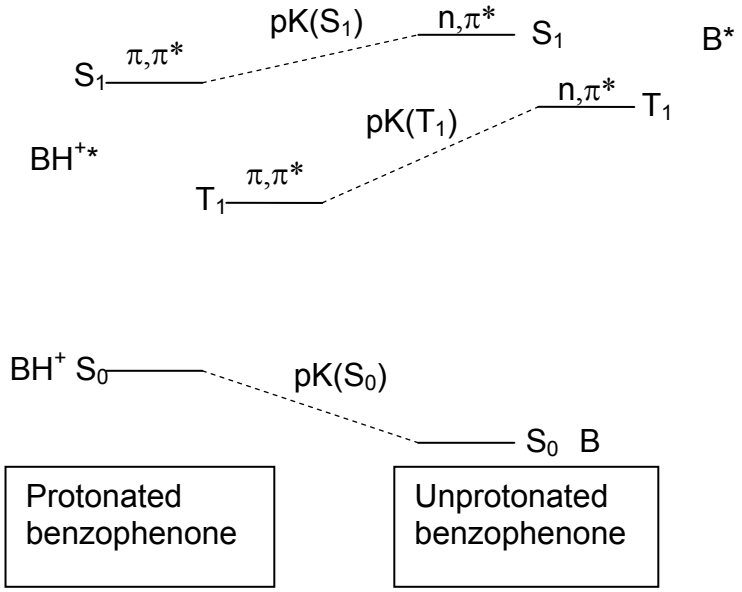

Figure 1.3 Relative Energies for the S_0, S_1 and T_1 States for Protonated and Unprotonated Benzophenone[35]

This suggests that the electron density for the excited state protonated benzophenone involves the aromatic ring system to a greater extent than for the unprotonated benzophenone.

1.5 Photochemistry of Benzophenones

The photochemistry and photophysics of benzophenones have been studied for over a century.[20,36,37,38,39] As mentioned earlier the benzophenone photoreduction in 2-propanol was one of the first photoreactions reported and despite many papers on the subject it wasn't until 60 years later that the mechanism was finally identified as proceeding via the triplet state.[40,41] Intersystem crossing efficiency of unity are typically ovserved for benzophenones and substituted derivatives.[42] Consequently, benzophenone is essentially nonfluorescent ($\Phi_F < 10^{-4}$) and possesses a very short singlet lifetime ($\tau_s \sim 10^{-11}$ s).[36] This extremely rapid ISC is typical of certain carbonyl compounds possessing S_1 states close in energy with triplet states.[43]

Benzophenone is one of the most commonly used triplet sensitizers as it efficiently undergoes intersystem crossing and has a triplet state energy above that of many compounds. In order for sensitization to occur, the energy of the triplet state of the sensitizer must be higher than that of the molecule to be sensitized. Sensitization is used with molecules that do not undergo intersystem crossing efficiently due to alternative fast photochemical processes such as *cis-trans* isomerism in olefins. The triplet sensitization leads to alternative pathways for the sensitized molecules that would otherwise not exist.[44]

The photochemical reactions of benzophenones are limited as many of the pathways for aliphatic ketones are unavailable for the doubly aromatic ketone. Neither Norrish Type I nor Type II reactions occur with benzophenone. The lack of a stable alkyl radical means that α-cleavage is unfavourable. Type II photoelimination is likewise not possible because there are no removable γ-hydrogens and the aromatic ring does not lend itself to photoeliminations.

The primary reaction observed for benzophenone is intermolecular hydrogen abstraction from the solvent or from other effective hydrogen donors. In alcoholic or hydrocarbon solvents this leads to ketyl radicals being formed and subsequently either photoreduction or recombination of the ketyl radicals to form benzpinacols.[45,46,47] Intramolecular hydrogen abstraction is also possible if there are abstractable hydrogens within reach (Eqn [1.13]). This reaction is particularly facile for *ortho*-substituted methylbenzophenone (**21**) or hydroxybenzophenone. These molecules result in photoenols (**22**) which thermally revert to the original substituted benzophenone.[48,12] These compounds have found use as photoprotection agents due to their ability to convert photoenergy into thermal energy.

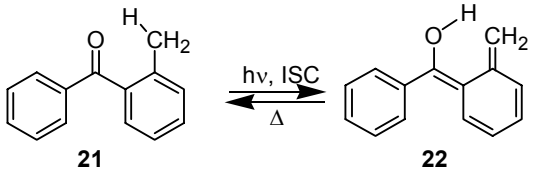

21 **22** [1.13]

Substituent identity and placement has significant affect on the photobehaviour of benzophenones. Hydrogen abstraction may be quenched if substituents such as OH, NH_2 or C_6H_5 are in the *para* position.[49,50,51] These substituents, because of their electron-donating capability, lower the energy of the (π,π*) triplet state so the electron density is

delocalized over the entire aromatic ring rather than focused on the carbonyl. Consequently the oxygen does not have appreciable radical character. Compounds especially reluctant to abstract hydrogen from 2-propanol such as *p*-aminobenzophenone appear to have intramolecular charge transfer states. These "charge transfer" triplet states, unlike those that are intermolecular, may be thought of as (π,π^*) triplet states in which the electron density is strongly directed by heteroatoms.[52] This CT state is highly sensitive to solvent and the quenching effect may be neutralized somewhat by using a hydrocarbon solvent rather than an alcoholic solvent. It is known that polar solvents stabilize the (π,π^*) triplet state while non polar solvents stabilize the (n,π^*) triplet state.[53] This is also the case for *p*-methoxybenzophenone (Figure 1.4).[54] Further evidence of the electron-donating effect on stabilizing the CT state may be observed with the addition of small amounts of HCl. Under those conditions *p*-aminobenzophenone may be photoreduced to the benzpinacol in 2-propanol as the amino group becomes protonated and its electron-donating character suppressed. The solvent effect on the triplet states' energy is also supported by the hypsochromic shift of the (n,π^*) absorption and the bathochromic shift of the (π,π^*) absorption on going from non-polar solvent to a polar protic solvent.[55] The shift in the (n,π^*) absorption and the (π,π^*) absorption upon changing polarity of solvents has also been directly correlated to photoreactivity by Porter.[49] The general trend when examining the reactivity of benzophenone towards hydrogen-abstraction is that the compounds with the most reactivity have (n,π^*) triplet states (benzophenone), those with moderate activity have (π,π^*) triplet states (*p*-phenylbenzophenone), and those with the least have (π,π^*) triplet states with significant charge transfer character (*p*-hydroxy and *p*-aminobenzophenone).

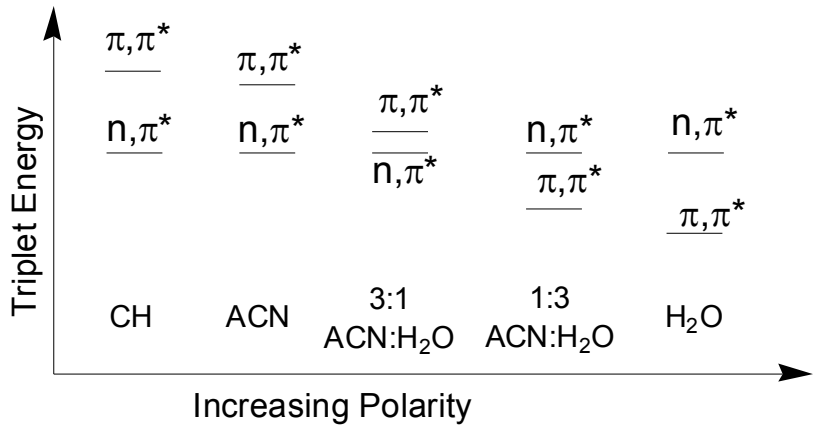

Figure 1.4 Energetics diagram for the lowest triplet states of *p*-methoxybenzophenone showing effect of solvent polarity on (π,π*) triplet energy.[54] The solvent systems vary from hydrocarbon (CH) to acetonitrile (ACN) to water.

Aqueous solutions, whose polarity and acid-base properties may result in (π,π*) triplet states being favoured have been examined in fewer studies than purely alcoholic and hydrocarbon solvents.[56, 57] The quenching of the benzophenone was observed by Ledger and Porter,[57] who noted that the phosphorescence of benzophenone was quenched by protons, although the mechanism was not understood at that time. Initially, it was thought that the quenching was due to the formation of the protonated triplet and Wyatt and co-workers[35,58] assigned a pK_a value of 1.5 ± 0.1 for the protonated triplet using Forster cycle. Further studies by Wirz[59] demonstrated that the transient observed was not the protonated triplet as previously assumed[60] but was instead the hydrated triplet and refined the pK_a value of the protonated triplet to be – 0.4 ± 0.1. Apparently, benzophenones, when photolyzed in moderately acidic aqueous solutions, become hydrated at the *ortho* and *meta* position with a preference at the *meta* position due to the *meta*-effect.[61] The mechanism is expected to involve the protonation of the carbonyl oxygen as it is well established[33] that aromatic ketones are much stronger bases when

excited ($pK_a(T_1)$ = -0.4)[59] than when in the ground state ($pK_a(S_0)$= -5.7).[35] The addition of water to the *ortho* and *meta* positions can be explained by an enhanced charge separation leading to positive charges at those positions that are readily hydrated.

1.6 Photodecarboxylation of Phenylacetic Acids

The efficient photodecarboxylation of ketoprofen (**23**) under aqueous conditions (pH > pK_a) has been known for over 10 years.[62,63] Disparate opinions upon the pathway of decarboxylation have existed; Sik *et al* favoured a radical mechanism[64] while Wan *et al* believed the reaction goes through an ionic pathway.[65] Subsequent research supported the ionic pathway that proceeds *via* a benzylic carbanion intermediate (**24**) to 3-ethylbenzophenone (**25**) after protonation (Eqn [1.14]).[66] Although AM1 calculations support a delocalized biradical type intermediate, Scaiano *et al*[67] suggest the decarboxylation proceeds through the singlet state.

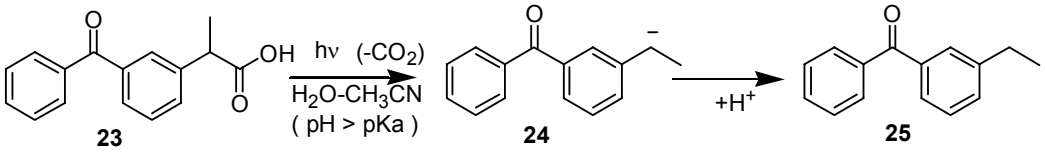

23 **24** **25** [1.14]

Photodecarboxylation is also observed for the simpler 3-benzoylphenylacetic acid (**26**) which also proceeds through a carbanion intermediate, however the multiplicity has not yet been determined. It was postulated that phenyl ketones, upon excitation, act as highly electron withdrawing groups that enhance the benzylic activation in a manner analogous to the behaviour of *p*-nitrophenylacetic acid (**27**).[68] A benzyl carbanion intermediate is also expected for the decarboxylation of **27**.

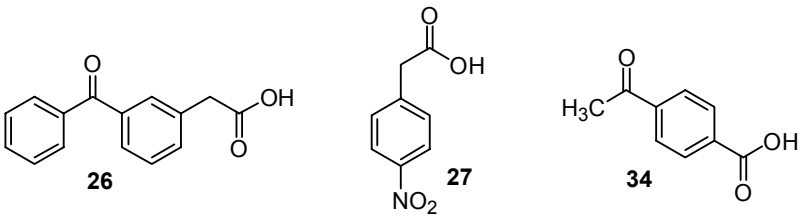

The benzyl carbanion has been implicated in photoredox reactions as well (see previous discussion on *meta* and *para*-nitrobenzyl alcohols) and in photodeuteration studies of 3-methylbenzophenone (**28**) (Eqn. [1.15]) and 3-methylacetophenone.[69] Subsequent investigations involving photodeuteration studies demonstrated that the aryl ketones alone were capable of inducing deprotonation in the excited state without requiring additional functional groups. In those studies *para*-substituted aryl ketones were completely unreactive towards deuteration, again supporting the *meta* effect.

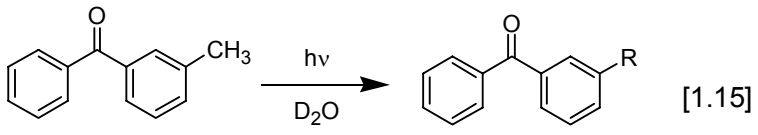

28

29 a R=CH_2D
b R=CHD_2
c R=CD_3

Subsequent investigation[70] suggests that when **26** or its acetophenone analogue **30** are photolysed in the presence of acid the mechanism does not directly produce a carbanion but instead forms a biradical enol **31** or **32** before undergoing protonation to yield the methyl compound **28** or **33**. This reaction mechanism (Eqn [1.16]), although not formally involving a carbanion, still undergoes decarboxylation in a similar method. Instead of forming a carbanion the pair of electrons becomes involved in a double bond. This acid catalysis is only observed for the *meta* compound. The *para* compound **34** does not react via an acid catalysis mechanism.

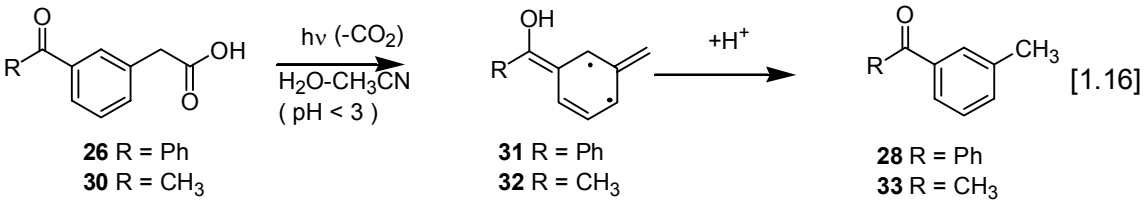

26 R = Ph
30 R = CH_3

31 R = Ph
32 R = CH_3

28 R = Ph
33 R = CH_3

1.7 Photoredox Chemistry of Pterins

Pterins, of which folic acid is a member, are a class of heterocyclic compounds that are commonly found throughout biological systems. It has been reported that they may act as light-harvesting antennas[71,72] and play a role in photosynthesis.[73] This participation in photobiological processes attracted interest and their photophysical and photochemical behaviour has been investigated in quite a few papers recently.[74,75,76]

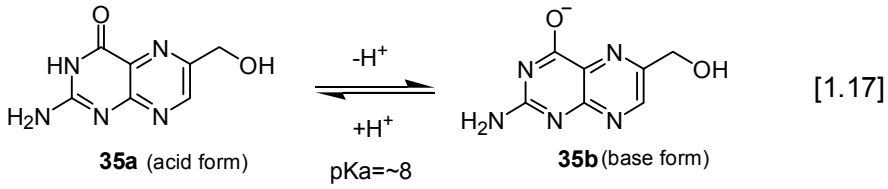

35a (acid form)

35b (base form)

The acid-base properties and multiple oxidation states available make pterins a complex system to study. The pterin heterocyclic system may be thought of as an aromatic amide as the carbonyl is α to the aromatic heterocycle. However, the pterin system differs from most other aromatic carbonyl compounds presented in this Thesis by the presence of a nitrogen α to the carbonyl. This allows facile deprotonation to yield a product that is an analogue of an enolate. Consequently there is an acid form and a base form for each pterin (see Eqn. [1.17]) with a pK_a of ~ 8.[77] Their photophysics and photochemistry vary dramatically depending on which form is dominant. For example the quenching of the fluorescence of the acid form seems to be related to its acid-base

properties and may occur through a proton-transfer mechanism.[78] This conclusion is supported by the fact that rate constant for quenching is readily correlated with the pK_b values of the anions and by the fact that the anions of strong acids such as chloride, sulfate and nitrate do not quench the fluorescence.

Of primary interest to this Thesis is the 6-hydroxymethylpterin (**35**). Upon photolysis the base form **35b,** oxidizes to 6-formylpterin (**36**) as the only reaction in the absence of oxygen ($\Phi_{disappearance}$=0.018). In the presence of oxygen the **36** is further oxidized to the carboxylic acid (**37**). The acid form **35a** has more complicated photochemistry, shown in Eqn [1.18]. In the presence of oxygen the reaction results in a mixture of ~15% **36**, ~85% **37** ($\Phi_{disappearance}$=0.0023). In the absence of oxygen the reaction proceeds to a new product, 6-formyl-5,8-dihydropterin (**38**). This product exhibits a change in absorption towards longer absorption bands[79] and is consistent with the reduction of the pterin moiety concurrent with the oxidation of the substituent through an intramolecular redox reaction. The pterin moiety of the redox product (**38**) is then thermally oxidized on admission of oxygen to yield the corresponding oxidized product (**36**) and hydrogen peroxide. A further intramolecular photoredox reaction is possible with the acid form of **36** being converted upon further photolysis into the redox product 6-carboxy-5,8-dihydropterin (**39**) which is then consequently thermally oxidized to the **37**.[80] Thus the main photoproduct is **37**.

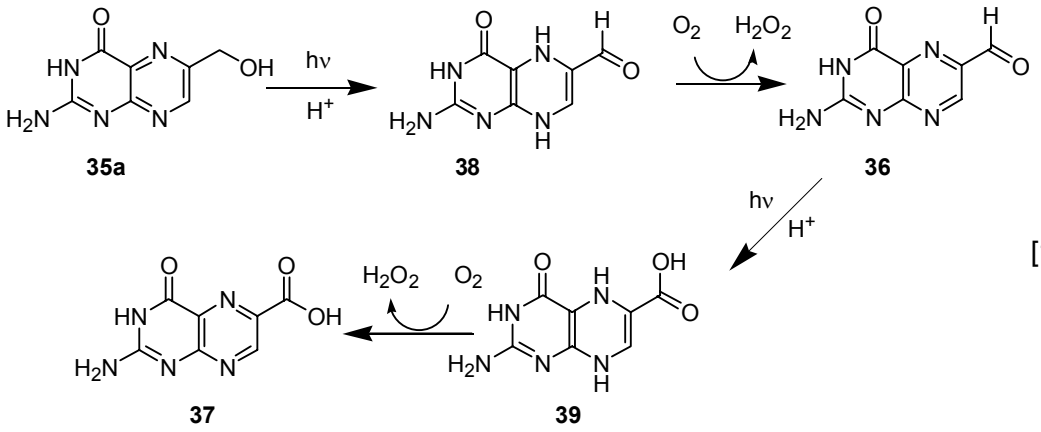

[1.18]

Although an in-depth mechanism has not yet been published, the product studies do suggest that the intramolecular photoredox reaction of pterins mirror some of the intramolecular redox reactions observed for substituted aromatic ketones to be reported in this Thesis.

1.8 Photoredox Chemistry of Anthraquinones

Anthraquinone (**40**) is a highly conjugated quinone that is very stable thermally. Its reduced form, 9,10-dihydroxyanthracene (**41**) is not thermally stable under oxygen and reverts to anthraquinone. The photochemistry of anthraquinone is similar to that of benzophenone in that it typically involves extremely efficient intersystem crossing to the triplet state.

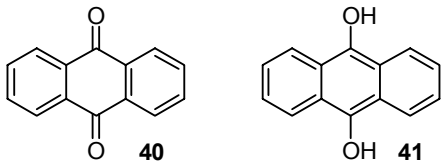

Similarly to benzophenone, anthraquinone is an excellent photosensitizer and has the added advantage that its main photoreduction product, **41**, reverts back to **40** upon contact

with oxygen.[81] Much work is currently being done on using water-soluble anthraquinone sulfonates as antennas for solar energy conversion,[82] or as photodeprotection agents.

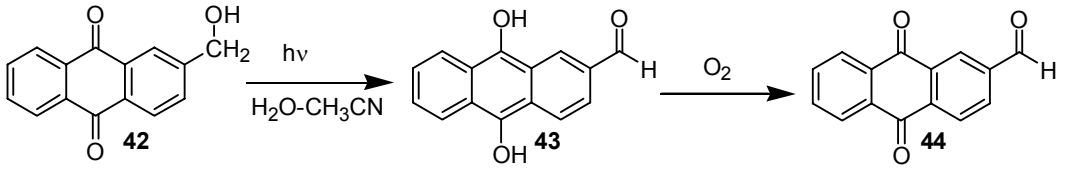

[1.19]

When 2-(hydroxymethyl)anthraquinone (**42)** is photolysed in 1:1 acetonitrile : water an intramolecular redox reaction occurs with high efficiency ($\Phi = 0.8$).[83] At first glance the reaction appears to be photooxidation but upon closer inspection it was noted that the reaction proceeded through an air-sensitive intermediate (**43**) that upon workup in air resulted in the 3-formylanthraquinone (**44**) observed as the final product. The intermediate was highly coloured and was readily visible via UV-vis traces. Photolysis in an NMR tube under argon yielded a product that was consistent with 2-formyl-9,10-dihydroxyanthracene (**43**). The oxygen sensitivity of the proposed intermediate is unsurprising as 9,10-dihydroxyanthracene reacts readily with oxygen to form anthraquinone. A mechanism was proposed[83] that is very similar to that proposed for *p*- and *m*-nitrobenzyl alcohols previously explored by Wan and Yates[10] involving a benzylic carbanion (**45**). No concentration dependence on quantum yield was observed over a concentration range of 10^{-6} M to 10^{-4} M which suggests that the reaction was unimolecular. Despite appearing to be an intramolecular reaction, the reaction was dependent on the presence of a protic solvent. The reaction is extremely efficient in water-acetonitrile, less so but still observable in methanol and non-existent in neat

acetonitrile. When examining the reaction, the initial deprotonation to form **45** and subsequent protonation to form **46** must involve solvent participation.

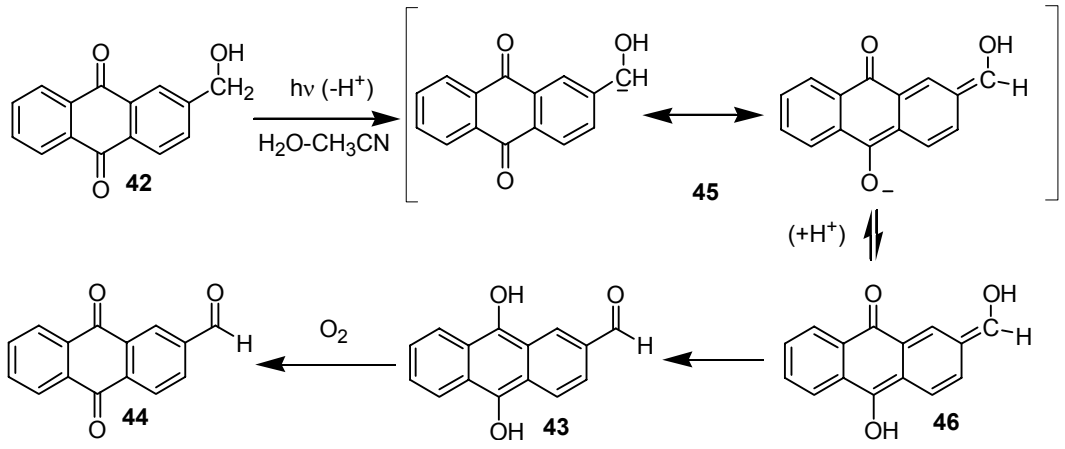

[1.20]

When 2-methylanthraquinone was photolysed under the same conditions no reaction was observed, not even simple photoreduction, even upon prolonged irradiation.

1.9 Proposed Research

Previous research in our group examined the intramolecular photoredox reaction of 2-(hydroxymethyl)anthraquinone (**42)**. This work was presented in a communication[83] which may be seen as pivotal to the direction of research for this Thesis and has been discussed previously. This was itself an extension of previous studies on *p*- and *m*-nitrobenzyl alcohols which exhibited intramolecular photoredox chemistry in the excited triplet state. The goal of that research was to explore the similarities between the nitro group, which is considered to be "enigmatic" and consequently difficult to explore, and the carbonyl group, which exhibits photobehaviour that is considerably better understood. The intramolecular photoredox chemistry observed suggested that the primary

photochemical step was water-mediated deprotonation of a benzylic C-H, to generate a carbanion intermediate. Studies examining the decarboxylation of ketoprofen (**23**) and phenylacetic acid (**26**) suggested that the carbonyl moiety could act as an enhanced electron-withdrawing group in the excited state akin to the nitro group. Based on that conclusion, various aromatic ketones were investigated and **42** was determined to exhibit efficient intramolecular photoredox behaviour.

The benzophenone chromophore will be the main focus of this Thesis towards the goal of understanding the intramolecular photoredox behaviour exhibited by certain aromatic ketones. Chapter 2 of this Thesis will explore the parent compound, 3-(hydroxymethyl)benzophenone (**47**)and its simple alkyl (**48**) and aryl derivatives (**49**). Their photobehaviour will be explored in detail and the effect of altering the benzylic carbon substituents examined. In addition, the role the hydroxyl group plays in the photoredox chemistry will be investigated by studying the photochemistry of 3-methylbenzophenone (**28**) and 3-(methoxymethyl)benzophenone (**50**). The effect of aromatic substitution will also be explored through the *ortho*- (**51**) and *para*-substituted (**52**) (hydroxymethyl)benzophenones. A mechanism, supported by evidence obtained via extensive product studies and laser flash photolysis will be presented.

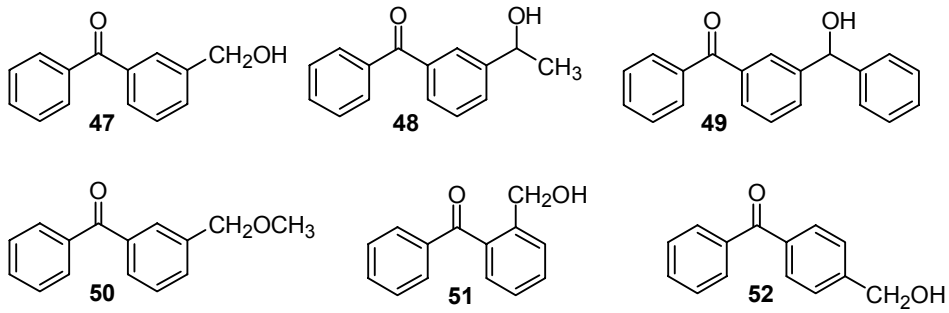

As the photobehaviour of benzophenones is governed by its lowest triplet excited state and the electronic behaviour of the aromatic rings are critical to any photochemistry

observed, Chapter 3 will explore alternative chromophores, specifically two different cyclic chromophores with very different electronic behaviour, xanthones and fluorenones. Consequently 2-(hydroxymethyl)xanthone (**53**) and 2-(hydroxymethyl)fluorenone (**54**) were synthesized and studied.

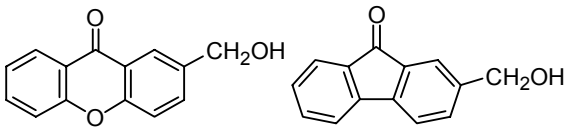

53 **54**

Previous research on the nitrobiphenylmethanols by Morrison[11] (presented in Section 1.3) demonstrated that intramolecular photoredox chemistry was not only possible but promoted by the enhanced polarizability of the extended biphenyl moiety. Chapter 4 will explore the possibility of extending the benzophenone chromophore using a substituted phenyl group. One complication that does not arise in the nitrobiphenyl case is that there are now two different chromophores, the benzoyl chromophore and the biphenyl chromophore. The effect of substituents' position will also be explored through the three compounds: 3-(2'-(hydroxymethyl)phenyl)benzophenone (**55**), 3-(3'-(hydroxymethyl)phenyl)benzophenone (**56**), 3-(4'-(hydroxymethyl)phenyl)benzophenone (**57**).

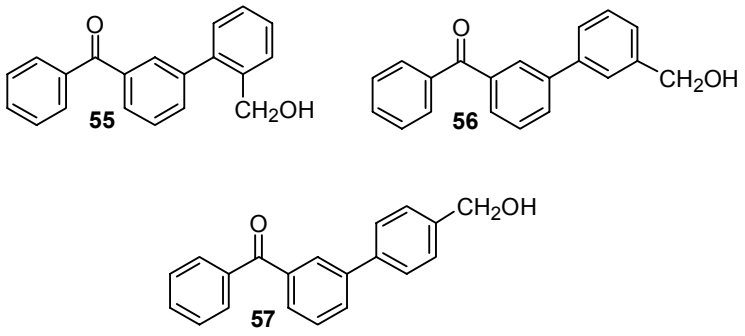

55 **56** **57**

Chapter 2
Intramolecular Photoredox Reactions of Benzophenones and Simple Derivatives

2.1 Introduction

The investigation into the photoredox behaviour of substituted aromatic ketones began by examining the parent compound, 3-(hydroxymethyl)benzophenone, (**47**). This Thesis focuses on this compound, and several sections of this chapter shall investigate in detail various aspects of the photoredox behaviour exhibited by **47**. Since the photobehaviour of all other compounds in this Thesis shall be compared with **47**, the UV-vis spectral and photoproduct studies on **47** are necessarily presented first. Details are presented in Section 2.2.2.1.

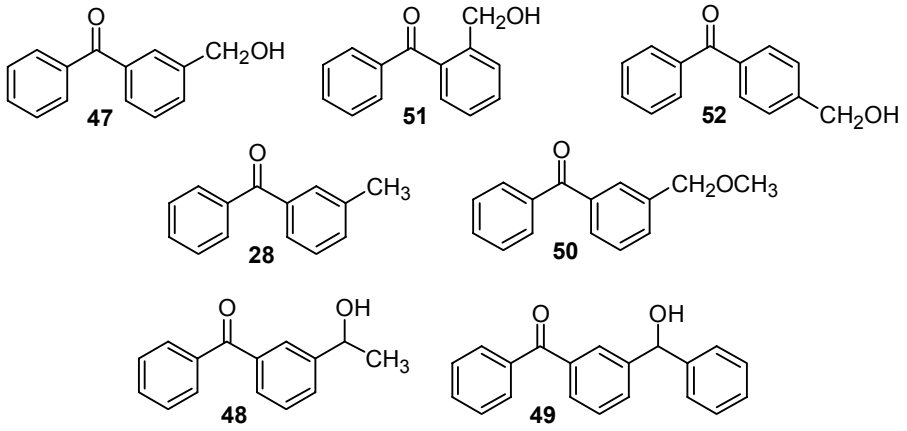

Figure 2.1 Compounds explored in Chapter 2

Because photochemical redox products depend greatly upon the electronic distribution in the molecule, it was felt that we might gain further insight into the observed photoredox behaviour by altering the position of the substituents, or by altering the identity of the benzylic substituents. To examine the effect substituent position has

on the photochemical behaviour of the benzophenones, the *ortho*- substituted compound **51** and the *para*- substituted compound **52** immediately present themselves as targets for investigation. The details of the photostudies on those compounds are presented in Section 2.2.2.3.

After determining the requirement for a *meta*- substituent in governing the efficiency of the photoredox reaction, the identity of the oxidizable group was next explored. First, the hydroxyl was removed to give the *meta*- methylbenzophenone (**28**). Although it is theoretically possible to oxidize the methyl group in order to observe photoredox behaviour, the loss of the hydroxyl group changes the electron distribution significantly. It is therefore unsurprising to observe significantly different photochemical behaviour in **28** compared with **47**. Next, the proton on the hydroxyl group was exchanged with a methyl group to give the methyl ether **50**. We anticipated that since a hydroxyl group has similar electron distribution to a methoxy group, the photoredox reaction observed for **47** would also be possible for **50**. This however turned out not to be the case. The photobehaviours of these two compounds are investigated in Section 2.2.2.4 and are contrasted with the photobehaviour of the parent **47**.

Other derivatives were investigated in order to study the effect of structural alteration of the benzylic carbon on the photobehaviour. It was felt that because the benzylic carbon seemed central to the photobehaviour of **47,** varying the attached atoms might yield some insight into the mechanism of reaction. Two different derivatives of **47** were studied in Section 2.2.2.5: 3-(1-hydroxyethyl)benzophenone (**48**), and 3-benzoylbenzhydrol (**49**). In the first of these, one of the hydrogens is replaced with a methyl group while in the second the same hydrogen is exchanged for a phenyl

substituent. Since the charge density on the benzylic carbon is expected to be largely the same for **48** as for **47**, the photochemistry of **48** may be similar to that of **47**. However, the additional phenyl group in **49** has the capability to stabilize charges at the benzylic carbon, and so may affect the photobehaviour significantly.

Since previous studies[8,9,70,83] on intramolecular photoredox reactions were dependent on the solvent mixture's identity, it was necessary to examine in detail the effects of different solvent systems on the photobehaviour of **47**. Particular attention was paid to the pH since the photoredox reaction is apparently catalyzed in the presence of acid. More detail concerning the effect of concentration (Section 2.2.2.6), and pH (Section 2.2.2.7) on the photobehaviour of **47** is also presented. These studies were invaluable in the task of determining the mechanism of the photoredox reaction of the benzophenone derivatives examined in this Thesis. Determining the origin of the benzhydrol proton is a further requirement towards elucidating the mechanism of the photoredox reaction. This was determined through photolysis in D_2O solvent. Results are presented in Section 2.2.2.8.

The nature of the excited state species often affects which photoreaction is observed. Since all of the compounds investigated in this Chapter are benzophenone derivatives it is expected that they should behave similarly to benzophenone itself and have efficient intersystem crossing to the triplet state. Regardless, no discussion of a mechanism is complete without at least a cursory examination of the nature of the excited state. Consequently, nanosecond laser flash photolysis (LFP) was performed on many of the compounds discussed in this Chapter. These results are presented in Section 2.2.3.

Finally, a postulated mechanism is presented in Section 2.2.5 that is consistent with all of the observed data. It is a amalgamation of several previously presented ideas, concerning the photoreactions of benzophenones.

2.2 Results and Discussion

2.2.1 Synthesis and Materials

Because none of the desired photosubstrates were available commercially, they all had to be prepared before photochemical studies could be accomplished. In most cases, the benzophenone alcohols that were the focus of the photochemical studies were prepared from initially purchased or prepared methyl substituted analogues via bromination and hydrolysis. The parent compound examined in this Thesis, **47**, was prepared from the commercially available 3-methylbenzophenone (**28**) via NBS bromination followed by hydrolysis (Eqn [2.1]).

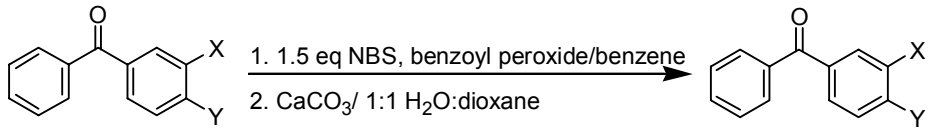

[2.1]

28 X: CH_3; Y: H
58 X: H; Y: CH_3

47 X: CH_2OH; Y: H; Z: H
52 X: H; Y: CH_2OH; Z: H

The *para*-substituted compound, **52**, was prepared via the analogous procedure, starting with the commercially available 4-methylbenzophenone (**58**). By contrast, the mono-deuterated compound, **47-αD,** could not be directly produced via this method. It was instead prepared from **28** by dibrominating with NBS and hydrolysing to form 3-formylbenzophenone (**59**), which was then selectively reduced using sodium borodeuteride (Eqn [2.2]).

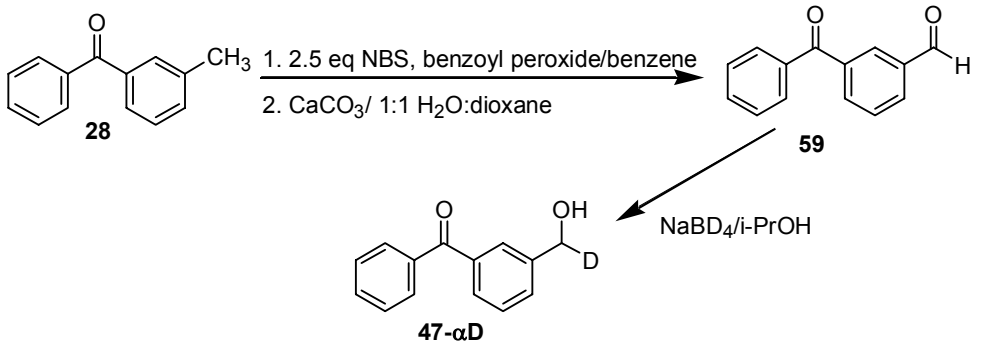

[2.2]

Although 3-ethylbenzophenone (**25**) is not available commercially, there is a simple photochemical procedure that produces pure **25** via the photodecarboxylation of ketoprofen, **23**, in 100% yield (see Section 1.6, Eq. [1.14]). Once **25** was produced, the synthesis of **48** was accomplished via the standard bromination and hydrolysis (Eqn [2.3]).

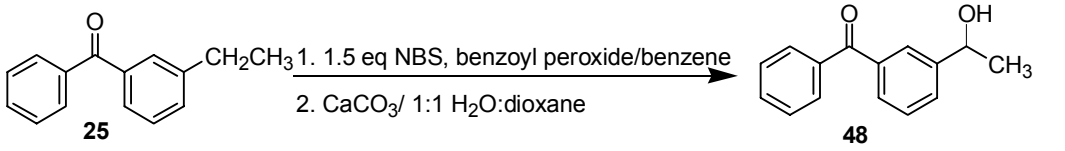

[2.3]

3-Benzoylbenzhydrol (**49**) and its deuterated version, **49-αD** were synthesized conveniently through the sodium borohydride (or sodium borodeuteride) monoreduction of the commercially available 3-benzoylbenzophenone (**60**) (Eqn. [2.4]).

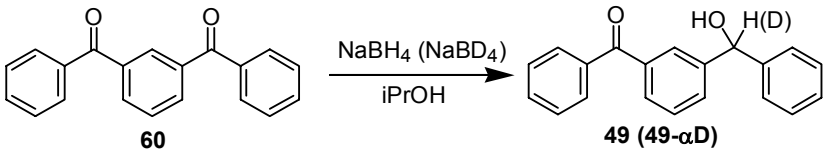

[2.4]

The synthesis of the *meta*-substituted methyl ether **50** was accomplished in a similar manner to the synthesis of **47** except that during the solvolysis step, methanol was used instead of water (Eqn. [2.5]).

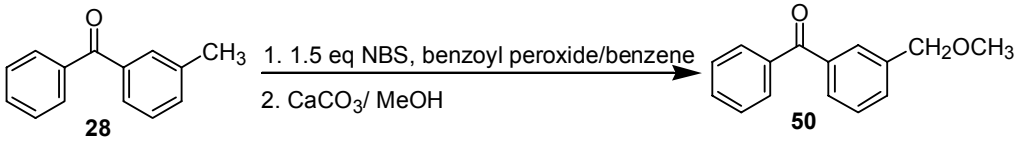

[2.5]

2.2.2 UV-Vis Spectral Studies and Product Studies

As discussed in Chapter 1, the primary focus of this Thesis involves an exploration of the photoredox behaviour of aromatic ketones originally exhibited by 2-(hydroxymethyl)anthraquinone (**42**) in Section 1.8.[83] Of particular focus will be the investigation into certain benzophenone derivatives explored in this Chapter.

2.2.2.1 Photostudies on Parent Compound 47

The novel photoredox reaction of **42** (See Section 1.8)[83] was mediated by water and was active at pH 7. Also presented in that work was a cursory examination of the analogous benzophenone, **47**. The evidence presented showed no photoredox chemistry; only the photoreduction typically observed for benzophenones was observed to take place. However, this experiment was only performed at pH 7 and at ~10^{-3} M. Subsequent investigation undertaken and presented in this Thesis concluded that these conditions were inappropriate for studying the photoredox reaction of substituted benzophenones. Unlike the analogous **42**, **47** requires the presence of moderate proton concentration (pH < 3) in order to observe significant photoredox chemistry. The effect of pH on the photobehaviour of **47** will be explored in more detail in Section 2.2.2.7. The photoredox reaction of **47** is more complicated than the photoredox reaction for **42** due to the competing photoreduction reaction of the benzophenone moiety. This competing reaction is primarily due to the ease of hydrogen abstraction that the carbonyl undergoes and was reviewed in Section 1.5. The photoreduction reaction is bimolecular and competes effectively with the photoredox reaction under conditions that are unfavourable to the latter transformation such as neutral or basic aqueous medium. The bimolecular photoreduction reaction is also concentration dependent, and therefore will be more

prevalent at higher concentrations. Consequently it is unsurprising that under the conditions examined in the study by Lukeman *et al*[83] only the successfully competing photoreduction reaction was observed. By decreasing the concentration of **47** it is possible to observe photoredox chemistry, even at pH 7, albeit with greatly reduced efficiency compared to pH 2. The effect of substrate concentration on the resulting photobehaviour will be presented in more detail in Section 2.2.2.6.

Upon photolysis under acidic aqueous conditions (while purging with argon), **47** underwent photoredox chemistry to form the intramolecular photoredox product, **61** (see Eq. [2.4]). This reaction is highly efficient with an estimated quantum yield of 0.6 (by using the photolysis of **42** ($\Phi = 0.8$) as a secondary standard (See Section 2.4.4.5 for full description)). Trace amounts of the oxidized product **59** were also visible in the NMR spectrum.

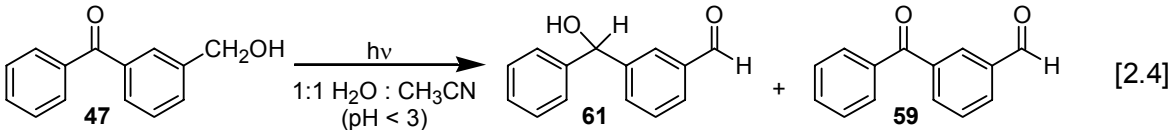

[2.4]

Initial UV-vis spectral traces performed for **47** were intriguing. Although immediate loss of the 255 nm peak was observed indicating loss of **47**, a new spectrum arose with peaks at 230 nm and 250 nm that was unassignable to either **61** or **59** (see Figure 2.2). UV-vis spectral traces of **61** and **59** also proceeded to the same spectrum following irradiation indicating that although the UV-vis spectral trace of **47** did not visibly proceed to **61**, a further reaction may have been possible under the conditions involved during acquisition of the trace (7.9×10^{-6} M 1:1 H_2O : CH_3CN (pH 2), Ar purged in quartz cuvette). The previously unassigned spectrum was essentially identical to 3-benzoylbenzoic acid (**62**). Thus, under UV-vis concentrations, instead of proceeding

to **59** or stopping at **61**, **47** was oxidized all the way to **62**, despite being purged with argon prior to photolysis.

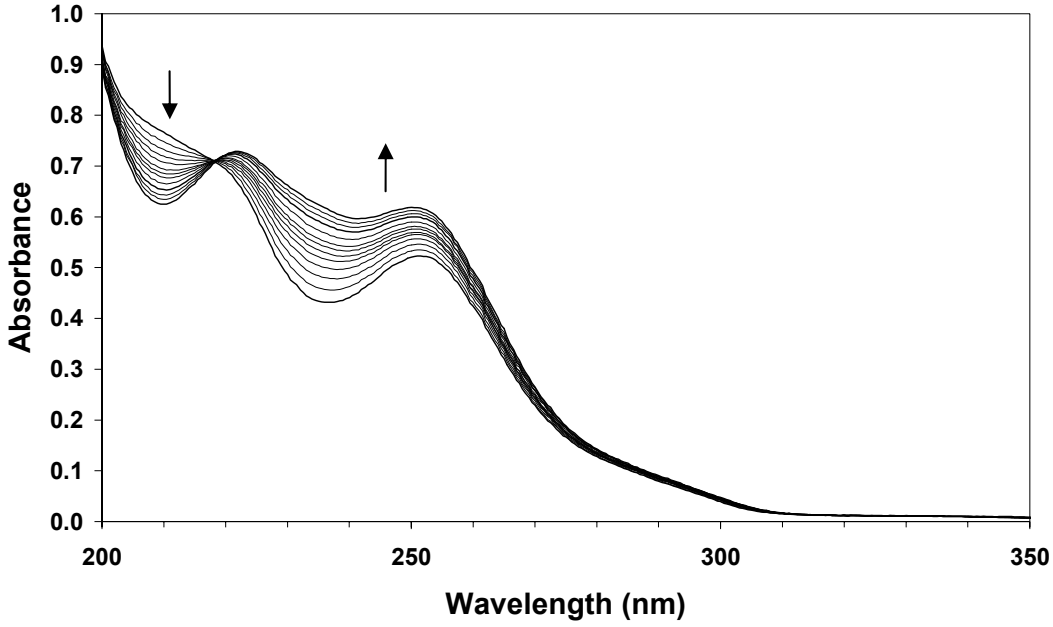

Figure 2.2 UV-vis spectral traces observed upon photolysis of **47** in 1:1 H_2O : CH_3CN (pH 2). Each trace is taken after 2 minutes irradiation at 300 nm using two lamps (7.9 x 10^{-6} M). The final spectrum is consistent with the spectrum for **62.**

This was unexpected as semi-preparatory photolysis of **47** results in **61** when purged with argon and **59** when purged with oxygen. Under the semi-preparatory photolysis conditions used with **47**, no **62** was observed, even after purging with oxygen. However, when **59** or **61** is irradiated further while saturating with oxygen, **62** results (Eqn. [2.5]). It is thought that because the concentration of the cuvette is so dilute (8 x 10^{-6} M), the residual dissolved oxygen has a greater effect than at the concentration used for semi-preparative photolysis (1.5 x 10^{-4} M). To avoid this complication an alternative technique was used. Compound **47** was photolysed on a semi-preparative scale with a concentration of 1.5 x 10^{-4} M. The photolysis run was stopped periodically and aliquots

removed. These were then diluted precisely and UV-vis spectra obtained. In this manner, Figure 2.3 was produced. As the photolysis proceeded, the spectral trace showed a loss of a band at 255 nm (due to **47**) concomitant with a growth of bands at 210 nm, 250 nm and 295 nm. The hypsochromic shift from 255 nm to 250 nm is consistent with an interruption of conjugation attributable to the benzophenone chromophore and the growth of two bands in the product is consistent with the two chromophores present in the photoredox product. The final trace is assignable to the expected photoredox product **61.** An isosbestic point is clearly visible suggesting that the photoreaction proceeds without the production of significant sideproducts.

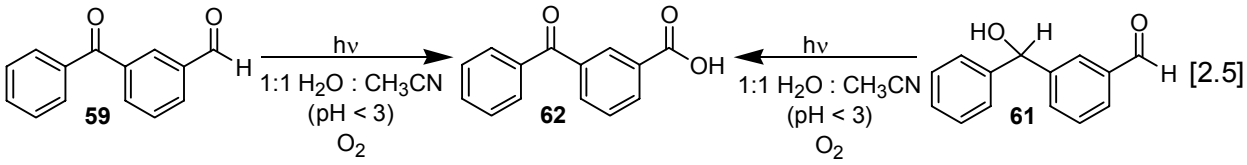

[2.5]

A second UV-vis spectral trace was obtained at pH 7 following the same experimental procedure as that used to obtain the UV-vis spectral trace at pH 2. The pH 7 spectral trace exhibited a loss of the band at 255 nm concomitant with a growth of a band at < 200nm. Unlike at pH 2, only loss of **47** was observed, with no **61** produced (see Figure 2.4). Analysis of the product mixture demonstrated a significant increase in sideproducts. The difference in photobehaviour with respect to pH suggests that the photoredox reaction is acid-catalysed. This shall be explored later in more detail.

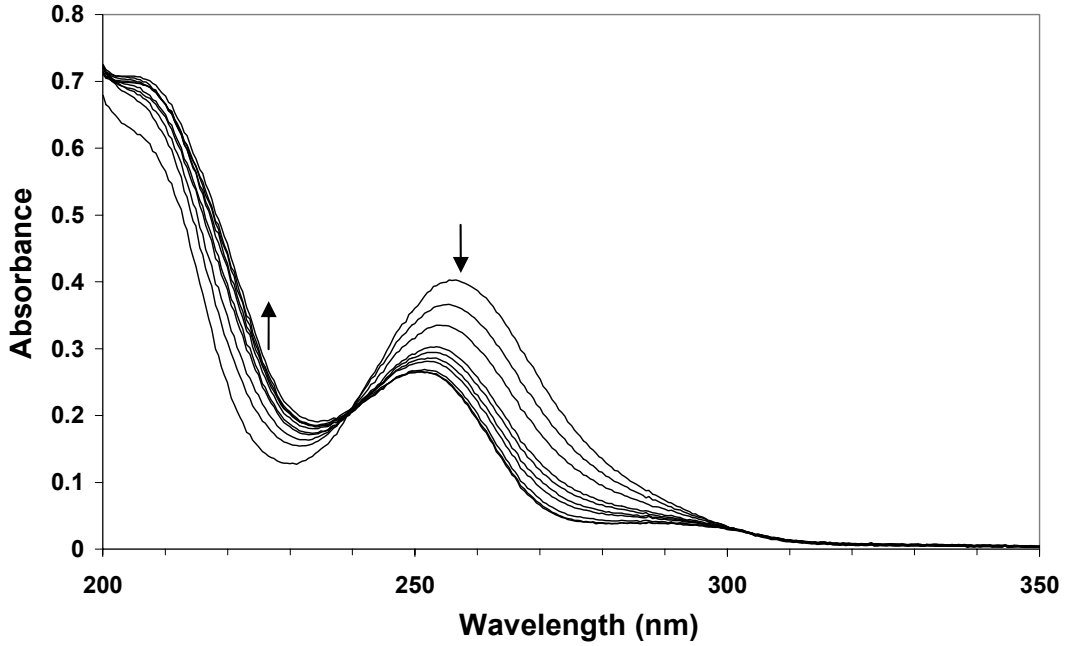

Figure 2.3 UV-vis spectral traces observed on photolysis of **47** in 1:1 H_2O : CH_3CN (pH 2). Each trace is taken after 30 second irradiation at 300 nm using four lamps at semi-preparative photolysis concentrations (1.5 x 10^{-4} M). The final spectrum is consistent with the spectrum for **61**.

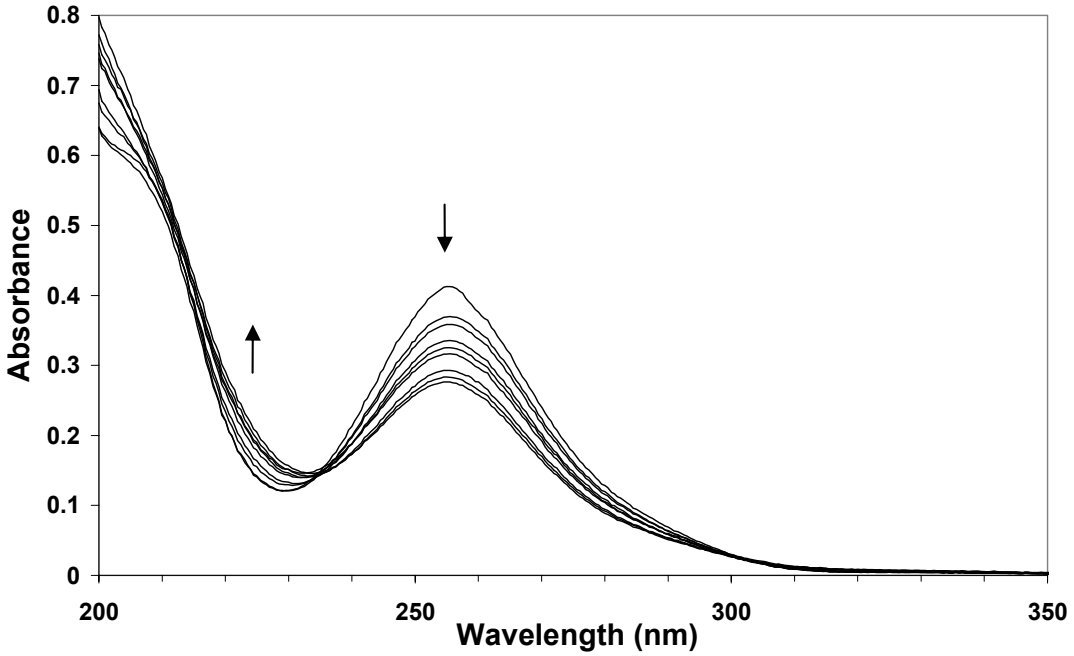

Figure 2.4 UV-Vis spectral traces observed on photolysis of **47** in 1:1 H_2O : CH_3CN (pH 7). Each trace is taken after 30 second irradiation at 300 nm using four lamps at semi-preparative photolysis concentrations (1.5 x 10^{-4} M).

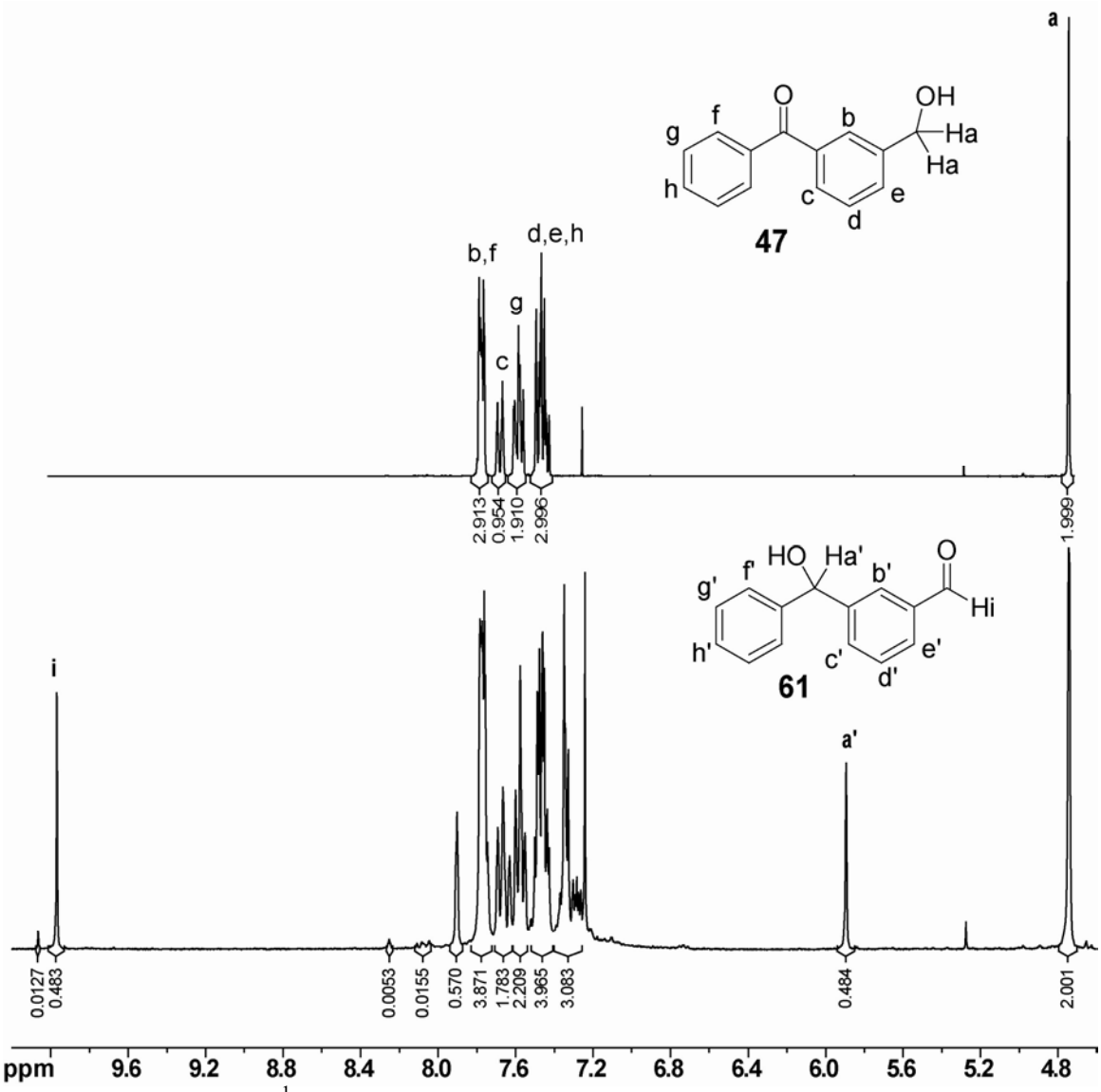

Figure 2.5 300 MHz ^{1}H-NMR spectra of **47** (in chloroform-*d*) before (top) and after (bottom) photolysis (1.6×10^{-4} M, 10.1 mg/300 mL) in 1:1 H_2O : CH_3CN (pH 2), for 2 minutes with two 300 nm lamps (argon purged). Product ratio: 67% **47**: 32% **61**: 1% **59**. Product ratio was determined by comparing the integrations for the peak due to the benzhydrol proton (**a'**: 5.90 ppm, 0.48H) to the singlet (**a**: 4.79 ppm, 2.0H). amounts (< 1%).

Both **61** and **59** are readily distinguishable by ^{1}H-NMR spectroscopy and the product ratios may be determined directly from NMR analysis of the product mixture (see Figure 2.5 for the NMR spectrum of the product mixture and the NMR spectrum of the unphotolysed **47**). The benzylic methylene protons (δ 4.79 ppm) are particularly

diagnostic for **47**. The benzhydrol proton (δ 5.90 ppm) and the aldehyde proton (δ 10.00 ppm) of **61** are also diagnostic and by comparing the ratios between the two a semi-quantitative percent conversion may be obtained (67% **47**: 32% **61:** 1% **59**). The second aldehyde peak (δ 10.10 ppm) arises from **59** and is only present in trace quantities. No significant amounts of oligomeric photoreduction side products (usually observable as broad aromatic signals at δ 7.0 -7.3 ppm when present) were observed when samples of **47** were photolysed under dilute conditions (~ 10^{-4} M) in acidic aqueous solvent media. These oligomeric photoreduction side products were present when **47** was photolysed at higher concentrations. The oligomeric material is made up of many similar compounds having masses above 500 (as shown by mass spectrometry). These likely originate from the photoreduction of the benzophenone moiety in the manner shown in Eqn. [2.6].

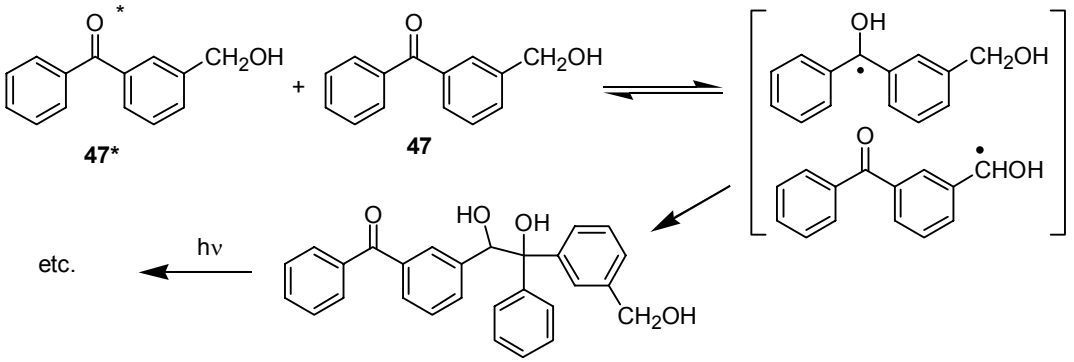

[2.6]

Photolysis while purging with oxygen results in a product mixture containing almost exclusively **59**. The presence of **59** in the photoreaction mixture while purging with argon may be due to residual oxygenation of either **61** or a reactive intermediate leading to **61**. The photolysis results showing the product ratios at increasing photolysis times at pH 2 are shown in Table 2.1. Results are also shown at pH 7 and pH 1 under comparable photolysis conditions to aid comparison. Detailed pH studies are presented later, but a trend is immediately obvious in that as the pH decreases the conversion from **47** increases.

Table 2.1 Comparison of Product Mixture Ratios from Photolysis of **47**[b]

Photolysis time 300 nm lamps	pH[a]	% **47**	%**61**	%**59**	%**OP**[c]
1 lamp, 1 min	2	89	9	1	1
1 lamp, 2 min	2	79	18	2	1
2 lamps, 2 min	2	63	33	2	2
2 lamps, 5 min	2	23	70	3	4
4 lamps, 5 min	2	5	85	2	8
2 lamps, 5 min	7	48	42	2	8
2 lamps, 5 min	1	28	65	3	5

[a]Using 10.2 mg **47** in 300 mL (1.60×10^{-4} M) in 1:1 H_2O : CH_3CN, pH of H_2O adjusted with H_2SO_4 to pH 2 prior to mixing with CH_3CN.
[b]Product mixture ratio determined by integration via ^{1}H-NMR($CDCl_3$).
[c]Oligomeric side product (**OP**) approximate, estimated from integration via ^{1}H-NMR($CDCl_3$).

2.2.2.2 The Effect of Solvent Mixture Ratio

The presence of water was determined to be necessary in order for the photoredox reaction to proceed. When **47** was photolysed in pure acetonitrile, no **61** was observed, and only side products consistent with hydrogen-abstraction photoreduction products resulted. Although water appears to be a necessary mediator of the intramolecular photoredox reaction, it is thought that acetonitrile is only necessary to facilitate the dissolution of **47**. The results of photolysis studies in various solvent mixtures are summarized in Table 2.2.

Table 2.2 Comparison of Product Mixture Ratios from Photolysis of **47** for Different Solvent Ratios[b]

Photolysis time 300 nm lamps	%H_2O	pH[a]	% **47**	%**61**	%**59**	%**OP**[c]
2 lamps, 2 min	99%	2	52	46	1	1
2 lamps, 2 min	95%	2	50	48	1	1
2 lamps, 2 min	90%	2	55	42	2	1
2 lamps, 2 min	50%	2	63	33	2	2
2 lamps, 2 min	10%	2	76	18	2	4
2 lamps, 2 min	5%	2	83	6	3	8
2 lamps, 2 min	1%	2	86	0	2	12

[a]Using 10.2 mg **47** in 300 mL (1.60×10^{-4} M) in different ratios of H_2O : CH_3CN, pH of H_2O adjusted with H_2SO_4 to pH 2 prior to mixing with CH_3CN.
[b]Product mixture ratio determined by integration via ^{1}H-NMR($CDCl_3$).
[c]Oligomeric side product (**OP**) approximate, estimated from integration via ^{1}H-NMR($CDCl_3$).

It becomes evident that as the percentage of water in the solvent mixture increases so does the conversion from the substrate (graphically illustrated in Figure 2.6). The polarity of the solution plays an important role in the photoredox reaction. This may be due to the stabilizing effect that a polar solvent has on the π,π^* triplet excited state.[54] When very little water is present in solution (below 10%) the redox reaction becomes very inefficient and the formation of oligomeric sideproducts becomes correspondingly more favourable.

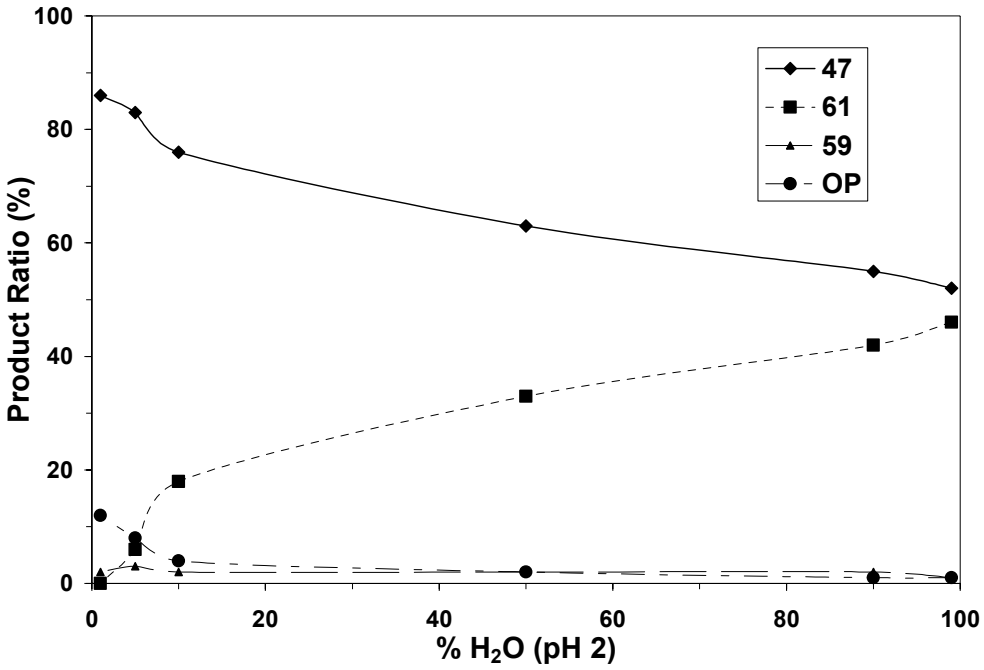

Figure 2.6 Product ratios as a function of the solvent ratio of water. Conversion from **47** using 10 mg/300 mL H_2O : CH_3CN, adjusted to pH 2 using H_2SO_4; photolysed for 2 minutes using two 300 nm lamps after purging with argon. The products were **59**, **61** and oligomeric side-product (**OP**).

2.2.2.3 Exploring the Effect of Substituent Position on the Photoredox Reaction

Substituent position on an aromatic ring is a great factor in ground state chemistry due to the delocalization of electron density around the aromatic ring and the ease with which charges may be stabilized through resonance. These same factors are present in the excited state molecules and substituent position has been noted to play a significant role in the photobehaviour of aromatic molecules.[36] Specific focus needed to be made on the *para* and *meta* positions as the anthraquinone analogue **42** has a carbonyl group in both the *para* and *meta* positions to the hydroxymethyl substitutent and is active at pH 7.

The *para* compound **52** was photolysed under equivalent conditions to **47** to gauge the relative reactivity between the two of them. These photolysis results for **52** are

summarized in Table 2.3. Although some photoredox product **63** was formed during the reaction the majority of **52** was consumed to produce oligomeric product of the type similar to Eqn [2.6]. As with **47**, a small amount of the oxidized product **64** was produced. The photoreaction observed is shown in Eqn [2.7].

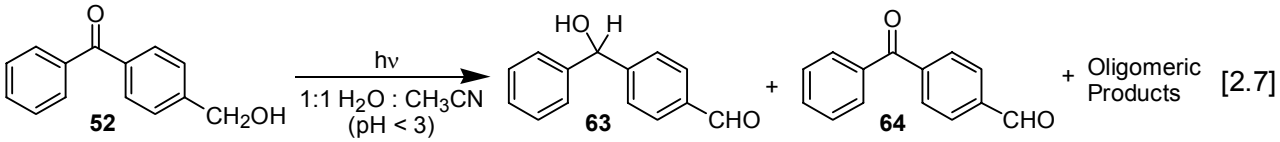

[2.7]

Photolysis of **52** under more acidic conditions (10% and 30% H_2SO_4) did not significantly improve the results but dramatically increased the amounts of oligomeric product that resulted. As the postulated mechanism (Section 2.2.5) suggests the dependence of deprotonation of the benzylic carbon as one of the important steps in the conversion of the substrate into the redox product, it was thought that by photolysing in base the reaction may be promoted. Photolysing **52** in base (pH 13), however, resulted in only a trace of redox product (**52**:97%; **63**: <1%; **64**: 2%; OP: <1%). This approach was evidently flawed. It appears that the presence of a moderate proton concentration is important. Interestingly, the acid-catalysis that is so prevalent in the photobehaviour of **47** seems almost absent during the photolysis of **52**. Although under equivalent photolysis time, **52** is consumed a greater amount at pH 2 than at pH 7 (**52** was 73% of the product mixture for pH 2 while 82% was remaining for pH 7), the product ratios do not vary nearly as dramatically as for the photolysis of **47**. These results are consistent with the *meta*- effect[61] explored by Zimmerman. Substituents at the *para* position to the absorbing chromophore are expected to be less reactive (often several orders of magnitude less) than at the equivalent *meta* position. Consequently, the significantly different reactivity between **47** and **52** is unsurprising. This would not affect the

hydrogen abstraction pathways however, and the efficiency of photoreactions leading to photoreduction oligomeric products should remain relatively unchanged. The observed oligomeric products seem to confirm this statement. The oligomeric products increase dramatically as the photolysis times increase and the redox product eventually becomes obscured by the presence of oligomeric products. Photolysis in oxygen appears to quench the reaction and prevents the oligomeric products from forming. Unfortunately it also seems to inhibit formation of **63** and **64** as well.

Table 2.3 Comparison of Product Mixture Ratios from Photolysis of **52**[b]

Photolysis time 300 nm lamps	pH[a]	% **52**	%**63**	%**64**	%**OP**[c]
2 lamps, 2 min	2	93	0	1	6
2 lamps, 5 min	2	85	1	1	13
4 lamps, 5 min	2	73	3	1	23
2 lamps, 5 min	7	78	<1	0	22
2 lamps, 5 min	1	93	0	3	4
2 lamps, 5 min	ACN[d]	93	0	0	7
4 lamps, 5 min	2[e]	98.6	0.8	0.2	0.4

[a]Using 10.2 mg **52** in 300 mL (1.6×10^{-4} M) 1:1 H_2O : CH_3CN, pH of H_2O adjusted with H_2SO_4 prior to mixing with CH_3CN.
[b]Product mixture ratio determined by integration via ^{1}H-NMR($CDCl_3$).
[c]Oligomeric side product (**OP**) approximate, estimated from integration via ^{1}H-NMR($CDCl_3$).
[d]Run contained no H_2O, only pure CH_3CN
[e]Run purged with O_2

When the substituent is in the *ortho* position it has complications that do not exist for either the *meta* or the *para* position. Like all *ortho*-substituted benzophenones with

accessible hydrogens (see Section 1.5), **51** may undergo rapid hydrogen abstraction which could compete strongly with any possible photoredox reaction. A possible reaction pathway for this reaction is shown for the photochemistry of **51** in Scheme 2.1. After excitation, internal hydrogen abstraction from the benzylic carbon would lead to the biradical **65** which may be viewed as the dienol **66**. Ketonization of **66** may result in either the redox product **67** or reversion to starting material.

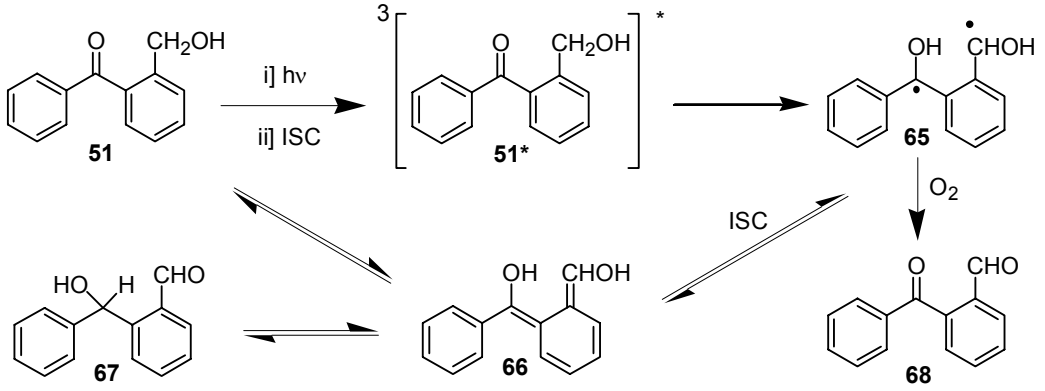

Scheme 2.1 Photoreactions Expected from the Excited Triplet State of **51**

It is important to note that this reaction mechanism does not rely on acid catalysis. In fact, protonation of the carbonyl oxygen should inhibit the hydrogen abstraction. During the photolysis of **47** at different pHs the inhibition of the oligomeric side-products as a factor of pH is observed and explored in more detail in Section 2.2.2.7. These results are expected as the oligomeric side-products are presumably due to a competing hydrogen-abstraction pathway. As the preferential reaction pathway available to **51** proceeds via initial intramolecular hydrogen abstraction, rather than through another mechanism, it differs significantly from the pathway available to the *para*, **52,** or the *meta*, **47,** compounds. Hydrogen abstraction pathways for **52** and **47** do not lead to photoredox product. Instead, for these compounds, hydrogen abstraction leads to oligomeric side-

products that compete with the photoredox pathway. Consequently, for the purposes of this Thesis the explorations into the mechanism for **51** are not applicable and shall not be discussed further.

The remainder of this Thesis shall focus on the *meta* position exclusively due to the lack of reactivity of the *para* position and the different reactivity exhibited by the *ortho* position.

2.2.2.4 The Effect of Removing the Hydroxyl Group

The hydroxyl group is an important structural feature and may play several roles within the photoredox reaction. Its ability to be oxidized to an aldehyde or carboxylic acid is key to the photoredox reaction as it is one half of the redox pair along with the carbonyl of the benzophenone. This will need to be investigated further. The oxygen of the hydroxyl group may act as an electron withdrawing group through the sigma bond to the benzylic carbon. However if the oxygen becomes conjugated to the aromatic ring as an enol it may donate the lone pair electrons into the ring.

By removing the hydroxyl group the *meta*-methyl compound **28** is formed which may be thought of as an important probe in studying the photobehaviour of **47**. Although it is theoretically possible for the hydrogens attached to the methyl carbon to be oxidized to a hydroxyl group, the attached hydrogens do not provide any of the electronic behaviour exhibited by an attached oxygen atom. When photolysed under the same conditions as **47** (shown in Eqn [2.8]), very little photoreaction is observed. No photoredox product, **69**, was observed. Evidence for any further oxidized products is

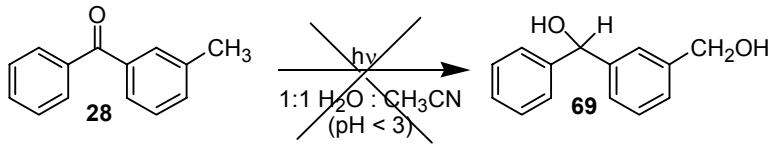

[2.8]

also absent. There is, however, a trace of product attributable to an oligomeric product analagous to that seen for in the photolysis of **47**. As this oligomeric product is expected for any benzophenone compound, its appearance is unsurprising. Rather, it is surprising that only a trace was present. Under the same reaction conditions, far more oligomeric product is observed for **47**. The increased number of abstractable hydrogens (3 for **28** compared to 2 for **47**) would suggest that **28** would be more susceptible to forming the oligomeric products than **47** would. As this is evidently not the case, either an alternative reaction proceeds that deactivates the excited molecules before they can react with one another or for some reason **28** does not proceed to the intermediate that results in the oligomeric side-products.

The answer to this question can be found in experiments undertaken in our lab by Huck *et al*[69] studying the photolysis of **28** in D_2O with acetonitrile as a co-solvent. When **28** was photolysed in acidic D_2O, deuteration of the methyl was observed with a quantum yield of 0.1 for monodeuterium incorporation. Although the primary reaction was monodeuteration, dideuteration and trideuteration were also observed (see Eqn. [1.15]. It is evident therefore that the excited state **28** is deactivated via proton exchange. Fewer molecules are therefore available to produce the oligomeric products.

Additionally there is a greater amount of oligomeric products resulting from the photolysis of 47 rather than 28 because the presence of an attached oxygen facilitates the removal of a hydrogen atom due to increased polar contributions to the transition state.[84]

The acid-catalyzed nature of the reaction was noted, as photolysis in organic solvents such as acetonitrile or in neutral D_2O solutions gave essentially no photochemistry under the same conditions that yielded significant deuterium incorporation in acidic D_2O solutions (pD < 3). The photochemical behaviour of **28** was intriguing because it is significantly different that exhibited by the *ortho* and *para* analogues (**21** and **58** respectively). Photolysis of the *para*-methyl analogue **58** resulted in no deuterium incorporation upon photolysis, regardless of the solvent conditions studied (pD 1-7). Photolysis of the *ortho*-methyl substituted compound **21** also results in deuterium incorporation. But unlike the photochemistry for **28**, the photodeuteration of **21** is well-known[85] to proceed via intramolecular hydrogen abstraction. This photobehaviour was independent of pH, in sharp contrast to the photobehaviour exhibited by **28**. As a different mechanism was clearly involved for the photolysis of **28**, Huck and co-workers proposed a mechanism similar to that proposed by Wirz and co-workers[59] for the photohydration of benzophenone. The difference in photobehaviour of **28** compared to **21** and **58** is strikingly similar to the difference in behaviour exhibited by the hydroxymethylbenzophenone derivatives **47**, **52** and **51**. The mechanism of the photodeuteration of **28** will be discussed in detail Section 2.2.5 when the mechanism of the photoredox reaction is explored in more depth. The two mechanisms will be compared and contrasted.

The importance of the alcohol group for the redox photobehaviour was probed by exchanging the hydroxyl group on the methylene carbon with a methyl ether. A methyl ether should have electronic effects quite similar to that of a hydroxyl group. In both cases the oxygen may act as both an electron withdrawing group through its sigma bond

to the benzylic carbon or as an electron donating group if it becomes involved in a pi system through the formation of an enol. Initially it was thought that the photobehaviour would essentially be identical to that of **47** as the postulated mechanism does not appear to directly depend on the identity of the group attached to the methylene carbon but instead relies on the inherent photobehaviour of the benzophenone chromophore (Eqn [2.9]). This should result in the ejection of methanol and would possibly be of interest as a photoreleasing agent.

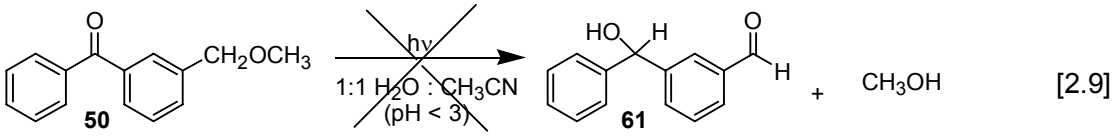

[2.9]

Unfortunately, this interpretation is evidently over-simplistic. Because methanol would be lost during the workup of the photolysis reaction the initial photostudies involved photolysing within an NMR tube. In this manner any methanol produced should be directly observed spectroscopically. Neither the photoredox product, **61**, nor methanol were observed. Instead, as is observed in the ^{1}H-NMR spectrum of the photoproduct mixture for the photolysis of **50** (Figure 2.7, middle spectrum), many products were present, none of them the expected photoredox product. Photoproduct studies at different pHs and for different amounts of time were performed and their results summarized in Table 2.4.

Extended photolysis at pH 2 results in the photodecay of **50** along with a concomitant increase in other products. As observed for the photolysis of the parent compound **47**, the photolysis of **50** also results in the formation of the oxidized product **59** (Eqn [2.10]). While the formation of the oxidized product **59** initially increases to a proportion around 2% of the product composition, it does not increase significantly upon

further photolysis. This is likely due to photooxidation by residual oxygen which is relatively constant between runs and would not increase upon further photolysis. Increasing photolysis times initially seems to increase the proportion of **59** with respect to **50**. However, this is an illusion as the apparent increase in the oxidized product **59** is merely an artifact of the decreasing proportion of **50** present. This conclusion is supported by the constant ratio between the solvent peaks and the peaks of **59** during the NMR tube photolysis described previously. Additionally, by examining the integration of the aromatic region as a whole instead of comparing just the integration attributable to **50**, one sees that the conversion to **59** appears to reach a maximum of ~2% and stays relatively constant despite further irradiation. Thus the formation of **59** proceeds until the supply of residual oxygen has been exhausted and then the photoreaction ceases.

Table 2.4 Comparison of Product Mixture Ratios from Photolysis of **50**[b]

Photolysis time 300 nm lamps	pH[a]	% **50**	% **59**	% Other
2 lamps, 2 min	2	59	1	40
2 lamps, 4 min	2	37	2	61
4 lamps, 5 min	2	9	2	88
2 lamps, 4 min	7	71	<1	28
2 lamps, 4 min	1	33	2	65
2 lamps, 4 min[c]	2	97	2	1

[a]Using 11.4 mg **50** in 300 mL (1.7×10^{-4} M) 1:1 H_2O : CH_3CN, pH of H_2O adjusted with H_2SO_4 prior to mixing with CH_3CN.
[b]Product mixture ratio determined by integration of the ^{1}H-NMR($CDCl_3$) spectrum. Determined by examining the integration of the aromatic region.
[c]Oxygen Saturated

The formation of **59** does not appear to be solely dependent on the concentration of oxygen however. The photoreaction also appears to be acid catalyzed, as the proportion of **59** formed is enhanced as the pH decreases from 7 to 2 to 1. At pH 7 virtually no **59** is observed while at pH 1 it is at its maximum. This suggests that although the final product mixture contains no photoredox product, the photolysis of **50** may share some mechanistic features with the photoredox behaviour observed during the photolysis of **47**. By photolysing in oxygen, a maximum amount of **59** is formed. This, too, is consistent with the behaviour observed for the photolysis of **47** while purging with oxygen.

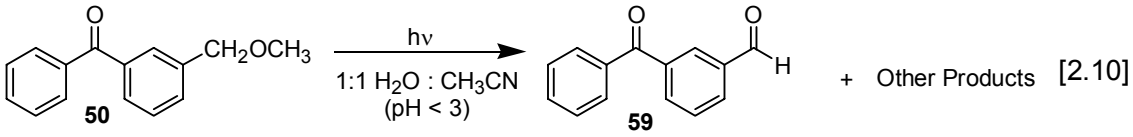

[2.10]

Photolysis in oxygen not only maximizes the amount of **59** produced but also prevents the other photoproducts from forming. This suggests a radical origin for the other products, but this has not been confirmed. Further studies are needed to definitively determine the nature of the multitude of photoproducts but they are beyond the scope of this Thesis as **50** does not undergo photoredox behaviour. The radical nature of the primary photoreaction is likely due to C-O bond cleavage (shown in Eqn [2.11]). This would result in a methoxyl radical and the resonance-stabilized benzylic radical **70**.

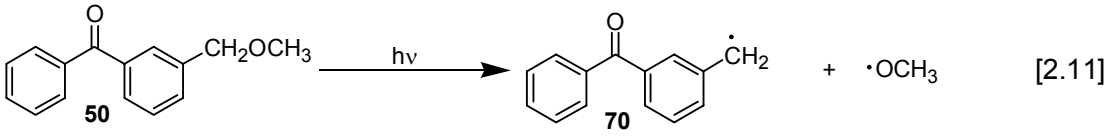

[2.11]

The other photoproducts (presumably of radical origin) also seem to be acid-catalyzed as their product ratio increases from 28% to 61% to 65% as the pH decreases from 7 to 2 to 1.

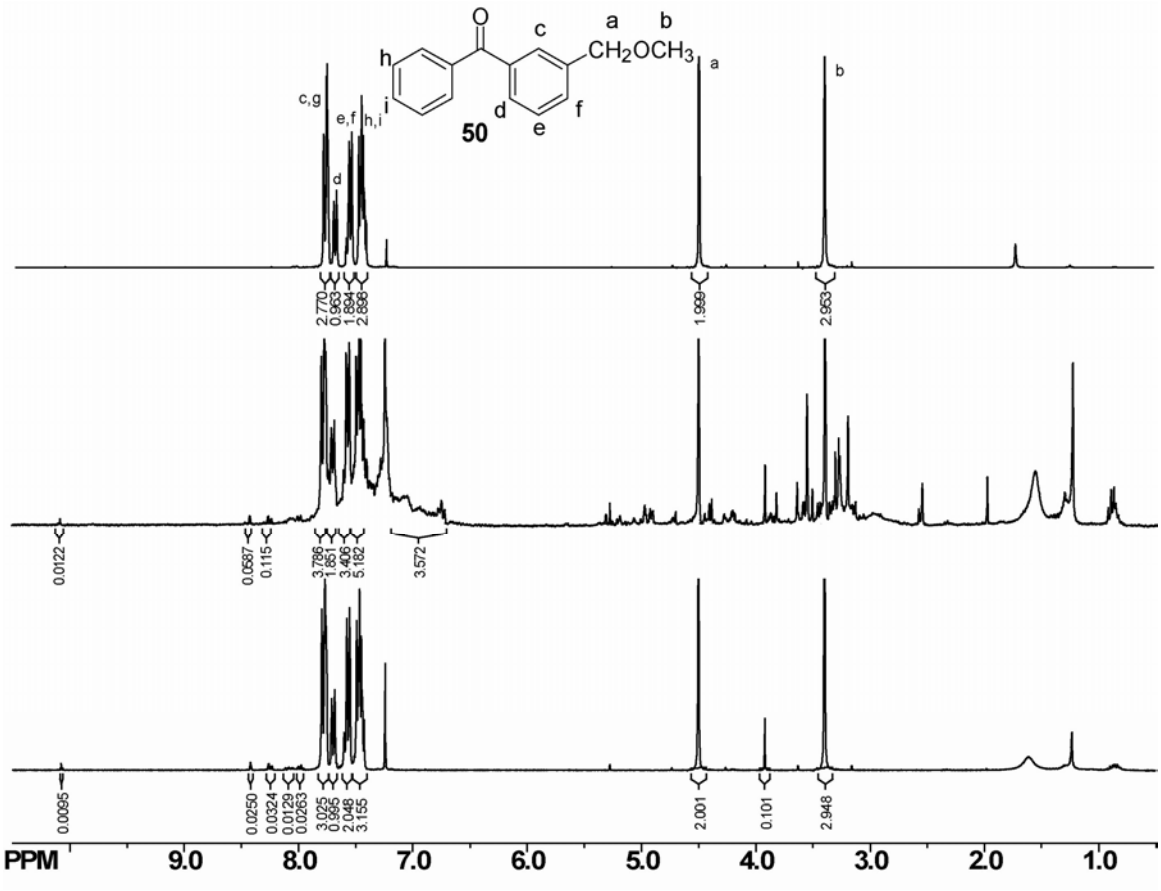

Figure 2.7 300 MHz ^{1}H-NMR spectra of **50** (in chloroform-*d*) before (top) and after photolysis (1.7×10^{-4} M, 11.4 mg/300 mL) in 1:1 H_2O : CH_3CN (pH 2), for 2 minutes with two 300 nm lamps purged with argon (middle) and purged with oxygen (bottom).

Although not directly related, some insight into the photobehaviour of **50** compared to **47** may be obtained from the work on the analogous 4-methoxymethylbenzophenone (**71**) and its comparison with the 4-hydroxymethyl compound **52**. Majima and coworkers[86] examined C-O bond cleavage using stepwise

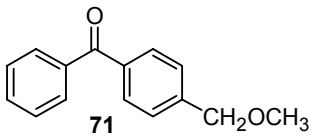

two-photon excitation. They reported that the bond dissociation energy for the C-O bond ($E_{BDE(C-O)}$) for **52** was 308 kJ/mol. This energy is higher than the energy of the lowest benzophenone triplet state (E_{T1} = 286 kJ/mol) so no cleavage was expected for the hydroxymethyl compound. However when the hydroxyl was replaced with a methoxy group the calculated $E_{BDE(C-O)}$ was lower than the energy of the first triplet state ($E_{BDE(C-O)}$ = 241 kJ/mol). Energetics alone was not sufficient to promote bond cleavage as no bond cleavage was observed from T_1, suggesting a significant energy barrier between the two states. A second laser pulse (532 nm) applied to the molecule in its T_1 state proved capable of initiating C-O bond cleavage of **71**. Despite having sufficient energy (E_{Tn} > 450 kJ/mol), **52** did not undergo C-O bond cleavage suggesting that substituent character was also important. Majima proposed that the delocalization of the T_n state including the C-O bond was also important. Thus, although bond cleavage is energetically favourable for both **52** and the **71**, only **71** undergoes cleavage because the anti-bonding character of the excited state may be delocalized in the C-O bond of the methyl ether. Such delocalization is not possible for **52** because a hydrogen atom is bonded to the oxygen. These observations are applicable in comparing the analogous *meta* compounds, **47** and **50**. No C-O bond cleavage was observed for **47** under any of the conditions tested. In contrast the methyl ether **50** apparently exhibited bond cleavage as a major photochemical pathway. The difference in reactivity between the *para* methyl ether and **50** is striking. Whereas **71** requires a second laser pulse to initiate bond cleavage, bond cleavage is accomplished in **50** within the single laser pulse and with notable efficiency. The discrepancy may be due to several factors.

Firstly, the *meta* position is known for being more reactive than the *para* position towards electronic effects (*meta* effect).[61] This makes it likely that a reaction exhibited at the *para* position may be more efficient at the *meta* position. This is especially important, when, as in the postulated mechanism put forth by Majima, delocalization of molecular orbitals between the substituents and the benzophenone chromophore is required. Secondly, the solvent conditions are quite different between the experiments performed for this Thesis and the research presented by Majima. The photolysis of **47** was accomplished in a water-acetonitrile solution at various pHs. By contrast the photolysis of **71** by Majima was accomplished in pure acetonitrile solution. In polar media the π,π* triplet state is known to be stabilized with respect to the n,π* state (see Figure 1.4). In addition, the protonation of the carbonyl oxygen is expected to accentuate the delocalization of the molecular orbitals. As the bond cleavage is expected to proceed via a π,π* triplet state in order to delocalize the anti-bonding character from the benzophenone character to the C-O bond, if the excited molecule is already in the π,π* triplet state the second laser pulse should not be required.

2.2.2.5 The Effect of Replacing One of the Benzylic Hydrogens

By altering the identitiy of the substituents, one can often gain useful information about the reaction mechanism by observing how the change in structure affects the reaction. The previous section discussed altering the hydroxyl group but this section will deal with altering the carbon backbone. By examining the effect of changing one of the hydrogens on the benzylic carbon with a methyl group or a phenyl group (**48** and **49** respectively) more information is obtained about the reaction mechanism. Exchanging

both hydrogens with alkyl groups will likely render the compound photoinert towards photoredox because the photoredox reaction results in the loss of a hydrogen on the benzylic carbon.

The photolysis of **48** in acidic aqueous media proceeds to the expected intramolecular photoredox product, **72** (Eq. [2.12]). The photoredox reaction was as efficient for the photoredox of **48** as for the photoredox of **47**. Using **47** as a secondary reference ($\Phi = 0.6$) the quantum yield of **48** was found to also be 0.6. Some residual photooxidation product **73** is visible and its origin is likely identical to that of **42**.

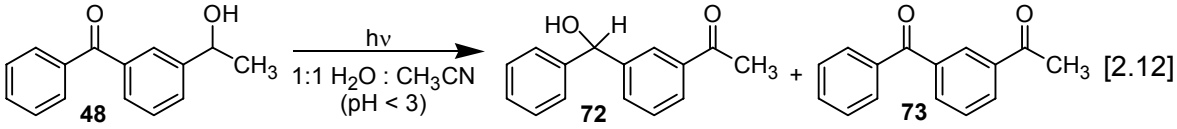

[2.12]

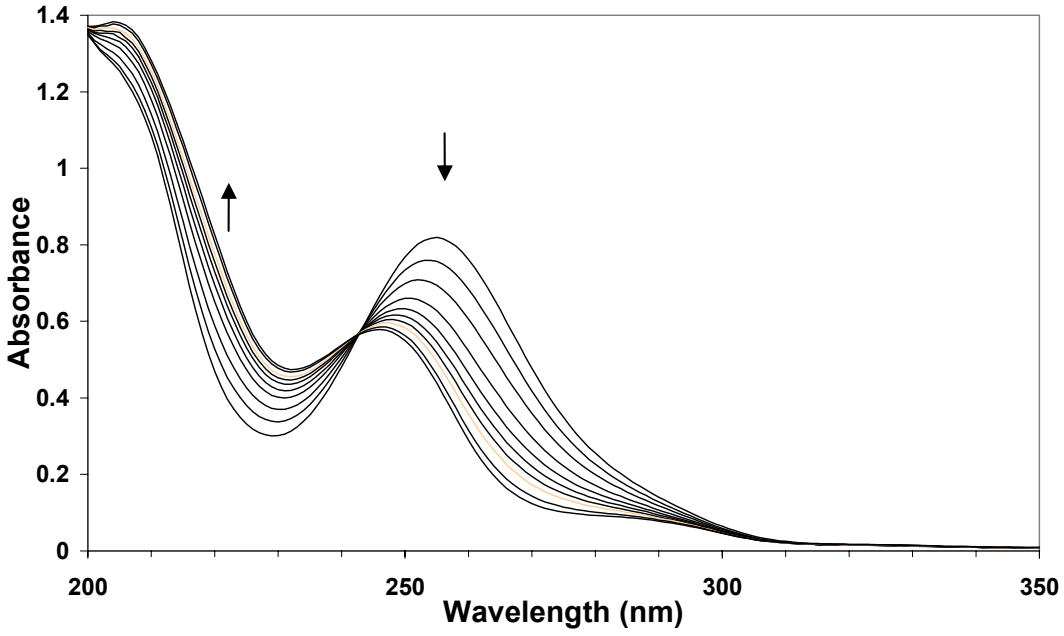

Figure 2.8 UV-vis spectral traces observed on photolysis of **48** in 1:1 H_2O : CH_3CN (pH 2), purged with argon. Each trace is taken after 30 second irradiation at 300 nm using one lamp at UV-vis concentration (10^{-5} M). The final spectrum is consistent with the spectrum for **72**.

Unlike the UV-vis spectral trace for **47**, which required following a semi-preparative photolysis (1.5×10^{-4} M), it was possible to follow the photolysis of **48** at UV-vis concentrations (1×10^{-5} M). This may indicate that **48** is less sensitive than **47** to residual oxygen. The UV-vis spectral trace of **48** at pH 2 has many similarities to the UV-vis spectral trace of **47** as expected for such similar molecules (see Figure 2.7 and Figure 2.3 for comparison). Both **47** and **48** have a band at 255 nm which decreases as the reaction proceeds. The photoreaction results in the growth of bands at 205 nm, 245 nm and 290 nm. The final spectral trace is assignable to **72** and has the same features as the UV-vis spectrum of **61** but with each band shifted 5 nm lower. As for the UV-vis spectral trace for **47**, an isosbestic point is clearly visible in the spectral trace for the photolysis of **48** suggesting that the photoreaction proceeds directly to **72** without many side reactions.

The UV-vis spectral trace obtained at pH 7 for the photolysis of **48** followed the same experimental procedure as used to obtain the UV-vis spectral trace at pH 2. The appearance of the spectral trace mirrored the spectral trace for **47** at pH 7 and exhibited a loss of the band at 255 nm concomitant with a growth of a band at < 200nm. At pH 7, only loss of **48** was observed and no **72** was readily observed in the UV-vis spectrum.

The photolysis product mixture ^{1}H-NMR spectrum is shown in Figure 2.10 with the NMR spectrum of **48** for comparison. As for the photolysis of **47**, the product mixture from the photolysis of **48** is easily decipherable using certain diagnostic peaks of **48** and the photoproduct. The benzylic methine proton of **48** is readily observed because it is isolated from the rest of the spectrum as a quartet (δ 5.00 ppm). The benzhydrol proton (δ 5.90 ppm) of **72** is also separate from the rest of the spectrum. By comparing

the integration of each the product ratio was obtained. Two peaks (δ 2.5-2.7 ppm) may be assigned as the acetyl methyl group present in **72** and **73** (the smaller peak). To facilitate comparisons between the two compounds, the same photolysis conditions were used for both and the ^{1}H-NMR spectrum of the product mixtures presented for **48** (Figure 2.10) and for **47** (Figure 2.5). By comparison to the photolysis of **47**, the photoreaction proceeds to photoproducts with similar efficiency but with fewer side products. The product ratio under these conditions is 68% **48** to 32% **72**.

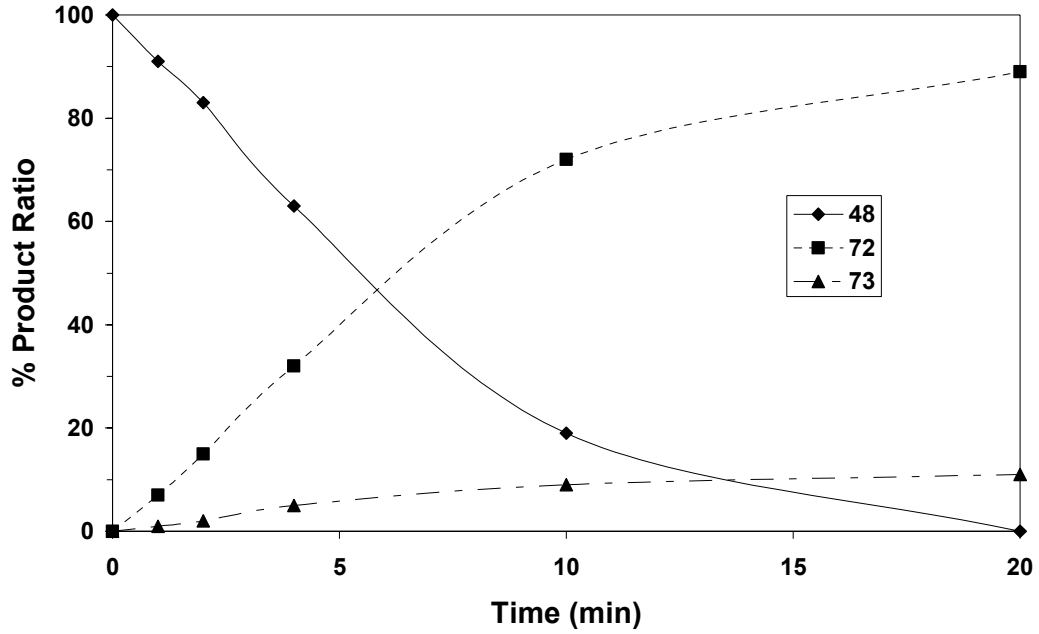

Figure 2.9 Percent conversion of **48** to **72** and **73** using 10 mg/300 mL 1:1 H_2O : CH_3CN (pH 2); photolysed using one 300 nm lamp after purging with argon (higher photolysis times converted from higher numbers of lamps to yield equivalent times for one lamp). Data from Table 2.5.

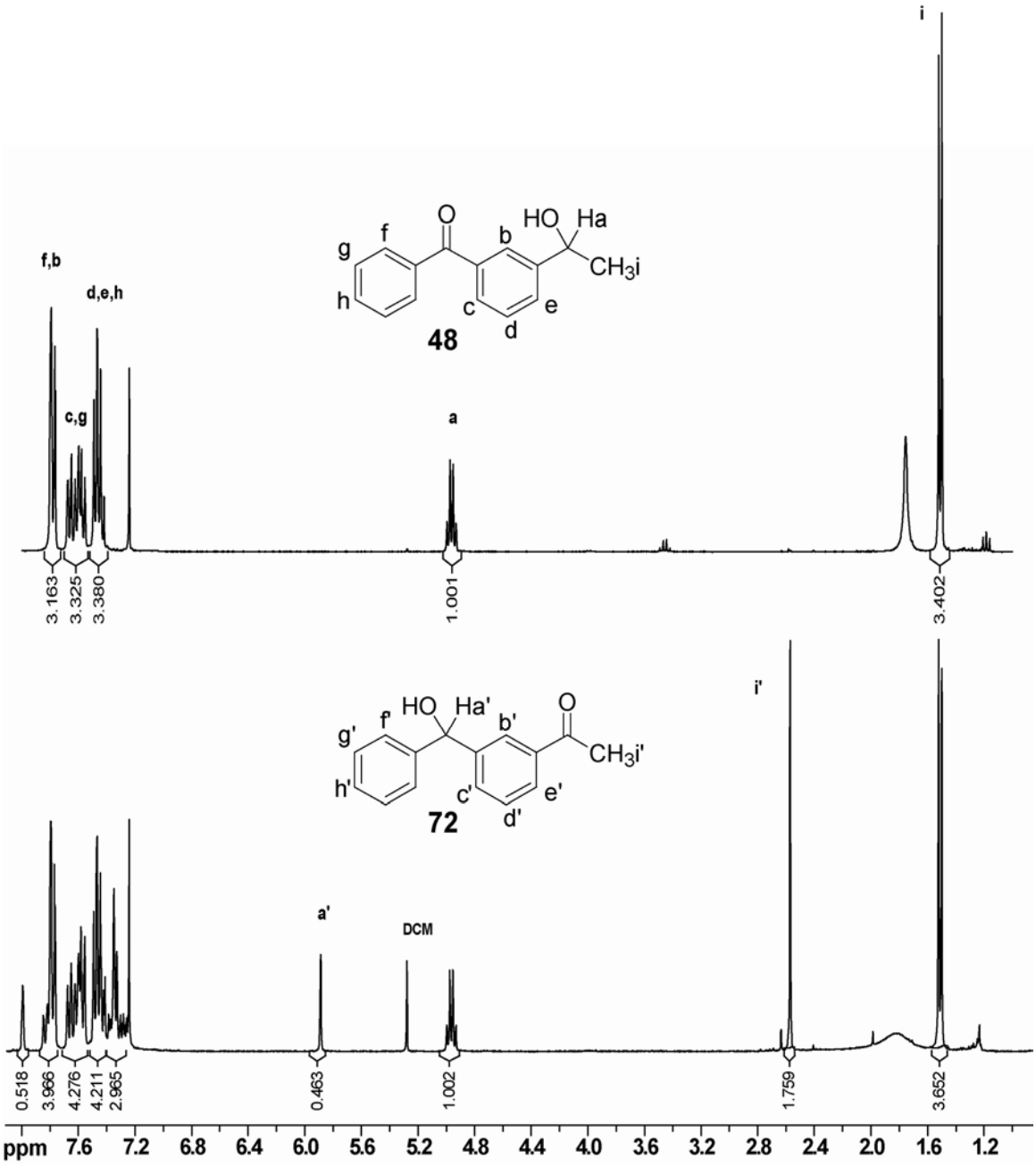

Figure 2.10 300 MHz ^{1}H-NMR spectra of **48** (in chloroform-*d*) before (top) and after (bottom) photolysis (1.5 x 10^{-4} M, 10.1 mg/300 mL) in 1:1 H_2O : CH_3CN (pH 2), for 2 minutes with two 300 nm lamps (argon purged). Product ratio: 68% **48**: 32% **72**. Product ratio was determined by comparing the integrations for the peak due to the benzhydrol proton (**a'**: 5.90 ppm, 0.13H) to the quartet (**a**: 4.97 ppm, 1.0H).

Only a trace of **73** is present in the product mixture. The exact proportion may be ascertained from the integration of the acetyl methyl at δ 2.7 ppm. As this reaction

produces few side-products, the reaction was photolysed to high conversion. It is possible to push the photolysis to 100% photoconversion with minimal formation of side products. The final product ratio is 89% **72** to 11% **73**. The progression of product ratio as a function of photolysis time is presented in Figure 2.9 and the photolysis data is given in Table 2.5. As expected, purging with oxygen leads to **73** as the only product.

Table 2.5 Comparison of Product Mixture Ratios from Photolysis of **48**[b]

Photolysis time 300 nm lamps	pH[a]	% **48**	% **72**	% **73**	%**OP**[c]
1 lamps, 1 min	2	91	7	1	0
1 lamps, 2 min	2	83	15	2	0
2 lamps, 2 min	2	63	32	5	0
2 lamps, 5 min	2	19	72	9	0
4 lamps, 5 min	2	0	89	11	0
2 lamps, 2 min	7	85	<1	4	11
4 lamps, 5 min	7	69	2	6	23
2 lamps, 2 min	1	63	34	1	2
2 lamps, 5 min	ACN[d]	94	0	2	5
4 lamps, 5 min	2[e]	62	0	38	0

[a]Using 10.1 mg **48** in 300 mL (1.5×10^{-4} M) 1:1 H_2O : CH_3CN, pH adjusted with H_2SO_4.
[b]Product mixture ratio determined by integration via ^{1}H-NMR($CDCl_3$).
[c]Oligomeric side product (**OP**) approximate, estimated from integration via ^{1}H-NMR($CDCl_3$).
[d]Run contained no H_2O, only pure CH_3CN
[e]Run saturated with O_2

The proton concentration is also a factor for the photoredox of **48**, just as it was for the photoredox of **47**. Photolysis at pH 7 does not lead to efficient conversion to **72**

but photolysis at pH 2 is extremely efficient with few side-products. Further increases in the acidity (pH 1) did not increase the conversion from starting material significantly but did increase the proportion of the product mixture assignable to **72**.

Photolysis in the absence of acidic aqueous media (pure acetonitrile) results in a small amount of **73** and an increased amount of oligomeric product. No photoredox product is observed under these conditions.

The general result of the intramolecular photoredox reaction studied in this Thesis is an exchange of oxidation states between a ketone and an alcohol. For both **47** and **48** this results in a change in the chemical structure and thus a new molecule. This makes spectroscopic analysis of the product mixture relatively straightforward. However, by replacing the methyl group of **48** with a phenyl group, the nearly symmetrical compound **49** results. An examination of **49** shows that the photoredox product of **49** has the identical structure to the original substrate. This complicates the photostudies because it is difficult to determine whether a photoredox reaction occurred and to what extent it progressed. A UV-vis spectral trace would not be useful in this case as the photoredox reaction would not result in any change in the UV-vis spectrum and only decomposition would be observed. Photoproduct studies using NMR spectroscopy would likewise be hampered by the impossibility of distinguishing the product and starting material. Thus any photostudies using NMR spectroscopy as a technique must involve deuteration. To do this two compounds were synthesized, **49** and **49-αD**. The two different benzoylbenzhydrols were photolysed under appropriate conditions. In 1:1 D_2O : CH_3CN **49** was photolysed to yield **49-αD** and conversely, **49-αD** was photolysed in 1:1 H_2O : CH_3CN to yield **49** (Eqn. [2.13]).

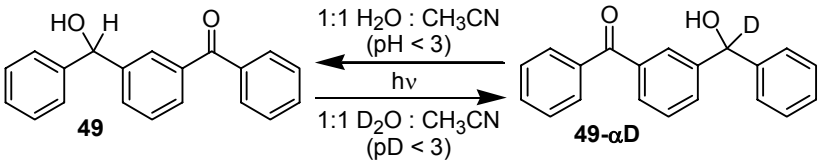

[2.13]

Product studies were complicated by the fact that more side-products arose during the photolysis of this compound. It was possible however to discern the conversion to the redox product in both cases. By examining the ^{1}H-NMR spectra of **49-αD** and the product mixture (Figure 2.11), it is possible to determine the product ratio in the photoreaction mixture. The conversion from **49-αD** to **49** may be followed by examining the growth in the benzhydrol proton (δ 5.90 ppm) as the deuterated benzhydrol is replaced with a proton. There is a minor signal due to residual protons that was present in the **49-αD**. This may easily be accounted for when calculating the product ratio. From these ratios the quantum yield of reaction for **49-αD** was estimated to be about 0.3 using **47** (Φ = 0.6) as a secondary reference. The trace low field signals at (δ 8.00 ppm and 8.10 ppm) may be assigned to the diketone **60**. Regardless of the concentration, significant oligomeric photoreduction products deriving from reactions analogous to the one shown in Eqn. [2.5] are present. These are visible in the ^{1}H-NMR spectrum as a broad aromatic region between δ 7-7.3 ppm. In contrast with **48**, when the photoreaction was pushed to higher conversions, the photoredox product conversion remained relatively constant at about 20% while the percentage of photooxidation and other side products rose. The increasing proportion of oligomeric side-products (**OP**) is visible in the plot showing how the product ratio changes over time (Figure 2.12). Although the photoredox product of **48** is itself, its ability to act as a possible photoprotecting molecule is limited by the large amount of side-products.

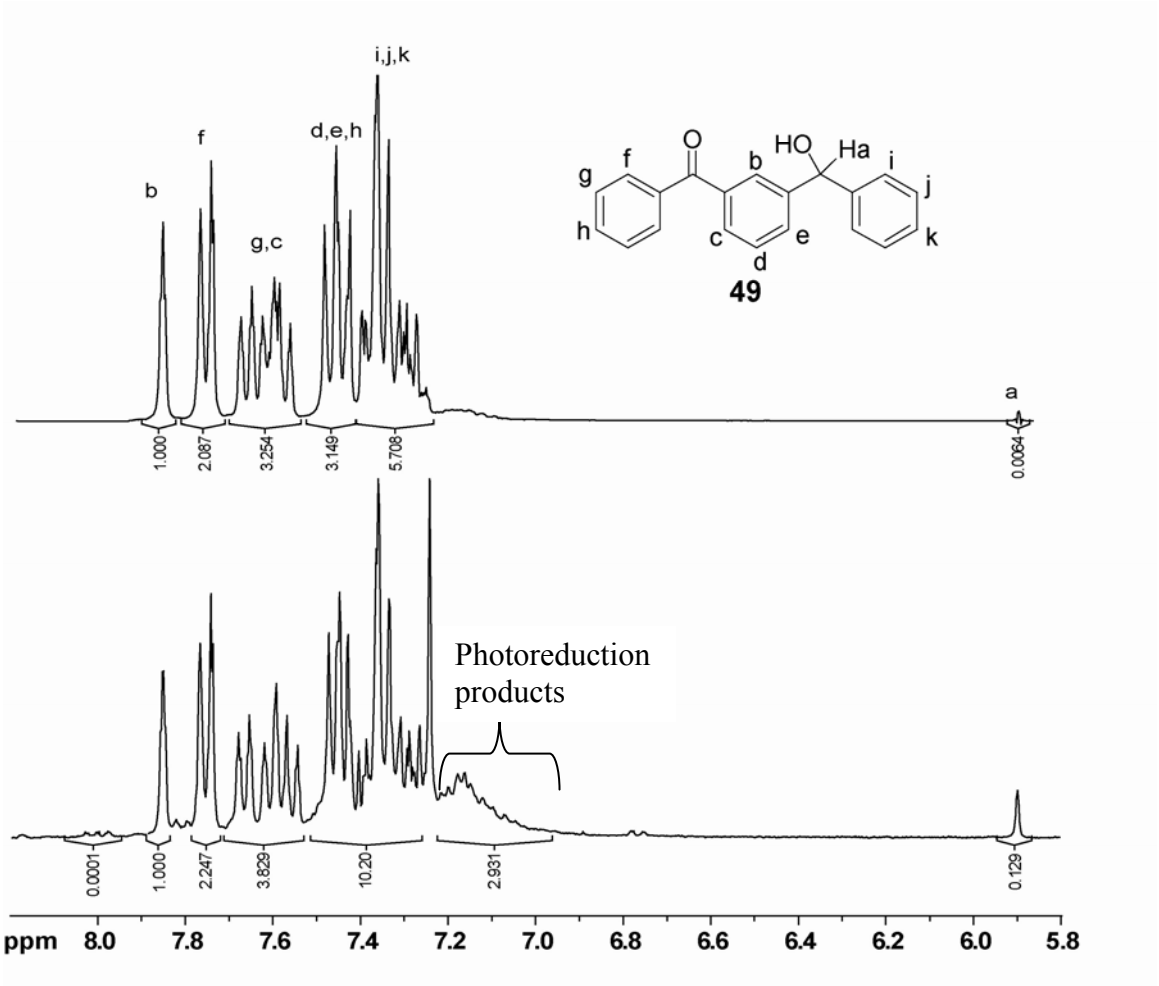

Figure 2.11 300 MHz ^{1}H-NMR spectra of **49-αD** (in chloroform-*d*) before (top) and after (bottom) photolysis (1.1×10^{-4} M, 9.8 mg/300 mL) in 1:1 H_2O : CH_3CN (pH 2), for 2 minutes with two 300 nm lamps (argon purged). Product ratio obtained via integration: 67% **49-αD**; 16% **49**; 2% **60**; 15% oligomeric photoreduction product. The product ratio was determined by comparing the integrations for the peak due to the benzhydrol proton (**a**: 5.90 ppm, 0.129H) to the singlet peak due to the aromatic proton adjacent to both the ketone and the alcohol (**b**: 7.85 ppm, 1.00H) and to the equivalent proton of **60** (8.17 ppm, 0.0001).

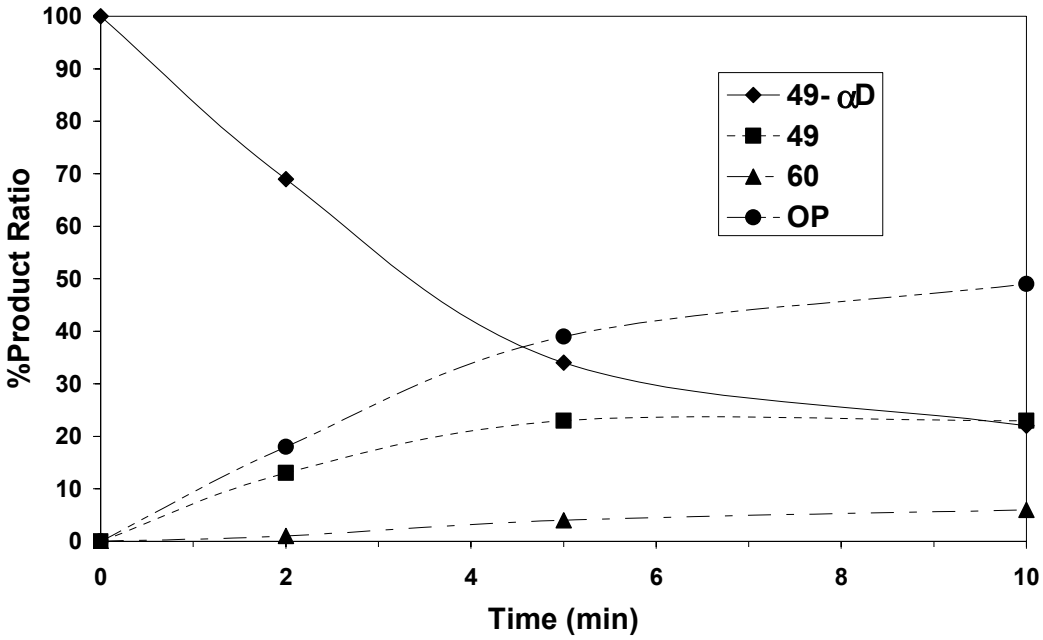

Figure 2.12 Percent conversion of **49-αD** to **49** and **60** using 10 mg/300 mL 1:1 H_2O : CH_3CN (pH 2); photolysed using two 300 nm lamp after purging with argon. Oligomeric side-products (**OP**) are also produced. Data from Table 2.6.

The photoconversion from **49-αD**, although difficult to calculate precisely due to the large amount of oligomeric photoreduction products, appears to be approximately the same as for both **47** and **48**. All three compounds under equivalent photolysis conditions resulted in photoconversions of approximately 33% from substrate. The differences between them arose from the degree of competition of side reactions. The increased amount of side-products arising from the photolysis of **49-αD**, compared with **48**, may be understood as arising from the increased lability of the doubly benzylic benzhydrol hydrogen as compared to the singly benzylic methine of **48**. A different argument may be used to explain the fact that **47** has more side-products than **48**. There are twice as many abstractable hydrogens on **47** as on **48**, leading to a higher probability of photoreduction products for **47**.

Table 2.6 Comparison of Product Mixture Ratios from Photolysis of **49-αD**[b]

Photolysis time 300 nm lamps	pH[a]	% **49-αD**	% **49**	% **60**	%**OP**[c]
2 lamps, 2 min	2	69	13	1	18
2 lamps, 5 min	2	34	23	4	39
2 lamps, 10 min	2	22	23	6	49
2 lamps, 2 min	1	68	12	4	17
2 lamps, 5 min	1	27	6	10	57
2 lamps, 5 min	7	84	1	3	13

[a]Using 9.8 mg **49-αD** in 300 mL (1.1x 10^{-4} M) 1:1 H_2O : CH_3CN, pH adjusted with H_2SO_4.
[b]Product mixture ratio determined by integration via ^{1}H-NMR($CDCl_3$).
[c]Oligomeric side product (**OP**)approximate, estimated from integration via ^{1}H-NMR($CDCl_3$).

2.2.2.6 Effect of Concentration on Reaction Pathway

In order to elucidate the mechanism of the intramolecular photoredox reaction, it is necessary to eliminate alternative pathways. As the overall reaction is an oxidation of the alcohol concomitant with the reduction of the ketone, it is important to discriminate between two possible mechanisms. One possible reaction mechanism (initial step shown in Eqn [2.14]) that could result in the photoredox of **47** would be if two molecules of **47** came together in such a way as to place the ketone of one molecule in close proximity with the methyl alcohol of another molecule. This should be highly dependent on concentration as it requires two molecules to come together. A second possible mechanism would involve solvent mediation, either by water or acetonitrile and this

pathway should be independent of the concentration of substrate. Consequently, concentration studies were performed in order to determine whether the reaction was unimolecular or bimolecular with regards to the substrate. The possible mechanisms are compared in Section 2.2.5.

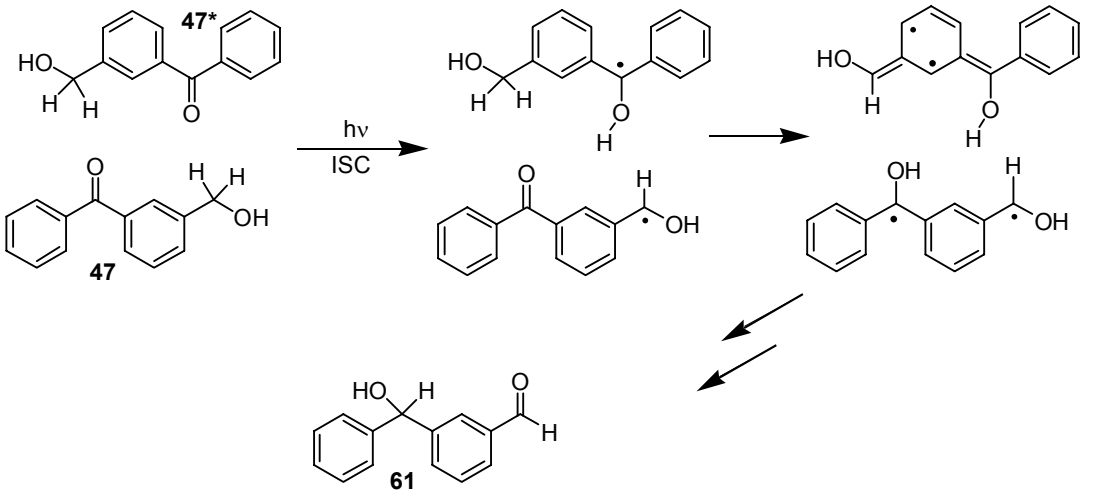

[2.14]

It is difficult to quantitatively compare the photolysis at different concentrations because concentration significantly affects the conversion rate. It is possible however, to make qualitative comparisons. By examining the product ratios at different concentrations it is evident that concentration plays an important role in the photobehaviour of **47**. The photoredox reaction is apparently unaffected by dilution and was observed down to the lowest concentration in which we were able to follow the reaction (~10^{-6} M). This evidence supports the unimolecular pathway as that would be independent of concentration. As the concentration was increased above ~10^{-3} M however, the amount of oligomeric side-product increased rapidly. It was these oligomeric side reactions that were competing successfully with the photoredox reaction at concentrations ~10^{-3} M that led to the erroneous conclusion that no photoredox reaction was possible for the benzophenone analogue of **42**, **47**.[83] The photoreduction side reaction is likely due to

hydrogen abstraction of the methylene hydrogens by the excited ketone oxygen as typically observed in benzophenone photolysis in hydrogen donating solvents and is consequently bimolecular. In order to minimize the side reactions most of the photostudies were accomplished using a substrate concentration of 10^{-4} M. The photolysis studies examining different concentrations are summarized in Table 2.7. Special attention should be paid to the two entries that had the same conversion (59% **47** remaining) from **47** (2 lamps, 2 min, 1.63 x 10^{-4} M and 4 lamps, 5 min, 2.61 x 10^{-3} M). As these two have the same conversion, comparison is simplified. Although conversion to **59** remains essentially identical, the conversion to **61** decreases and the conversion to

Table 2.7 Comparison of Product Mixture Ratios from Photolysis of **47** at Different Concentrations[b]

Photolysis time 300 nm lamps	Concentration	pH[a]	% **47**	%**61**	%**59**	%**OP**[c]
2 lamps, 2 min	1.63 x 10^{-4} M	2	59	35	2	4
2 lamps, 2 min	3.14 x 10^{-4} M	2	66	28	2	4
4 lamps, 5 min	1.62 x 10^{-4} M	2	4	82	9	5
4 lamps, 5 min	1.18 x 10^{-3} M	2	39	40	6	15
4 lamps, 5 min	2.61 x 10^{-3} M	2	59	24	2	15
8 lamps, 5 min	1.57 x 10^{-4} M	2	3	72	16	9
8 lamps, 5 min	2.40 x 10^{-3} M	2	33	32	5	30

[a]Using **47** at different concentrations in 1:1 H_2O : CH_3CN, pH adjusted with H_2SO_4 to pH 2.
[b]Product mixture ratio determined by integration via ^{1}H-NMR($CDCl_3$).
[c]Oligomeric side product (**OP**) approximate, estimated from integration via ^{1}H-NMR($CDCl_3$).

oligomeric products increases as the concentration increases from ~10^{-4} M to ~10^{-3} M. It appears as though the oligomeric reaction pathway is in direct competition to the

photoredox reaction and methods that decrease the favourability of the oligomeric reaction pathway should increase the product ratio of **61**. Concentration of substrate is one such factor. The proton concentration is also a factor and shall be discussed in the next section (Section 2.2.2.7).

2.2.2.7 The Effect of pH on the Photobehaviour

Under neutral conditions, no photoredox product had been previously observed.[83] This seems to have been an oversimplification. Photoredox does indeed occur but the yield of the reaction under neutral conditions is far lower than the hydrogen-abstraction photoreduction which competes successfully. The side-products from thise competing reaction thus swamp the product mixture making isolation of the redox product difficult. Photolysis under high dilution (10^{-5} M to 10^{-6} M) minimizes the side products and allows the observation of **61** under neutral conditions. The reaction is still not very efficient at pH 7 compared to its behaviour under acidic conditions, however. The acid catalysis of this reaction is significant and readily visible in Figure 2.13.

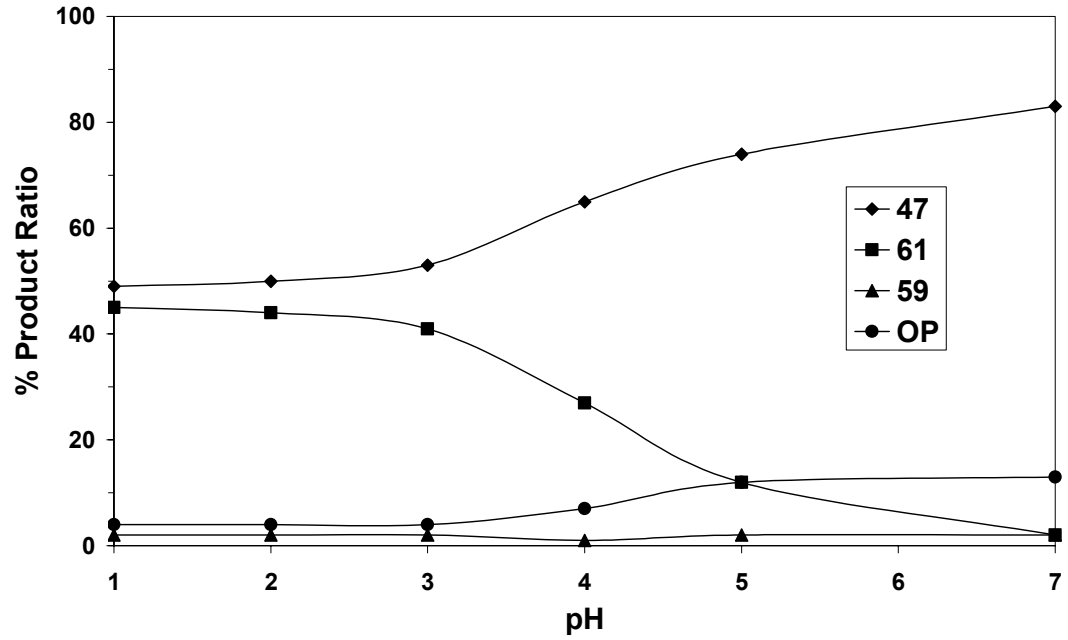

Figure 2.13 Percent conversion of **47** to **61** using 10 mg/300 mL 1:1 H_2O : CH_3CN; photolysed for 2 minutes using two 300 nm lamps after purging with argon. Oligomeric side-products (**OP**) are also produced.

The range at which acid catalysis is observed for this reaction is between pH 4 and pH 1. As explained previously, the intramolecular redox reaction does not occur outside of those ranges. The photoredox reaction is not apparent under basic conditions, consistent with the concept of acid catalysis. Under stronger acidic conditions more side products become visible, possibly due to protonation of the alcoholic oxygen. Photolysis in 20% and 40% H_2SO_4 leads to a complex product mixture with many products, some of which appear to be polymeric in nature. As this Thesis is directed towards the study of intramolecular photoredox reactions, it is unnecessary to explore highly acidic reaction conditions and therefore focuses on milder conditions.

Table 2.8 Comparison of Product Mixture Ratios from Photolysis of **47** at Varying pHs[b]

Photolysis time 300 nm lamps	Concentration	pH[a]	% **47**	%**61**	%**59**	%**OP**[c]
4 lamps, 5 min	1.62 x 10^{-4} M	5%[d]	1	68	6	25
4 lamps, 5 min	1.62 x 10^{-4} M	1	1	84	3	12
4 lamps, 5 min	1.62 x 10^{-4} M	2	4	82	9	5
4 lamps, 5 min	1.62 x 10^{-4} M	3	1	92	1	5
4 lamps, 5 min	1.62 x 10^{-4} M	4	6	82	3	9
4 lamps, 5 min	1.62 x 10^{-4} M	7	47	26	6	21
2 lamps, 4 min	1.57 x 10^{-4} M	5%[d]	24	49[e]	9	18
2 lamps, 4 min	1.57 x 10^{-4} M	1	49	45	2	4
2 lamps, 4 min	1.57 x 10^{-4} M	2	50	44	2	4
2 lamps, 4 min	1.57 x 10^{-4} M	3	53	41	2	4
2 lamps, 4 min	1.57 x 10^{-4} M	4	65	27	1	7
2 lamps, 4 min	1.57 x 10^{-4} M	5	74	12	2	12
2 lamps, 4 min	1.57 x 10^{-4} M	7	83	2	2	13

[a]Using **47** at different concentrations in 1:1 H_2O : CH_3CN, pH adjusted with H_2SO_4.
[b]Product mixture ratio determined by integration via ^{1}H-NMR($CDCl_3$).
[c]Oligomeric side product (**OP**) approximate, estimated from integration via ^{1}H-NMR($CDCl_3$).
[d]pH ~0 (5% H_2SO_4)
[e]product ratio for redox product **74** is for condensed product consisting of 1 molecule each of **47** and **61**

One interesting result occurred when using 1:1 5% H_2SO_4 : CH_3CN as the photolysis solvent. No redox product was observed upon photolysis but the ^{1}H-NMR spectrum (Figure 2.14) of the product mixture shows a peak due to both an aldehyde and a benzyhydrol but at different shifts than for **61**. In addition, a new doublet of doublets in a similar region to the benzylic methylene is apparent. Upon isolation of the product,

both the MS and ^{1}H-NMR spectroscopy are consistent with a condensation product, **74**, formed between **47** and **61**. This may be formed via protonation of the benzhydrol alcohol (Scheme 2.2) followed by nucleophilic attack by **47**.

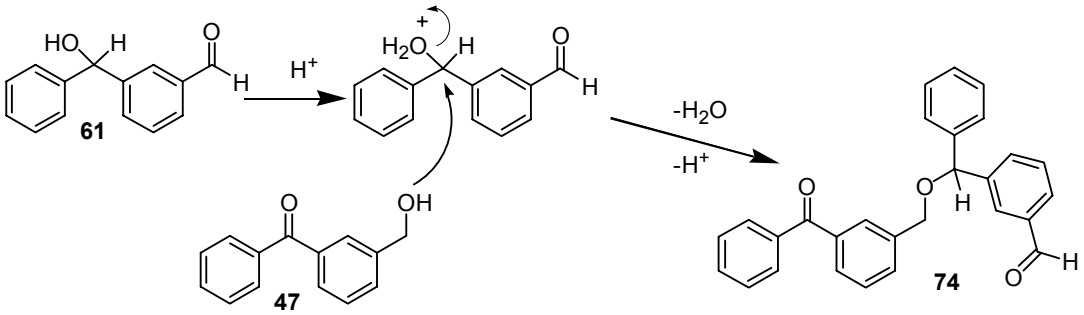

Scheme 2.2

Further confirmation arises from the fact that by placing **47** in a 1:1 5% H_2SO_4 : CH_3CN solvent mixture and slowly adding **61** dropwise, **74** is produced. It is likely that during photolysis of **47**, any **61** formed would immediately react with the higher concentration **47.** Thus, **47** acts as an effective trap for the unstable (under those conditions) **61** to form the more acid stable ether, **74.** The condensation is not limited to the condensation of **47** and **61**. Spontaneous formation of the dimer, **75**, occurs from the dark reaction of **61** in 5% H_2SO_4.

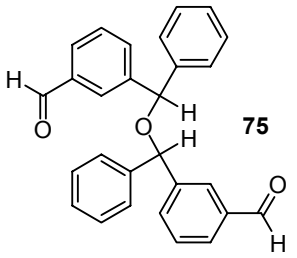

By contrast **59** is stable to both photo and thermal reaction in 5% H_2SO_4. No change is observed in the product mixture and only **59** is recovered. As **59** contains only carbonyl groups and does not contain a hydroxyl group this result is to be expected.

According to Scheme 2.2 it is the hydroxyl group that is protonated and acts as an effective leaving group. Consequently the condensation reaction requires the presence of a hydroxyl group. Additionally it appears as though the primary hydroxyl group also acts as the nucleophile as no product was isolated that involved the aldehyde of **61**.

The acid catalysis of the intramolecular photoredox reaction is also observed for **48** and **49-αD**, both of which see a significant increase in the conversion from starting material as the pH increases from pH 7 to pH 2. Unfortunately, although decreased pH leads to higher photoconversion, other side products are also increased. Just as photolysis of **47** in highly acidic media results in more photooxidation products, so does **48**. As the pH decreases from pH 2 to pH 1 the ratio of photooxidized product, **73**, to photoredox product, **72**, increases. After photolysis in 5% H_2SO_4 solution, the product mixture was exceedingly complex and resembled the photolysis runs of **47** at higher proton concentrations. Product ratios were not obtainable from that run due to complexity of the product mixture. Presumably the condensation product is also present in the product mixture.

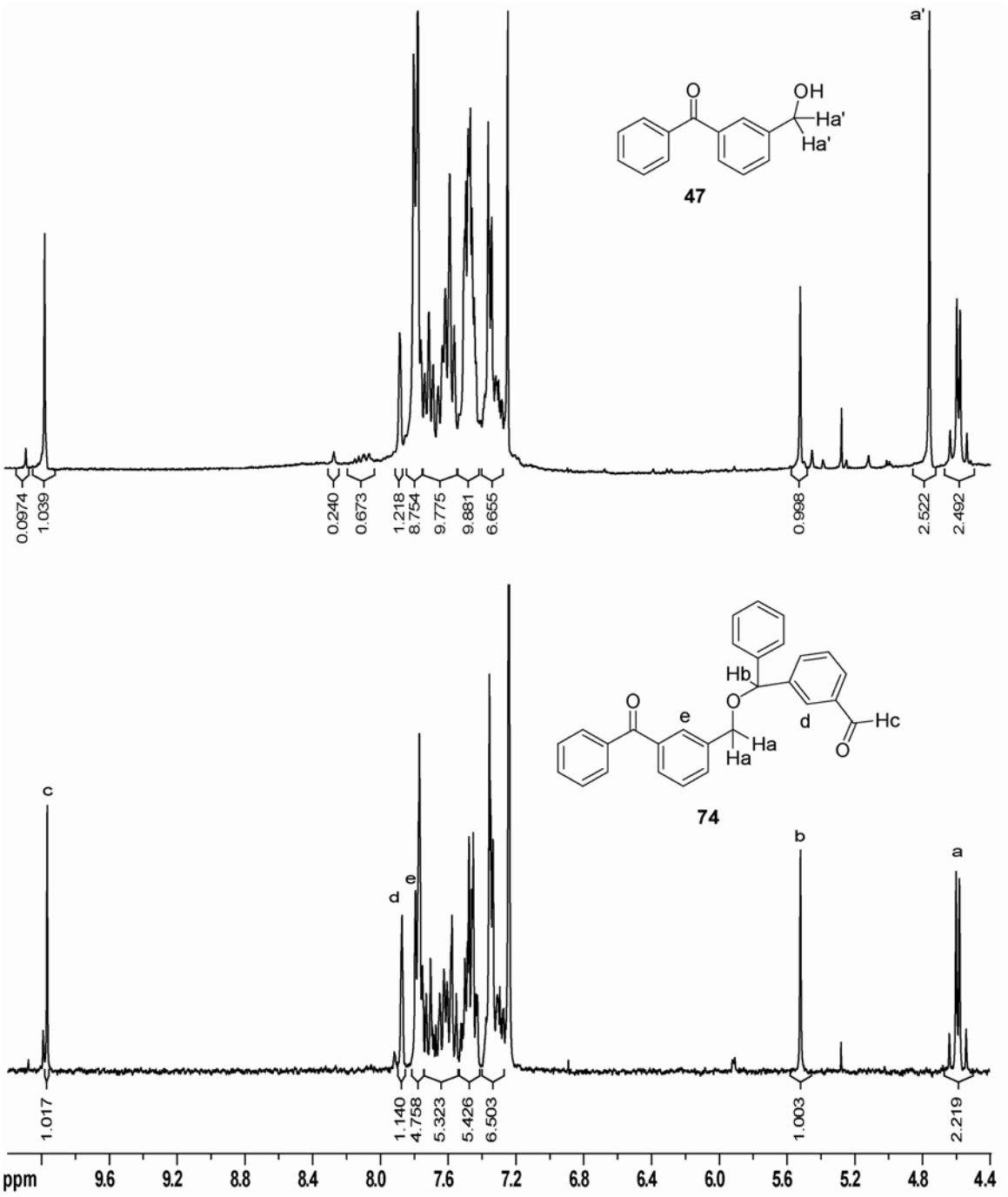

Figure 2.14 300 MHz ^{1}H-NMR spectra of **47** (in chloroform-*d*) after (top) photolysis (1.5 x 10^{-4} M, 10.1 mg/300 mL) in 1:1 5% H_2SO_4 : CH_3CN, for 2 minutes with two 300 nm lamps (argon purged). Product ratio: 43% **47**: 42% **74**: 8% **59**: 7% other products The product ratio was determined by comparing the integrations for the peak due to the benzylic methylene of **47** (**a'**: 4.8 ppm, 2.5H) to the doublet of doublets due to the benzylic methylene of **74** (**a**: 4.6 ppm, 2.5H) to the proton associated with **59** (8.25ppm, 0.24H). Subtraction of the integration due to those compounds from the integration of the entire aromatic region leads to the product ratio for the other products.

The acid catalysis of **49-αD** is immediately evident in the increased photoconversion to **49** going from pH 7 to pH 2. However, as **49-αD** is even more sensitive than **48** to side products, it is therefore hardly surprising that, although conversion from starting material increases going from pH 2 to pH 1, the conversion to **49** actually decreases. The ^{1}H-NMR spectrum of the product mixture at pH 1 is complex with a higher proportion of both **60** and photoreduction oligomers making assignment more difficult.

2.2.2.8 Determining the Source of the Benzhydrol Proton

The investigations into the effect of concentration of substrate upon the photobehaviour of **47** (Section 2.2.2.6) suggest that the mechanism for photoredox is likely unimolecular albeit solvent assisted. As the oxidation and reduction sites are too far away for direct transfer of hydrogen between them, the reaction must be mediated in some way. If the solvent is the assumed mediator there are two different possible sources of protons for the methine proton of the benzhydrol: water and acetonitrile. Depending on which solvent is the source, the mechanism of the photoredox reaction would be considerably different as water would necessarily be a proton transfer and acetonitrile would most likely be a hydrogen atom transfer. When **47** is photolysed in 1:1 D_2O : CH_3CN (adjusted to pD = 2 using D_2SO_4) full deuteration of the benzhydrol proton of **61** is observed with no benzhydrol proton observed in the ^{1}H - NMR spectrum (Figure 2.15, top spectrum). This result is a strong indication that the methine proton of **61** arises from water, not from acetonitrile. This is consistent with a water-mediated pathway towards the intramolecular photoredox product.

Slight deuteration of the aldehyde was also observed and initially it was thought that this might be due to photolysis of deuterated **47**. The deuteration of the aldehyde increases with further photolysis (a higher conversion run shown in Figure 2.13 has 80% deuteration of the aldehyde). It was hypothesized that deuteration of the starting material might arise via a pathway which proceeds through a common intermediate that instead of forming the redox product, forms the starting material again. The deuterated starting material **47-αD** could then undergo the photoredox chemistry in a manner similar to Eqn [2.15]. Subsequent investigation demonstrated that there was no deuteration of the

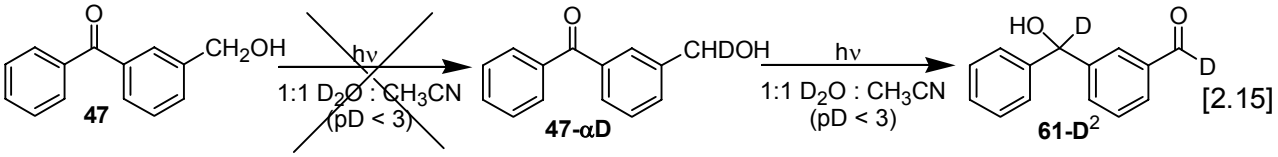

[2.15]

starting material, even at high conversion levels, as no deuterated starting material was ever isolated (See Figure 2.13, bottom spectrum). Direct deuteration of the aldehyde is the likely source of the deuteration of the aldehyde of **61** as photodeuteration of benzaldehyde has been previously reported in the literature in deuterated aqueous medium.[87]

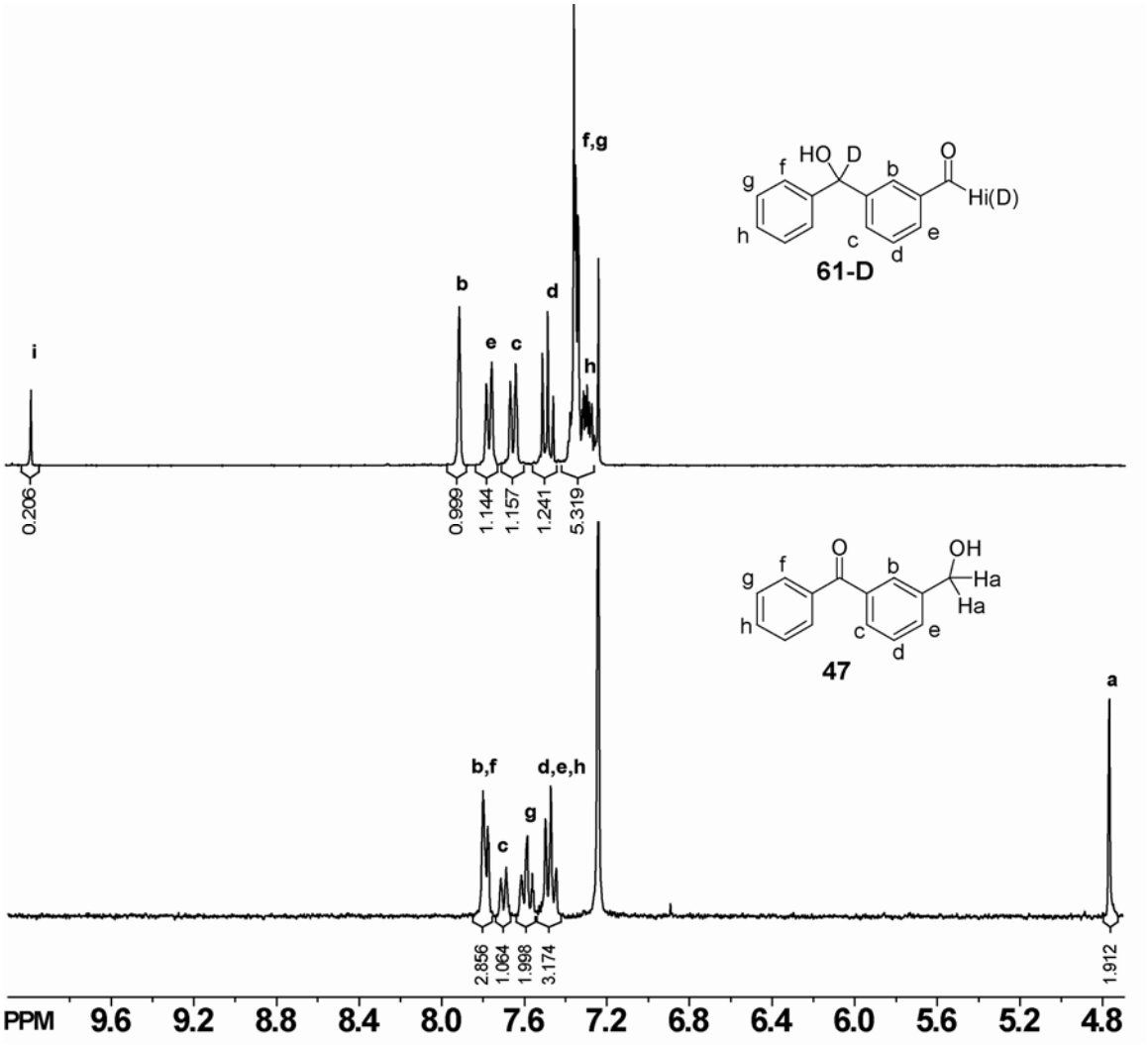

Figure 2.15 300 MHz ^{1}H-NMR spectra of **61-D** (top) and **47** (bottom) isolated from product mixture following high conversion photolysis run of **47** (50.2 mg in 100 mL (2.37×10^{-3} M) 1:1 D_2O : CH_3CN (pD 2), argon purged) using eight 300 nm lamps for 14 minutes. Deuteration of aldehyde of **61 (H_i)** is approximately 80% by comparison of integration.

2.2.2.9 Examining the Deprotonation of the Benzylic Hydrogens

In the previous section (Section 2.2.2.8) the source of the benzhydrol proton was examined and determined to arise from the aqueous solvent. It is also important to determine what part the deprotonation of the benzylic hydrogens play in the mechanism. For this reason deuterium isotopic exchange reactions were performed. By photolysing the monodeuterated parent compound **47-αD** and comparing the proportion of deuterium to hydrogen left on that benzylic carbon (by examining the integration of the aldehyde proton compared to the benzhydrol proton, see Figure 2.15), one can get an idea of the importance of the deprotonation in the mechanism. Several runs were performed at different amounts of irradiation and two typical runs are presented in Table 2.9. The two different runs, one at ~40% conversion and the other at ~85% conversion, gave similar values for the deuterium : hydrogen ratio of 1.6 and 1.4 respectively. Although the value for the lower conversion run is considered more reliable due to additional possible reactions observed at high conversion photolysis, the two values should be considered essentially the same. The fact that there was a noticeable difference in the deuterium : hydrogen ratio suggests that the deprotonation step plays an integral part in the reaction. No kinetics studies were performed however so rate constants are not available definitively.

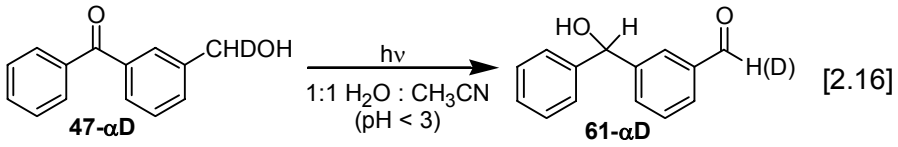

[2.16]

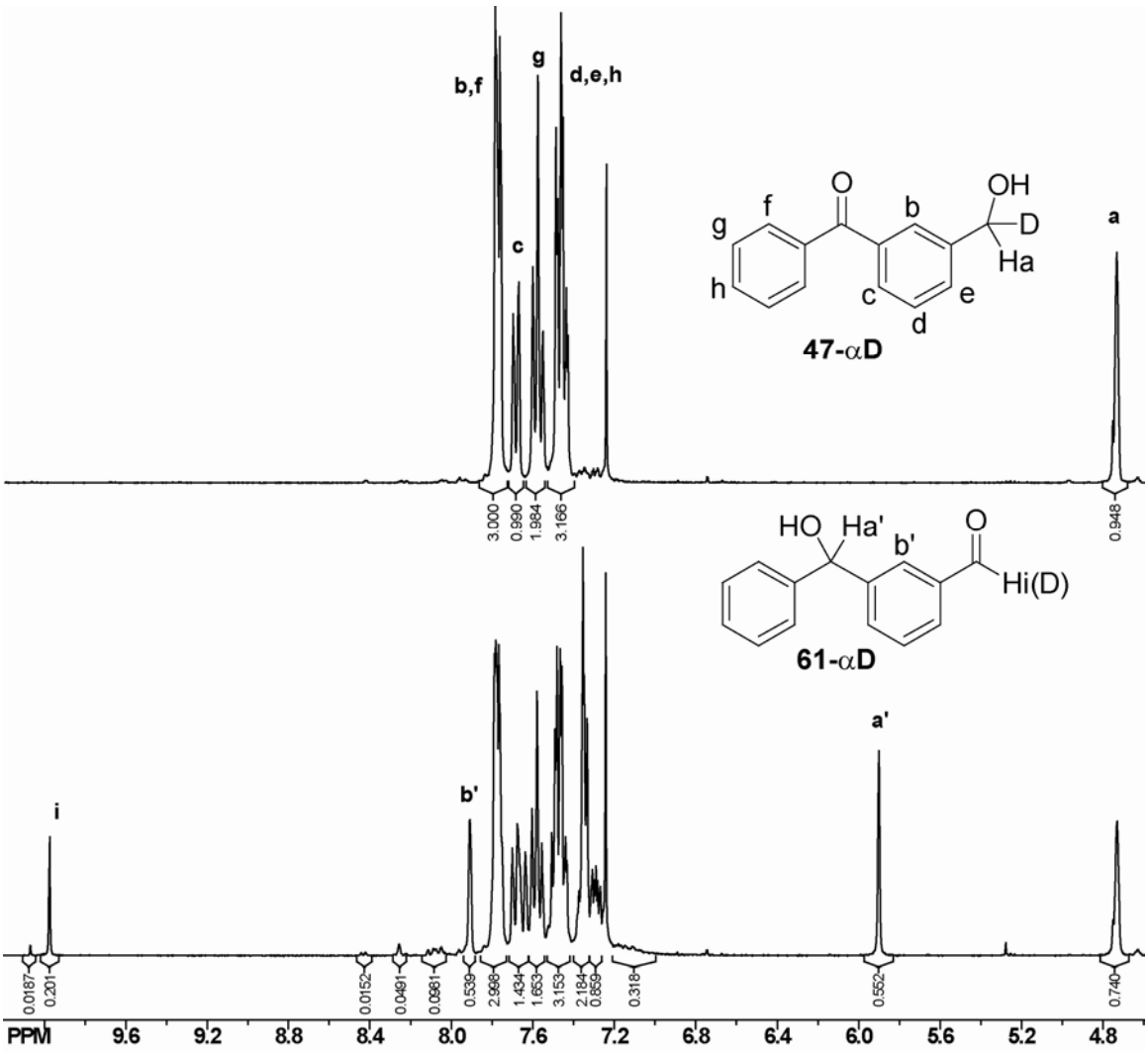

Figure 2.16 300 MHz ^{1}H-NMR spectra of 10.4 mg in 300 mL (1.63×10^{-4} M) 1:1 H_2O : CH_3CN (pH 2), argon purged) **47-αD** before (top) and after photolysis using two 300 nm lamps for 2 minutes. D/H ratio: 1.6. Product ratio: **47-αD**: 62%, **61** + **61(-αD)**: 34%**, 59**: 2%, OP: 2%

Table 2.9 Comparison of Product Mixture Ratios from Photolysis of **47-αD** at Varying Conversions[b]

Photolysis time 300 nm lamps	**Concentration**[a]	**% 47**	**%61**[d]	**%59**	**%OP**[c]	D/H[e]
2 lamps, 2 min	1.63×10^{-4} M	62	34	2	2	1.6
2 lamps, 5 min	1.78×10^{-4} M	16	75	4	5	1.4

[a]Using **47** at different concentrations in 5:1 H_2O : CH_3CN, pH 2 adjusted with H_2SO_4.
[b]Product mixture ratio determined by integration via ^{1}H-NMR($CDCl_3$).
[c]Oligomeric side product (**OP**) approximate, estimated from integration via ^{1}H-NMR($CDCl_3$).
[d]Total **61** determined by using integration of benzhydrol proton
[e]Deuterium to Hydrogen ratio (D/H) determined by comparing integration between the benzhydrol and the aldehyde peaks

2.2.3 Related Results

Dr. Nikola Basarić, in our research group explored the photochemistry of several derivatives of **49**.[88] These results are presented in this section as they contribute to the understanding of the photoredox reaction. The *para*-methyl derivative **76** is structurally very similar to **49** but the photochemistry is easier to study due to its asymmetry. This asymmetry allows the reaction to be followed by UV-vis spectroscopy and also allows product studies without resorting to deuteration. The *para*-methoxy derivative **77** and *meta*-methoxy derivative **78** have significantly different electronic distribution both from each other and from **76**. They are consequently expected to exhibit considerably different photobehaviour due to their different electronic withdrawing or donating capacities. As such **77** and **78** are effective probes in determining the effect of substituent's position and identity on the terminal phenyl ring.

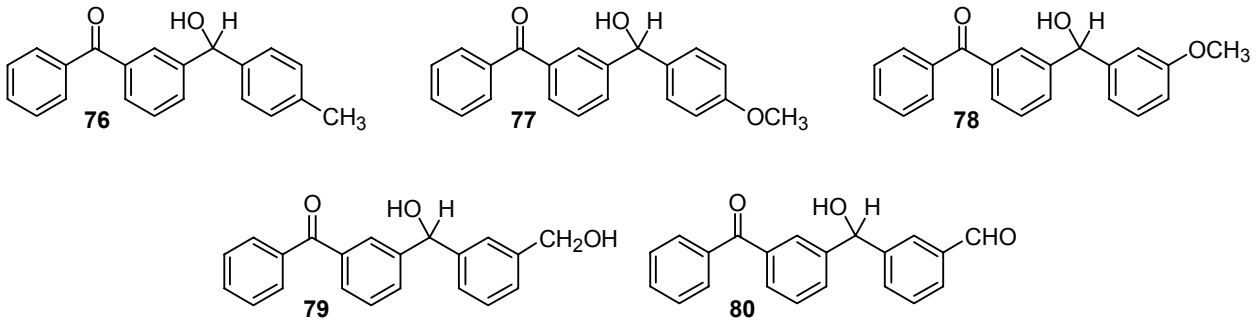

Photolysis of **76** produces the intramolecular photoredox product **81** (Eqn. [2.16]) in a photoredox reaction that exhibited behaviour almost identical to that of **49**. The major product was the photoredox product **81** but the oxidized product **82** was also produced in a minor quantity. Although the efficiency of the reaction is similar to **49** at pH 2 ($\Phi \approx 0.3$), the photolysis of **76** produced the highest proportion of oligomeric products of any of the phenyl derivatives. Even at the lowest concentration (10^{-5} M), significant oligomeric products were observed. The increased susceptibility towards oligomeric products may be correlated with the significantly greater availability of abstractable benzylic hydrogens (four for **76** as compared to one for **49**). The addition of naphthalene (a known efficient triplet quencher) resulted in a much less efficient reaction (up to ten-fold increase in photolysis times) but a significant decrease in the amount

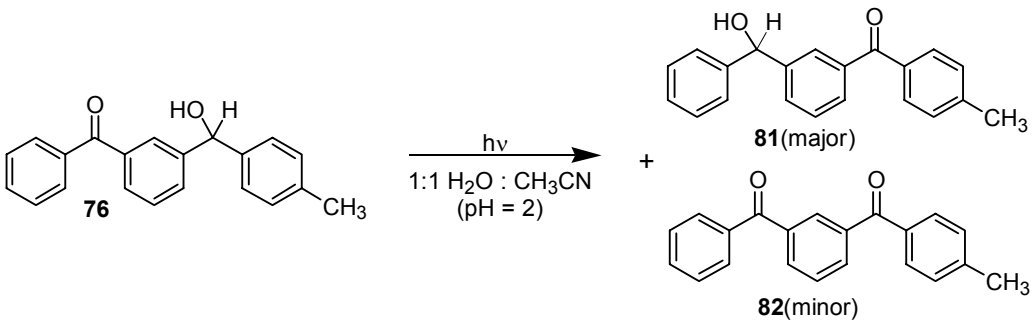

[2.16]

of side products. This allowed **76** to be photolysed almost to completion with only 20-30% oligomeric material. This experiment is valuable for several reasons. Primarily, it presents evidence that the photoredox reaction occurs from the triplet state rather than the singlet state. If the reaction proceeded exclusively from the singlet state, the addition of naphthalene would not have affected the efficiency of the reaction. Although it can not be stated definitively that no portion of the reaction occurs via the singlet state, the triplet state's importance to the reaction pathway is evident. Additionally, the triplet quenching experiment is also important as the results support the assertion that the photoredox reaction is unimolecular while the competing reaction (formation of oligomeric material) is bimolecular with regards to substrate. The decreased lifetime of the triplet limits bimolecular reactions more than unimolecular reactions as bimolecular reactions require enough time for the excited molecule to interact with another molecule of substrate.

Complete conversion of **76** to **81** does not appear to be possible however, even with added naphthalene. At the wavelength used (300 nm) a photostationary state seems to result with the ratio consisting of 92% **81** to 8% **76**. Although **81** could not be fully separated from the substrate **76** to prove the photostationary state ratio from the photolysis of **81**, the product mixture of the presumed photostationary state was photolysed at pH 2 (300 nm). No change in the product ratio was observed, thus suggesting that the photostationary state had been reached. The product ratio highly favours the product over the reactant which suggests that the reverse photoredox reaction from **81** to **76** is relatively disfavoured compared to the forward photoredox reaction.

The methoxy derivatives had significantly different behaviour from each other. As expected, photoredox behaviour was exhibited by the *para*-methoxy isomer **77**, albeit

with significantly lower quantum yields ($\Phi \approx 0.02$) than either **49** or **76**. The photoredox reaction (Eqn. [2.17]) resulted primarily in the photoredox product **83** but some photooxidized product **84** was also visible. Furthermore, photolysis of **77** resulted in considerably fewer side products than **49.** This enabled the photoredox reaction to be observed not only at pH2 but also at pH 7 ($\Phi \approx 0.007$) when photolysed at 10^{-5} M substrate. By contrast, the *meta*-methoxy isomer **78** exhibited no evidence of photoredox behaviour at either pH 7 or pH 2. Instead, all that was observed was a loss of substrate and formation of oligomeric material.

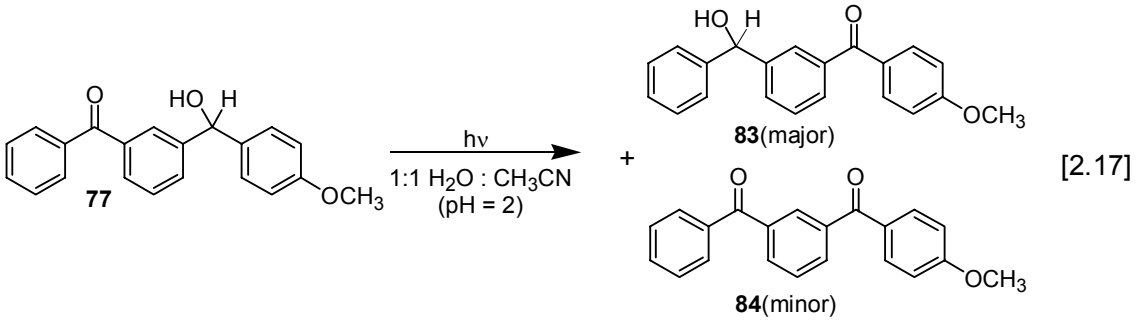

[2.17]

Continuing the investigation into the effect substitution of the phenyl group has on the photoredox reaction the *meta*-hydroxymethyl **79** and the *meta*-formyl **80** compounds were studied.[88] Compound **79** is an interesting extension of the research of this Thesis as the redox product **85** has a moiety identical to **47**. This suggests that a two step photolysis reaction might be possible, the first step resulting in **85** and the subsequent photolysis of **85** resulting in **86**. Photolysis of **79** at pH 2 (Eqn. [2.18]), in addition to a small amount of **80**, yielded both **85** and **86**, with **86** being produced in a greater quantity. It was not possible to produce **85** alone even at the lowest conversions that were carried out. This suggests that **85** is more reactive than **79** with regards to the photoredox reaction because any photon flux that could produce **85** from **79** would also convert **85** into **86**. An alternative explanation is that **85** has two potential pathways for

photoredox, one being the reverse reaction back to **79** while **79** only has one. Compound **80** was observed for all runs at both pH 2 and pH 7 and it is likely that it arises from the residual oxygenation pathway characteristic of all of these reactions.

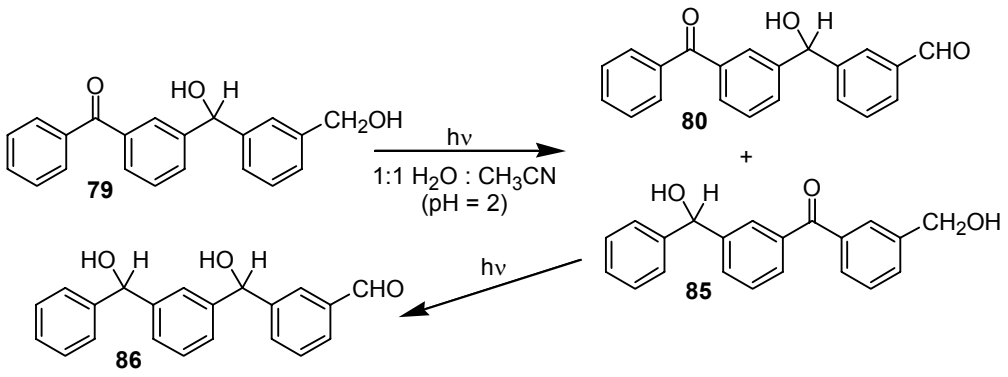

[2.18]

Compound **80** was itself photoinert towards the photoredox reaction. Similarities exist between **80** and **78**. Both are electron-withdrawing groups at the *meta* position to the benzhydrol position ($\sigma_m = 0.35$ for CHO and $\sigma_m = 0.12$ for OCH_3). As both are photoinert towards the photoredox reaction, it could be reasonably assumed that the position and electronic behaviour has a significant effect on the reaction. The methoxy group behaves as an electron-donating group via resonance and as an electron-withdrawing group via induction (Field effects).[89] The predominant effect is a matter of position. Resonance only affects the *para* and *ortho* position while the induction effect is a factor of distance through bonds. Induction is thus strongest at the *ortho* position and weakest at the *para* position with the *meta* position being intermediate. The *meta* position therefore only experiences the electron-withdrawing effect of the methoxy group with none of the electron-donating character due to resonance effects. By contrast the *para* position consequently has the strongest electron-donating character due to the combination of resonance effect and the weakest inductive effect. The *ortho* position has

somewhat weaker electron-donating character because of the conflicting inductive and resonance effects but still acts as an electron-donating position.

Evidence suggests that most asymmetric compounds undergo photoredox reactions in only one direction and the photoredox product is relatively photoinert towards the reverse reaction. This is demonstrated with the parent compound **47** and the alkyl compound **48**. For the derivatives of **49**, although photolysis of the photoredox products were not performed for most compounds, evidence suggests that the photoredox products are also relatively photoinert towards the photoredox reaction. It also appears that the more electronically asymmetric the molecule the more likely the photoredox reaction is to be unidirectional. Thus, although the photostationary state of **76** lies far to the right, the reaction does not actually go to completion. By contrast **77**, having a methoxy group rather than just a methyl group, proceeds to completion and its photoproduct is therefore photoinert at that wavelength. Although untested, **85** is a likely candidate for a reverse reaction as it could be argued that the similarity in quantum yield of loss of substrate for **47** and **49** could allow competition between the two oxidizable benzylic alcohol moieties. With this in mind it is possible that any compound that appears to be photoinert towards the photoredox reaction, may actually be the photoredox product of a different compound.

2.2.4 Nanosecond Laser Flash Photolysis (LFP)

Product studies and UV-vis spectral traces, although exceedingly useful for examining the product mixtures and identifying the direction of the photoreactions, do not provide any information about the excited singlet or triplet states. The excited triplet state is central to any investigation of benzophenone derivatives as benzophenones undergo extremely efficient intersystem crossing to the triplet state. Nanosecond laser flash photolysis (LFP) is one way of directly observing the excited triplet state. The timescale of the nanosecond LFP suggest that transients assignable to reactive intermediates other than the reactive triplet are unlikely.

As neither **51** or **52** exhibit photobehaviour relative to the photoredox reaction, no LFP studies were performed on them. Instead, LFP studies concentrated on the compounds that were shown through photoproduct studies to behave in a similar manner such as **47**, **48** and **49** and to a lesser extent **50**.

LFP studies were carried out on **47**, **48** and **49** at a variety of different proton concentrations. In each case the transient absorption spectra resemble each other and match the triplet-triplet absorption spectra typical of benzophenones with two bands, one at 320 nm and another at 525 nm (Figure 2.17).[59] This is unsurprising as the benzophenone chromophore is identical in each case. Neither **47** nor **48** have another chromophore so their absorption spectra are fundamentally that of benzophenone. The additional phenyl group of **49** does not alter the absorption spectrum significantly as it is unconjugated to the benzophenone moiety. Complications to the spectra arise from overlap by the benzophenone ketyl radical which absorbs at 545 nm.[90] This complicates the 525 nm band making kinetic analysis challenging.

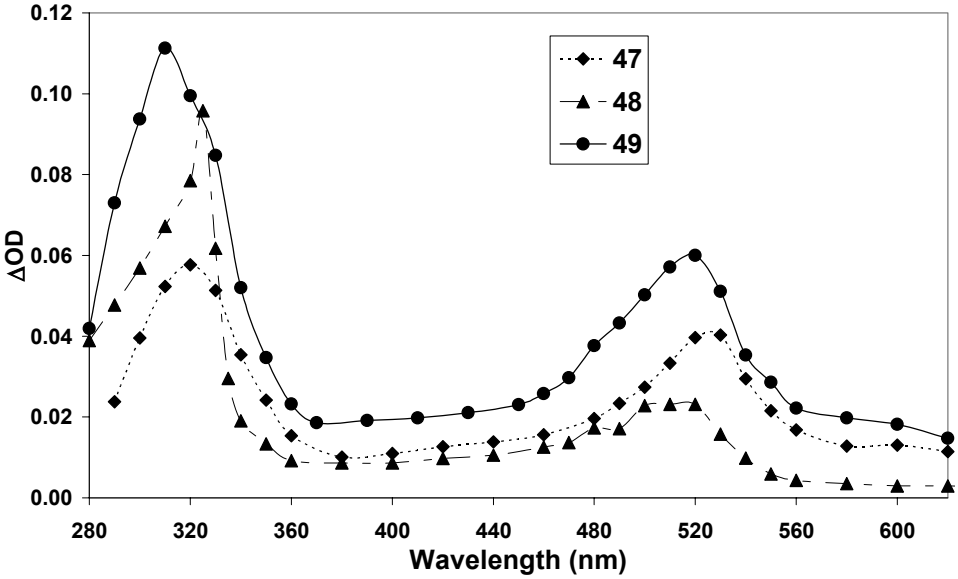

Figure 2.17 Triplet –triplet absorption spectra of **47**, **48,** and **49**, detected by LFP (λ_{ex} 266 nm) in 1 : 1 H_2O : CH_3CN (pH 7) using a flow cell with continuous N_2 purging. Data points were taken immediately after the laser pulse.

Aside from the appearance of the triplet-triplet absorption spectra, which yield information on the identity of the triplet state, the decay of those spectra also gives information about the lifetime of the triplet state. By examining the decay of the spectra one can determine whether only one transient exists or whether there is more than one. If only one transient exists the decay should be monoexponential but if more than one is present the decay may be biexponential or more. A qualitative examination of the decay of **47** as shown in Figure 2.18 shows that the two bands do not decay at the same rate. Many decays do not fit first-order exponential decays and typically require a sum of two first-order decays, especially those for the band at 325 nm. It is likely that the polyexponential decay arises from the hydrogen-abstraction pathways that yield the oligomeric products. This is consistent with the finding that increased dilution of **76** leads to longer lifetimes.[88]

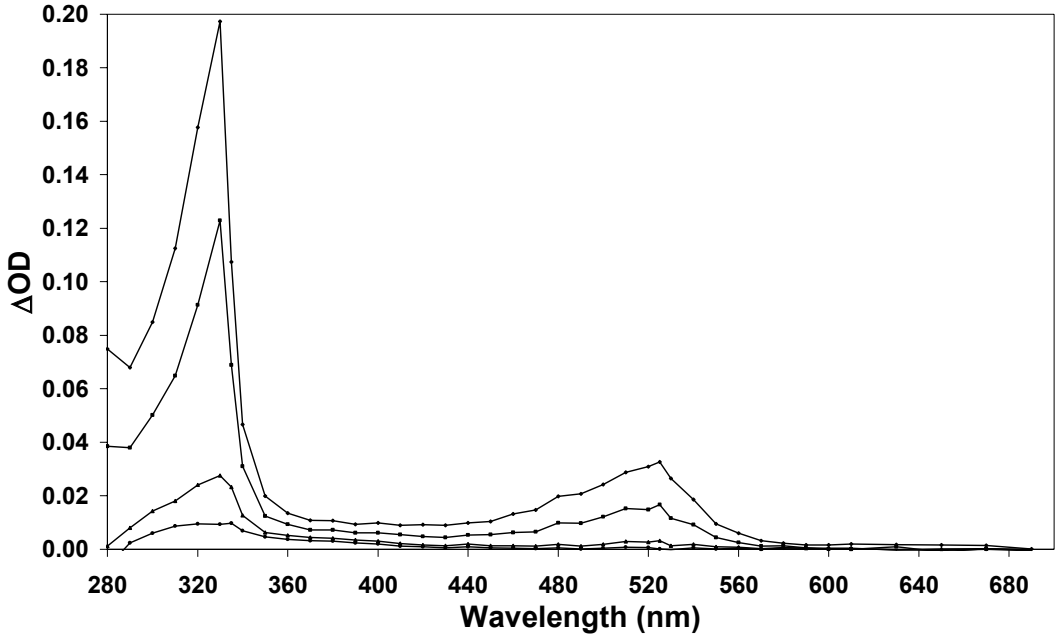

Figure 2.18 Triplet-triplet absorption spectrum observed on LFP (λ_{ex} 266nm) of **47** in 1:1 H_2O : CH_3CN (pH 2), using a flow cell with continuous N_2 purging. The four spectra are taken at the following intervals: immediately after the laser pulse, after 1 μs, after 7 μs and after 22 μs.

The band at 325 nm does not decay completely by the time the band at 520 nm decays. As the band at 520 nm decays to the baseline before the band at 325 nm, it is evident that there is a second, longer-lived species that absorbs at a slightly shorter wavelength, around 320 nm. This second transient is observable under more acidic conditions (pH 1 and pH 2) but seems to be absent at pH 7. However, direct comparison of the spectra at pH 2 and pH 7 shows very little difference (Figure 2.19). Although difficult to discern, the shorter-lived species seems to be slightly shifted to higher wavelengths (325 nm vs 320 nm) at pH 2. The longer lived species seems to have a relatively constant lifetime (~3 μs) independent of pH while the shorter-lived species is extremely pH dependent. It is unknown whether the longer lived species is present at pH 7 or is only present under

acidic conditions. At pH 7 both bands experience monoexponential decay traces but at pH 2 and pH 1 the 320 nm band has a biexponential decay trace (see Figure 2.20). As the band at 525 nm does not show the biexponential behaviour observed for the band at 320 nm, the decay lifetimes were reported for the band at 525 nm.

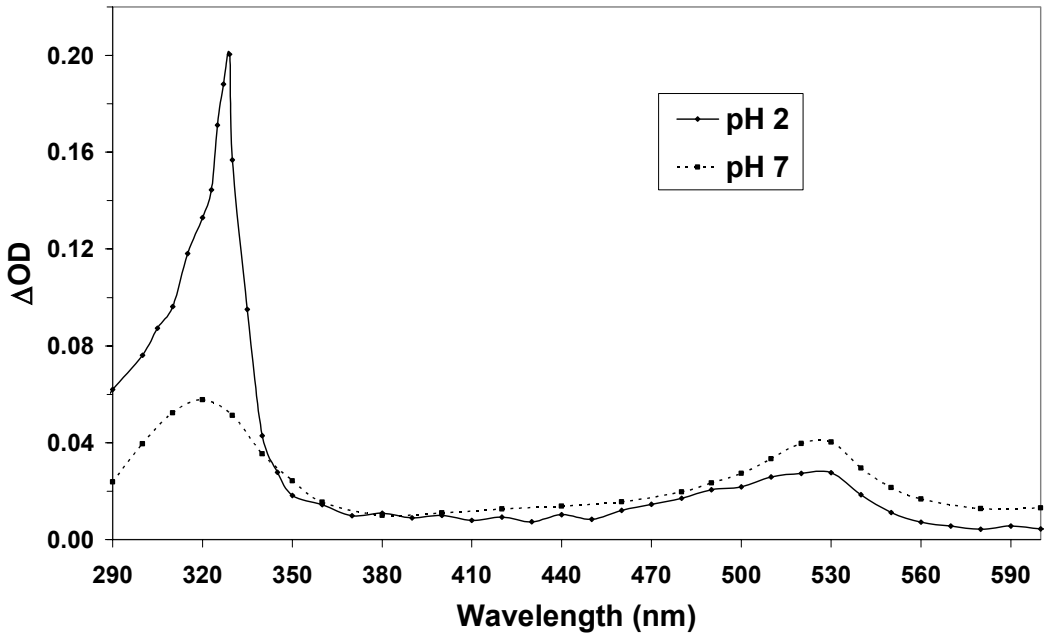

Figure 2.19 Triplet-triplet absorption spectra for **47** at pH 2 and pH 7 detected by LFP in 1:1 H_2O : CH_3CN (N_2 purged). Spectral traces are shown immediately after the laser pulse.

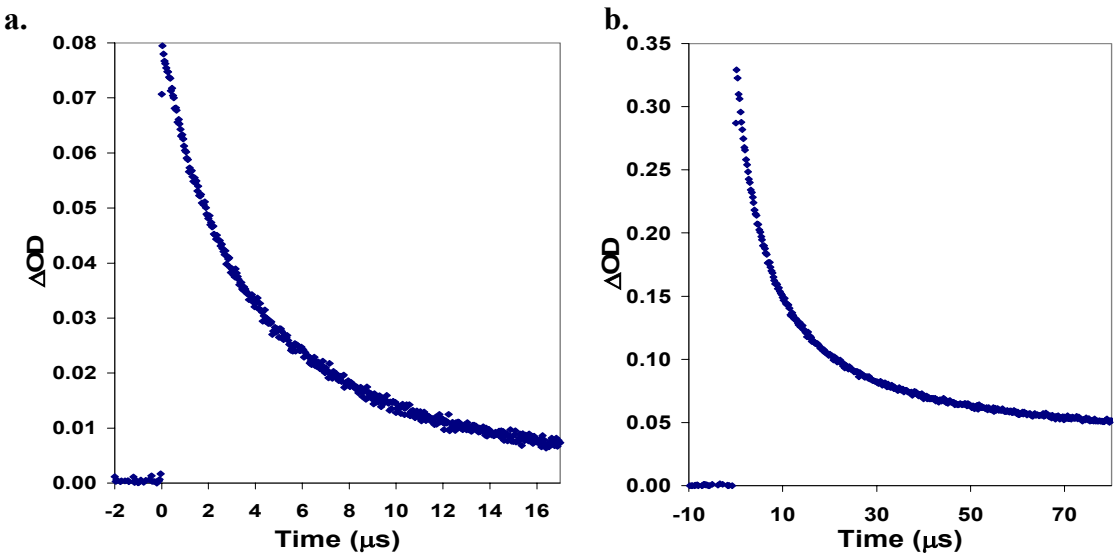

Figure 2.20 Decay traces of **47** 1:1 H_2O : CH_3CN (N_2 purged) measured at 330 nm at different pHs. Trace **a.** (left) is at pH 7 while trace **b** (right) is at pH 2.

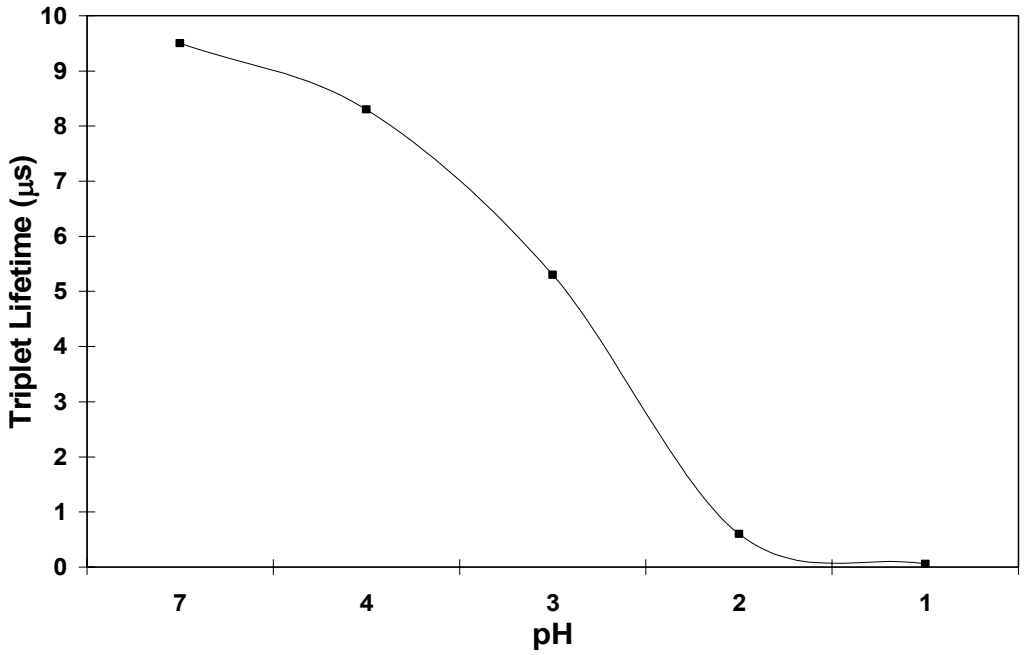

Figure 2.21 - Observed proton quenching of the triplet lifetimes for **47** in 1:1 H_2O : CH_3CN. The decay lifetimes observed at 525 nm.

Lifetimes of **42** were collected at a variety of pH by measuring the decay of the transient absorption spectra for **47** at the 525 nm band. A clear indication of proton

quenching of the transient can be seen in Figure 2.21. The transient lifetime at pH 7 is an order of magnitude longer than at pH 2 and two orders of magnitude longer than at pH 1.

Quenching by oxygen was observed for all species (**47**, **48** and **49**) and the lifetimes were all about 100 ns. As it is expected that the transient is a triplet rather than a singlet it is unsurprising that it would be quenched by oxygen.

All three compounds exhibit proton quenching as observed from Table 2.10. The similar lifetimes of **47** and **48** match their similar photoreactivity. Equivalently, the lifetime of **49** was significantly longer and was biexponential. The implication that there are multiple transients with absorption around 520 nm is in agreement with the product studies that found that **49** produces many oligomeric side products.

Table 2.10 Comparative Lifetimes of Benzophenone Derivatives obtained via LFP

Molecule		**Lifetimes (μs), O_2[a]**	**Lifetimes (μs), N_2[a]**
		520 nm	**520 nm**
47	pH 2	0.084	0.56
47	pH 7	0.094	9.5
48	pH 2	0.10	0.92
48	pH 7	0.10	2.3
49	pH 2	0.11	1.9[b]
49	pH 7	0.14	2.7

[a] Lifetimes were obtained by exponential fitting of decay traces in 1:1 H_2O : CH_3CN, (pH 7 or pH 2), N_2 or O_2 purged; Fitting was monoexponential unless otherwise indicated; $[O_2]_{acetonitrile} = 9.1 \times 10^{-3}$ M; $[O_2]_{water} = 1.27 \times 10^{-3}$ M

[b] Decay trace was biexponential, lifetime reported is that of the shorter lifetime

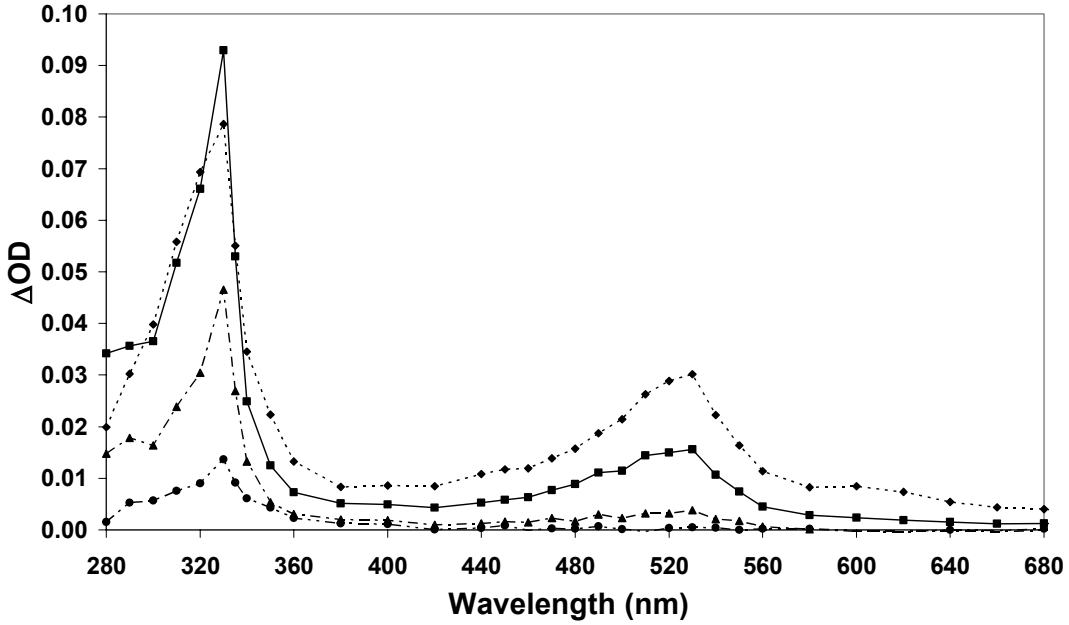

Figure 2.22 Triplet-triplet absorption spectrum observed on LFP (λ_{ex} 266nm) of **50** in 1:1 H_2O : CH_3CN (pH 2), using a flow cell with continuous N_2 purging. The four spectra are taken at the following intervals: immediately after the laser pulse, after 1 μs, after 7 μs and after 22 μs.

Compound **50** has a very similar triplet-triplet absorption spectra (Figure 2.22) to those observed for the other benzophenone derivatives. There are two maxima in the spectrum, one at 320 nm and the second at 530 nm. Decay of the band at 330 nm resulted in a triplet lifetime of 3.1 μs. Decay of the band at 530 nm was biexponential and exponential fitting of the decay trace gives lifetimes of 3.7 μs and 0.9 μs when purged with N_2. When purged with oxygen, the spectrum had the same bands, both of which had lifetimes of 120 ns.

2.2.5 Proposed Mechanism

As the concentration studies presented in Section 2.2.2.6 demonstrated, the photoredox reaction is unimolecular with respect to substrate and consequently the mechanism presented must only involve interactions between the substrate and the solvent and no interactions between two substrate molecules. The postulated mechanism shown in Scheme 2.3 is consistent with these findings.

The proton concentration has a significant effect on the photobehaviour of **47** as explored in Section 2.2.2.7. It was noted that as the pH decreased the efficiency of the photoredox reaction increased dramatically. Although unsurprising, it was reassuring to discover that this same behaviour was also present during the photobehaviour of **48** and **49**. This pH effect also seemed to be active during the decomposition of **50** and during the photoactivity of **51**. The acid catalysed nature of the photoredox reaction suggests that protonation of the substrate is necessary for the reaction to proceed. In the ground state, protonation of the ketone is negligible at the pH values used in the experiments (pH >0). However, as mentioned in Section 1.5, excited-state ketones are much stronger bases ($pK_a(S_o) = -5.7$, $pK_a^*(T_1) = -0.4$).[59,31] Protonation of the excited triplet state should therefore be relatively facile and would account for the proton quenching of the triplet observed in the LFP studies.

The presence of water plays an important role in the photoredox reaction. Not only does the aqueous medium provide protons necessary for the acid-catalysis of the photoredox reaction, but the solvent polarity is also important. As explored in Section 2.2.2.2, the percent of water present as the solvent media exerts a marked effect on the photoredox reaction. As the solvent ratio may be directly correlated with the solvent

polarity it is interesting to note that as the solvent polarity increases (increasing amounts of water present) the photoredox reaction becomes more efficient, reaching a maximum near 100% water. By contrast, when there is less than 10% water in the solvent medium the ratio of redox product drops off dramatically and the amount of oligomeric product increases at the same time. Although one may postulate that when the concentration of water drops below 10% the lack of water affects photoredox reaction but even at the lowest proportion of water at pH 2 (1%) there is still 0.56 M water (1.0×10^{-4} M H^+) present so there should be sufficient protons available to interact with the substrate in order to promote the redox reaction. This is especially true when one considers that at pH 4 of 1:1 H_2O : CH_3CN the concentration of protons is 5.0×10^{-5} M and there is still nearly 30% photoredox product formed. However this is not the case at low water to acetonitrile ratios. At a solvent ratio of 1% water no redox product is observed and 12% of the product ratio was oligomeric product. Even when the solvent was 5% water, only 6% redox product is observed with 8% of the product ratio being oligomeric product. This suggests that polarity plays a large role and that there might be a switch in the identity of the lowest triplet state below 10% water. As this reaction is expected to go through a π,π^* lowest triplet state, and hydrogen abstraction is favoured by a n,π^* lowest triplet state, it could be postulated that below a 10% water mixture the lowest triplet state is no longer π,π^* but is instead n,π^*. This is consistent with the result that polar solvents stabilize the π,π^* lowest triplet state, reviewed in Section 1.5. [53]

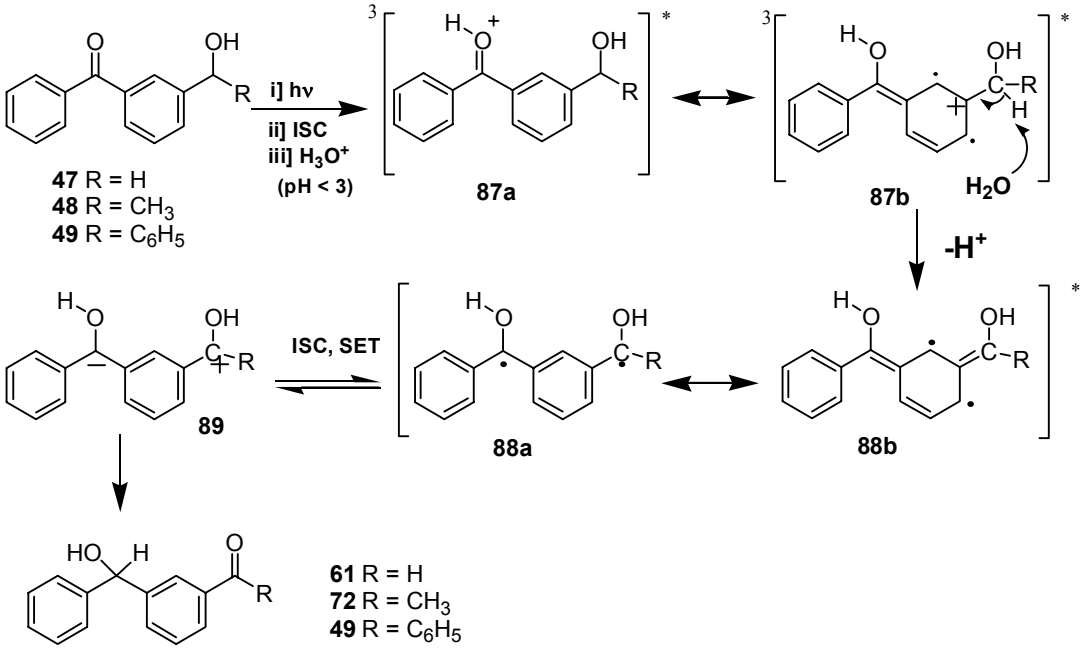

Scheme 2.3 Postulated mechanism for the acid catalysed intramolecular photoredox reaction of **47**, **48** and **49**

Simple HOMO/LUMO (Chem3D, MOPAC/AM1) calculations were performed for the compounds discussed in this chapter. Although by no means comprehensive, these HOMO/LUMO molecular orbital visualizations give a qualitative glimpse into the electronic behaviour of the excited state. The excited state of a molecule may be visualized as involving the promotion of an electron from the HOMO to the LUMO. Consequently, by examining both the HOMO and the LUMO one can see how electron density changes upon excitation. The HOMO/LUMO molecular orbitals are shown for **47** in Figure 2.23, for **48** in Figure 2.24 and for **49** in Figure 2.25. Upon examination and comparison between those three figures, it becomes evident that the HOMO and LUMO orbital representations for each compound appear strikingly similar. Thus, for simplicity sake the explanation will be made with regards to **47** alone as the arguments are valid for

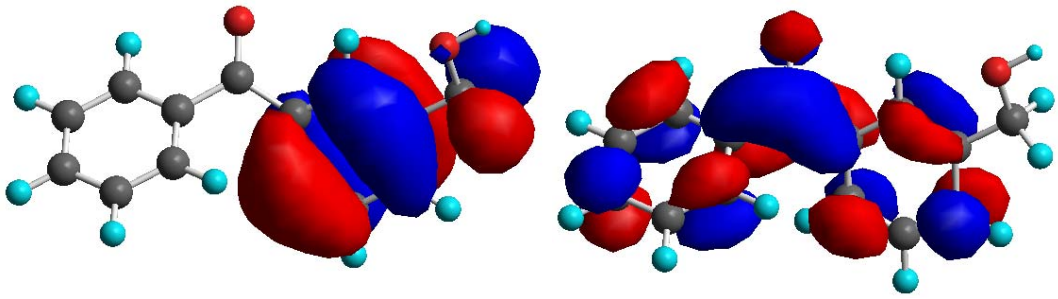

Figure 2.23 HOMO (left) and LUMO (right) of **47** calculated using Chem3D (AM1)

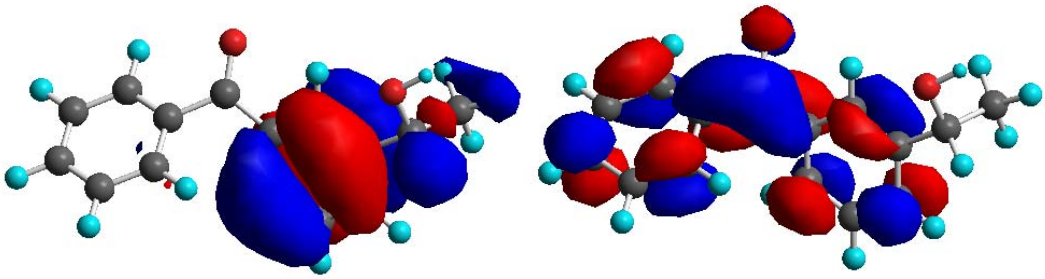

Figure 2.24 HOMO (left) and LUMO (right) of **48** calculated using Chem3D (AM1)

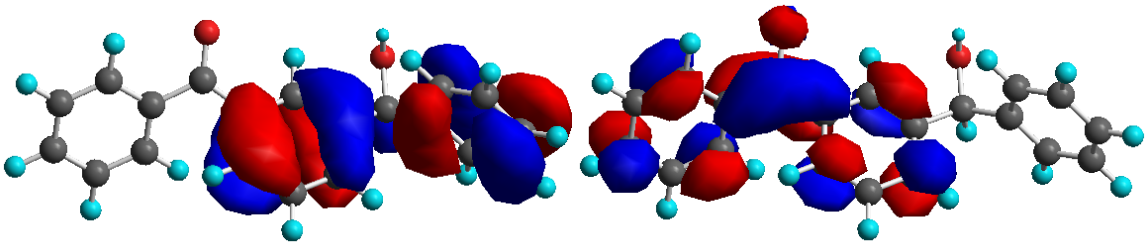

Figure 2.25 HOMO (left) and LUMO (right) of **49** calculated using Chem3D (AM1)

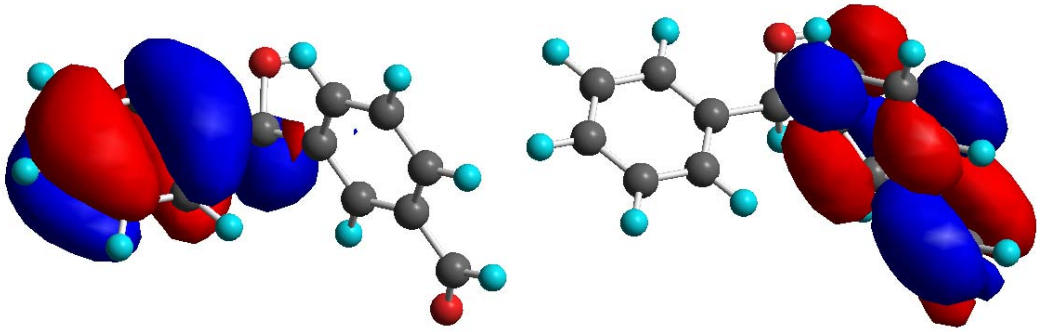

Figure 2.26 HOMO (left) and LUMO (right) of **61** calculated using Chem3D (AM1)

all three compounds. The proposed mechanism shown in Scheme 2.3, is likewise valid

for all three compounds. As shown in Figure 2.23, upon excitation there should be charge migration from the benzene ring with the attached hydroxymethyl group (phenyl ring on the right of the molecule) to the benzophenone carbonyl group and the other benzene ring. This would have the effect of increasing the charge density on the carbonyl group, increasing its basic character. It is thus predictable that the benzophenone ketone should exhibit enhanced basicity. Upon protonation (**87a**), it is reasonable to assume that the charge distribution should be essentially unchanged, assuming the compound is still in the excited state. If this is true, then the benzene ring with the attached hydroxymethyl group should be expected to have less electron density as some of its previous charge has been transferred to the carbonyl and the other benzene ring. This leaves that benzene ring with a net partial positive charge represented in the reaction mechanism by **87b**. This intermediate is analogous to the intermediate postulated for the acid-catalyzed photohydration of benzophenone by Wirz[59] and has also been suggested as an intermediate in the deuteration of **28**.[70] Although the simple HOMO/LUMO calculations do not show the positional effect of the substituents, the positional reactivity of the photoredox reaction was explored in Section 2.2.2.3. The significant reactivity of the *meta*-substituted **47** when compared to the almost complete absence of reactivity of the *para*-substituted **52** is consistent with the *meta*-effect described by Zimmerman *et al*.[61] The activation of the *meta* position to a much greater degree than the *para* position is also consistent with the work on the acid-catalyzed photohydration of benzophenone which saw activation primarily at the *meta* position, and at the *ortho* position to a lesser extent.[59] Although the previous studies by Zimmerman and Wirz suggest that photoredox chemistry, via an equivalent mechanism, is possible for the *ortho* compound **51**, the

photochemistry is more complicated. This is because **51** has access to an alternative pathway, proceeding via hydrogen abstraction rather than through the protonation and deprotonation pathway discussed in this section. As the hydrogen abstraction pathway is likely more efficient **51** is a poor choice for contributing to the discussion of mechanism of photoredox of **47**.

In the case of the photohydration of benzophenone, water attacks the carbocation that is the analogue of **87b**. Although this may occur in the *meta*-substituted compounds as well, the photohydration would lead to an unstable product that would revert to substrate and would not be isolated. However, unlike benzophenone itself, as studied by Wirz, the substituted benzophenones have an alternative pathway available to them. Instead of photohydration, the charge transfer away from the substituted benzene ring promotes the deprotonation of a benzylic proton to form the biradical dienol **88b**. This is supported by the observed isotopic effect of 1.5 presented in Section 2.2.2.9. This value was obtained from deuterium isotope effect exchange experiments involving the photolysis of mono-deuterated **47-αD** and suggests that the deprotonation of the benzylic proton of **87b** is an integral step in the mechanism.

The deprotonation of the benzylic proton appears to be common in the photoreaction of several similar compounds. The methyl compound **28** is thought to proceed through a benzylic anion when it undergoes photodeuteration. Likewise the base-catalyzed pathway of the decarboxylation of **30** and **34**[70] is thought to proceed through a benzylic anion. For these two systems the mechanism proposed results in the anion rather than the enol proposed in the mechanism. However the acid catalyzed pathway for the decarboxylation, shown in Eqn [1.16], is significantly different. This

pathway shares many similarities to the mechanism proposed by Wirz[59] for the photohydration of benzophenone. This in turn shares many similarities with the mechanism proposed in this Thesis. In all three cases, protonation of the excited state leads to positive charge at the *meta* position which promotes deprotonation of benzylic hydrogens (or decarboxylation).

As discussed in Section 1.8 Lukeman *et al*[83] proposed a mechanism for the photoredox chemistry of the anthraquinone analogue **42** that proceeded through a carbanion intermediate similar to one previously proposed for the photoredox chemistry of *meta* and *para*-nitrobenzyl alcohols.[10] This reaction pathway involving carbanion formation could be viewed as the base catalysed route. As the experiments were conducted under neutral conditions, one could equally propose an acid mechanism. This mechanism would behave in a manner akin to Scheme 2.3. By that perspective **42** and **47** are not significantly different from one another from a mechanism point of view. This is especially true in the light of the investigations into the photoredox of **47** at pH 7 in Section 2.2.2.7. Compound **47** just requires more acid to approach the efficiency of reaction of **42**.

Like the photolysis of **42,** photolysis of 6-hydroxymethylpterin (**29**) results in intramolecular photoredox chemistry (See Section 1.7). The substituent is oxidized and the aromatic pterin moiety is reduced. The redox product reacts with oxygen to produce the oxidized product in a manner reminiscent of the oxidation of dihydroxyanthracene to anthraquinone during workup.[83] In this way aromaticity is restored. By contrast benzophenone does not involve a loss of aromaticity during the photoredox reaction and thus the photoredox product is stable to oxygen.

It is likely that residual oxygenation of the resulting **88a** or **88b** leads to **59** via the trapping of the biradical with oxygen. The mechanism of photooxidation has not been explored, however, and alternative mechanisms may be involved.

The final photoredox product **61** involves ketonization of the dienol **88b**. The deuteration studies (Section 2.2.2.8) suggest that that the only way the redox product would have a deuterated methine proton would be if the intermediate reacts with D_2O. It has not been determined whether this ketonization may occur through a concerted mechanism or through a stepwise mechanism. However, regardless of the pathway, the intermediate must undergo intersystem crossing before attaining the singlet ground state of the product. If the mechanism proceeds in a concerted manner, it may not involve a zwitterion and should proceed in a manner similar to Eqn [2.20]. If the mechanism proceeds stepwise the zwitterionic intermediate **89** is the most likely to be involved as water rarely reacts homolytically. Protonation from water is known to be involved in the formation of the redox product as the benzhydrol proton was deuterated fully when **47** was photolysed in D_2O (pD 2).

The alternative zwitterion **90b**, with the negative charge on the benzylic carbon and a positive benzhydrol carbon is not likely to play much of a part as no deuterated starting material was recovered after photolysis in acidic D_2O, even after photolysis to high conversion yields. This result is interesting as the alternative zwitterion is easily accessible, and is essentially already formed from **87b** according to Eqn. [2.19]. This is likely the pathway that occurs during the photodeuteration of the 3-methyl analogue **28** (See Section 2.2.2.4).

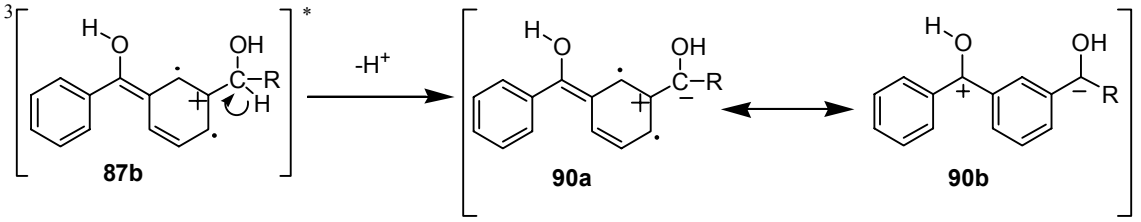

It is unknown why precisely one zwitterion is favoured over the other or why the presence of a hydroxyl group favours the protonation at the carbonyl carbon while its absence favours protonation at the benzylic carbon. However an explanation may be made by examining the two different zwitterions and the factors of the substrate molecules that stabilize said zwitterions. If the mechanisms do not go through a zwitterion and instead involve the direct protonation of the double bond Eqn [2.20] and Eqn [2.21] result. It is immediately noticeable that in order to form **61** a different carbon is required to be protonated than to form **28**. Apparently the presence of the hydroxyl group exerts a significant enough electronic effect to reverse the behaviour. It is possible that the lone pair on the oxygen may be transmitted through the conjugated electronic system in both cases to make the *meta* position more basic allowing ketonization of the extended enol. In the case of **31** only one direction is possible so the benzylic methylene is protonated to produce **28**. This behaviour is also consistent with a zwitterionic model as the resonance contributor with the cation at the carbonyl carbon is more stabilized than the contributor with the anion in that position. For **88b** there are two enols and therefore two possible directions for ketonization. In the cases of **47** and **48**, these two directions are not equal and directionality is observed. The lone pair of the hydroxyl group may conceivably stabilize a cation by allowing delocalization of the positive charge. As the phenyl group acts as an electron withdrawing group adjacent to the benzhydrol position, it could stabilize the anion. These two factors should stabilize the resonance contributor

with the anion at the benzhydrol position relative to the resonance contributor with the cation at that position. This would favour protonation at the benzhydrol position and consequently only the redox product would be formed, not starting material. As the substrate molecule becomes more symmetrical, the difference between the different zwitterions decrease and eventually the forward photoredox reaction should no longer be favoured.

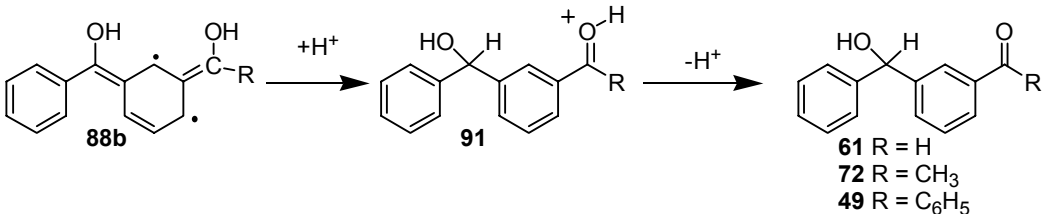

[2.20]

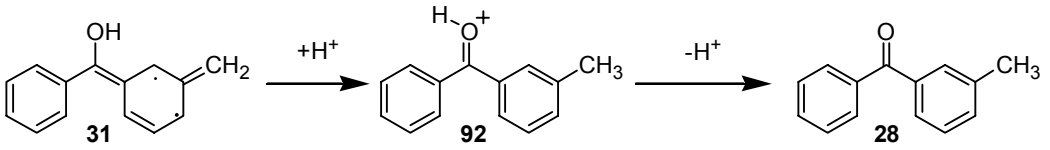

[2.21]

HOMO/LUMO calculations were also carried out on the photoredox product **61** to gain insight into why the reverse reaction is not possible. As shown in Figure 2.26 electronic excitation results in charge transfer from the one benzene ring to the carbonyl but this time the extended ring system is not involved. Thus the charge density at the benzhydrol proton is not decreased sufficiently to deprotonate and consequently the reverse reaction is not as favourable.

As discussed in detail in Section 2.2.3, the charge that the substituents induce on the benzhydrol or the benzylic carbon plays a large role in the direction and reversibility of the reaction. By altering the substituents attached to the added phenyl ring, many different kinds of photochemical behaviour were observed. If the substituent was electron-donating in character at the hydroxymethine carbon the forward reaction towards

the photoredox product was favoured. If the substituent was electron-withdrawing in character the compound was photoinert towards photoredox leading to the suggestion that the reverse reaction was probably favoured. Thus the direction was favoured that stabilized the appropriate carbocation. For the forward reaction the carbocation needs to be present on the methylene carbon and thus by stabilizing that position the forward reaction is favoured. The reverse is also true. If the carbanion is stabilized at that position relative to the benzophenone carbon then the reverse reaction would be more favoured and no forward reaction would be evident. This is consistent with the research done on **28** where, as a comparison to **47**, the benzophenone carbocation was stabilized and thus **28** would not proceed to a photoredox product.

2.3 Summary and Conclusions

The electronic differences between **47**, **48** and **49** are subtle and so all three molecules undergo similar intramolecular photoredox chemistry. However the three differ in their reactivity and in the amount of side products produced in the reaction. Although the three different compounds differ in quantum yield of formation of photoredox product, they all have similar quantum yields of loss of substrate. The primary difference lies in the yield of side products. The two main side products consistently observed are the photooxidation product and the oligomeric photoreduction products. The photooxidation product is due to residual oxidation and is present in similar quantities for all three independent of substrate. By contrast, the oligomeric

photoreduction products are highly dependent on concentration and substrate chemical structure.

The oligomeric photoreduction products arise via bimolecular hydrogen abstraction. Consequently, the pathway is highly concentration dependent. Substrate chemical structure also plays a role. The competitiveness of the pathway that produces the oligomeric photoreduction products may be correlated with the number of abstractable hydrogens and the ease of abstracting those hydrogens. Compound **48** has fewer benzylic hydrogens as compared to compound **47** so appears cleaner with respect to oligomeric side products. Compound **49** however, has the highest proportion of oligomeric side products despite having the same number of benzylic hydrogens. In this case, the answer lies with the fact that benzhydrol type hydrogens are more readily removed due to the stabilizing effect of the two phenyl rings as opposed to just one for **47** and **48**. This explanation also holds for the phenyl derivatives investigated by Basarić[88] as the *para*-methyl derivative **76**, with its four abstractable hydrogens, one of which being a benzhydrol type, has the most oligomeric photoreduction products of any of the phenyl derivatives studied.

The essential steps in the photoredox mechanism are: (a) protonation of the carbonyl oxygen of the photoexcited substrate, (b) deprotonation of the benzylic alcoholic carbon and (c) subsequent protonation of the former carbonyl to form the benzhydrol. The reaction is solvent mediated and acid-catalysed. If any of those essential steps are hindered the photoredox reaction is inhibited. The two protonation steps require a protic solvent and the efficiency of the photoredox reaction may be correlated with the acidity of the solvent medium. The deprotonation of the benzylic

alcoholic carbon is more dependent on the chemical structure of the substrate than the solvent media. Decreasing the ability of the benzylic alcoholic carbon to deprotonate has the effect of decreasing the efficiency of the reaction and may explain the photoinertness of several compounds such as the *meta*-methoxy phenyl derivative **78**.

These conclusions agree with research done by Dr. Nikola Basarić in our lab. In addition to the product studies, the LFP triplet lifetimes of the substituted phenyl derivatives of **49** could be correlated to their electron donating or electron withdrawing capability. The longest lived species is the transient for the *meta*-methoxy compound **78**, followed by the parent **49**, then the *para*-methyl substituted **76** and finally by the *para*-methoxy substituted compound **77**. This order corresponds to an increasing electron donating character as the lifetime shortens. This correlates well at pH 7 but at pH 2 the two methoxy substituted compounds have lifetimes that are greatly affected by the pH of the solution. This is likely because the methoxy oxygen may be solvated by H_3O^+.

Much of the reactivity a compound shows towards photoredox behavour is a result of the structural effects on the electronic charge distribution throughout the molecule. As mentioned in Section 2.2.5, if a resonance contributor is stabilized in such a manner as to favour either the cation at the benzylic methylene or the anion at the benzophenone carbonyl carbon, the photoredox reaction is favoured. If the reverse is stabilized then the compound is photoinert towards photoredox reaction, such as in the case of **28**, **78** and **80**.

Although **50** should be a promising candidate for photoredox chemistry due to its structure, no photoredox chemistry was observed. Instead many radical products were observed leading to the conclusion that under those photolysis conditions the C-O bond

for methoxy was weak enough to undergo homolytic photolysis. This conclusion was supported by similar results obtained for photolysis of the equivalent *para* compound **71**.

2.4 Experimental

2.4.1 General

^{1}H NMR spectra were recorded on either a Bruker AC300 (300 MHz) instrument or a Bruker AVANCE 500 (500MHz) instrument using chloroform-*d* as the solvent unless otherwise specified. Chemical shifts are reported in ppm and *J*-values are reported in Hz. Splitting patterns are reported as s (singlet), d (doublet), t (triplet), dd (doublet of doublets), dt (doublet of triplets), tt (triplet of triplets) and m (multiplets). Mass spectra and High-resolution-mass spectra (HRMS) were obtained on a Kratos Concept 1H (EI and HRMS) instrument. UV–vis spectra were recorded on a Varian Cary 1, or 5 spectrometer instrument using baseline correction. Infrared spectra were recorded on a Perkin Elmer FTIR Spectrometer Spectrum 1000 using NaCl plates with neat product or thin film obtained from a solution of dichloromethane. Only strong and medium peaks are reported. Melting point values were obtained using a Gallenkamp Melting Point Apparatus. Measurements of pH(D) values were obtained using a Fisher Accumet 915 pH meter prior to mixing with acetonitrile co-solvent. Transient absorption spectra and kinetic measurements were carried out at the University of Victoria nanosecond LFP facility. Excitation was achieved by a Spectra Physics YAG laser (GCR-11, λ_{ex} 266 nm). Preparative photolysis were performed using a Rayonet RPR 100 photochemical reactor using 300 nm lamps unless otherwise noted. I wish to acknowledge Dr. Nikola Basarić

for the studies performed upon the substituted benzoylbenzophenones reported in this chapter.

2.4.2 Common Laboratory Reagents

All solvents used for synthesis (ACS grade) were purchased from Aldrich Chemical Company and used as received unless otherwise noted. THF, diethyl ether and toluene used in syntheses were either distilled over Na (using benzophenone as an indicator) or used directly from a Solvent Purification System. Acetonitrile (HPLC grade) used for photolyses was checked for impurities by NMR. Organic extracts were dried over anhydrous magnesium sulfate and filtered. Deuterated solvents; D_2O, $CDCl_3$ were purchased from Cambridge Isotope laboratory containing 99.9% D. D_2SO_4 was obtained Aldrich Chemical company and contained 99.9% D. Preparative TLC was carried out on 20 cm x 20 cm silica gel GF Uniplates (Analtech). The following compounds were purchased from Aldrich: 3-benzoylbenzophenone, 3-methylbenzophenone, 4-methylbenzophenone, sodium borohydride, sodium borodeuteride, magnesium turnings, N-bromosuccinimide, benzoyl peroxide, 4-bromotoluene, 4-bromoanisole, 3-bromoanisole, 3-bromobenzaldehyde, ketoprofen, 2-(hydroxymethyl)anthraquinone.

2.4.3 Synthesis

3-(Hydroxymethyl)benzophenone (**47**)

3-Methylbenzophenone (**28**) (9.10 mL, 51.0 mmol) was combined with 1.5 molar equivalents N-bromosuccinimide (13.6 g, 76.5 mmol) and catalytic amounts of benzoyl peroxide (0.10 g, 0.7 mmol)(1.4 mol%) in 40 mL benzene. The system was flushed with N_2 and the reaction mixture was refluxed under N_2 for 12 hours. After allowing the mixture to cool to room temperature the mixture was washed twice with 50 mL distilled H_2O and a further 25mL CH_2Cl_2 was added to enhance separation. The reaction mixture was then separated in a separatory funnel and the organic layer dried with anhydrous $MgSO_4$. After filtration and removal of the solvent via rotary evaporator, the crude 3-(bromomethyl)benzophenone was used directly in the next step. The crude residue was then hydrolysed by dissolving in 150 mL dioxane and combining with 5 molar equivalents $CaCO_3$ (25.4 g, 254 mmol) and 150 mL distilled H_2O and refluxing overnight for 16 hours. The solvent was removed via rotary evaporator. The resulting crude solid mixture was dissolved by alternately adding 1M HCl and CH_2Cl_2. Bubbles stopped evolving when enough HCl had been added (~ 200 mL CH_2Cl_2, ~300 mL HCl). The organic layer was collected and the aqueous layer further extracted twice with 100 mL CH_2Cl_2. The organic layers were combined and washed twice with 200mL saturated $NaHCO_3$ solution. They were then dried with anhydrous $MgSO_4$, filtered and the solvent removed via rotary evaporator. After purifying via silica column using 1:1 ether:hexanes as the eluent, **47** was obtained as a colourless oil in 21% yield (2.27 g, 10.7mmol). ^{1}H-NMR (300MHz, $CDCl_3$) δ: 7.78-7.74 (m, 3H), 7.67-7.65 (d, 1H), 7.59-7.54 (m, 2H), 7.47-7.40 (m, 2H), 4.72 (s, 2H); ^{13}C-NMR (125 MHz, $CDCl_3$) 197.01, 141.48, 138.02,

137.67, 132.72, 131.09, 130.24, 129.50, 128.65, 128.51, 128.44, 64.91; IR (thin film from CH_2Cl_2 solution, NaCl plates, Air Background): ν = 3417, 3057, 2920, 2870, 1654, 1593, 1446, 1316, 1280, 1047, 1025, 720, 709 cm^{-1}; UV-Vis (1:1 pH 2 H_2SO_4 - CH_3CN): λ_{max} = 255 nm (ε = 21,500); MS (EI) *m/z*; 212 (80, M+), 181 (10), 135 (70), 105 (100), 89, (15), 77 (70), 51 (25); HRMS, calculated for $C_{14}H_{12}O_2$ 212.0837; observed 212.0832.

3-(Hydroxymethyl)benzophenone-αd_1 (47-αD)

Compound **59** (0.247 g, 1.17 mmol) was dissolved in 30 mL isopropanol. Sodium borodeuteride (0.0160 g, 0.383 mmol) (1.3 molar equivalents) was then added and washed into the flask with another 20 mL of isopropanol. The reaction mixture was stirred for 1 hour and then quenched in 50 mL of distilled water. This was then extracted twice with 50 mL CH_2Cl_2, washed with 50 mL distilled water and then dried with anhydrous $MgSO_4$, filtered and the solvent removed via rotary evaporator to yield a pale yellow oil with a yield of 0.2230 g (89% yield). A ^{1}H-NMR spectrum of the crude oil shows nearly quantitative reduction with vary little other products. Pure **47-αD** was obtained as a colourless oil in 0.1968 g yield (79% yield) by using a prep TLC (2 plates) using ether as the developing solvent.

^{1}H-NMR (300MHz, $CDCl_3$) δ: 7.72-7.68 (m, 3H), 7.62-7.48 (m, 3H), 7.44-7.34 (m, 3H), 4.62 (s, 1H), 3.40 (s, 1H); ^{13}C-NMR (125 MHz, $CDCl_3$) δ: 197.01, 141.48, 138.02, 137.67, 132.72, 131.09, 130.24, 129.50, 128.65, 128.51, 128.44, 64.91 (t) ; 125 MHz); UV-Vis (1:1 pH 2 H_2SO_4 - CH_3CN): λ_{max} = 255 (ε = 20,500); MS (EI) *m/z* 213 (55, M^+),

181 (10), 136 (60), 105 (100), 90 (15), 77 (55), 51 (20) ; HRMS, calculated for $C_{14}H_{11}DO_2$ 213.0899; observed 213.0895.

3-(1'-Hydroxyethyl)benzophenone (48)[66]

Ketoprofen (**17**) (0.300 g, 1.20 mmol) was dissolved as much as possible in 150 mL H_2O and brought to a pH ~8 by the addition of NaOH which completed the dissolution. A further 150 mL CH_3CN was added and the resulting solution photolysed (after purging for 15 min with Ar) in a photochemical reactor using sixteen lamps (300nm) for 15 min to form **19** in 100% conversion. A ^{1}H-NMR spectrum showed that the photolysis produced pure **19** with no additional purification needed. The product from the previous reaction was used directly for the next step of the reaction. It was then brominated with 1.2 molar equivalents of N-bromosuccinimide (0.250 g, 1.4 mmol) and catalytic amounts of benzoyl peroxide (0.0034 g, 0.014 mmol)(1.1 mol%) in 40 mL benzene. The reaction mixture was refluxed 5 hours under N_2. After the mixture cooled much solid was present in the reaction flask. The solution was decanted off into a separatory flask, washed twice with 50 mL distilled H_2O and dried with anhydrous $MgSO_4$. The resulting mixture was filtered and the solvent removed under vacuum. This crude 3-(1'-bromoethyl)benzophenone was then combined with 5 molar equivalents of $CaCO_3$ (0.6 g, 6 mmol) in 100 mL 1:1 H_2O: dioxane and refluxed overnight for 17 hours. After the reaction mixture had cooled, the solvent was removed *in vacuo*. Then 100 mL of CH_2Cl_2 and ~100 mL 1 M HCl was added until all solid had been dissolved. The organic phase was separated and the aqueous phase extracted twice with 50 mL CH_2Cl_2.

The organic fractions were combined and washed twice with 100 mL saturated $NaHCO_3$. Next, the organic fraction was dried with anhydrous $MgSO_4$, filtered and the solvent removed via rotary evaporator. A pale yellow crude product that consisted of primarily **48** with the major impurity being **73** with a crude yield of 0.153 g. A colourless oil resulted after chromatography (silica gel, CH_2Cl_2). Final yield: 0.033 g (12 %) ^{1}H-NMR (300MHz, $CDCl_3$) δ: 7.78-7.74 (m, 3H), 7.66-7.54 (m, 3H), 7.48-7.40 (m, 3H), 4.94 (q, 1H, 6.6 Hz), 1.50 (d, 3H, 6.6 Hz); ^{13}C NMR ($CDCl_3$, 125 MHz) δ: 197.00, 146.44, 137.94, 137.73, 132.68, 130.23, 129.67, 129.39, 128.59, 128.49, 127.12, 70.13 (s) 25.53; IR (neat, NaCl plates): v = 3434, 3060, 2972, 2926, 2875, 1662, 1646, 1597, 1446, 1313, 1283, 1204, 1178, 1136, 1075, 1023, 970, 902, 819, 786, 723, 701 cm^{-1}; UV-Vis (1:1 pH 2 H_2SO_4 - CH_3CN): λ_{max} = 255nm (ε = 21,600); MS (EI) *m/z*; 226 (20, M+), 211 (50), 183 (40), 149 (20), 133 (20), 105 (100); HRMS, calculated for $C_{15}H_{14}O_2$ 226.0994; observed 226.0998.

3-Benzoylbenzhydrol –α*D*$_1$ (49-αD)

3-Benzoylbenzophenone (0.300 g, 1.1 mmol) was dissolved in 60 mL isopropanol sodium borodeuteride (for **49-αD**) (0.0235 g, 0.56 mmol) in 25 mL isopropanol was added slowly dropwise while stirring at room temperature. After addition, the mixture was stirred for a further 1.5 hours at room temperature with a $CaCl_2$ tube as a vent. The mixture was refluxed for 45 min and then quenched with 100 mL distilled H_2O. The resulting mixture was extracted twice with 100 mL CH_2Cl_2, and the organic phase washed with 100 mL distilled H_2O before drying over anhydrous magnesium sulfate.

The solvent was evaporated to give a yellow film. Pure **49-αD** was obtained via preparative TLC using 1:24 ether : CH_2Cl_2 (2 plates). (Final yield 55%)

^{1}H-NMR (500MHz, $CDCl_3$) δ:7.84 (t, 2H, 1.8 Hz), 7.74 (dd, 2H, 8.2 Hz and 1.4 Hz), 7.65 (dt, 1H, 7.6 Hz and 1.5 Hz), 7.60 (dt, 1H, 7.7 Hz and 1.6 Hz), 7.56 (tt, 1H, 7.5 and 1.3 Hz), 7.46-7.40 (m, 3H), 7.37-7.35 (m, 2H), 7.34-7.31 (m, 2H), 7.28-7.24 (m, 1H).^{13}C NMR ($CDCl_3$, 125 MHz) δ: 196.87, 144.37, 143.60, 137.81, 137.61, 132.68, 130.65, 130.27, 129.46, 128.83, 128.60, 128.45, 128.21, 128.01, 126.72; IR (thin film from CH_2Cl_2 solution, NaCl plates): *v* = 3435, 3059, 3026, 1656, 1651, 1596, 1447, 1318, 1282, 1196, 1179, 1134, 1053, 713, 698, 640 cm^{-1}; UV-Vis (1:1 pH 2 H_2SO_4 - CH_3CN): λ_{max} = 256 nm (ε = 22,200); MS (EI) *m/z*; 289 (M+, 40), 286 (M^+, 45), 273 (40), 209 (80), 196 (35), 184 (100), 166 (40), 152 (20); HRMS, calculated for $C_{20}H_{15}DO_2$ 289.1212; observed 289.1206.

3-Benzoylbenzhydrol (49)

Preparation identical to preparation of **49-αD** but instead of sodium borohydride, sodium borodeuteride was used.

^{1}H-NMR (500MHz, $CDCl_3$) δ: 7.84 (t, 2H, 1.8 Hz), 7.74 (dd, 2H, 8.2 Hz and 1.4 Hz), 7.65 (dt, 1H, 7.6 Hz and 1.5 Hz), 7.60 (dt, 1H, 7.7 Hz and 1.6 Hz), 7.56 (tt, 1H, 7.5 and 1.3 Hz), 7.46-7.40 (m, 3H), 7.37-7.35 (m, 2H), 7.34-7.31 (m, 2H), 7.28-7.24 (m, 1H). 5.90 (s, 1H);).^{13}C NMR ($CDCl_3$, 75 MHz) δ: 196.84, 144.39, 143.67, 137.92, 137.68, 132.72, 130.66, 130.31, 129.54, 128.90, 128.66, 128.50, 128.25, 128.10, 126.78; UV-Vis (1:1 pH 2 H_2SO_4 - CH_3CN): λ_{max} = 254 nm (ε = 22,400); MS (EI) *m/z* 288 (M^+, 15), 286

(15), 272 (10), 209 (30), 195 (10), 183 (50), 105 (100), 77 (60); HRMS, calculated for $C_{20}H_{16}O_2$ 288.1150; observed 288.1152.

4-(Hydroxymethyl)benzophenone[91] (52)

This synthesis proceeded in the same manner as for **47** but starting with 4-methylbenzophenone (**58**)(10.00 g, 51.0 mmol),purchased from Aldrich. The crude yield obtained was 82% (8.83 g, 41.6 mmol) and after silica column purification a white solid with a yield of 21% (2.32 g, 10.9 mmol) was obtained.

mp. 59-65°C (lit.61-64°C)[92]; ^{1}H-NMR (300MHz, $CDCl_3$) δ: 7.68-7.65 (m, 4H), 7.53-7.48 (m, 1H), 7.41-7.35 (m, 4H), 4.67 (s, 2H), 3.94 (s, 1H)); ^{13}C NMR ($CDCl_3$, 125 MHz) δ: 196.69, 145.74, 137.87, 137.00, 132.63, 130.62, 130.22, 128.51, 126.63, 64.92 (s) ; IR (neat from CH_2Cl_2 solution, salt plates): ν = 3415, 3057, 2869, 1651, 1607, 1597, 1577, 1446, 1413, 1317, 1279, 1202, 1175, 1048, 1015, 938, 924, 840, 786, 731, 701 cm^{-1}; UV-Vis (1:1 pH 2 H_2SO_4 - CH_3CN): λ_{max} = 253 nm (ε = 23,000); MS (EI) *m/z* 212 (60, M^+), 181 (10), 135 (80), 105 (100), 89 (10), 77 (70), 69 (10); HRMS, calculated for $C_{14}H_{12}O_2$ 212.0837; observed 212.0836.

3-Formylbenzophenone (59)[93]

3-Methylbenzophenone (**28**)(9.10 mL, 51.0 mmol) was combined with 2.5 molar equivalents of N-bromosuccinimide (22.8 g, 128 mmol) and benzoyl peroxide (0.11 g, 0.80 mmol) as an initiator in 100 mL benzene. The reaction mixture was refluxed overnight for 17 hours under N_2. After the mixture cooled, it was washed twice with 50 mL distilled H_2O, dried with anhydrous magnesium sulfate, filtered and the solvent

removed under vacuum. This crude 3-dibromomethylbenzophenone was then combined with 5 molar equivalents of $CaCO_3$ (25.8 g, 258 mmol) in 300 mL 1:1 H_2O: dioxane and refluxed overnight for 17 hours. After the reaction mixture had cooled, the solvent was removed under vacuum. Then 200 mL of CH_2Cl_2 and ~400 mL 1 M HCl was added until all solid had been dissolved. The organic phase was separated and the aqueous phase extracted twice with 100 mL CH_2Cl_2. The organic fractions were combined and washed twice with 200 mL saturated sodium bicarbonate. The organic fraction was dried with anhydrous magnesium sulfate, filtered and the solvent removed to yield a thick yellow oil that slowly crystallized into a waxy solid. Pure white crystals were obtained after chromatography (silica gel, 1:1 ether : hexanes). (final yield 35%)

mp. 90-96 ^{o}C (lit. 91-99 °C)[93]; ^{1}H-NMR (300MHz, $CDCl_3$) δ: 10.08 (s, 1H), 8.27 (s, 1H), 8.12-8.05 (m, 2H), 7.82-7.78 (m, 2H), 7.69-7.58 (m, 2H), 7.53-7.48 (m, 2H); ^{13}C NMR ($CDCl_3$, 75 MHz) δ: 195.70, 191.65, 138.73, 137.05, 136.56, 135.67, 133.23, 132.91, 131.56, 130.24, 129.48, 128.80; IR (neat from CH_2Cl_2 solution, salt plates) ν = 3417, 3061, 3029, 2846, 2736, 1694, 1600, 1582, 1493, 1449, 1385, 1281, 1236, 1137, 1037, 1023, 915, 783, 754, 700, 650 cm^{-1}; UV-Vis (1:1 pH 2 H_2SO_4 : CH_3CN): λ_{max} = 233 nm (ε = 18,700), 250 nm (ε = 23,000); MS (EI) *m/z*: 210(M^+, 100), 181 (10), 133 (40), 105 (60), 104 (95), 77 (50), 51 (20); HRMS, calculated for $C_{14}H_{10}O_2$ 210.0681; observed 210.0686

3-Formylbenzhydrol (61)[94]

Compound **59** (0.421 g, 2.00 mmol) and $ErCl_3 \cdot 6H_2O$ (0.385 g, 1.00 mmol) was dissolved in 2.5 mL methanol. To this trimethyl orthoformate was added (0.77 mL, 7.0 mmol). The reaction mixture was stirred for 15 minutes at room temperature before adding sodium borohydride (80.4 mg, 2.1 mmol) all at once. An immediate vigourous reaction occurred. The reaction mixture was left to stir for 5 min before adding 1 M HCl to acidify the solution to pH 3. After 20 minutes 30 mL saturated sodium chloride solution was added and the reaction mixture extracted twice with 50 mL ether. The organic layers were combined and dried with anhydrous magnesium sulfate. After filtration the solvent was removed on the rotary evaporator. The crude residue (0.316 g, 75% yield) was purified using chromatography (silica gel, 1:1 ether : hexanes) to give a colourless oil. Final yield: 0.283 g (67%)

^{1}H-NMR (300MHz, $CDCl_3$) δ: 9.97 (s, 1H), 7.91 (s, 1H), 7.76 (d, 1H, 7.4 Hz), 7.65 (d, 1H, 8.1 Hz), 7.48 (dd, 1H, 7.7, 8.1), (m, 5H), 5.90 (s, 1H); ^{13}C-NMR ($CDCl_3$, 75 MHz) δ: 192.56, 145.11, 143.45, 136.76, 132.73, 129.41, 129.07, 129.01, 128.29, 127.85, 126.82, 75.95; IR (neat from CH_2Cl_2 solution, salt plates): ν = 3417, 3061, 3029, 2846, 2736, 1694, 1600, 1582, 1493, 1449, 1385, 1281, 1236, 1137, 1037, 1023, 915, 783, 754, 700, 650 cm^{-1}; UV-Vis (1:1 pH 2 H_2SO_4 : CH_3CN): λ_{max} = 250 nm (ε = 18,000), 291 nm (ε = 6,000); MS (EI) *m/z* 212 (30, M^+), 165 (15), 152 (10), 133 (35), 105 (100), 77 (60), 51 (25) ; HRMS, calculated for $C_{14}H_{12}O_2$ 212.0837; observed 212.0840.

3-(Methoxymethyl)benzophenone (50)

3-Methylbenzophenone (**28**)(9.10 mL, 51.0 mmol) was combined with 1.5 molar equivalents N-bromosuccinimide (13.6 g, 76.5 mmol) and catalytic amounts of benzoyl peroxide (0.10 g, 0.7 mmol)(1.4 mol%) in 40 mL benzene. The system was flushed with N_2 and the reaction mixture was refluxed under N_2 for 12 hours. After allowing the mixture to cool to room temperature the mixture was washed twice with 50 mL distilled H_2O and a further 25 mL CH_2Cl_2 was added to enhance separation. The reaction mixture was then separated in a separatory funnel and the organic layer dried with anhydrous $MgSO_4$. After filtration and removal of the solvent via rotary evaporator, the crude 3-(bromomethyl)benzophenone was used directly in the next step. The crude residue was then reacted by dissolving in 300 mL methanol and combining with 5 molar equivalents of $CaCO_3$ (25.38 g, 254 mmol) and refluxing overnight for 16 hours. The solvent was removed under vacuum yielding a heterogeneous solid residue. The resulting crude solid mixture was dissolved by alternately adding 1M HCl and CH_2Cl_2. Bubbles stopped evolving when enough HCl had been added (~200 mL CH_2Cl_2, ~300 mL HCl). The organic layer was collected and the aqueous layer further extracted twice with 100 mL CH_2Cl_2. The organic layers were combined and washed twice with 200 mL saturated sodium bicarbonate solution. They were then dried with anhydrous magnesium sulfate, filtered and the solvent removed via rotary evaporator. After purifying via silica column using 1:1 ether:hexanes as the eluent, pure **50** was obtained as a colourless oil in 19% yield (2.27 g, 10.0 mmol).

^{1}H-NMR (300MHz, $CDCl_3$) δ: 7.79-7.76 (m, 3H), 7.69 (d, 1H), 7.59-7.54 (m, 2H), 7.48-7.40 (m, 2H), 4.50 (s, 2H), 3.39 (s,3H); ^{13}C-NMR (125 MHz, $CDCl_3$) 196.77, 138.65,

137.61, 132.44, 131.58, 130.05, 129.42, 129.06, 128.37, 128.30, 74.50, 58.34; UV-Vis (1:1 pH 2 H_2SO_4 - CH_3CN): λ_{max} = 254 nm (ε = 27,700); MS (EI) *m/z* 226 (20, M^+), 210 (15), 181 (10), 163 (20), 149 (20), 133 (10), 105 (100), 77 (50), 51 (20); HRMS, calculated for $C_{14}H_{12}O_2$ 226.0994; observed 226.0998.

2.4.4 Product Studies

2.4.4.1 General

All photolysis reactions were performed using a Rayonet RPR 100 photochemical reactor with 300 nm lamps varying from one lamp to sixteen lamps, and a water-cooled cold finger. Solutions of substrate (~10^{-4} to 10^{-3} M, 100 mL to 300 mL total) were photolysed for times ranging from 1 minute to 10 minutes. The quartz photolysis tubes were purged with argon for 15 minutes prior to photolysis and then purged continuously with argon (unless otherwise noted) during photolysis, both to remove oxygen from the solution and to provide continuous mixing during photolysis.

After photolysis of aqueous samples, the photolysis mixture was placed in a separatory funnel and extracted twice with dichloromethane (100 mL). The organic fractions were combined and dried over anhydrous magnesium sulfate before filtering and removing the solvent under vacuum. The residue was placed on a vacuum line for 30 minutes to remove any remaining solvent before characterization of the product mixture via NMR spectroscopy. Samples consisting entirely of organic solvents (acetonitrile) were directly evaporated under vacuum. The progress of reaction was followed by ^{1}H-NMR spectroscopy and the product ratio of the product mixture determined by

integration when possible. If separation of the product mixture was warranted, the separation was accomplished using preparatory scale TLC. A maximum of 100 mg was placed on any one plate. The individual separated bands were scraped off into beakers and extracted several times with the appropriate solvent (usually CH_2Cl_2 or diethyl ether) and the solvent removed to yield the purified photoproducts. For aqueous solutions at pH values other than 7, the pH of the aqueous portion was adjusted before combination with acetonitrile. For acidic solutions the pH was adjusted with H_2SO_4 (or D_2SO_4) and for basic solutions the pH was adjusted with NaOH (or NaOD).

2.4.4.2 Individual Product Study Details

Photolysis of 47

Using a 500 mL quartz photolysis tube, **47** (10 mg) was dissolved in 150 mL CH_3CN and then 150 mL pH 2 H_2SO_4 was added to give a concentration of 1.6×10^{-4} M. This was purged with Ar for 15 minutes prior to photolysis with two 300 nm lamps for 2 minutes. The photolysis tube contents were placed in a separatory flask after photolysis and extracted twice with 50 mL CH_2Cl_2. The organic layer was then dried with anhydrous $MgSO_4$ and gravity filtered. The solvent was then removed *in vacuo* and the flask placed on a vacuum line for 20 minutes to remove any remaining solvent. The reaction was then characterized via ^{1}H-NMR($CDCl_3$) and yielded a conversion of 32% of **61** with 1% **59**. Photolysis for 5 minutes with 4 lamps using the same concentration yields a conversion of 97% via ^{1}H-NMR ($CDCl_3$). Separation of the product mixture by preparative TLC yielded pure **61** and **59**

61: ^{1}H-NMR (300MHz, $CDCl_3$) δ: 9.97 (s, 1H), 7.91 (s, 1H), 7.76 (d, 1H, 7.4 Hz), 7.65 (d, 1H, 8.1 Hz), 7.48 (dd, 1H, 7.7, 8.1), (m, 5H), 5.90 (s, 1H); ^{13}C-NMR ($CDCl_3$, 75 MHz) δ: 192.56, 145.11, 143.45, 136.76, 132.73, 129.41, 129.07, 129.01, 128.29, 127.85, 126.82, 75.95; UV-Vis (1:1 pH 2 H_2SO_4 : CH_3CN): 250 nm (ε = 18,000), 291 nm (ε = 6,000);

59: ^{1}H-NMR (300MHz, $CDCl_3$) δ: 10.08 (s, 1H), 8.27 (s, 1H), 8.12-8.05 (m, 2H), 7.82-7.78 (m, 2H), 7.69-7.58 (m, 2H), 7.53-7.48 (m, 2H); ^{13}C NMR ($CDCl_3$, 75 MHz) δ: 195.70, 191.65, 138.73, 137.05, 136.56, 135.67, 133.23, 132.91, 131.56, 130.24, 129.48, 128.80; UV-Vis (1:1 pH 2 H_2SO_4 : CH_3CN λ_{max} = 233 nm (ε = 18,700), 250 nm (ε = 23,000);

Photolysis of **47** in 1:1 H_2O : CH_3CN pH 7(~10^{-4} M, oxygen purged, 4 lamps, 5 minutes) results in only **59** as a product

Photolysis of **47** using 1:1 5% H_2SO_4 : CH_3CN (~10^{-4} M) with two 300 nm lamps and 4 minutes, argon purged results in a different product mixture with 49% condensed product **74**, 9% **59** and 18% oligomeric side products.

3-[(3-Benzoyl-benzyloxy)-phenyl-methyl]-benzaldehyde (74): ^{1}H-NMR (500MHz, $CDCl_3$) 9.96 (s, 1 H), 7.87 (s, 1 H), 7.75-7.80 (m, 4H), 7.71 (d, 1H), 7.63 (d, 1H), 7.55-7.61 (m, 2H), 7.43-7.49 (m, 4H), 7.31-7.37 (m, 4H), 7.26-7.30 (m, 1H), 5.52 (s, 1H), 4.59 (dd, 2H)δ: ^{13}C NMR ($CDCl_3$, 125 MHz) δ: 196.77, 192.42, 143.63, 141.26, 138.64, 138.05, 137.77, 136.83, 133.12, 132.70, 131.84, 130.28, 129.70, 129.44, 129.40, 129.14, 128.97, 128.69, 128.53, 128.33, 128.29, 127.37, 82.59, 70.52; MS (EI) *m/z*; 406 (M^+, 10), 223 (10), 211 (100); MS (LSIMS) *m/z* 407.2 (M^++1, 100), 329.1 (70); UV: λ_{max} = 245 nm (e = 14,000) (1:1 pH 2 H_2SO_4 : CH_3CN)

Photolysis of **47** in 1:1 D_2O : CH_3CN (pD 2) at high concentration and high conversion (2.37 x 10^{-3} M) using eight 300nm lamps for 14 minutes resulted in deuteration of **57**. Full deuteration of the benzhydrol was observed along with partial deuteration of the aldehyde proton by comparison of integration.

Photolysis of **47** was accomplished at many different irradiation times and conditions. Data on the photolysis of **47** at different irradiation times as a summary is summarized in Table 2.1. Data on the photolysis of **47** in different solvent ratio of aqueous to acetonitrile is summarized in Table 2.2. Table 2.7 summarizes the product ratio as a factor of concentration while Table 2.8 summarizes the product ratio as a factor of the pH.

Photolysis of 47-αD

Irradiation of **47-αD** in 1:1 H_2O : CH_3CN (~10^{-4} M, argon purged, 2 lamps, 2 minutes) gives a conversion of 38% with a product ratio of 34% **61** and 2% **59** and 2% oligomeric products as judged via ^{1}H-NMR($CDCl_3$). A Deuterium / Hydrogen ratio was determined to be 1.6 for this run. Irradiation for 5 minutes results in a conversion of 84% with a product ratio of 75% **61** and 4% **59** and 5% oligomeric products. A Deuterium / Hydrogen ratio was determined to be 1.4 for this run. Data on the photolysis of **47-αD** is summarized in Table 2.9.

Photolysis of 48

Irradiation of **48** in 1:1 H_2O : CH_3CN (pH 2)(1.5 x10^{-4} M, argon purged, 2 lamps, 2 minutes) gives a conversion of 37% with a product ratio of 32% **72** and 5% **73** and no oligomeric products as judged via ^{1}H-NMR spectroscopy. Irradiation of **48** with 4 lamps for 5 minutes results in 100% conversion with a product ratio of 89% **72** to 11% **73** as judged via ^{1}H-NMR spectroscopy.

Photolysis of **48** in 1:1 H_2O : CH_3CN (pH 2)(1.5 x10^{-4} M, oxygen purged, 4 lamps, 5 minutes) gives a conversion of 38% with **73** as the only product.

Photolysis of **48** was accomplished at many different irradiation times and conditions. This data on the photolyses of **48** is summarized in Table 2.5.

Photolysis of 49-αD

Irradiation of **49-αD** in 1:1 H_2O : CH_3CN (pH 2)(1.1 x10^{-4} M, argon purged, 2 lamps, 2 minutes) gives a conversion of 31% with a product ratio of 13% **49** and1% **60** and 18% oligomeric products as judged via ^{1}H-NMR spectroscopy.

Irradiation of **49-αD** in 1:1 H_2O : CH_3CN (pH 7)(1.1 x10^{-4} M, argon purged, 2 lamps, 5 minutes) gives a conversion of 16% with a product ratio of <1% **49** and 3% **60** and 13% oligomeric products as judged via ^{1}H-NMR spectroscopy.

Photolysis of **49-αD** was accomplished at different irradiation times and conditions. This data on the photolysis of **49-αD** is summarized in Table 2.6.

Photolysis of 49

Irradiation of **49** in 1:1 D_2O : CH_3CN (pD 2)(1.1 x10^{-4} M, argon purged, 2 lamps, 2 minutes) gives a conversion of 31% with a product ratio of 13% **49** and1% **60** and 18% oligomeric products as judged via ^{1}H-NMR spectroscopy. Separation of the product mixture by preparative TLC yielded pure **49-αD** and **60** as well as other unidentified oligomeric products.

49-αD: ^{1}H-NMR (500MHz, $CDCl_3$) δ:7.84 (t, 2H, 1.8 Hz), 7.74 (dd, 2H, 8.2 Hz and 1.4 Hz), 7.65 (dt, 1H, 7.6 Hz and 1.5 Hz), 7.60 (dt, 1H, 7.7 Hz and 1.6 Hz), 7.56 (tt, 1H, 7.5 and 1.3 Hz), 7.46-7.40 (m, 3H), 7.37-7.35 (m, 2H), 7.34-7.31 (m, 2H), 7.28-7.24 (m, 1H).^{13}C NMR ($CDCl_3$, 125 MHz) δ: 196.87, 144.37, 143.60, 137.81, 137.61, 132.68, 130.65, 130.27, 129.46, 128.83, 128.60, 128.45, 128.21, 128.01, 126.72; MS (EI) *m/z*; 289 (M+, 40), 286 (M^+, 45), 273 (40), 209 (80), 196 (35), 184 (100), 166 (40), 152 (20);

Photolysis of 50

Irradiation of 11.4 mg **50** in 300 mL of 1:1 H_2O : CH_3CN (pH 2)(1.7 x10^{-4} M, argon purged, 2 lamps, 2 minutes) resulted in a conversion of 41% with a product ratio of 1% **59** and 40% other products. Many products were formed, assumed to be radical in origin.

Photolysis of **50** was accomplished at different irradiation times and conditions. This data on the photolysis of **50** is summarized in Table 2.4.

Photolysis of 52

Irradiation of 10.2 mg **52** in 300 mL 1:1 H_2O : CH_3CN (pH 2)(1.6 x10^{-4} M, argon purged, 2 lamps, 2 minutes) resulted in a conversion of 7% with a product ratio of 0% **63,** 1% **64** and 6% oligomeric side products.

Irradiation of the same concentration using 4 lamps and 5 minutes of irradiation resulted in 27% conversion with a product ratio of 3% **63,** 1% **64** and 23% oligomeric side products.

Photolysis of **52** was accomplished at different irradiation times and conditions. This data on the photolysis of **52** is summarized in Table 2.3.

Photolysis of 61

Irradiation of 49.6 mg **61** in 100 mL 1:1 H_2O : CH_3CN (pH 2) (2.4 x10^{-3} M, argon purged, 8 lamps, 10 minutes) This yielded no identifiable products and is essentially photoinert. Some trace additional aromatic peaks were visible via ^{1}H-NMR ($CDCl_3$).

Photolysis of **61** at 1.2 x 10^{-3} M in 100 mL 1:1 H_2O : CH_3CN (pH 2) using 4 lamps for 5 minutes also yielded no identifiable products. Some additional aromatic peaks were visible via ^{1}H-NMR spectroscopy

Photolysis of 59

Irradiation of **59** in 1:1 H_2O : CH_3CN (pH 2)(10.0 mg/100 mL (1.2 x 10^{-3} M), argon purged, 4 lamps, 5 minutes) This yielded no identifiable products. Some additional aromatic peaks were visible via ^{1}H-NMR spectroscopy.

2.4.4.3 UV-Vis Studies

Using 1 cm quartz cuvettes or quartz fluorescence cells, solutions were prepared by filling with 3 mL of the appropriate solvent mixture and spiking with 1-30 μL of concentrated solution of substrate in acetonitrile to get the desired OD. Final concentrations are ~10^{-6} to 10^{-5} M. Cuvettes were then bubbled using fine needles through septa with argon or nitrogen for 15 minutes to remove any dissolved oxygen. Parafilm was then placed over the septa before the UV-vis traces were performed.

Following the semi-preparative photolysis run via UV-vis used the following technique. The semi-preparative solution was prepared as for a typical photolysis run to concentrations of ~1.5 x 10^{-4} M. The photolysis run was stopped periodically and aliquots removed. These were then diluted precisely and UV-vis spectra obtained.

2.4.4.4 Laser Flash Photolysis (LFP)

Laser flash photolysis was performed in the University of Victoria LFP facility using an excitation wavelength of 266 nm (pulse width ≈ 20 ns) using a Nd-YAG Spectra Physics laser (GCR-11), power kept under 25 mJ / pulse using attenuation of power.

The LFP spectra were collected using a flow cell containing 1:1 H_2O : CH_3CN purged with N_2 prior to excitation for 15 minutes. The flow cell consisted of a chamber consisting of ~100 mL of solution containing substrate of ~10^{-5} M with an OD = 0.4 at 266 nm determined by UV-vis. From the flow chamber the solution was pumped continuously into a 7 mm x 7 mm quartz cell at flow rates of ~1.5 mL / min.

Spectra were obtained by plotting the absorbance value at a fixed time after laser excitation for a given wavelength and repeating for other wavelengths at 10 or 20 nm increments across the UV-vis region (280 nm – 700 nm). Multiple shots (4 to 10) were taken and averaged before plotting. Four different time windows were examined to yield data at various times after excitation. This allowed simultaneous generation of spectra at four different times. Windows were selected to illustrate important points in the decay of the transient.

Decay data was obtained by measuring 500 absorbance points at equivalent time intervals within a chosen time scale. Time scales used varied between 50 ns and 1 ms. Lifetimes were determined from fitting of the exponential decay. Polyexponential decays were estimated by fitting different regions of the decay with monoexponential fitting.

2.4.4.5 Reaction Quantum yields

Reaction Quantum yields (Φ) were obtained for **47**, **48** and **49**. The photoredox reaction of 2-(hydroxymethyl)anthraquinone (**42**) was used as a secondary standard to determine the quantum yields. Intramolecular photoredox reaction of **42** (1.5×10^{-4} M) was observed on irradiation in 1:1 pH 7 H_2O : CH_3CN solution ($\Phi = 0.8$)[83] (Eqn. [1.19]). The quantum yields for all benzophenone derivatives (**47**, **48**, and **49**) were determined in solutions of 1:1 pH 2 H_2O : CH_3CN at the same concentration (1.5×10^{-4} M) and the same degree of photolysis (two 300 nm lamps for 2 minutes) by comparing the photoredox conversion compared to the photoredox conversion observed for **42**. Φ was

determined to be 0.60 ± 0.05 for **47**, 0.63 ± 0.05 for **48** and 0.30 ±0.05 for **49-αD**. These values were obtained from the average of three trials.

As the photoredox reaction is highly dependent on pH each quantum yield is dependent on the pH at which the substrate was photolysed and comparisons of quantum yield must take that into account. Also the lower value of 0.30 for the quantum yield for **49-αD** reflects the increased amounts of oligomeric side-products that correspondingly decrease the production of the photoredox product. If the loss of substrate were compared instead, all three substrates (**47**, **48** and **49**) have approximately the same quantum yield.

Chapter 3
Intramolecular Photoredox Reactions of Xanthone and Fluorenone Derivatives

3.1 Introduction

As the photophysical and photochemical behaviour depends in part on the relative energy levels of the electronically excited states it is important to explore this aspect in some detail for the photoredox reactions discovered in this Thesis. The relative energy levels of the singlet and triplet electronically excited states vary widely between compounds with different chromophores. Previous research into an alternative chromophore, anthraquinone, has already been presented in Section 1.8 and its relation to the benzophenone analogue discussed in Section 2.2.5.[83] Like the benzophenone system explored in detail in this Thesis, the anthraquinone analogue **42** also undergoes photoredox chemistry. This photochemistry was reviewed in Section 1.8. The anthraquinone system differs from the benzophenone system in that the photoredox reaction is quite efficient under neutral conditions and does not form any noticeable oligomeric sideproducts.

The major structural difference between benzophenone and anthraquinone is that in benzophenone the two rings may be viewed as being more separated, where in anthraquinone the two phenyl rings are rigidly affixed by two ketone moieties. This has the effect of planarizing the entire aromatic system, unifying the two benzene rings into a single chromophore. By exploring alternative structural methods of fixing the rings while retaining the carbonyl in a consistent position it was hoped that further insights into the intramolecular photoredox reaction would be obtained. The two additional chromophores

chosen for study in this Thesis were the xanthone moiety and the fluorenone moiety. The hydroxymethyl analogues were respectively 2-(hydroxymethyl)xanthone (**53**) and 2-(hydroxymethyl)fluorenone (**54**). The xanthone moiety binds the two phenyl rings with an oxygen to create a six membered ring, while the fluorenone directly attaches the phenyl rings to yield a five membered ring.

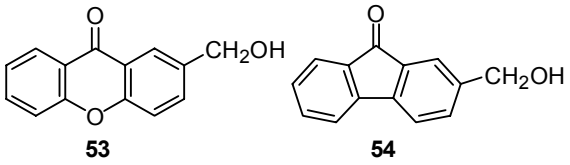

53 **54**

Figure 3.1 Compounds explored in Chapter 3

This structural difference leads to significantly different photophysical and photochemical behaviour. Insight into the photobehaviour may be gained by examining the nature of the lowest energy singlet and triplet excited states. The electronic states are affected by solvation to a greater or lesser extent depending on solvent polarity. The solvent polarity has a great effect on the energy levels of the electronic states of both fluorenone and xanthone.

Xanthone is very sensitive to the solvent media polarity. In nonpolar solvents, such as carbon tetrachloride, xanthone is very reactive towards 2-propanol in hydrogen abstraction reactions. This is symptomatic of ^{3}n,π* character. The reactivity decreases significantly when reacted in neat 2-propanol, suggesting that the ^{3}π,π* becomes lower in energy under those conditions.[98] This decrease in reactivity towards hydrogen abstraction to form the ketyl radical is combined with a concomitant increase in reactivity towards hydride donors such as $NaBH_4$ to form non-ketyl radicals of the cyclohexadienyl type.[95] This is consistent with reaction with the ^{3}π,π* state. In the absence of a hydride

donor, the xanthone triplet electronically excited state has a relatively long lifetime. These data along with triplet-triplet absorption maxima exhibiting pronounced hypsochromic shifts[98] as the solvent polarity increases led many researchers to conclude that in nonpolar solvents the lowest triplet state was n,π* but that in polar solvents the lowest triplet excited state was π,π*.[96,97] This exchange of states was explained as arising from the increased stabilization of the π,π* triplet excited state observed in polar solvents.

The π,π* state can be stabilized in polar media because it has a larger dipole moment than the ground state[98] whereas the n,π* state has an increased energy in polar media because it has a smaller dipole moment than the ground state.[36] Because of the small energy gap between T_1 and T_2, a switch between n,π* and π,π* is possible. Subsequent work by Connors *et al*[99] suggested that instead of a complete exchange of energy levels in the nonpolar solvents, the T_1 (π,π*) and T_2 (n,π*) states are close enough in energy that thermal exchange occurs and that at room temperature sufficient occupation of the T_2 (n,π*) state exists that the spectroscopic evidence of a lowest state being n,π* may be observed (via the observation that the absorption spectrum blueshifts in polar solvents). This interpretation was consistent with the temperature dependence observed in the change in phosphorescence spectrum by Pownall.[96] These two interpretations are presented in Figure 3.2.

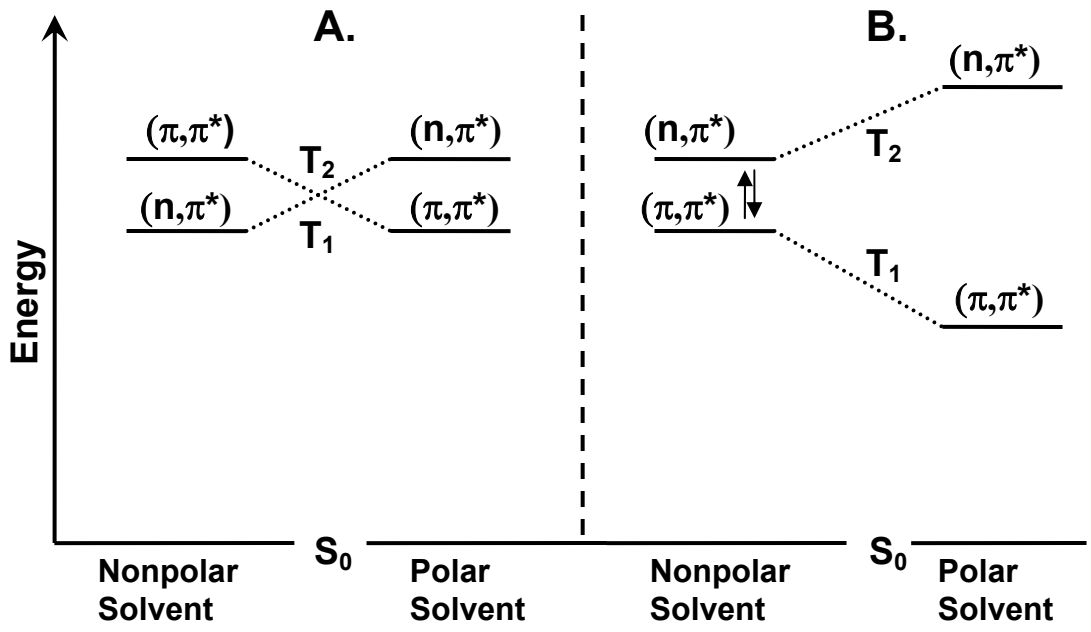

Figure 3.2 Effect of solvent polarity on the $T_1$and T_2 electronically excited states for xanthone (adapted from reference 99). Interpretation **A.** is presented in reference 96, **B.** is presented in reference 99.

Comparison of the electronically excited states of fluorenone (Figure 3.3) shows the lowest singlet electronically excited state (S_1) to be very close in energy to an upper triplet electronically excited state (T_3) when in nonpolar solvent media. The T_3 excited state (n,π*) is stabilized by nonpolar solvents and electron withdrawing groups.[100] This stabilization results in the energy level of the T_3 excited state being lower than that of the S_1 excited state. In addition, the S_1 and T_3 excited states become relatively close in energy and consequently efficient ISC is observed in nonpolar solvents. By contrast, in polar solvents the T_3 state is not involved as it is higher than the S_1 state and the energy difference between the S_1 and the next lowest triplet state, T_2 is much greater. This results in a much smaller ISC and increased fluorescence quantum yields and lifetimes in

polar solvents than in nonpolar solvents. When water is used as the solvent, very low ISC is observed but fluorescence is also minimized ($\Phi_F < 1.5 \times 10^{-4}$).[97]

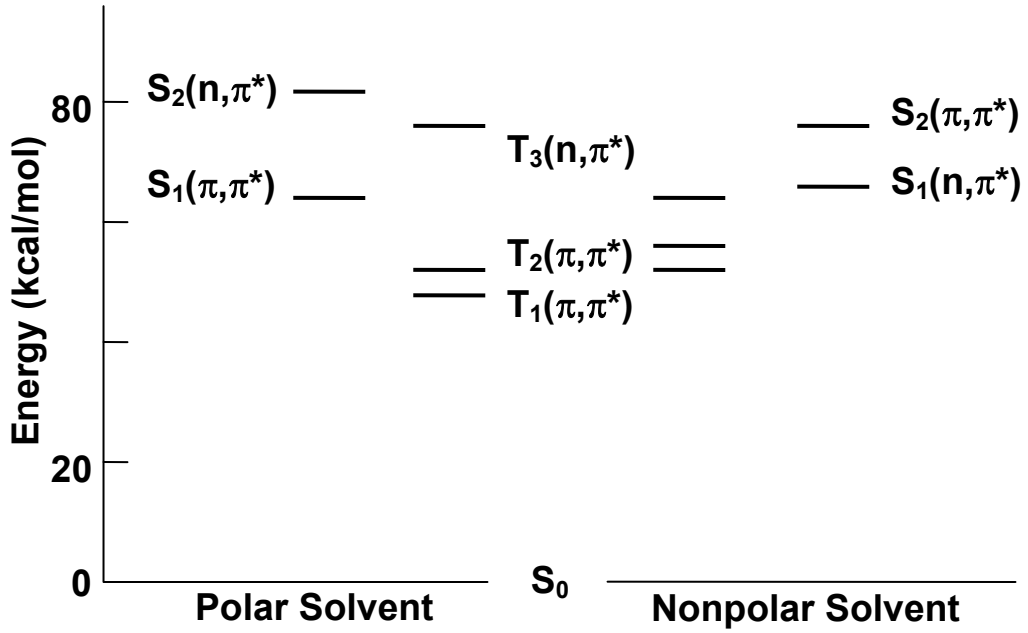

Figure 3.3 Energy level diagram for fluorenone in polar and nonpolar solvents (adapted from reference 100)

In addition hydrogen bonding solvents are known to inhibit triplet formation and quench fluorescence.[101,102] This has been attributed to the intermolecular hydrogen bond between the hydroxyl proton of the solvent and carbonyl oxygen of fluorenone. The intermolecular hydrogen bond enhances the internal conversion rate constant thus decreasing both the fluorescence and the intersystem crossing. Thus in the solvent media used in this Thesis (1:1 H_2O : CH_3CN) it is expected that fluorenone will not exhibit significant ISC and may consequently be relatively photoinert.

3.2 2-(Hydroxymethyl)xanthone (53)

3.2.1 Results and Discussion

3.2.1.1 Synthesis and Materials

As **53** was not available for purchase it had to be synthesized. In order to capitalize on the previously used synthetic technique of bromination followed by hydrolysis to produce the alcohol, the 2-methylxanthone (**96**) first needed to be obtained. As this is not available commercially, it too needed to be synthesized. The synthesis of **96** was accomplished in relatively large yield (4.5 grams formed) using a literature preparation.[103] The synthesis proceeded via a modified Ullmann reaction to form the coupled intermediate **95** before cyclization to form **96** (shown in Eqn [3.1]). This reaction used heavy mineral oil as a solvent and required fairly extreme conditions (200 ^{o}C) so care had to be taken to prevent a fire.

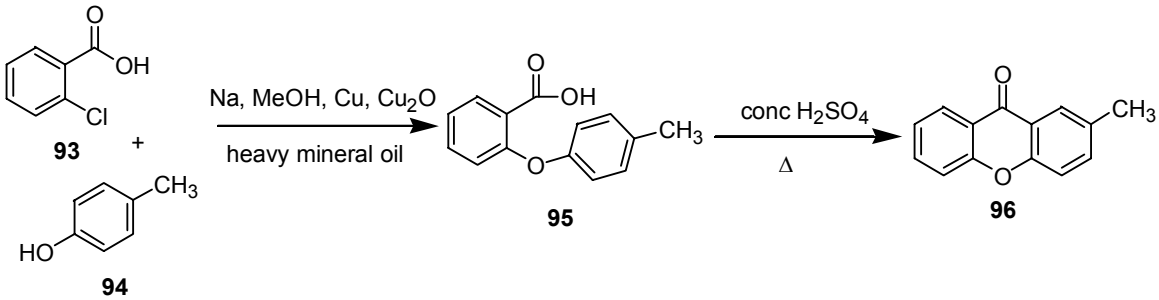

[3.1]

The formation of **96** allowed direct access to **53** via N-bromosuccinimide bromination and hydrolysis (shown in Eqn [3.2])

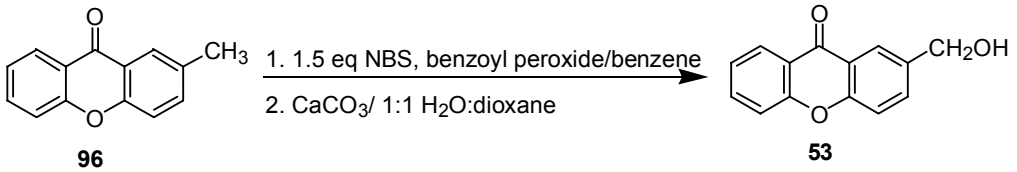

[3.2]

3.2.1.2 UV-Vis and Product Studies

If the photoredox reaction of **53** proceeds via the same mechanism as for **47** the reaction should result in the redox product **97** and some residual oxidation product **98** according to Eqn [3.3]. However this turns out not to be the case. Instead, when **53** was photolysed in 1:1 H_2O : CH_3CN with a pH of 2, the product mixture (Figure 3.4) shows

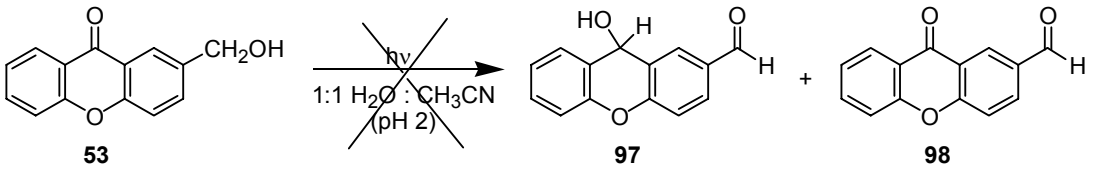

[3.3]

that only **98** was recovered along with a significant amount of oligomeric product (Eqn. [3.4]). A possible trace amount of **97** may be observable as the additional aldehyde observed in Figure 3.4 but the benzhydrol peak is missing suggesting that that assignment is questionable.

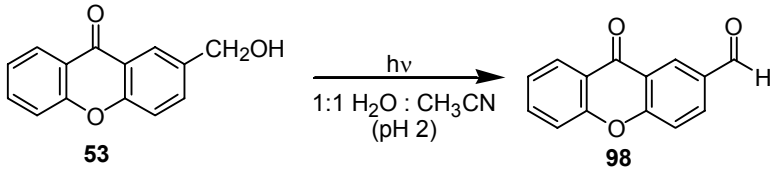

[3.4]

The photoreaction was, however, more efficient compared to the photolysis of the benzophenone derivative **47** (55% conversion from **53** compared to 41% from **47** under the same conditions and with the same concentration).

Although the photoredox reaction of **47** is inefficient at pH 7, the increased efficiency of the conversion from **53** suggests that investigation into the photobehaviour of **53** at pH 7 may prove fruitful. It was thought that perhaps the photoredox reaction product **97** was not stable under acidic conditions and may consequently be observed under neutral photolysis conditions.

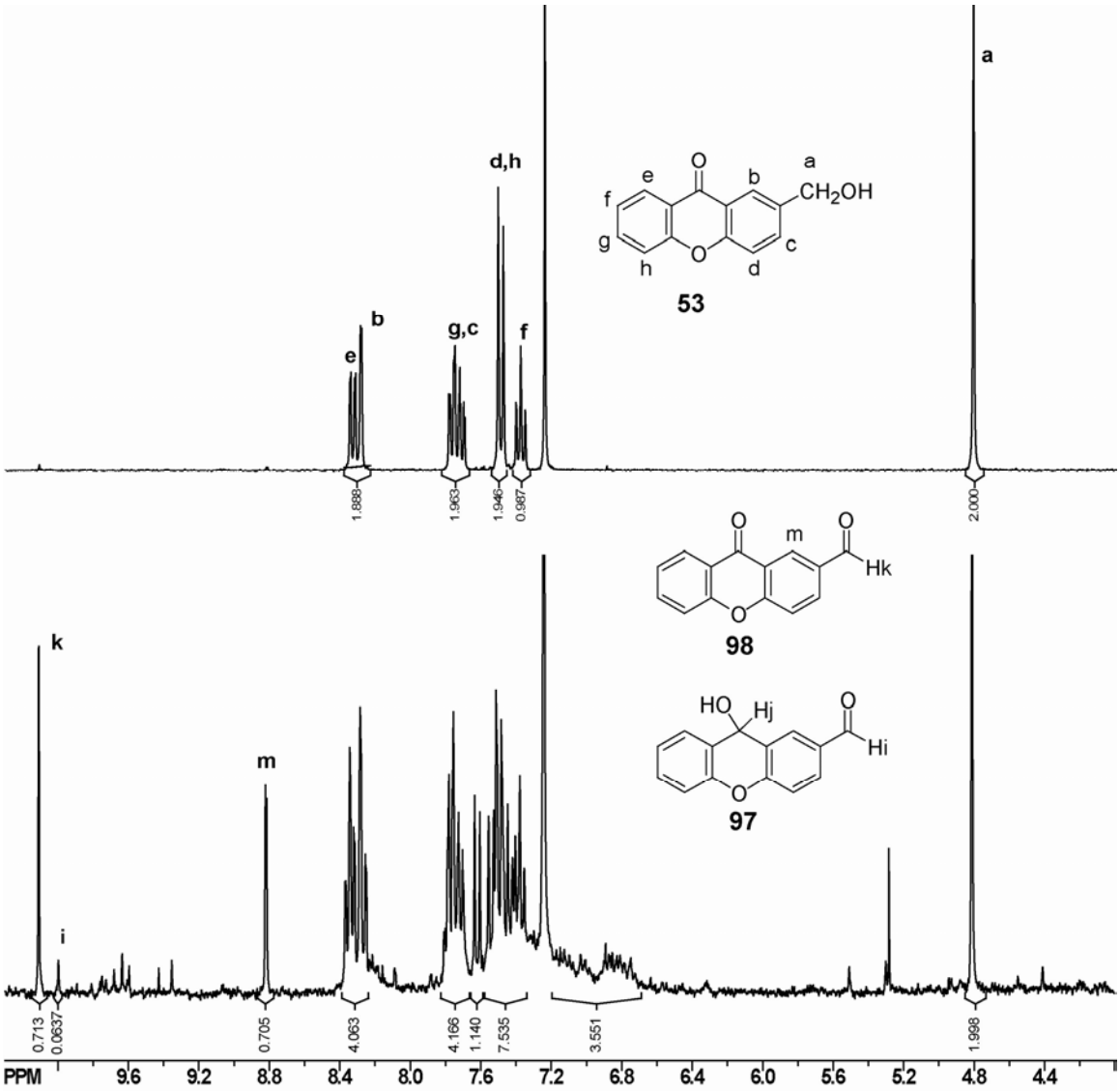

Figure 3.4 300 MHz ^{1}H-NMR spectra of **53** (in chloroform-*d*) before (top) and after (bottom) photolysis (1.6 x 10^{-4} M, 10.7 mg/300 mL) in 1:1 H_2O : CH_3CN (pH 2), for 2 minutes with two 300 nm lamps (argon purged). Product ratio: 44% **53**: 3% **97**: 31% **98**: 22% oligomeric product. Product ratio was determined by comparing the integrations for the peak due to the aldehyde of **97** (**i**: 9.98 ppm, 0.064H) to the singlet (**a**: 4.80 ppm, 2.0H) and the singlet due to the aldehyde of **98** (**k**: 10.10 ppm, 0.71H).

The photolysis reaction of **53** was followed at pH 7 by taking UV-vis spectral traces in a manner similar to that performed for **47** in Chapter 2. There were however notable differences in the behaviour of **53** when compared with **47**. Initial examination of

the UV-vis spectrum of **53** shows significant complexity compared to **47**. This complexity is observed in the initial trace of the spectra shown in Figure 3.5. Whereas **47** had one major band and one minor band **53** has the four bands typical of xanthones. This is an indication of the rigidity inherent within the xanthone system compared to the benzophenone system.

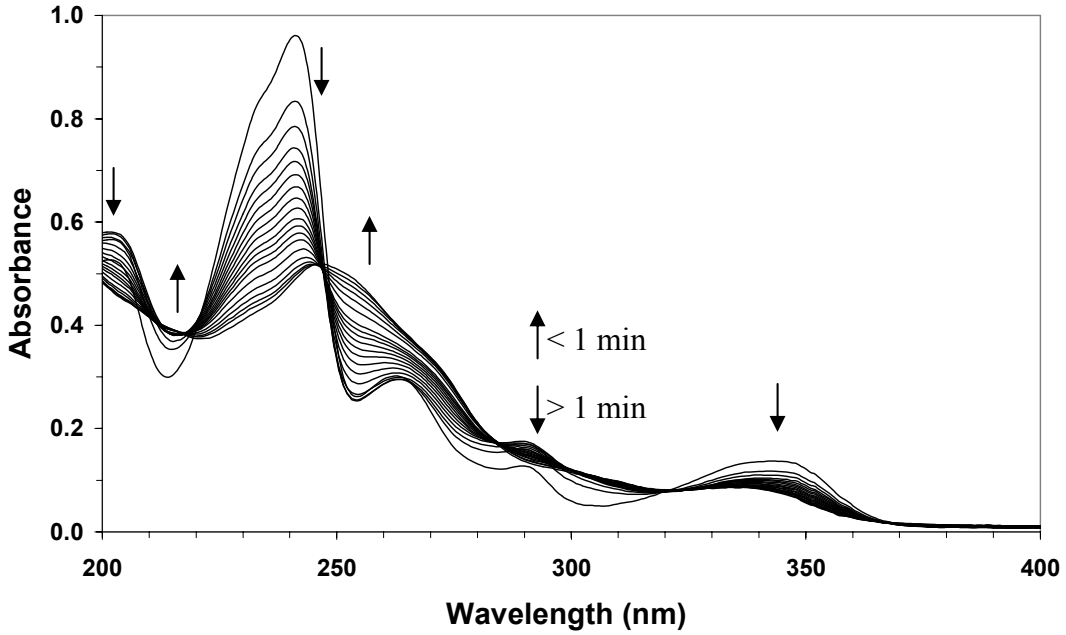

Figure 3.5 UV-vis spectral traces observed on photolysis of **53** in 1:1 H_2O : CH_3CN (pH 7). Irradiation was accomplished at 300 nm using four lamps (7.9×10^{-6} M). Initial traces are taken after 15 seconds with later traces taken after 1 or 2 minutes. Final trace is consistent with the UV-vis spectrum of **98**.

Closer examination of the peak at 290 nm shows a reversal of the trend after about 1 minute of photolysis. Initially, growth of the band at 290 nm was observed but the growth reaches a maximum at 1 minute after which the peak decays. The UV-vis trace should consequently be presented as two figures, one showing the behaviour before one minute (Figure 3.6) and the other showing the subsequent behaviour (Figure 3.7).

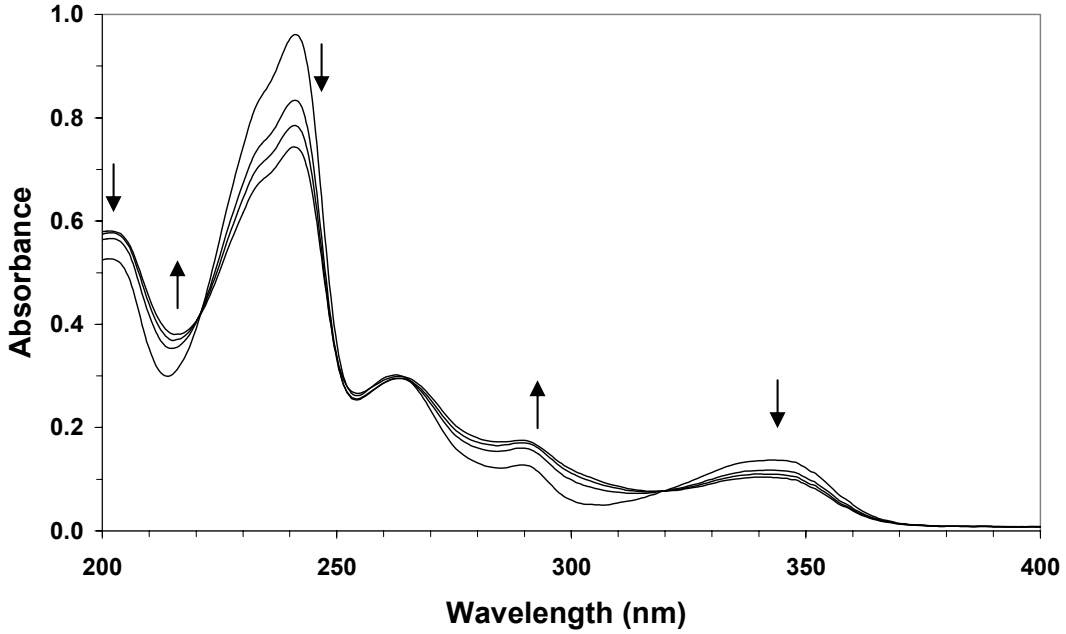

Figure 3.6 UV-vis spectral traces observed on photolysis of **53** in 1:1 H_2O : CH_3CN (pH 7). Irradiation was accomplished at 300 nm using four lamps (7.9×10^{-6} M). Traces are shown here from 0 second to 1 minute with intervals of 15 seconds irradiation.

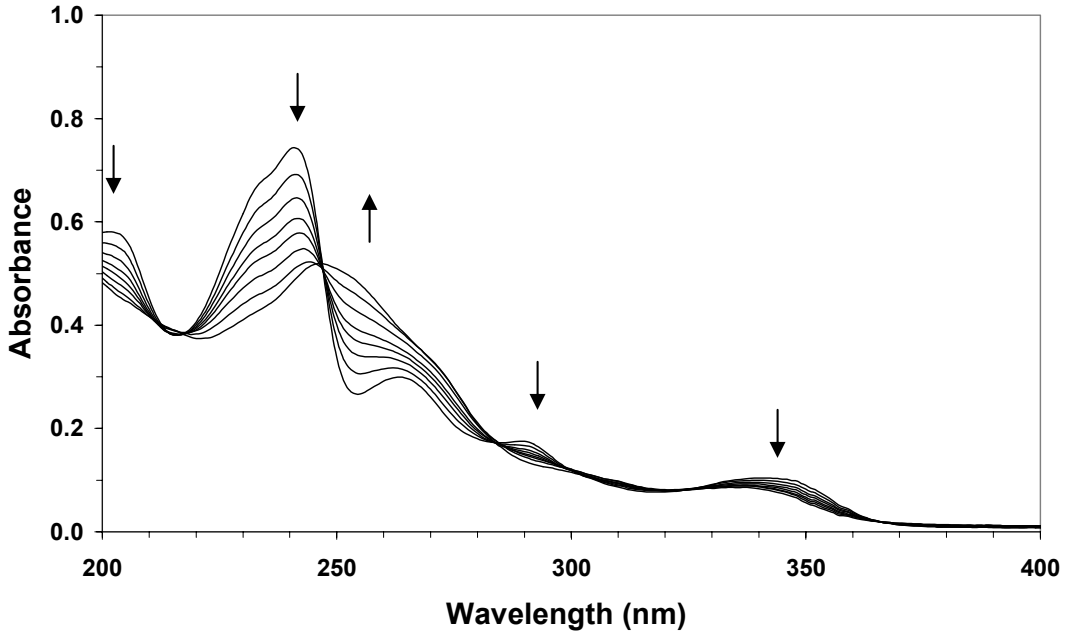

Figure 3.7 UV-vis spectral traces observed on photolysis of **53** in 1:1 H_2O : CH_3CN (pH 7). Irradiation was accomplished at 300 nm using four lamps (7.9×10^{-6} M). Traces shown from 1 minute with photolysis time of 2 minutes between traces (after 10 minutes photolysis times increase).

The changing UV-vis spectral traces indicate that there is more than one product being formed. The photobehaviour is evidently more complicated than a straightforward photoredox conversion. Apparently there is initial formation of one compound before subsequently proceeding towards another compound.

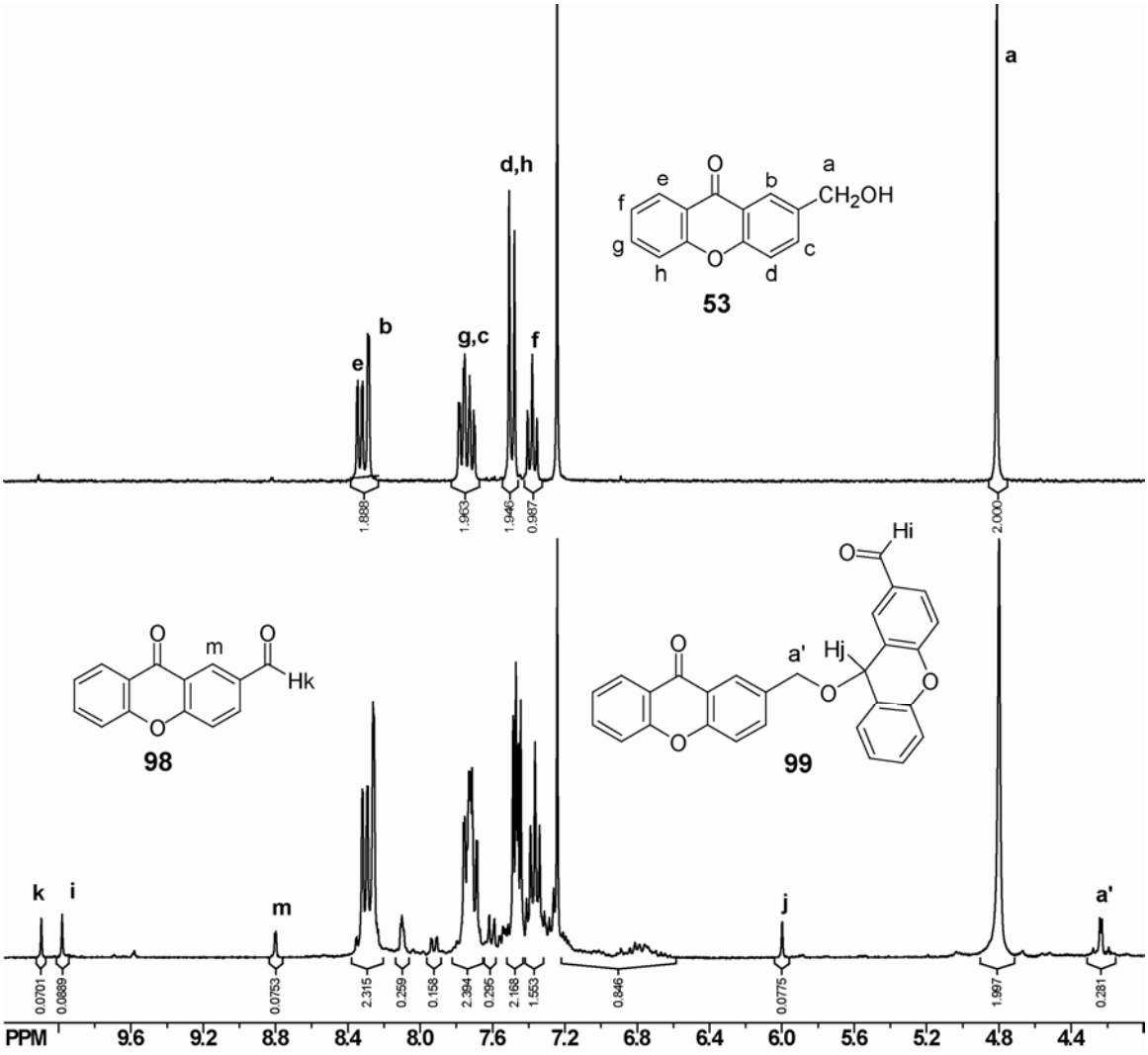

Figure 3.8 300 MHz ^{1}H-NMR spectra of **53** (in chloroform-*d*) before (top) and after (bottom) photolysis (1.6 x 10^{-4} M, 10.7 mg/300 mL) in 1:1 H_2O : CH_3CN (pH 7), for 5 minutes with four 300 nm lamps (argon purged). Product ratio: 78% **53**; 7% **99**; 5% **98**; 10% oligomeric product. Product ratio was determined by comparing the integrations for the peak due to the aldehyde of **99** (**i**: 9.98 ppm, 0.090H) to the singlet (**a**: 4.80 ppm, 2.0H) and the singlet due to the aldehyde of **98** (**k**: 10.10 ppm, 0.070H).

Unlike the photobehaviour of **47** at pH 7 (simple photodecomposition observed in the UV-vis spectral trace), the photobehaviour of **53** under neutral conditions is more complicated and bears further investigation.

When photolysed in 1:1 H_2O : CH_3CN at low conversion the photoredox reaction resulting in both **97** and **98** appears to be occurring. The expected photoredox reaction is shown in Eqn. [3.5]. Closer inspection of the apparent redox product present in the ^{1}H-NMR spectrum of the product mixture (Figure 3.8) shows several additional peaks at δ: 4.3 ppm which are not assignable to either **98**, **97** or **53**.

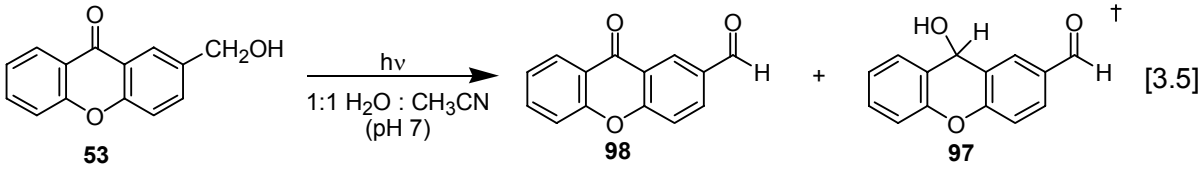

53 **98** **97** [3.5]

†redox product does not have this structure

The isolated product mixture (^{1}H-NMR spectrum shown in Figure 3.8) is consistent with the condensed product **99**, whose origin may be rationalized as deriving from the nucleophilic attack of **53** upon the redox product **97** (Scheme 3.1). The additional peaks observed at δ: 4.3 ppm are attributable to the diastereotopic benzylic protons. It is unknown whether this reaction proceeds via SN_1 or SN_2 mechanism but it could be argued that the exceptional stability of the carbocation **100** buttresses the argument in favour of the SN_1 mechanism. The stability of **100** arises from the aromaticity of the central ring. This would promote the loss of hydroxide, even under neutral conditions.

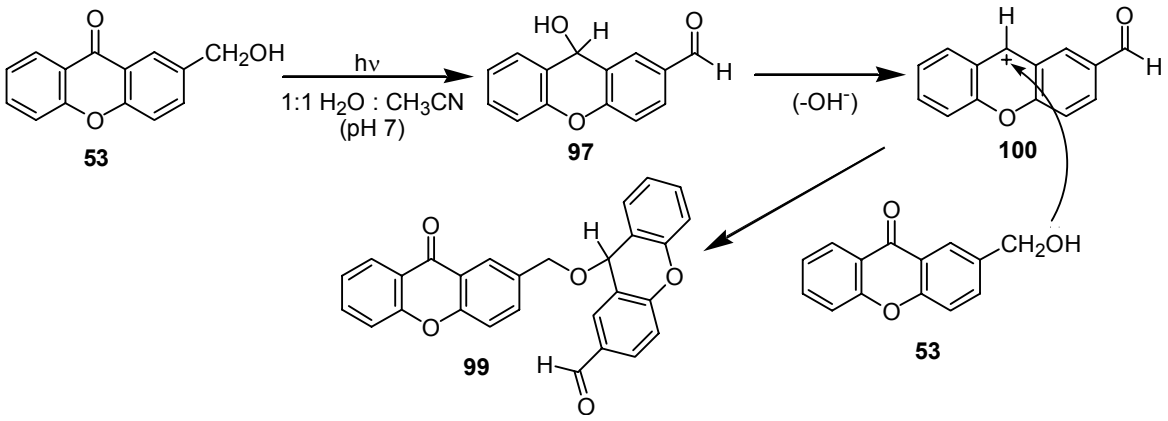

Scheme 3.1

This condensation reaction resembles that observed for **47**, described in Section 2.2.2.7. Although the behaviour is similar, the conditions under which this reaction occurs are quite different. While the parent benzophenone only condenses when under highly acidic conditions (5% H_2SO_4), **53** condenses at pH 7. The likely explanation is due to the more stable intermediate **100**. Compound **47** does not have a corresponding stable cation so must first protonate the hydroxyl group (Scheme 2.2).

It is interesting to note that **99** is only observed under relatively low photoconversions. Further irradiation decreases the ratio of **99** : **98** and the proportion of product mixture attributable to **99**. The most likely situation is that photolysis of **99** results in **98**. Although isolation proved difficult due to the necessarily low conversion and the similarity in polaritities with both **98** and **53**, isolation of a small quantity was obtained via preparative TLC. Photolysis of this isolated **99** resulted in **98** being formed. Compound **99** is not stable over time and decomposes into **98** and **53** upon standing for less than a week. It is uncertain whether the action is due to the presence of oxygen or due to residual light. Because the final product is an oxidation product the possibility of

oxidation of **99** by oxygen is quite plausible, especially as the benzhydrol proton on the central ring should have a relatively weak C-H bond (Eqn [3.6]).

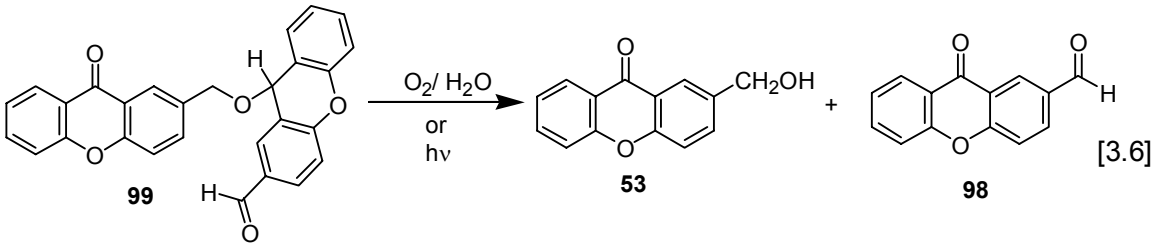

[3.6]

As **99** is not present at higher photoconversions, the photobehaviour observed for **53** at pH 2 is consistent with the photobehaviour observed at pH 7. Photolysis of **53** in pH 2 solution results in only **98** as the conversions are considerably higher in more acidic solutions. This is consistent with the acid-catalysis observed for the benzophenone analogue **47**, presented in detail in Section 2.2.2.7.

Table 3.1 Photoproduct studies for **53**[a,b]

Photolysis time, 300 nm lamps	pH	% **53**	%**99**	%**98**	%OP[c]
4 lamps, 5 min	2[d]	31	0	28	41
4 lamps, 2 min	2[d]	38	0	53	8
2 lamps, 2 min	2	44	3	31	22
2 lamps, 2 min	7	82	5	2	11
4 lamps, 5 min	7	78	7	5	10
8 lamps, 10 min	7	69	4	11	16

[a]Using **53** at 1.6 x 10^{-4} M(10.7 mg / 300 mL) in 1:1 H_2O : CH_3CN, pH adjusted with H_2SO_4.
[b]Product mixture ratio determined by integration via ^{1}H-NMR($CDCl_3$).
[c]Oligomeric side product approximate, estimated from integration via ^{1}H-NMR($CDCl_3$) (δ: 6.8-7.2ppm).
[d]Solvent ratio of 5:1 H_2O : CH_3CN

3.2.1.3 Nanosecond Laser Flash Photolysis (LFP)

The structural similarities between xanthone and benzophenone suggest that the triplet - triplet absorption spectra should be similar. This is indeed the case. The LFP spectrum of **47** resulted in 2 bands, one at 320 nm and one at 525 nm and was shown in Figure 2.17. By comparison, LFP of **53** led to the spectrum shown in Figure 3.9 and features two bands, one at 300 nm and one at 600 nm. This is consistent with the triplet state characterized by Wilkinson and Garner for xanthone which observed a λ_{max} at 590 nm in aqueous solutions and a lifetime of 17.9 μs.[104,105,106] The ketyl radical (λ_{max} =475) is only weakly present in aqueous solution.

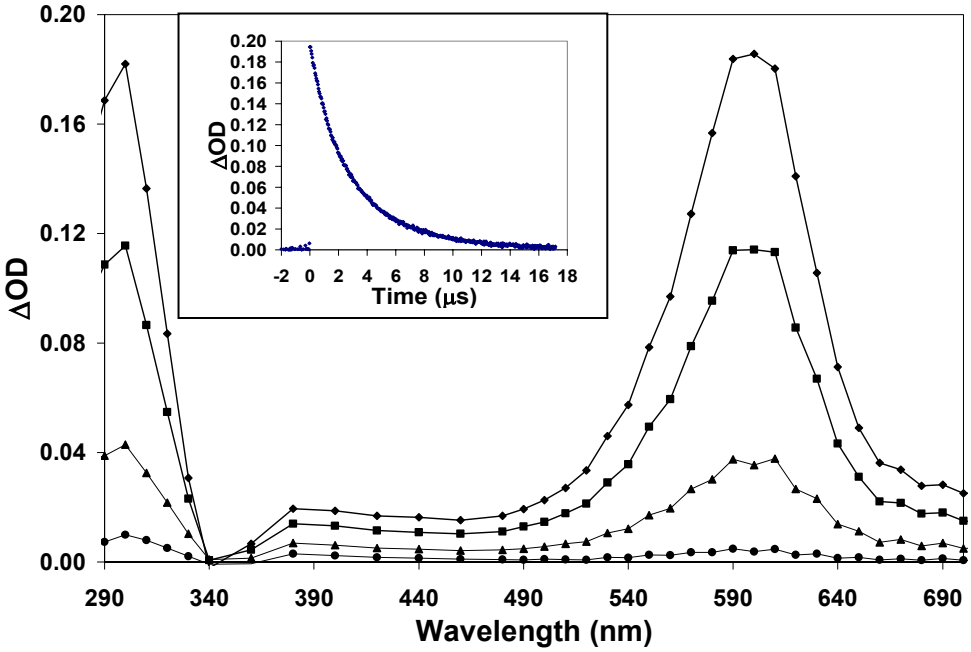

Figure 3.9 Triplet-triplet absorption spectrum observed on LFP (λ_{ex} 266 nm) of **53** in 1:1 H_2O : CH_3CN (pH 7), using a flow cell with continuous N_2 purging. The four spectra are taken at the following intervals: immediately after the laser pulse, after 2 μs, after 6 μs and after 15 μs. Inset is the decay trace taken at 600 nm.

In order to study the effect of the solvent on the lifetime of the triplet, LFP was performed in 1:1 H_2O : CH_3CN (pH 7) and in acetonitrile and the spectra and lifetimes compared. A significant shift in the peak of the band at 600 nm occurs when **53** is photolysed in pure acetonitrile. The band exhibits a bathochromic shift from 600 nm to 630 nm. This significant shift may indicate the stabilization of the π,π^* transition over the n,π^* transition, as the n,π^* transition generally shows hypsochromic behaviour due to a decreased dipole of the n,π^* excited state relative to the ground state.[99,107]

The triplet decays for both bands in 1:1 H_2O : CH_3CN (pH 7) are mono-exponential and both have triplet lifetimes of 2.9 μs. When the solvent is altered to pure acetonitrile the triplet decays are still monoexponential with similar lifetimes of 2.1 μs for both bands. The slightly shorter decay for the pure acetonitrile is consistent with the results found by Scaiano for xanthone.[98] Because **53** has additional benzylic protons additional reaction pathways become available towards the formation of oligomeric products shortening the triplet lifetime compared to xanthone. Other substituted xanthones[108] exhibit lifetimes in the 5 μs range so values of 2-3 μs are reasonable.

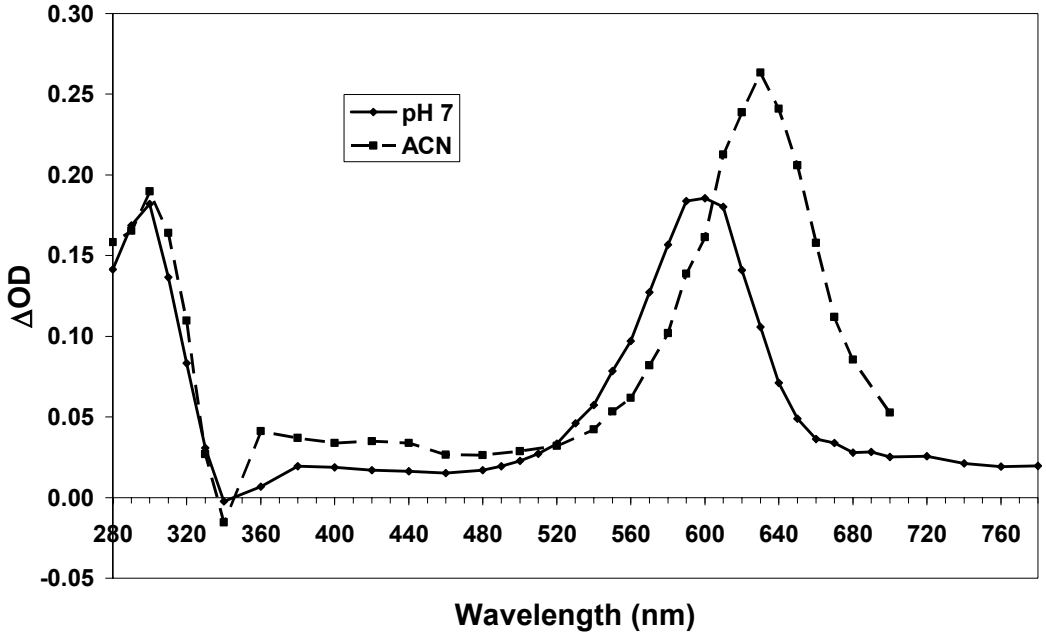

Figure 3.10 Triplet-triplet absorption spectrum observed on LFP (λ_{ex} 266 nm) of **53** in 1:1 H_2O : CH_3CN (pH 7) and pure CH_3CN (ACN), using a flow cell with continuous N_2 purging.

Supporting the identification of the transient as being a triplet excited state is the fact that significant quenching is observed upon purging with oxygen. The lifetime of **53** was found to be 120 ns in 1:1 H_2O : CH_3CN (pH 7) under O_2 purging and ~ 20 ns in CH_3CN under O_2 purging. The differences may be explained by comparing the different oxygen concentrations in the two solvent mixtures. The concentration of oxygen in a oxygen saturated acetonitrile solution is 9.1 mmol/L while it is 1.27 mmol/L in water.[109] As the acetonitrile solution has a higher concentration of dissolved oxygen it is expected that the the lifetimes will be shorter in pure acetonitrile than in a water – acetonitrile solution.

Table 3.2 Lifetime Comparison of **53** in Differing Solvent Media[a]

pH 7	300 nm (μs)	600 nm (μs)	CH_3CN	300 nm (μs)	630 nm (μs)
N_2	2.9	2.9	N_2	2.1	2.1
O_2	0.12	0.12	O_2	0.025	0.021

[a] Lifetimes were obtained by exponential fitting of decay traces in 1:1 H_2O : CH_3CN, (pH 7) or pure CH_3CN, N_2 or O_2 purged; fitting was monoexponential; $[O_2]_{acetonitrile} = 9.1 \times 10^{-3}$ M; $[O_2]_{water} = 1.27 \times 10^{-3}$ M.

3.2.1.4 Proposed Mechanism

The mechanism of reaction for the photoredox behaviour of **53** is expected to proceed via a similar pathway to that of the benzophenone analogue **47** and the proposed mechanistic scheme (Scheme 3.2) is essentially the same as that proposed for **47** in Chapter 2. As for the mechanism of **47**, the main parts inherent in the reaction pathway of **53** are: (1) protonation of the carbonyl oxygen; (2) promotion of deprotonation of the benzylic group in the *meta* position; (3) electron transfer; and (4) subsequent protonation and deprotonation to yield the final redox product.

The acid catalysis present in the photoredox behaviour of benzophenone derivatives is expected to be prevalent with the xanthone chromophore as well because it is a general function of aromatic ketones. The presence of the additional basic oxygen of the ether adds additional complexity for xanthone that is not present for benzophenone. However, in the excited state aromatic ketones tend to become more basic while phenols tend become more acidic. Thus, it is likely that upon excitation it is only the ketone oxygen that will experience protonation and a similar mechanism to that presented for **47** may be

written for the photoredox behaviour of **53**. The acid catalysis of **53** is not necessary as the reaction is active even at pH 7. In fact, when photolysed at pH 2, only the oxidation product **98** is formed. Additionally, the redox product **97** appears to be photoreactive and is converted into **98** upon photolysis. Consequently, low conversion runs are necessary to observe **97**.

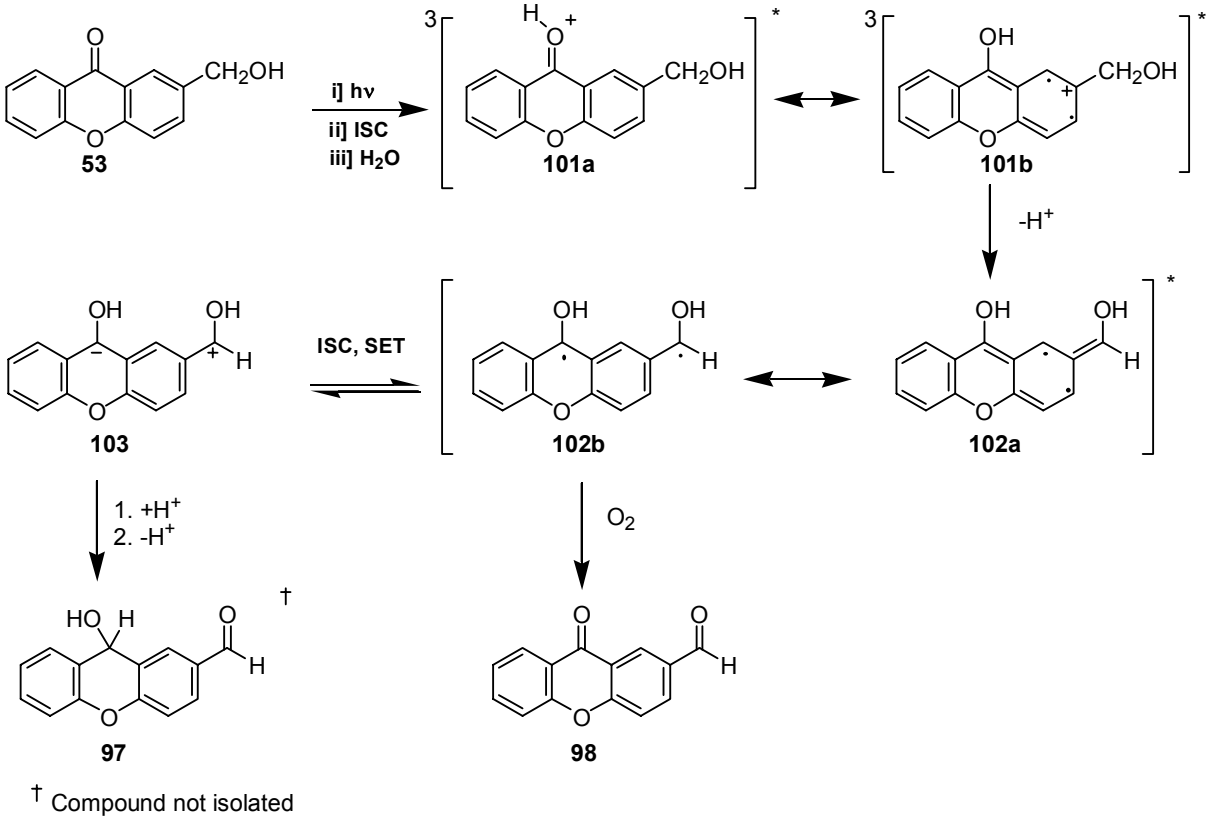

Scheme 3.2

The protonated species **101a** should favour the deprotonation of the benzylic group due to the positive charge in the *meta* position of the resonance contributor **101b**.

Protonation directly of the deprotonated compound **102a** or through the zwitterion **103** should lead to the photoredox product **97**. This product was not isolated, however, and as mentioned in Section 3.2.1.2 the condensed product **99** was isolated instead. This compound has an analogue in the benzophenone system as the condensed product **74** is

observed when photolysing **47** in 5% H_2SO_4. While fairly acidic conditions are required for **47**, this condensation happens to **53** in solvent media at pH 7. The dramatically different requirements arise from the nature of benzophenone and xanthone. Xanthone contains a central ring that may become aromatic under certain conditions. In the ground state, a cation at the carbon bridge of **100** (see Scheme 3.1) has a ring containing 6π electrons making it aromatic by Huckel's rules.[89] This extra stability promotes the loss of the hydroxyl group even under neutral conditions. By contrast, the hydroxyl of benzhydrol must be protonated before it may leave, as the corresponding carbocation is not stabilized to the same degree. Studies involving the photodehydroxylation of 9-phenylxanthen-9-ol (**104**) support this interpretation.[110] The dehydroxylation of **105** is possible via either a thermal or photochemical route (See Scheme 3.3). The thermal route involves reversible protonation of the hydroxyl group to form **105** before subsequent dehydration to form **106**. It is through this pathway that **99** is proposed to be formed.

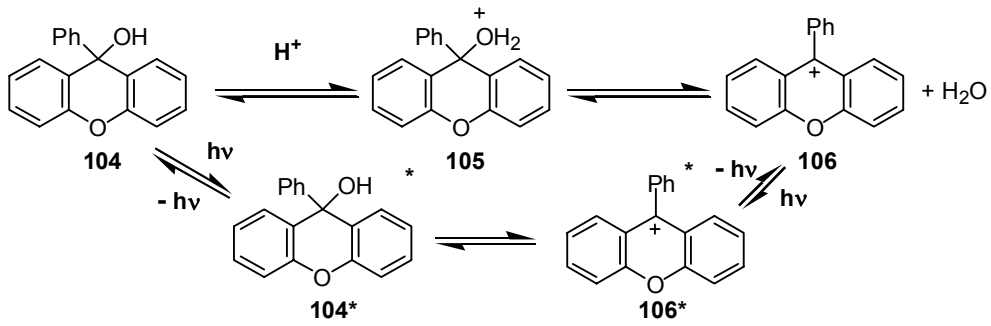

Scheme 3.3

Once formed the condensed product **74** is relatively stable and can easily be isolated due to the difficulty in forming the corresponding carbocation. The same can not be said for the xanthone condensed product **99** as it seems to be both photo and oxygen sensitive. This instability may also be attributable to the relative stability of the carbocation **100**. However, as Huckel's rules are the opposite for excited state systems

(4nπ systems are aromatic and 4nπ+2 systems are anti-aromatic), excitation of **99** may result in deprotonation of the carbon bridge proton to result in the now aromatic carbanion **107** (8π electrons) which may then decompose into **98** as shown in Eqn [3.7]. Problems exist with this explanation however as no significant amounts of 2-methylxanthone (**96)** were recovered. Oxidation must occur to explain the observed results but the pathway is not known.

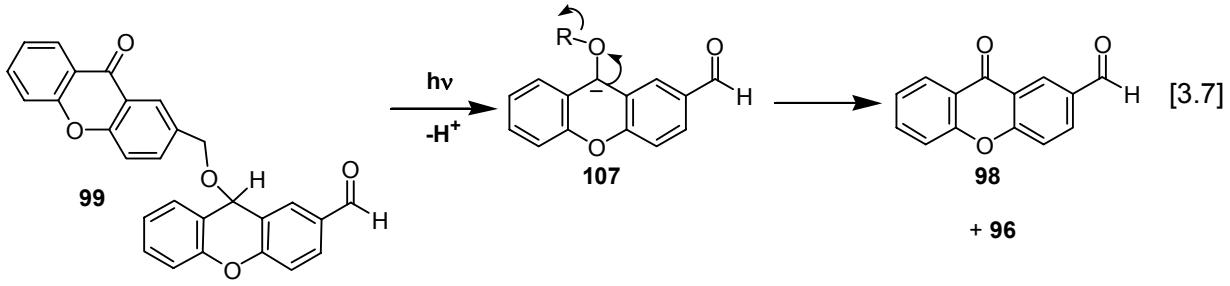

[3.7]

The comparison between **53** and **47** is facilitated by a comparison of simple HOMO/LUMO (Chem3D, MOPAC/AM1) representations. These were presented for **47** in Section 2.2.5. The HOMO/LUMO representations are presented in Figure 3.11. Unlike **47**, both the HOMO and the LUMO involve both rings. However, like **47**, the transition from the HOMO to the LUMO of **53** involves a decrease in electron density at the *meta* position of the substituted aromatic ring and an increase in the electron density at the carbonyl carbon. Thus it is understandable that **53** would behave in a similar manner to **47** and become protonated at the carbonyl oxygen and deprotonated at the benzylic carbon. The reverse reaction, as illustrated via the HOMO/LUMO representations of **97** (Figure 3.12) is not possible because the electron density at the benzhydrol position does not decrease and the carbonyl does not experience an increase in electron density.

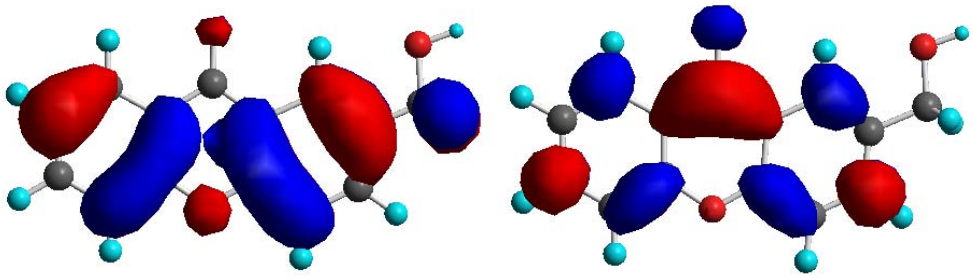

Figure 3.11 HOMO (left) and LUMO (right) of **53** calculated using Chem3D (AM1)

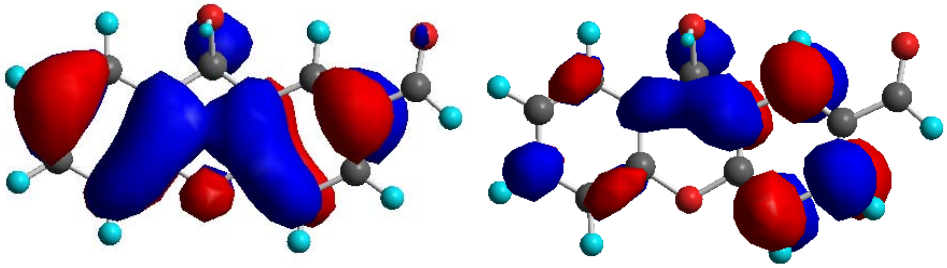

Figure 3.12 HOMO (left) and LUMO (right) of **97** calculated using Chem3D (AM1)

In Chapter 2, the requirement of the lowest π,π* excited triplet state was described in detail in Section 2.2.5 as the aromatic ring needs to be involved in order for the photoredox reaction to be effective. It is reasonable that this requirement should also be applicable for **53** as the intramolecular photoredox reaction necessarily involves conjugation of the carbonyl with the benzene ring. The π,π* excited triplet state was favoured for **47** when the solvent media was polar and that correlated well with the increasing reactivity towards photoredox as the polarity of the solvent media increased. Scaiano[98] presented data that shows that the solvent media affects the photochemistry of xanthone to a greater amount than was observed for benzophenone and acetophenone. By examining the hydrogen abstraction reaction rates in different solvent mixtures he

compared the relative reactivities of acetophenone with xanthone. Acetophenone is a reasonable compound to use as a comparison as its triplet energy and xanthone are almost identical.[44] The change in reactivities of acetophenone when going from a polar solvent to a non-polar solvent is just under a factor of three. Contrastingly, the reactivity of xanthone changes by 3 orders of magnitude upon changing the polarity of the solvent. In polar solvents the energy gap is significant enough to conclude that the lowest energy triplet excited state is π,π*. However, any n,π* present will produce oligomeric product, and as the n,π* triplet of xanthone is more reactive than the triplet state of benzophenone,[20] more oligomeric product is expected to be formed for **53** than for **47**. This is indeed the case as seen Table 3.1.

3.3 2-(Hydroxymethyl)fluorenone (54)

3.3.1 Results and Discussion

3.3.1.1 Synthesis and Materials

As **54** was not available for purchase it had to be synthesized. The most straightforward method was the reduction of the carboxylic acid to the benzyl alcohol using a borane solution (1 M BH_3·THF) as the reducing agent (Eqn [3.8]). This yielded the desired product but also produced significant further reduced 2-methylfluorenone.

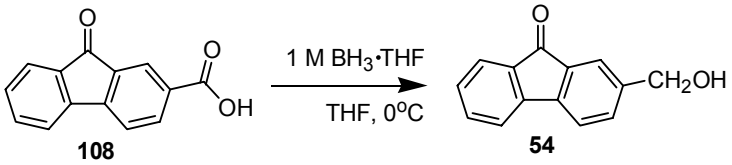

108 **54** [3.8]

3.3.1.2 UV-Vis and Product Studies

The photoredox reaction is expected to proceed via Eqn [3.9].

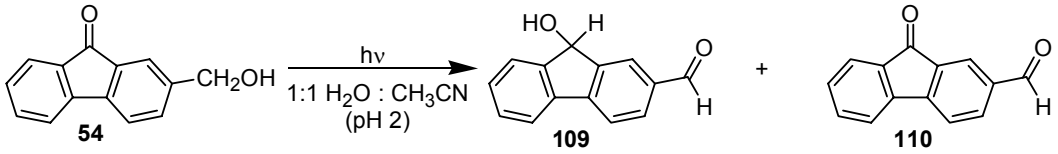

[3.9]

However, preliminary photolysis of **54** showed no photoreaction via NMR spectroscopy under the same photolysis conditions that exhibited photoredox behaviour for **47** and for **53** (1:1 H_2O : CH_3CN, pH 2 or pH 7 respectively). Consequently, the photolysis of **54** was followed by UV-vis spectroscopy under several different solvent conditions. The first at pH 7 (Figure 3.13) showed no change in the UV-vis spectrum despite photolysis for 40 min using 16 lamps at 300 nm.

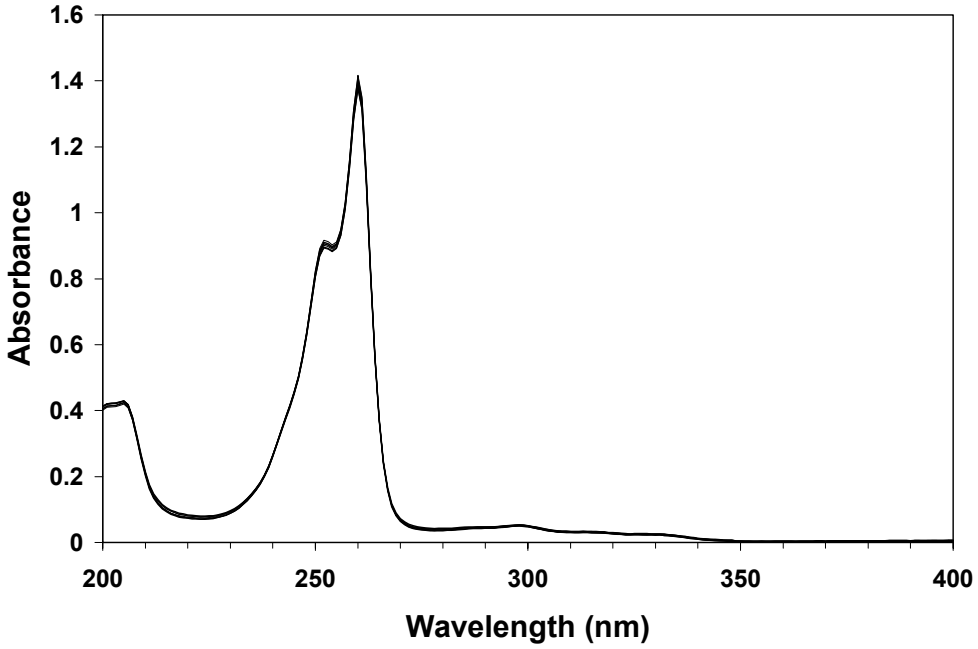

Figure 3.13 UV-vis spectral traces observed on photolysis of **54** in 1:1 H_2O : CH_3CN (pH 7). Each trace is taken after 5 minutes irradiation at 300 nm using sixteen lamps at 5.1 x 10^{-5} M.

The next two UV-vis spectral traces were produced using two different solvent media. The first uses a 1:1 H_2O : CH_3CN (pH 2) solution (Figure 3.14) while the second uses a 100% H_2O (pH 2) solution (Figure 3.15). Both exhibited a loss of the band at 260 nm with a concomitant increase in a broad band centered at 305 nm. The primary difference between the two traces was that the photolysis of **54** in pure pH 2 solution was slightly more efficient. Although the traces look very similar, Figure 3.14 takes one fewer trace to complete the decay of the band at 260 nm despite having a slightly lower absorbance.

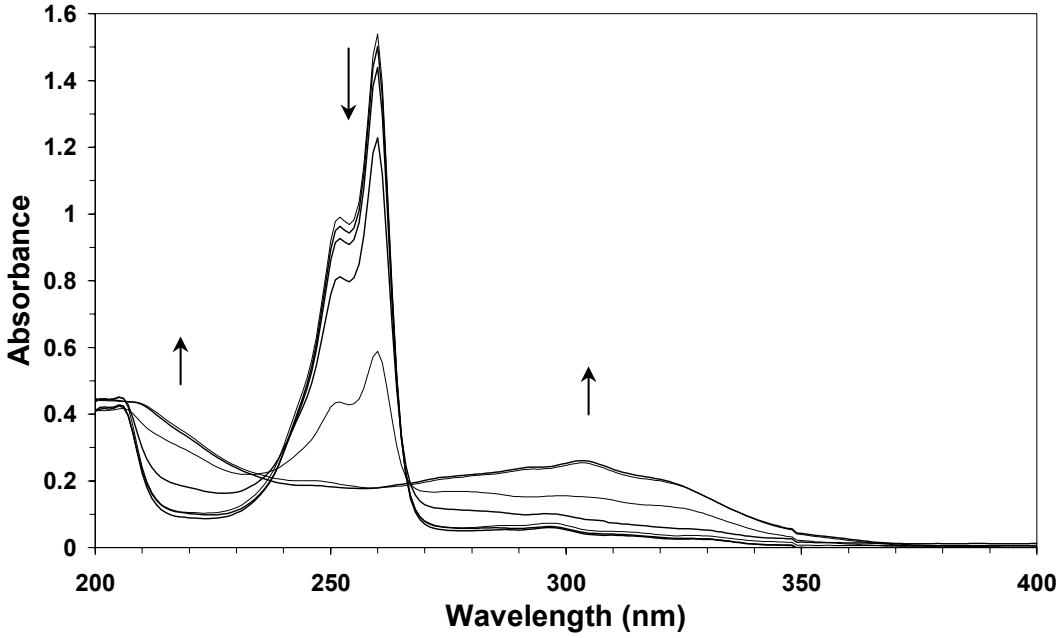

Figure 3.14 UV-vis spectral traces observed on photolysis of **54** in 1:1 H_2O : CH_3CN (pH 2). Each trace is taken after 5 minutes irradiation to a maximum of 30 minutes at 300 nm using sixteen lamps at 5.1 x 10^{-5} M.

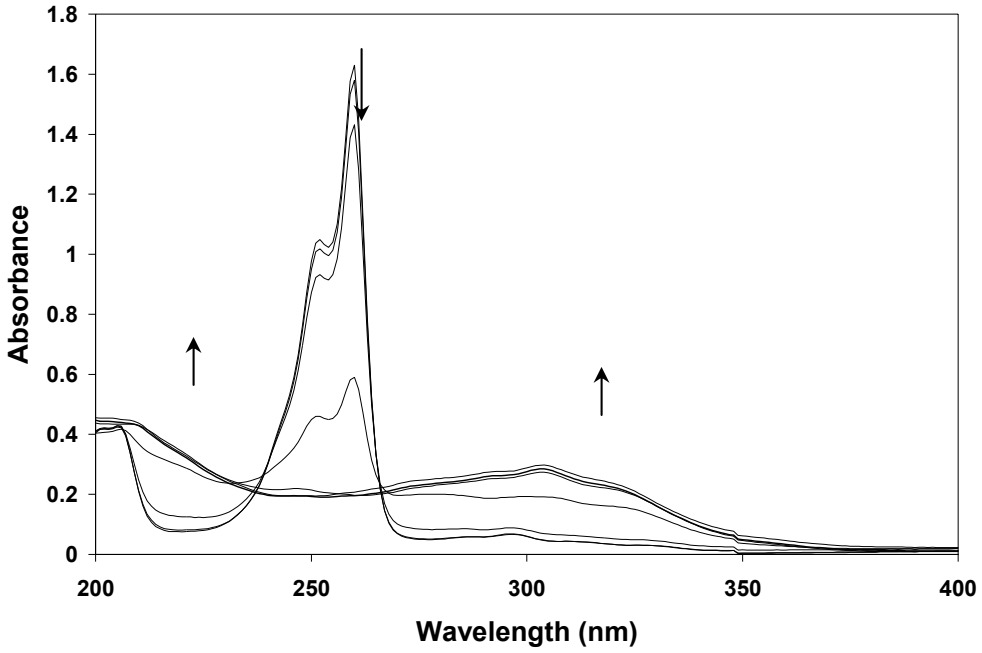

Figure 3.15 UV-vis spectral traces observed on photolysis of **54** in H_2O (pH 2). Each trace is taken after 5 minutes irradiation at 300 nm to a maximum of 30 minutes using sixteen lamps at 5.1 x 10^{-5} M.

As it became evident that a reaction was proceeding at concentrations used in UV-vis studies, **54** was investigated under varying conditions and photolysis times. Only when the photolysis times reached 60 minutes in length in a solvent mixture of 1:1 H_2O : CH_3CN (pH 2) was an appreciable amount of **109** observed, and then only in ~10% yield. Thus, although the photoredox reaction is possible for **54**, it is extremely inefficient compared to both the xanthone and the benzophenone chromophore derivatives. Although admittedly the xanthone is ultimately isolated as a different product, **99**.

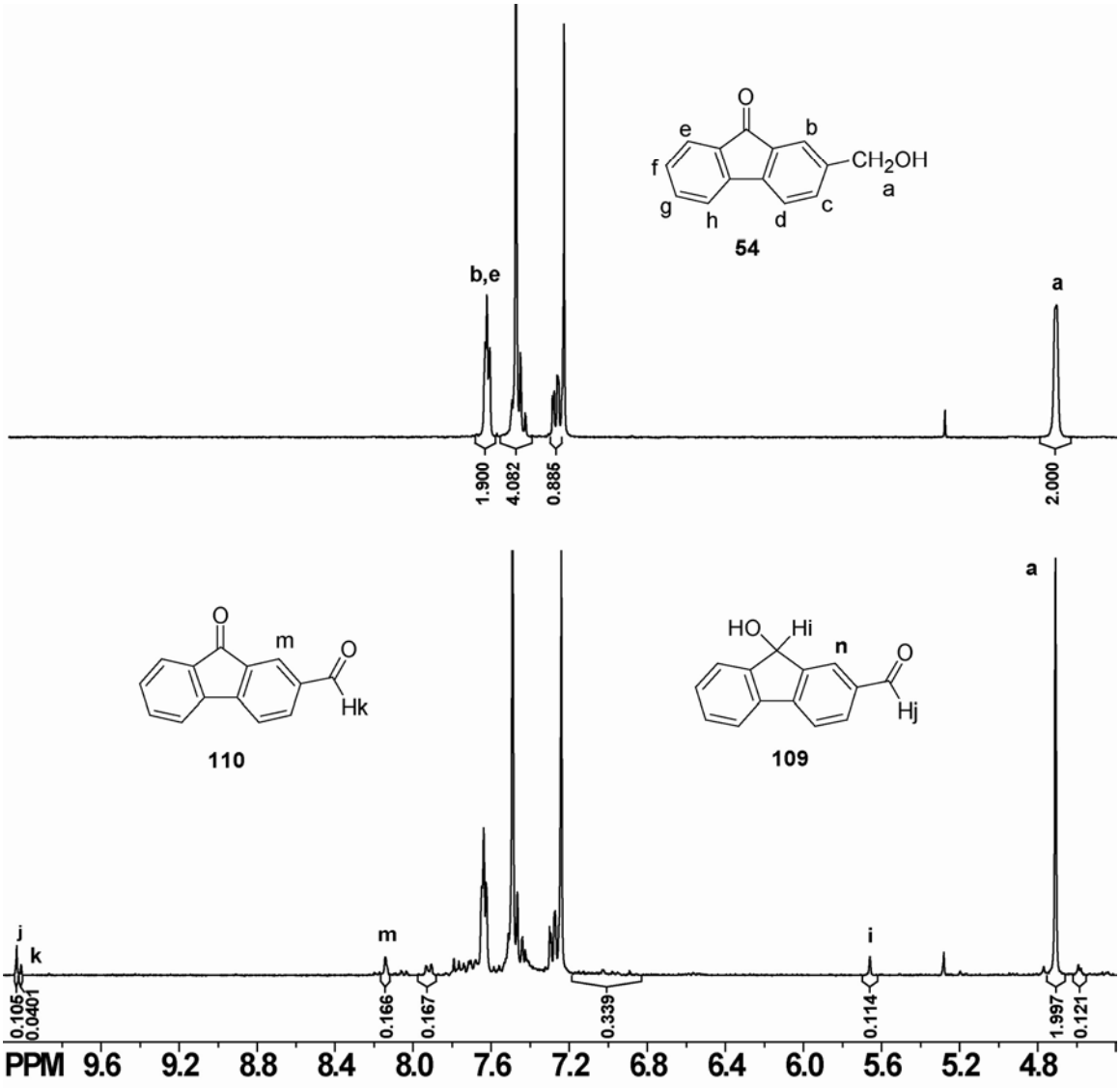

Figure 3.16 300 MHz ^{1}H-NMR spectra of **54** (in chloroform-*d*) before (top) and after (bottom) photolysis (1.6 x 10^{-4} M, 5 mg/150 mL) in 1:1 H_2O : CH_3CN (pH 2), for 60 minutes with sixteen 300 nm lamps (argon purged). Product ratio: 76% **54**; 9% **109**; 12% **110**; 3% oligomeric product. Product ratio was determined by comparing the integrations for the peak due to the methine peak of **109** (**i**: 5.66 ppm, 0.11H) to the singlet (**a**: 4.71 ppm, 2.0H) and the singlet due to the aromatic proton of **110** (**m**: 8.15 ppm, 0.17H).

Compound **54** was photolysed in deuterated solvent in an attempt to determine whether the lack of reactivity was due to the reverse reaction being present. If the opposite zwitterion in the mechanism was present, deuterated starting material should be produced and should be isolable. However no deuterated **54** was observed.

Table 3.3 Photoproduct studies for **54**[a,b]

Photolysis time, 300 nm lamps	pH	% **54**	%**109**	%**110**	%**OP**[c]
4 lamps, 5 min	2[d]	99	0	0	1
16 lamps, 15 min	2[d]	100	0	0	0
16 lamps 5 min	2[e]	99	0	<1	<1
16 lamps 15 min	2[e]	99	0	1	<1
16 lamps, 60 min	2	76	9	12	3
16 lamps 15 min	pD 2	98	0	2	<1
16 lamps, 60 min	pD 2	89	3	5	3

[a]Using **48** at 1.6 x 10^{-4} M(10.0 mg / 300 mL) to 1.7 x 10^{-4} M (5.2 mg / 150 mL) in 1:1 H_2O : CH_3CN, pH adjusted with H_2SO_4.
[b]Product mixture ratio determined by integration via ^{1}H-NMR($CDCl_3$).
[c]Oligomeric side product (**OP**) approximate, estimated from integration via ^{1}H-NMR($CDCl_3$). (δ: 6.8-7.2ppm).
[d]Solvent ratio of 5:1 H_2O : CH_3CN
[e] 100% pH 2

3.3.1.3 Nanosecond Laser Flash Photolysis (LFP)

9-Fluorenone has significantly different photochemical and photophysical behaviour compared to both benzophenone and xanthone. It has been shown[111] to have a significant fluorescence quantum yield (Φ_F = 0.027) centered at 510 nm while the fluorescence of benzophenone is essentially absent. Whereas benzophenone has a Φ_{ISC} of approximately unity, fluorenone has a Φ_{ISC} of 0.34 and many of its derivatives have lower values. Thus, although all other compounds required a flow cell for LFP

measurements, the relative inertness of the photoreaction of **54** led to LFP being performed using a static cell.

Literature[112] ascribes the absorption bands of 9-fluorenone of the triplet-triplet transitions to 420 nm and 620 nm. However in acetonitrile the band at 620 nm is significantly smaller than the 420 nm band and is appreciably deformed by the relatively strong fluorescence. This is consistent with the spectrum obtained in acetonitrile for **54** (Figure 3.17). There are three bands, one at 290 nm, one at 450 nm and another at 630 nm. There is another possible band at 340 nm but that might just be an artifact of the low signal to noise ratio. The spectra presented in the literature[112] start at 340 nm so would not have shown the peak at 290 nm. In the spectrum of **54** the weak band at 630 nm is much lower in intensity. There is a significant bathochromic shift of 30 nm from 420 nm to 450 nm. Like **47**, the band at 290 nm is biexponential as it does not decay to baseline while the band at 430 nm does. This is likely due to another transient that absorbs at that wavelength.

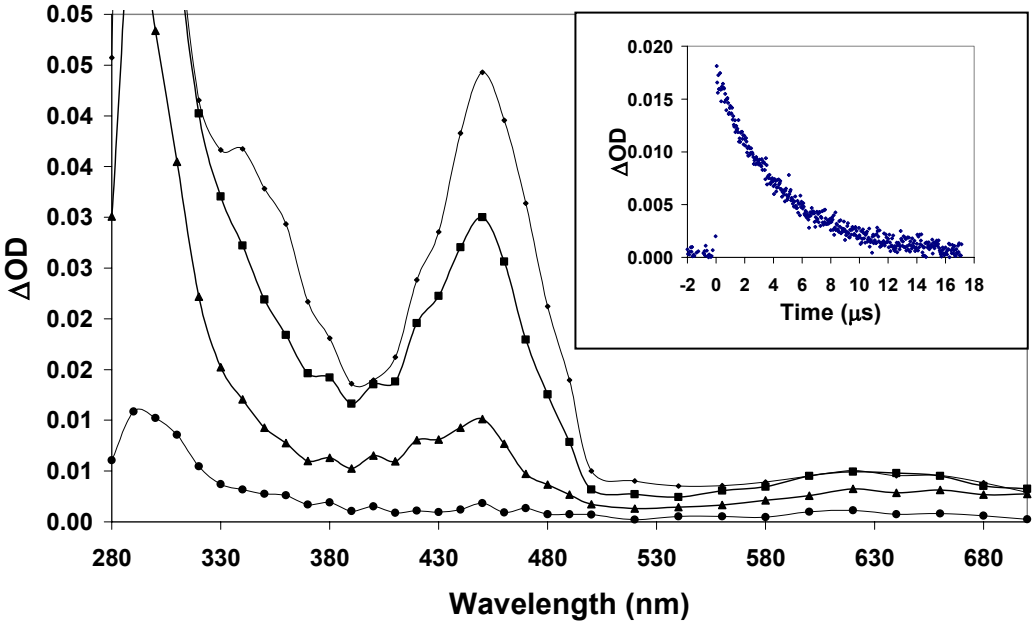

Figure 3.17 Triplet-triplet absorption spectrum observed on LFP (λ_{ex} 266 nm) of **54** in CH_3CN, using a static cell with N_2 purging. The four spectra are taken at the following intervals: immediately after the laser pulse, after 1.5 μs, after 6 μs and after 17 μs. Inset is decay trace taken at 430 nm.

The LFP spectra in aqueous media were also performed for 1:1 H_2O : CH_3CN (pH 2 and pH 7) and for 100% H_2O (pH 2) for **54**. The amplitude of the absorbance of the spectra in the aqueous solvent media was a factor of 20 weaker than the spectrum obtained using acetonitrile as the solvent medium. This supports the assertion that water quenches the triplet state through hydrogen bonding.[111] The signal to noise ratios for the spectra were correspondingly smaller and consequently the data obtained was limited. However the spectra do show the three bands (300 nm, 430 nm, and 650 nm) attributable to the triplet of **54**. Significant fluorescence is observable as a negative signal at 570 nm is present in the pH 7 run.

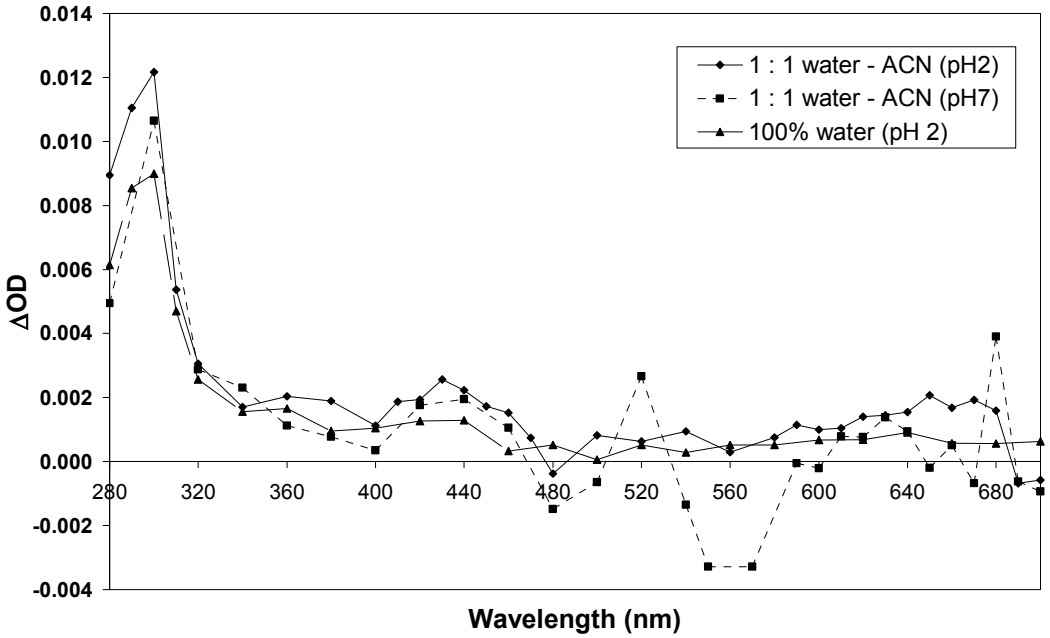

Figure 3.18 Comparison of the triplet-triplet absorption spectrum observed on LFP (λ_{ex} 266 nm) of **54** in 1 : 1 H_2O : CH_3CN (pH 2), 1 : 1 H_2O : CH_3CN (pH 7) and pure H_2O (pH 2), using a static cell with N_2 purging.

The triplet lifetimes are given for the band at 310 nm and 430 nm for each of the different solvent media listed in Table 3.4. Unfortunately, lifetimes were not obtainable for the band at 430 nm for all solvent media. Compound **54** exhibits its shortest lifetime when irradiated in acetonitrile as the solvent medium. A short lived component was also observed with a lifetime about 17 ns. This short lived transient was not observed for the other compounds. This is likely due to the relatively large amounts of noise observed for the decay traces measured for the solvent mixtures containing water. Proton quenching of the triplet appears active by examining the lifetimes of the 310 nm band at the different solvent pHs.

Purging with oxygen resulted in a quenching of the lifetime in each case and resulted in a decrease of the lifetime by 2 orders of magnitude. This supports the supposition that the transient being observed is a triplet. The changing lifetimes for the

oxygen purged system is consistent with the different dissolved oxygen content in acetonitrile (9.1 mmol/L) and in water (1.27 mmol/L).[109]

Table 3.4 Lifetime Comparison of **54** in Differing Solvent Media[a]

Solvent		**310 nm (μs)**	**430 nm (μs)**
100% pH 2	N_2	51	100[c]
	O_2	0.44	
50% pH 2	N_2	79	73
	O_2	0.26	0.30
0% pH 2	N_2	6.3 (16.8 ns)[b]	4.8 (18.6 ns)[b]
	O_2	0.072	0.054
50% pH 7	N_2	86	60
	O_2	0.21	
50% pH 1	N_2	8.2	
	O_2	0.18	

[a] Lifetimes were obtained by exponential fitting of decay traces in 1:1 H_2O : CH_3CN, (pH 7) or pure CH_3CN, N_2 or O_2 purged; fitting was monoexponential unless otherwise indicated. $[O_2]_{acetonitrile} = 9.1 \times 10^{-3}$ M; $[O_2]_{water} = 1.27 \times 10^{-3}$ M

[b]Second exponentials in ns present at short time scales

[c]This value has a high degree of scatter so should be considered to be highly approximate

3.3.1.4 Proposed Mechanism

Although **54** has significantly lower photoreactivity than either **47** or **53** the behaviour can still be illustrated using a similar mechanism, shown in Scheme 3.3, as photoredox chemistry is observed.

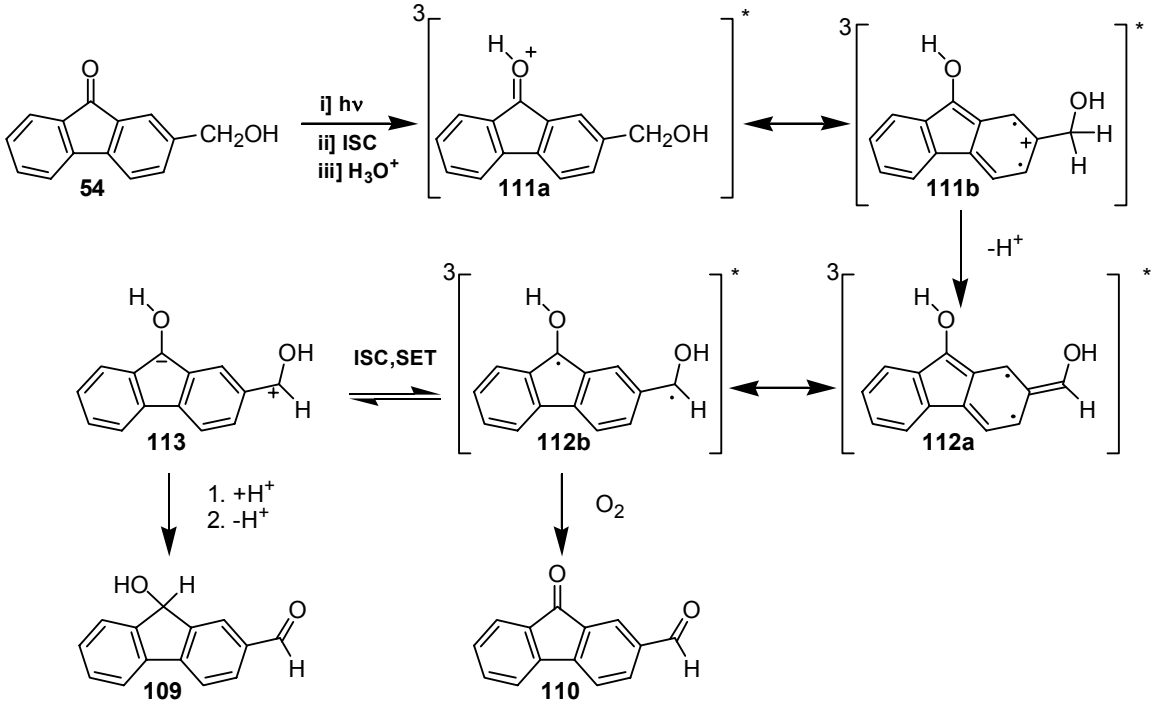

Scheme 3.4

The acid catalysis evident in both the benzophenone system **47** and the xanthone system **53** is also present for the photoredox reaction of **54**. In Section 3.3.1.2 the UV-vis spectral trace at pH 7 saw no photoreaction while the spectral trace at pH 2 produced a photoreaction. Additionally, in Section 3.3.1.3 there was a clear quenching of the triplet state as the pH was lowered from pH 7 to pH 2 to pH 1. Consequently, the first step is likely to proceed in a manner similar to that observed for **47** and result in the protonated

structure **111**. As the *meta* position will be activated (**111**), deprotonation is expected to produce **112**.

Oxidation of **112** by residual oxygen would lead to the oxidation product **110** but the photoredox product would occur from solvation of the zwitterion **113** or through direct reaction with the dienol **112**.

Of primary importance for the photoredox reaction to occur is the presence of a lowest excited triplet state in π,π*. As the reaction necessarily involves the conjugation of the two oxygens through an aromatic system, the π,π* transition is required. This does not seem to be a hinderance as the lowest triplet state of 9-fluorenone has been established as being of π,π* character. This is in contrast to benzophenone which has n,π* character and whose π,π* must be stabilized by using polar solvents and acidic solvent media. In polar solvents both the S_1 and T_1 states of 9-fluorenone have π,π* configuration but the intersystem crossing quantum yield decreases by 2 orders of magnitude open going from nonpolar solvents to polar solvents.[100] Benzophenone by contrast has an ISC rate 400 times faster. Thus, **54** has a much lower proportion of π,π* triplet present in the excited state than either **47** or **53** and it is therefore reasonable to expect that the quantum yield of any photoreaction deriving from **54** should be correspondingly lower. A comparison of Table 2.1 and Table 3.2 shows that the two runs that show similar photoconversion are 1 lamp for 2 min for **47** and 16 lamps for 60 min for **54**. A rough calculation of the amount of irradiation needed to obtain equivalent photoconversions results in a 480 times greater amount of photons needed for **54**. This corresponds well with the tabulated literature value for the ISC rate difference between benzophenone and fluorenone.

One benefit of the π,π* lowest energy singlet and triplet excited states is that the competing pathway towards oligomeric side-products is minimized. This allows photolysis times much longer than is possible for **47** or **53**.

It is interesting to compare the core ring of **54** with the core ring of **53**. When a negative charge is at the methylene carbon, the core ring of **54** is aromatic in the ground state according to Huckel's rules.[89] By contrast the core ring of **53** is aromatic when there is a positive charge at the methylene carbon. The stabilization of the anion at the carbon bridge should favour the zwitterion **113** that leads to the redox product.

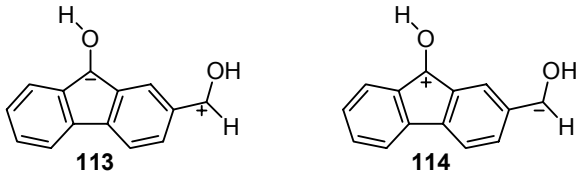

The other zwitterion **114** should result in reversion to starting material and may be detected by photolysing in D_2O and searching for **54-D** by the presence of a decrease in the integration of the methylene peak. Preliminary photolysis in 1:1 D_2O : CH_3CN (pD2) however did not lead to any decrease in the integration of the methylene peak (Eqn [3.10]).

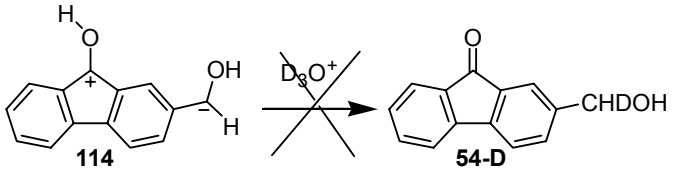

[3.10]

Although further investigation is wise before a definitive statement may be made, it appears as though **113** is favoured over **114**.

As explored for **47** and **53,** simple HOMO/LUMO (Chem3D, MOPAC/AM1) representations were calculated for **54** (Figure 3.19) and for **109** (Figure 3.20) to give

some qualitative information about the relative electron densities upon excitation. The transition from the HOMO to the LUMO of **54** leads to an increase in the electron density

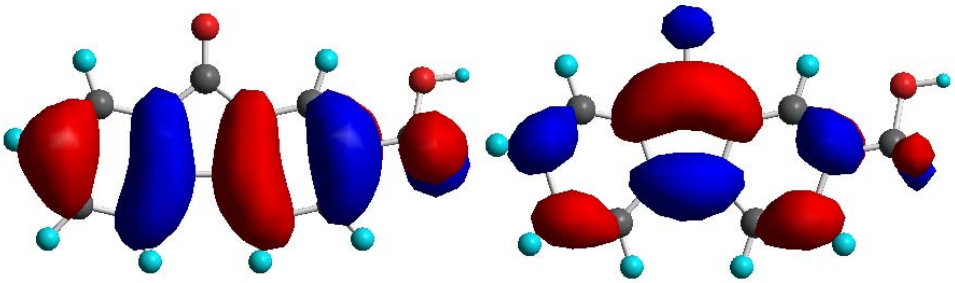

Figure 3.19 HOMO (left) and LUMO (right) of **54** calculated using Chem3D (AM1)

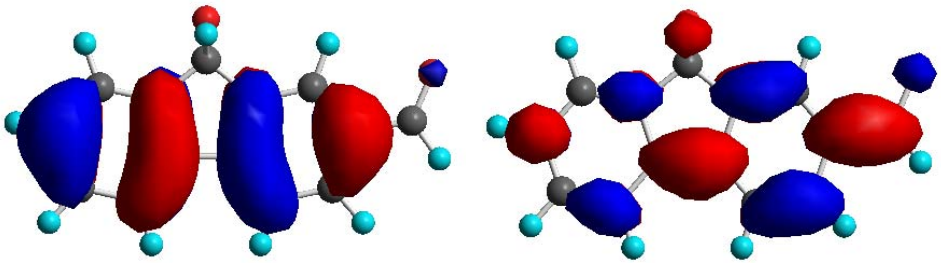

Figure 3.20 HOMO (left) and LUMO (right) of **109** calculated using Chem3D (AM1)

at the carbon bridge corresponding to the increased basicity observed for all of the aromatic ketones explored thus far in this Thesis. Along with the increase in electron density, a decrease in electron density at the *meta* position was also observed. This was consistent with the increased polarization of **111** that should lead to deprotonation of a benzylic proton. As the HOMO/LUMO representation for **54** is analogous to the HOMO/LUMO representations observed for both **47** and **53** it is not surprising that the photoredox reaction is present in **54** as well, albeit at much lower efficiency. An interesting variation on the behaviour arises from the HOMO/LUMO representation of the redox product **109** however. Unlike the HOMO/LUMO representations of the

photoredox products of **47** and **53**, the HOMO/LUMO representation of **109** shows a decrease in the electron density at the carbon bridge atom with a concomitant increase in the electron density at the aldehyde. This suggests that the reverse reaction may be viable. Although no evidence was collected for this Thesis, this might be an interesting angle to pursue.

3.4 Comparison of Results

The difference between the photobehaviour of **53** and **54** is striking. While **53** is more active than benzophenone and is capable of undergoing photoredox chemistry at pH 7 (albeit not being stable under those conditions), **54** is nearly photoinert under the same conditions. This is true even towards photodecomposition. The lack of reactivity of **54** may be traced to the low ISC rate. The redox product stability also differs between the two compounds. The increased reactivity of **53** is also exhibited in the stability of the photoredox product **97**. This product is never actually isolated and instead the condensation product **99** is formed. This condensation product is not stable either and upon photolysis produces the oxidation product **98**. By contrast, the redox product of **54**, **109**, appears to be stable but is not produced in great amounts.

Despite the difference in efficiency of reaction the generality of the reaction is evident in fact that both **53** and **54** undergo similar photoredox behaviour to that exhibited by **47**. This is especially significant due to the great electronic differences between the xanthone and the fluorenone chromophores evident in their different electronically excited states and the opposite aromaticity of their central ring .

3.5 Experimental

3.5.1 General

^{1}H NMR spectra were recorded on either a Bruker AC300 (300 MHz) instrument or a Bruker AVANCE 500 (500MHz) instrument using chloroform-*d* as the solvent unless otherwise specified. Chemical shifts are reported in ppm and *J*-values are reported in Hz. Splitting patterns are reported as s (singlet), d (doublet), t (triplet), dd (doublet of doublets), dt (doublet of triplets), tt (triplet of triplets) and m (multiplets). Mass spectra and High-resolution mass spectra (HRMS) were obtained on a Kratos Concept H (EI) instrument. UV–vis spectra were recorded on a Varian Cary 5 instrument using baseline correction. Infrared spectra were recorded on a Perkin Elmer FTIR Spectrometer Spectrum 1000 using NaCl plates with neat product or thin film obtained from a solution of dichloromethane. Only strong and medium peaks are reported. Melting point values were obtained using a Gallenkamp Melting Point Apparatus. Measurements of pH(D) values were obtained using a Fisher Accumet 915 pH meter. Preparative photolyses were performed using a Rayonet RPR 100 photochemical reactor using 300 nm lamps unless otherwise noted.

3.5.2 Common Laboratory reageants

All solvents used for synthesis (ACS grade) were purchased from Aldrich Chemical Company and used as received unless otherwise noted. Acetonitrile (HPLC grade) used for photolyses was checked for impurities by NMR spectroscopy. Organic extracts were dried over anhydrous magnesium sulfate and filtered. Deuterated solvents; D_2O, $CDCl_3$ were purchased from Cambridge Isotope laboratory containing 99.9% D.

D_2SO_4 was obtained Aldrich Chemical company and contained 99.9% D. Preparative TLC was carried out on 20 cm x 20 cm silica gel GF Uniplates (Analtech). The following compounds were purchased from Aldrich: Sodium metal, 2-chlorobenzoic acid, p-cresol, Cu powder, Cu_2O, N-bromosuccinimide, benzoyl peroxide, Na_2CO_3, activated charcoal, $CaCO_3$, 9-fluorenone-2-carboxylic acid, 1 M BH_3·THF .

3.5.3 Synthesis

2-(4'-Methylphenoxy)benzoic acid (95)[103]

Sodium metal (2.4 g, 100 mmol) was cleaned in hexanes and added piece by piece to 50mL MeOH. After all of the sodium had been added and evolution of gas ceased, the newly formed sodium methoxide was added to a 250 mL flask containing 2-chlorobenzoic acid (7.87 g, 50.3 mmol), p-cresol (15.8 mL, 151.1 mmol), Cu powder (0.1663 g, 2.6 mmol) and Cu_2O (0.066 g, 0.5 mmol). The flask was then evaporated to dryness on the rotary evaporator. To this residue, 50 mL of heavy mineral oil was and the mixture stirred at ~200^{o}C using a silicon oil bath for approximately 3.5 hours keeping the temperature relatively constant. The mixture was cooled overnight and 50 mL benzene was added before transferring to a sintered glass filter frit. The precipitate was washed twice with 50 mL aliquots of benzene. The precipitate was dissolved in 130 mL of 10% Na_2CO_3 and the aqueous layer decolourised by boiling with activated charcoal. The mixture was then filtered, cooled to room temperature and 10% H_2SO_4 added. The resulting precipitate was collected and recrystallized from 70% EtOH to give a product yield of 38%.

^{1}H-NMR (300MHz, $CDCl_3$) δ: 8.22 (dd, 1H, 7.7 Hz, 1.5 Hz), 7.47-7.40 (m, 1H), 7.23-7.15 (m, 2H), 7.02 (d, 2H, 8.4 Hz), 6.88 (d, 1H, 8.3 Hz), 2.37 (s, 3H)

2-Methylxanthone (96)[103]

The recrystallized 2-(4'-methylphenoxy)benzoic acid (4.46 g, 19.5 mmol) was placed in a 100 mL round bottom flask with 15 mL concentrated sulfuric acid (280 mmol, >10 eq) and stirred while heating on a water bath for 2 hours. The mixture was then allowed to cool to room temperature and stirred overnight. The next day the mixture was poured into 100 mL of ice water immediately resulting in an off-white precipitate. The precipitate was collected by filtration and subsequently washed twice with 50 mL 10% Na_2CO_3. After drying under vacuum the crude **96** was obtained as an off-white solid in 42 % yield (4.44 g). mp 116-120 ^{o}C (lit. 122-123 ^{o}C)[103]; ^{1}H-NMR (300MHz, $CDCl_3$) δ: 8.33 (dd,1H, 8.0 Hz,1.4 Hz), 8.11 (d,1H, 0.95 Hz), 7.70 (ddd, 1H, 1.4 Hz, 6.9 Hz, 6.9 Hz), 7.55-7.45 (m, 2H), 7.41-7.32 (m, 2H), 2.46 (s, 3 H); ^{13}C-NMR (125 MHz, $CDCl_3$) δ:177.55, 156.42, 154.63, 136.32, 134.87, 133.93, 126.96, 126.25, 123.93, 122.03, 121.69, 118.17, 117. 97, 21.07; MS (EI) *m/z*; 210 (100, M+), 181, (40), 152 (10), 105 (10); HRMS, calculated for $C_{14}H_{10}O_2$ 210.0681; observed 210.0678.

2-(Hydroxymethyl)xanthone (53)

2-Methylxanthone (**96**) (2.30 g, 10.9 mmol) was dissolved in 40 mL benzene. N-bromosuccinimide (2.34 g, 13.1 mmol) and benzoyl peroxide (0.010 g, 0.07 mmol) were added and the mixture refluxed overnight for 12 hours under an atmosphere of nitrogen. The following day much off-white precipitate was visible. The precipitate was dissolved

in 200 mL dichloromethane and washed twice with 100 mL distilled water before drying with anhydrous magnesium sulfate. Upon filtration and solvent removal, crude 2-(bromomethyl)xanthone was produced (crude yield: 2.62 g). The crude product was used directly to produce the alcohol through hydrolysis. The crude product was dissolved in 75 mL dioxane and then calcium carbonate (5.53 g, 55.2 mmol) was added along with 75 mL distilled H_2O. This mixture was the reluxed overnight for 17 hours. The solvent was removed using a rotary evaporater and the residue subsequently dissolved by alternately adding 1 M HCl and CH_2Cl_2 until all the solid had dissolved. The organic layer was removed and the aqueous layer was extracted three times with 50 mL dichloromethane until all of the solid had dissolved. The organic layers were combined, washed twice with 100 mL saturated sodium bicarbonate solution and dried with anhydrous magnesium sulfate. Filtration and solvent removal resulted in the crude product (1.11 g) in 45 % yield (3:1 alcohol to aldehyde ratio). Recrystallization from ethanol resulted in the pure **53** (white needle-like crystals) in 10% yield. Selective reduction with sodium borohydride will also reduce the aldehyde to alcohol with less loss than recrystallization or column.

mp 140 - 145 ^oC; ^1H-NMR (300MHz, $CDCl_3$) δ: 8.31 (dd, J = 1.4,7.7 1H), 8.26 (d, J = 1.8, 1H), 7.76 – 7.67 (m, 2H), 7.44 - 7.43 (m, 2H), 7.37 (t, J = 7.8,1H), 4.80 (s, 2H); ^{13}C-NMR (125 MHz, $CDCl_3$) δ: 177.37, 156.30, 155.73, 136.98, 135.03, 134.05, 126.89, 124.79, 124.13, 121.90, 121.62, 118.48, 118.14, 64.62; IR (neat from CH_2Cl_2 solution, salt plates): ν = 3367, 1659, 1608, 1488, 1467, 1320, 1243, 1207, 1139, 1015, 834, 760 cm^{-1}; UV-Vis (1:1 pH 7 H_2SO_4 - CH_3CN): λ_{max} = 341 nm (ε = 13,000), 262 nm (ε = 26,000), 241 nm (ε = 91,000), 204 nm (ε = 38,000); MS (EI) *m/z*; 226(80, M+), 209 (20),

197 (100), 180 (15), 149 (50), 139 (25), 69 (30), 57 (30), 55 (30), 44 (30); HRMS, calculated for $C_{14}H_{10}O_3$ 226.0630; observed 226.0629.

2-(Hydroxymethyl)fluorenone (54)[113]

9-Fluorenone-2-carboxylic acid (**108**) (2.31 g, 10 mmol) was placed in a clean dry 2 necked round-bottom flask with a pressure-equalizing dropping funnel. The system was flushed with nitrogen and 200 mL dry THF was added via syringe. This partially dissolved the starting material. Using a syringe, 11.8 mL (11.8 mmol) 1 M BH_3·THF was added to the dropping funnel. Dry THF (20.0 mL was then added to the dropping funnel and the reaction flask cooled in an ice bath to 0^{o}C. The borane solution was added dropwise over 30 minutes. After addition, the reaction mixture was allowed to warm up to room temperature slowly and left to stir overnight (8 hours). The next day 50 mL of 1 M H_2SO_4 and 50 mL of distilled water were added to quench any remaining borane (no noticeable change was observed) and the mixture placed in a separatory funnel. An additional 200 mL dichloromethane and 200 mL saturated sodium bicarbonate were added, leaving a yellow aqueous fraction. The organic fraction was separated and the aqueous fraction extracted twice more with 200 mL dichloromethane. The organic fractions were combined and then washed three times with saturated sodium bicarbonate. The organic portion was then dried with anhydrous magnesium sulfate, filtered and the solvent removed under vacuum. The crude residue was than placed on a vacline for 30 minutes. Column purification using dichloromethane as the eluent resulted in 0.062 g of product (3% yield after column). As this mainly pure sample had a small amount of

aldehyde product it was further purified by preparative TLC (two plates were performed, the first with dichloromethane and the second with ether). This resulted in the pure **54** (a yellow solid) with a yield of 0.030 g (1.4% yield pure).

mp 135 -141 ^{o}C; ^{1}H-NMR (300MHz, $CDCl_3$) δ: 7.64-7.60 (m, 2H), 7.51-7.44 (m, 4H), 7.30-7.25 (m, 1H) 4.70(s,2H) ; ^{13}C-NMR (125 MHz, $CDCl_3$) 193.96, 144.50, 144.04, 142.46, 134.97, 134.78, 134.59, 133.34, 129.27, 124.61, 123.09, 120.63, 120.54, 64.98; IR (neat from CH_2Cl_2 solution, salt plates): ν = 3409, 1713, 1602, 1455, 1342, 1288, 1255, 1174, 1102, 1047, 989, 824, 760, 733 cm^{-1}; UV-Vis (1:1 pH 2 H_2SO_4 - CH_3CN): λ_{max} = 252nm (ε = 14,000), 260 nm (ε = 22,000), 298 nm (ε = 600) ; MS (EI) *m/z*; 210 (95,M+), 193 (20), 181 (100), 165 (10), 152 (70), 76 (10); HRMS, calculated for $C_{14}H_{10}O_2$ 210.0681; observed. 210.0681

3.5.4 Product Studies

3.5.4.1 General Workup

All photolysis reactions were performed using a Rayonet RPR 100 photochemical reactor with 300 nm lamps varying from one lamp to sixteen lamps, and a water-cooled cold finger. Solutions of substrate (~10^{-4} M, 150 mL to 300 mL total) were photolysed for times ranging from one minute to 120 minutes. The quartz photolysis tubes were purged with argon for 15 minutes prior to photolysis and then purged continuously with argon (unless otherwise noted) during photolysis, both to remove oxygen from the solution and to provide continuous mixing during photolysis.

After photolysis of aqueous samples, the photolysis mixture was placed in a separatory funnel and extracted twice with dichloromethane (100 mL). The organic fractions were combined and dried over anhydrous magnesium sulfate before filtering and removing the solvent under vacuum. The residue was placed on a vacuum line for 15 minutes to remove any remaining solvent before characterization of the product mixture via NMR spectroscopy. Samples consisting entirely of organic solvents (acetonitrile) were directly evaporated under vacuum. The identities of the products of the photoreactions were primarily determined by ^{1}H-NMR spectroscopy and the product ratio of the product mixture determined by integration when possible. If separation of the product mixture was warranted, the separation was accomplished using preparatory scale TLC. A maximum of 100 mg was placed on any one plate. The individual separated bands were scraped off into beakers and extracted several times with the appropriate solvent (usually CH_2Cl_2 or diethyl ether) and the solvent removed to yield the purified photoproducts. For aqueous solutions at pH values other than 7, the pH of the aqueous portion was adjusted before combination with acetonitrile. For acidic solutions the pH was adjusted with H_2SO_4 (or D_2SO_4) and for basic solutions the pH was adjusted with NaOH (or NaOD).

3.5.4.2 Individual Product Study Details

Photolysis of 53

Using a 500 mL quartz photolysis tube, **53** (10.7 mg) was dissolved in 150 mL CH_3CN and then 150 mL pH 7 H_2O was added to give a concentration of 1.6 x 10^{-4} M. This was purged with Ar for 15 minutes prior to photolysis with two 300 nm lamps for 2 minutes. The photolysis tube contents were placed in a separatory flask after photolysis and extracted twice with 50 mL CH_2Cl_2. The organic layer was then dried with anhydrous $MgSO_4$ and gravity filtered. The solvent was then removed *in vacuo* and the flask placed on a vacuum line for 20 minutes to remove any remaining solvent. The reaction was then characterized via ^{1}H-NMR spectroscopy and yielded a conversion of 5% of **61** with 2% **59** and 11% oligomeric product. Photolysis for 10 minutes with 8 lamps using the same concentration yields a conversion of 97% via ^{1}H-NMR ($CDCl_3$). Separation of the product mixture by preparative TLC yielded **99** and **98**.

99: ^{1}H-NMR (300MHz, $CDCl_3$) δ: 9.98 (s,1H), 8.35-8.29 (m, 3H), 8.09-8.07 (m, 2H), 7.92-7.90 (m, 1H), 7.79-7.61 (m, 3H), 7.50-7.40 (m, 3H), 7.40-7.35 (m, 2H), 6.00 (s, 1H), 4.30 (m, 2H)

98: ^{1}H-NMR (300MHz, $CDCl_3$) δ: 10.10 (s, 1H), 8.81 (s, 1H), 8.39-8.22 (m, 2H), 7.80-7.68 (m, 2H), 7.60 (d, 1H), 7.40 (m, 1H)

Photolysis of **53** in pH 2 (two 300 nm lamps for 2 minutes) results in a product ratio of 44% **53**; 3% **99**; 31% **98**; 22% oligomeric products.

Photolysis of **53** was accomplished at different irradiation times and conditions. This data on the photolyses of **53** is summarized in Table 3.1.

Photolysis of 54

Using a 500 mL quartz photolysis tube, **54** (5 mg) was dissolved in 75 mL CH_3CN and then 75 mL pH 2 H_2SO_4 was added to give a concentration of 1.6 x 10^{-4} M. This was purged with Ar for 15 minutes prior to photolysis with sixteen 300 nm lamps for 60 minutes. The photolysis tube contents were placed in a separatory flask after photolysis and extracted twice with 30 mL CH_2Cl_2. The organic layer was then dried with anhydrous $MgSO_4$ and gravity filtered. The solvent was then removed *in vacuo* and the flask placed on a vacuum line for 20 minutes to remove any remaining solvent. The reaction was then characterized via ^{1}H-NMR spectroscopy and yielded a conversion of 9% of **106** with 12% **107** and 3% oligomeric products. Photolysis for 15 minutes with 16 lamps using the same concentration yielded a conversion of only 1% **107** with <1% oligomeric products and no observable quantity of **106** via ^{1}H-NMR spectroscopy.

Photolysis of **54** was accomplished at different irradiation times and conditions. This data on the photolyses of **54** is summarized in Table 3.3.

3.5.4.3 UV-Vis Studies

Using 1 cm quartz cuvettes or quartz fluorescence cells, solutions were prepared by filling with 3 mL of the appropriate solvent mixture and spiking with 1-30 μL of concentrated solution of substrate in acetonitrile to get the desired OD. Final concentrations are ~10^{-6} to 10^{-5} M. Cuvettes were then bubbled using fine needles through septa with argon or nitrogen for 15 minutes to remove any dissolved oxygen. Parafilm was then placed over the septa before the UV-vis traces were performed.

3.5.4.4 Laser Flash Photolysis (LFP)

LFP was performed in the University of Victoria LFP facility using an excitation wavelength of 266 nm (pulse width ≈ 20 ns) using a Nd-YAG Spectra Physics laser (GCR-11), power kept under 25 mJ / pulse using attenuation of power.

The LFP spectra for **53** were collected using a flow cell containing the solvent mixture purged with N_2 prior to excitation for 15 minutes. The solvent mixtures used were 1:1 H_2O : CH_3CN (pH 7) and pure CH_3CN. The flow cell consisted of a chamber consisting of ~100 mL of solution containing substrate of ~10^{-5} M with an OD = 0.4 at 266 nm determined by UV-vis spectroscopy. From the flow chamber the solution was pumped continuously into a 7 mm x 7 mm quartz cell at flow rates of ~1.5 mL / min.

The LFP spectra for **54** were collected using static cells containing the solvent mixture containing the substrate of ~10^{-5} M with an OD = 0.4 at 266 nm determined by UV-vis spectroscopy. These static cells used quartz fluorescence cells and were purged with N_2 prior to excitation for 15 minutes. Solvent mixtures used in these cells include 100 % H_2O (pH 2), 100% CH_3CN, and 1 : 1 H_2O : CH_3CN (pH 2, pH 7 or pH 1). Spectra were obtained by plotting the absorbance value at a fixed time after laser excitation for a given wavelength and repeating for other wavelengths at 10 or 20 nm increments across the UV-vis region (280 nm – 700 nm). Multiple shots (4 to 10) were taken and averaged before plotting. Four different time windows were examined to yield data at various times after excitation. This allowed simultaneous generation of spectra at four different times. Windows were selected to illustrate important points in the decay of the transient. Decay data was obtained by measuring 500 absorbance points at equivalent time intervals within a chosen time scale. Time scales used varied between 50 ns and 1

ms. Lifetimes were determined from fitting of the exponential decay. Polyexponential decays were estimated by fitting different regions of the decay with monoexponential fitting. Lifetime data for **53** is listed in Table 3.2 while the lifetime data for **54** is listed in Table 3.4.

Chapter 4
Intramolecular Photoredox Reactions of Biphenyl Derivatives

3.6 Introduction

Formal transmission of charge from one moiety to another is required for the intramolecular photoredox reaction to occur. This "conduction" of electric charge relies on π system conjugation to conduct electric charge from one end of the molecule to the other end. This chapter involves the extension of that conjugation by the addition of an additional phenyl ring.

In the ground state the torsional angle of biphenyl varies tremendously. In the solid state it is planar or nearly so.[114, 115] However, dihedral angles between 10^{o} and 40^{o} have been observed in the solution state for biphenyl.[116, 117, 118] Although planarity would be electronically favoured for the extended conjugation of the aromatic system, steric hindrance between the *ortho-ortho'* hydrogens results in the twisting around the carbon-carbon bond. The conjugation is thus disrupted between the two phenyl rings as the two phenyl rings are twisted with respect to one another. Biphenyl is consequently a relatively poor conductor.[119] Evidence suggests that upon excitation the electronic effects appear to prevail over the steric hindrance favouring a planar alignment of the two benzene rings that gives a better π-system overlap.[120] The ground state of biphenyl exhibits a rather featureless absorption spectrum, consistent with the flexibility inherent in the twisted conformation. Contrastingly, the assignment of planarity of the singlet state is consistent with the observed sharp fluorescence spectrum with distinct features.[121,122] The lowest excited triplet state conformation has also been assigned as

planar.[123] Further evidence of coplanarity in the excited state arises from the photoracemization of optically active biphenyls.[124,125]

This planarization may be utilized to extend the chain of conjugation for an intramolecular photoredox reaction as previously presented for nitroaromatic systems (Section 1.3).[11] This chapter shall examine the effect extension of the aromatic system has on the intramolecular photoredox reaction of benzophenone derivatives.

When biphenyl is substituted with a donating and withdrawing group on either ring (both *para* to central carbon-carbon) a large change in the dipole moments is observed upon excitation, supporting the assertion of significant charge transfer between the phenyl rings.[126] In this Thesis, the two substituents on the biphenyl are a benzoyl group (an electron withdrawing group) and a hydroxymethyl group.

The compounds that will be explored in this chapter are 3-((2'-hydroxymethyl)phenyl)benzophenone (**55**), 3-((3'-hydroxymethyl)phenyl)benzophenone (**56**) and 3-((4'-hydroxymethyl)phenyl)benzophenone (**57**).

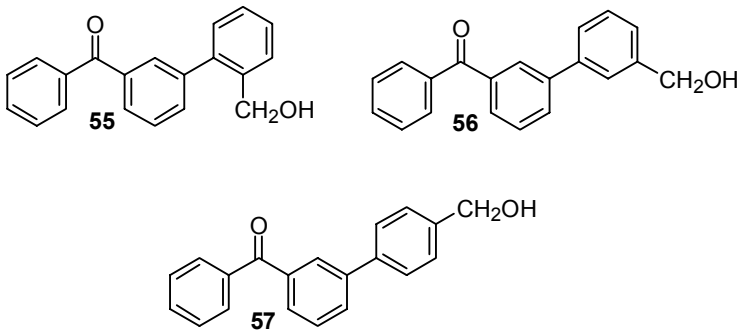

Figure 0.1 Compounds explored in Chapter 4

The potential bichromophoric nature of 3-phenylbenzophenone (**115**) (biphenyl and benzophenone) leads to additional complexity not seen with the monochromophoric nature of the compounds presented in Chapter 2 and Chapter 3. As the photochemistry of

this reaction is believed to proceed via the lowest triplet state it is necessary to identify the nature of the lowest triplet state of these derivatives.

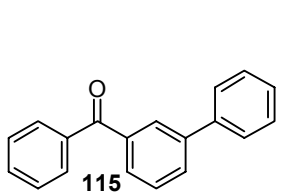

115

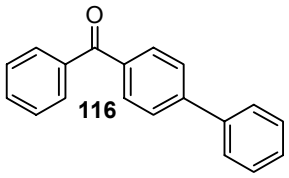

116

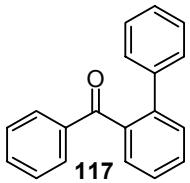

117

A survey of the literature shows no photochemical or photophysical studies of **115** but Tahara *et al*[127] examined the photophysics of 4-phenylbenzophenone (**116**) and Scaiano examined the 2-phenylbenzophenone (**117**)[128] system. Compound **117**, while very interesting does not provide a useful model because it involves significantly more steric hindrance from the close proximity of the ketone and extra benzene ring than the other two systems and shall not be explored further.

Tahara and coworkers[127] presented the case that not only does the biphenyl planarize in **116** upon excitation but that the lowest triplet state involves the excitation being delocalized across the carbonyl and the biphenyl moieties. It is unknown whether the amalgamation of the carbonyl and the biphenyl is possible from the *meta* position as well as from the *para* position but it has been shown that decarboxylation may be accomplished for both the *para*- substituted carboxylic acid and the *meta*-substituted carboxylic acid.[129] Indeed, not only is the *meta*-substituted derivative reactive but is actually more efficient than the *para*-substituted compound. Since the decarboxylation mechanism is believed to be related to the photoredox reaction, it is reasonable to expect that the *meta*-substituted biphenyl derivatives may exhibit electronic communication between the carbonyl and the alcoholic substituent on the biphenyl. This Chapter shall present the results associated with that electronic communication.

3.7 Results and Discussion

3.7.1 Synthesis and Discussion

All target substrates (**55**, **56** and **57**) require synthesis because they are unavailable commercially. It was decided that the most straightforward route, that allowed sufficient flexibility to access all three of the target compounds, was through a Suzuki coupling reaction. Consequently, the first step was to make the two aryl moieties that were to be coupled: 3-trifluoromethanesulfonylbenzophenone (**118**) and the boronic acids: 2-methylboronic acid (**119**), 3-methylboronic acid (**120**), and 4-methylboronic acid (**121**).

Compound **118** was synthesized from the commercially available 3-hydroxybenzophenone (**122**) using trifluoromethanesulfonyl anhydride (Tf_2O) in dichloromethane with pyridine as a non-coordinating base (Eqn. [4.1]). This was obtained in sufficient purity to allow direct usage without further purification.

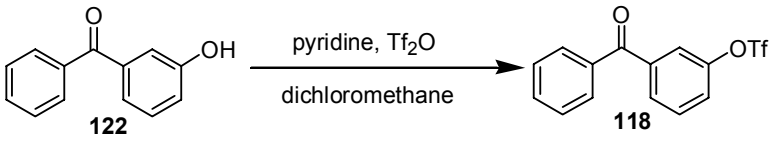

122 **118** [4.1]

The three boronic acids, **119**, **120** and **121** were all synthesized from the relevant commercially available bromotoluenes (**123**, **124** or **125**) by first forming the Grignard reagent and then reacting with trimethyl borate (Eqn. [4.2]). After recrystallization the boronic acids were ready for coupling.

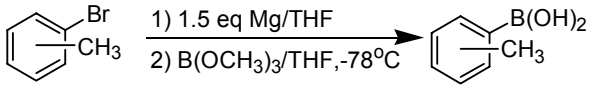

[4.2]

123: o-CH_3
124: m-CH_3
125: p-CH_3

119: o-CH_3
120: m-CH_3
121: p-CH_3

Now that the different aryl moieties were synthesized, they were coupled using a Suzuki coupling reaction (Eqn. [4.3]) to form the relevant 3-(methylphenyl)benzophenones, 3-(2'-methylphenyl)benzophenone (**126**), 3-(3'-methylphenyl)benzophenone (**127**) and 3-(4'-methylphenyl)benzophenone (**128**). Column purification was required to obtain **126**, **127** and **128** in sufficient purity for the next step.

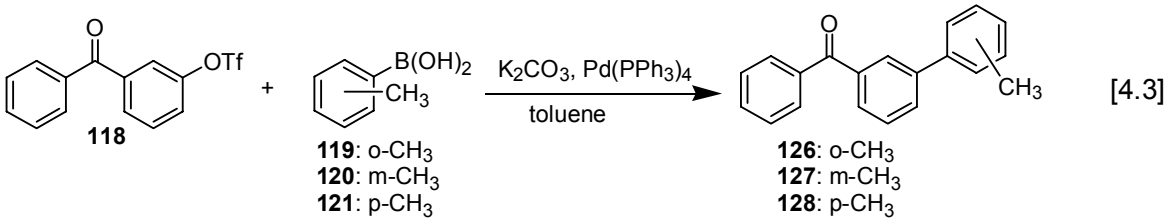

[4.3]

Subsequent bromination of the 3-(methylphenyl)benzophenones was accomplished using N-bromosuccinimide in benzene with benzoyl peroxide as a radical initiator. Hydrolysis in 1:1 water : dioxane with calcium carbonate as a base yielded the final product (Eqn [4.4]). Column purification was necessary to yield the product in sufficient purity for photolysis.

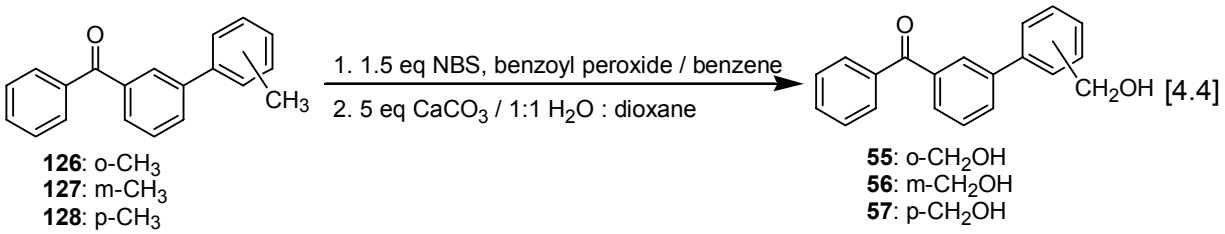

[4.4]

3.7.2 UV-Vis and Product Studies

3.7.2.1 Photoproduct Studies of 55

Proceeding under the assumption that the conjugation of the biphenyl should result in electronic communication between the carbonyl of the benzophenone moiety and the benzylic alcohol, the photoredox chemistry of **55** should be possible with the photoredox product **129** being formed along with trace amounts of the oxidized product **130** (shown in Eqn. [4.5]).

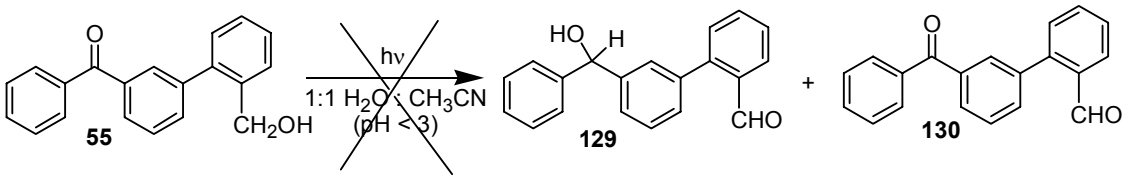

[4.5]

Although **130** was indeed formed in small quantities, **129** was not observed. Instead a new compound was formed providing a ^{1}H-NMR spectrum containing a benzhydrol peak at δ: 5.66 ppm but no aldehyde peak (see Figure 4.2 for product mixture).

Product isolation of the reaction mixture led to two products whose ^{1}H-NMR spectra are presented in Figure 4.3. The lower spectrum is consistent with the oxidized product **130** while the upper spectrum is consistent with the cyclized product **131**. Thus the actual photoreaction observed is that presented in Eqn [4.6].

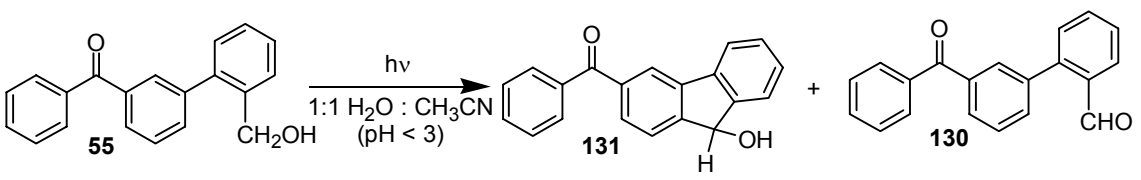

[4.6]

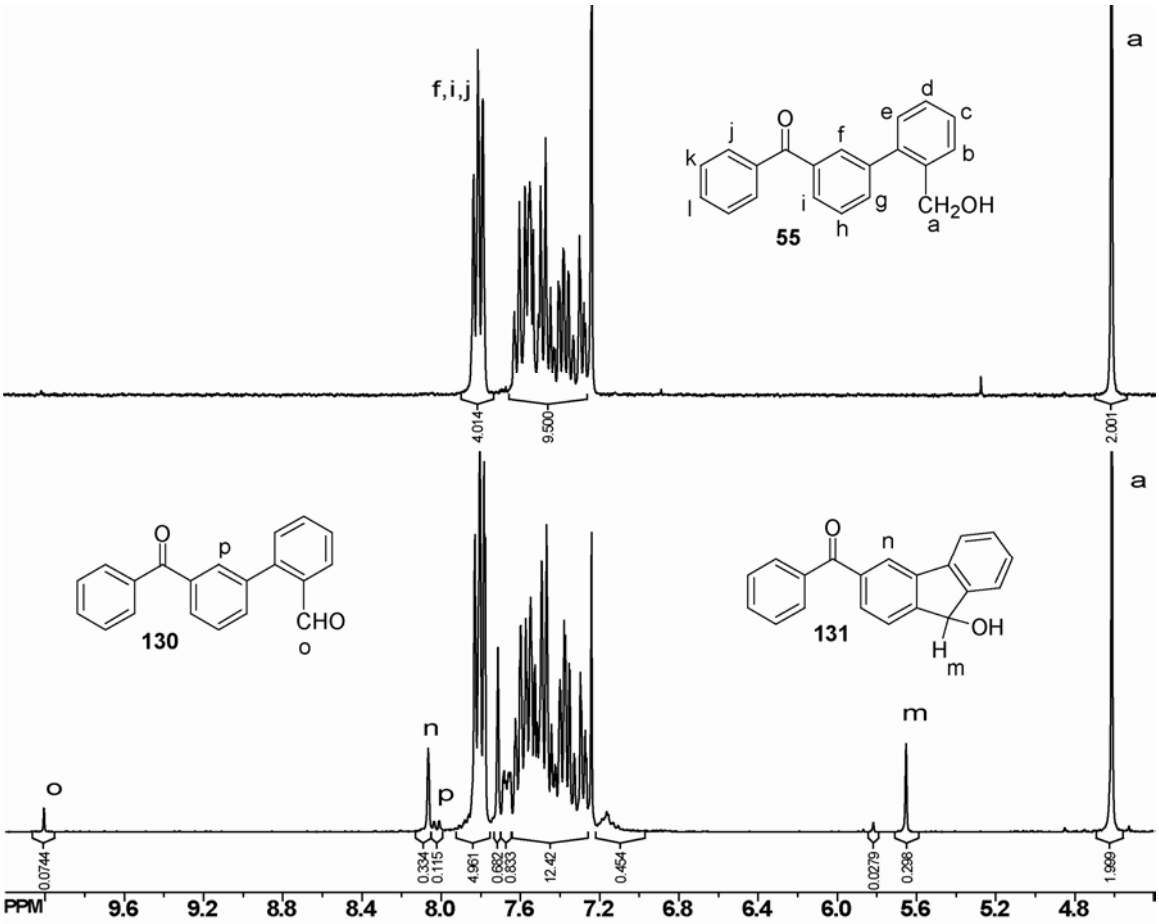

Figure 0.2 300 MHz ^{1}H-NMR spectra of **55** (in chloroform-*d*) before (top) and after (bottom) photolysis (1.6×10^{-4} M, 13.7 mg/300 mL) in 1:1 H_2O : CH_3CN (pH 2), for 2 minutes with two 300 nm lamps (argon purged). Product ratio:84% **55**: 10% **131**: 5% **130**: 1% oligomeric product. Product ratio was determined by comparing the integrations for the peak due to the fluorenol peak of **131** (**m**: 5.61 ppm, 0.298H) to the singlet of **55** (**a**: 4.60 ppm, 2.00H) and the singlet due to the aldehyde of **130** (**o**: 10.10 ppm, 0.0744H).

The isolated compound **131** is not the expected photoredox product. It is formally an additional oxidation product as two hydrogens have been lost. However, as will be presented in Section 3.7.4 the structure of **131** is consistent with a trapping of the photoredox product via cyclization.

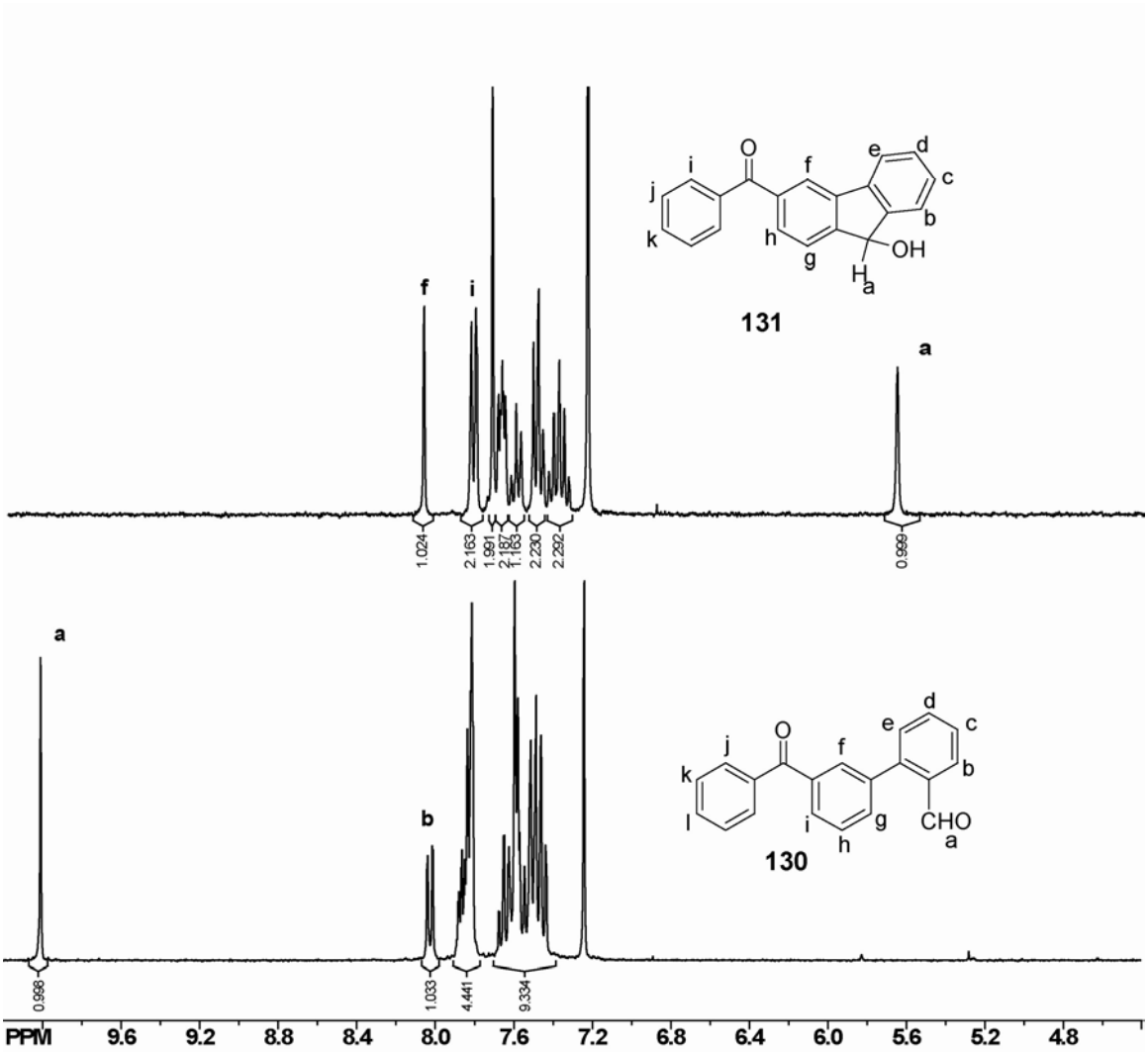

Figure 0.3 300 MHz ^{1}H-NMR spectra (in chloroform-*d*) of **131** (top) and **130** (bottom) isolated from the photoproduct mixture. This photoproduct mixture arose from photolysis of **55** (1.6 x 10^{-4} M, 13.7 mg/300 mL) in 1:1 H_2O : CH_3CN (pH 2), for 2 minutes with two 300 nm lamps (argon purged).

The photolysis reaction of **55** was followed using a solvent medium of 1:1 H_2O : CH_3CN with two different proton concentrations (pH 2 and pH 7). The run under acidic conditions (pH 2) is presented in Figure 4.4. The trace shows the decay in the original spectrum of **55** with a concomitant increase in bands at both lower and higher wavelengths along with a noticeable bathochromic shift of the original peak at 253 nm as it decays. The bathochromic shift is consistent with increased conjugation of **131** caused

by the planarization of the ground state via cyclization. The UV-vis spectral trace follows the photolysis reaction between zero and eight minutes of irradiation. Within that irradiation time the reaction proceeds fairly smoothly from **55** with two noticeable isosbestic points. Further irradiation showed deviation from those isosbestic points and may be the result of secondary reactions under higher conversions.

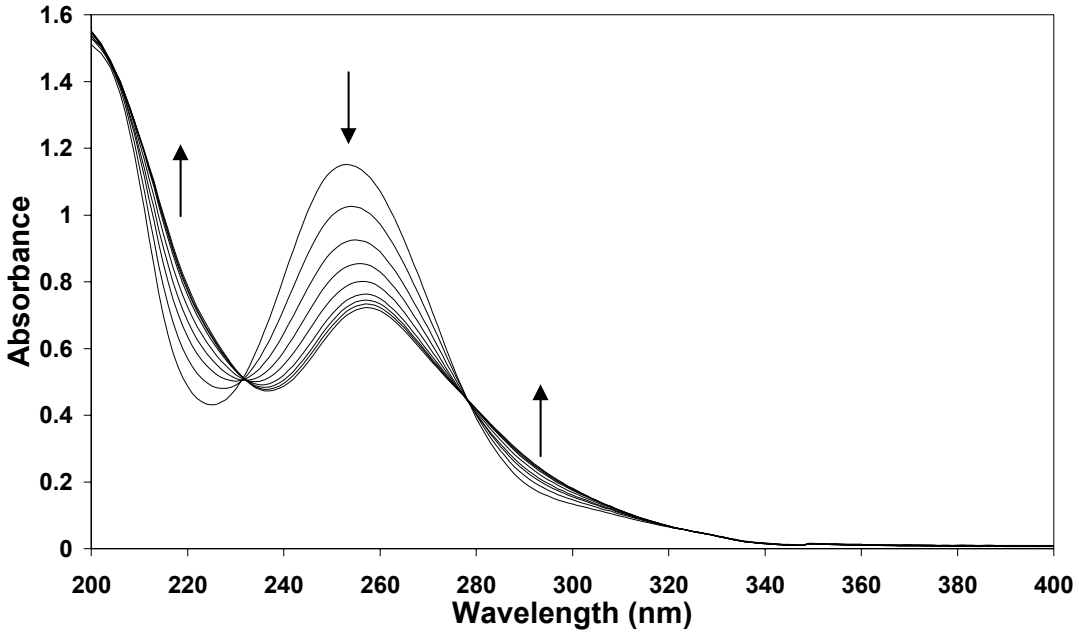

Figure 0.4 UV-vis spectral traces observed on photolysis of **55** in 1:1 H_2O : CH_3CN (pH 2). Each trace is taken after increasing irradiation time at 300 nm using two lamps at 6.5 x 10^{-5} M. The first four spectra are taken after irradiation by successive 30 second intervals. Subsequent traces are taken after successive 1 minute irradiation intervals.

Photolysis under neutral conditions is presented in Figure 4.5. Although some photoreaction was observed at pH 7, the efficiency is quite obviously lower than under acidic conditions indicating acid catalysis of the photoreaction is present. This would be consistent with a mechanism that proceeded via the protonated carbonyl oxygen.

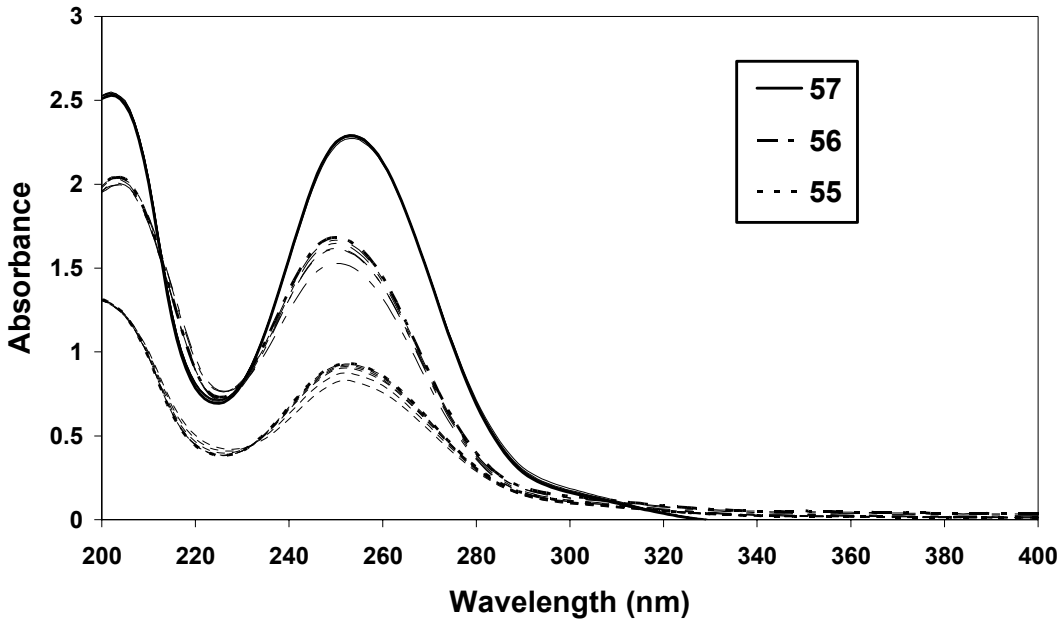

Figure 0.5 UV-vis spectral traces observed on photolysis of **55**, **56** and **57** in 1:1 H_2O : CH_3CN (pH 7). Each trace is taken after increasing irradiation time at 300 nm using two lamps at 6.5 x 10^{-5} M. The irradiation time doubles with each trace, starting with 1 minute and ending after 32 minutes.

By examining the product mixture under different solvent conditions, more information was obtained. Increasing the proton concentration from pH 2 to pH 1 decreases the proportion of **130** produced but does not significantly affect the amount of **131** produced. However, when the proton concentration was lowered to pH 7 primarily **130** was produced. Compound **131** was still produced but in a much smaller proportion of the product mixture than at pH 2 or pH 1. The different proton concentration dependence exhibited by **130** and **131** illustrates different origins. This is consistent with **130** arising from residual oxygen. Compound **131**, however, proceeds via a mechanism involving acid catalysis. A mechanism consistent with this data is presented in Section 3.7.4.

In addition to **130** and **131**, significant oligomeric product was produced at pH 7. Other unknown products were formed in increasingly larger proportions as irradiation increased. Photolysis in 100% acetonitrile resulted in only a trace of **131** with the product mixture primarily consisting of **130** and the oligomeric product. Results of photolysis in different solvent mixtures and at different photolysis times are presented in Table 4.1.

Table 4.1 Comparison of Product Mixture Ratios from Photolysis of **55** at Varying pHs[b]

Photolysis time 300 nm lamps	**pH[a]**	% **55**	%**131**	%**130**	%**OP**[c]	%other
2 lamps, 1 minutes	2	91	6	2	1	0
2 lamps, 2 minutes	2	84	10	5	1	0
2 lamps, 5 minutes	2	71	21	5	3	0
4 lamps, 5 minutes	2[d]	42	48	2	8	0
2 lamps, 5 minutes	7	69	0	19	10	2
2 lamps, 20 minutes	7	38	4	27	23	8
4 lamps, 20 minutes	7	20	4	27	35	14
2 lamps, 5 minutes	1	72	22	1	3	2
2 lamps, 10 minutes	1	55	34	2	6	3
2 lamps, 20 minutes	1	32	46	1	17	4
2 lamps, 10 minutes	ACN	80	1	11	7	1

[a]Using 13.7 mg of **55** in 300 mL (1.58×10^{-4} M) 1:1 H_2O : CH_3CN, pH adjusted with H_2SO_4.
[b]Product mixture ratio determined by integration via ^{1}H-NMR($CDCl_3$).
[c]Oligomeric side product (**OP**)approximate, estimated from integration via ^{1}H-NMR($CDCl_3$).
[d]Using 15.1 mg of **55** in 300 mL (1.75×10^{-4} M) 5:1 H_2O : CH_3CN, pH adjusted with H_2SO_4.

Photolysis was also performed in 1:1 D_2O : CH_3CN (pD 2) and the products isolated via preparative TLC. No deuterium incorporation was observed in either **131** or **130** via ^{1}H-NMR spectroscopy or mass spectrometry (EI). This result eliminates the possibility of incorporation of a proton from the solvent.

3.7.2.2 Photoproduct studies of 56

The photolysis of **56** differs in a number of ways from the photolysis of **55**. Following the photolysis in 1: 1 H_2O : CH_3CN (pH 2) by UV-vis spectroscopy (Figure 4.6) resulted in a decay of the peak at 256 nm with a concomitant increase in a band at lower wavelengths. However, unlike the bathochromic shift observed for **55**, the peak at 256 nm undergoes a slight hypsochromic shift.

The photolysis of **56** was also followed under neutral conditions (1: 1 H_2O : CH_3CN (pH 7)). This is shown along with the traces of **55** and **57** for ease of comparison in Figure 4.5. The reaction efficiency is similar to **55** and is significantly less reactive than it is under acidic (pH 2) conditions.

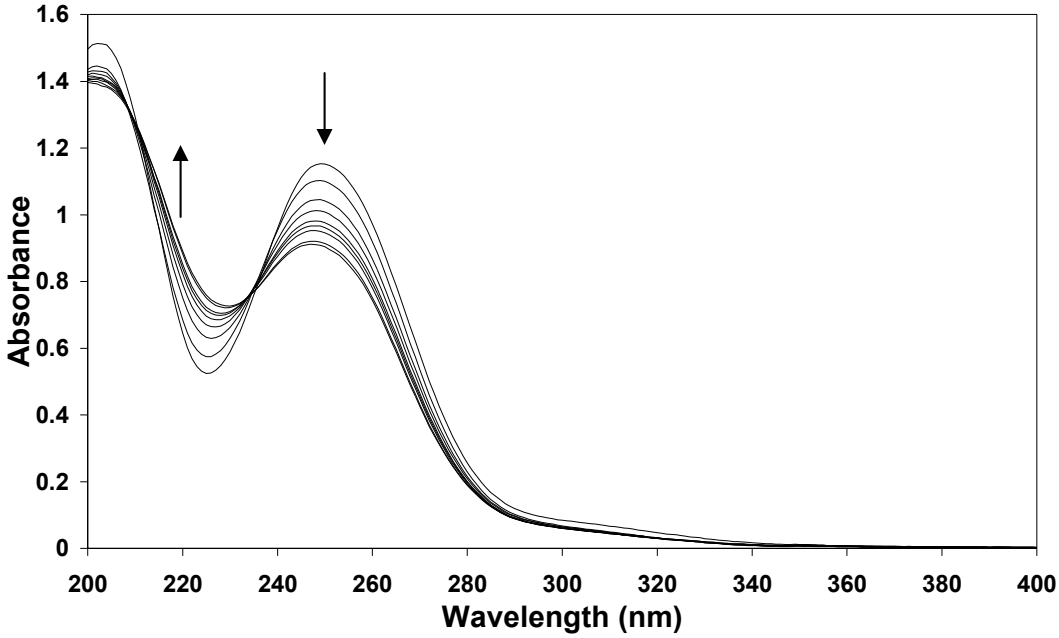

Figure 0.6 UV-vis spectral traces observed on photolysis of **56** in 1:1 H_2O : CH_3CN (pH 2). Each trace is taken after increasing irradiation time (successive two minute intervals) at 300 nm using two lamps at 6.5 x 10^{-5} M.

Photolysis of **56** at pH 2 (shown in Eqn. [4.7]) did not result in any observable redox product **132**, but the oxidized product **133** was observable with significant quantities of oligomeric product. Photolysis in pH 1 however, shows two different compounds with similar integrations in the appropriate regions to correspond to **132**. Both show benzhydrol protons in the region δ: 6.2 - 6.0 ppm and aldehyde protons in the region δ: 10.0 -9.8 ppm.

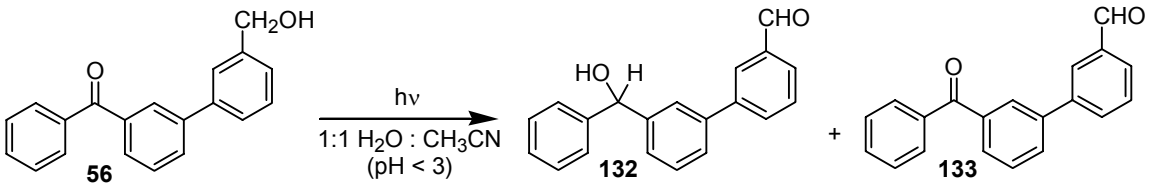

[4.7]

This information was not sufficient to categorically state which peaks are assignable to **132** and unfortunately the products of this reaction were never isolated to

confirm the identity. Regardless, the main product appears to be **133** in stark contrast to the results from the photolysis of **55** that strongly favoured the formation of **131**. This is likely because cyclization is not possible for **56**. The results of the photoproduct studies under different solvent conditions and different irradiation times are listed in Table 4.2.

Table 4.2 Comparison of Product Mixture Ratios from Photolysis of **56** at Varying pHs[b]

Photolysis time 300 nm lamps	**pH[a]**	**% 56**	**%132**	**%133**	**%OP[c]**
2 lamps, 2 minutes	2	90	0	7	3
2 lamps, 5 minutes	2	88	0	9	3
2 lamps, 10 minutes	2	85	1	9	5
2 lamps, 10 minutes	7	97	0	3	<1
2 lamps, 5 minutes	1	72	2	11	13
2 lamps, 10 minutes	1	51	2	15	31

[a]Using 13.7 mg of **56** in 300 mL (1.58×10^{-4} M) 1:1 H_2O : CH_3CN, pH adjusted with H_2SO_4.
[b]Product mixture ratio determined by integration via ^{1}H-NMR($CDCl_3$).
[c]Oligomeric side product (**OP**)approximate, estimated from integration via ^{1}H-NMR($CDCl_3$).

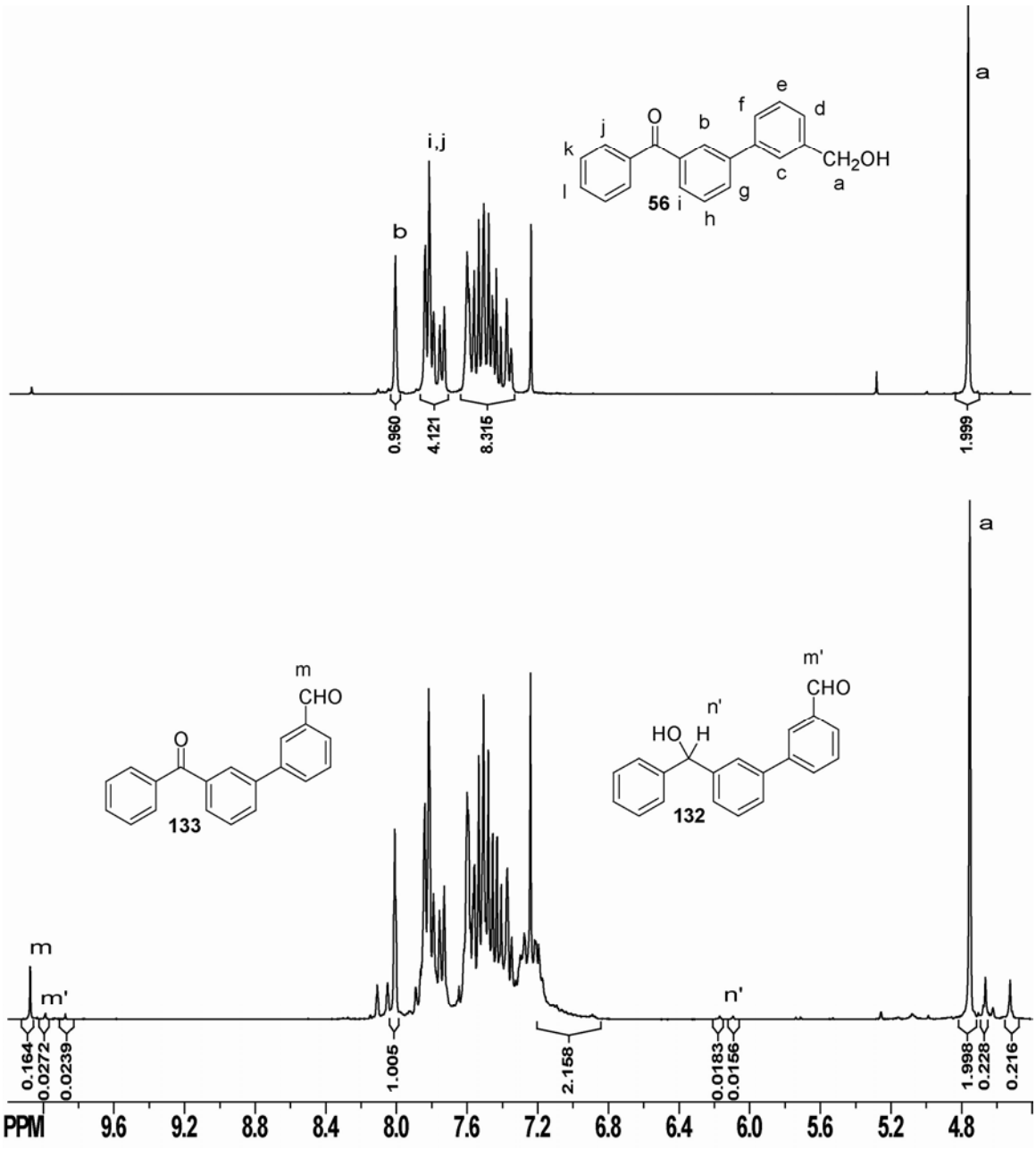

Figure 0.7 300 MHz ^{1}H-NMR spectra of **56** (in chloroform-*d*) before (top) and after (bottom) photolysis (1.6 x 10^{-4} M, 13.7 mg/300 mL) in 1:1 H_2O : CH_3CN (pH 2), for 5 minutes with two 300 nm lamps (argon purged). Product ratio: 72% **56**: 2% **132**: 11% **133**: 13% oligomeric product. Product ratio was determined by comparing the integrations for the peak due to the aldehyde of **132** (**m'**: 9.98 ppm, 0.027H) to the singlet of **56** (**a**: 4.80 ppm, 2.0H) and the singlet due to the aldehyde of **133** (**m**: 10.10 ppm, 0.16H).

3.7.2.3 Photoproduct Studies of 57

Photolysis of **57** in 1: 1 H_2O : CH_3CN (pH 2) leads primarily to oligomeric product with the oxidized product **134** as a secondary product.

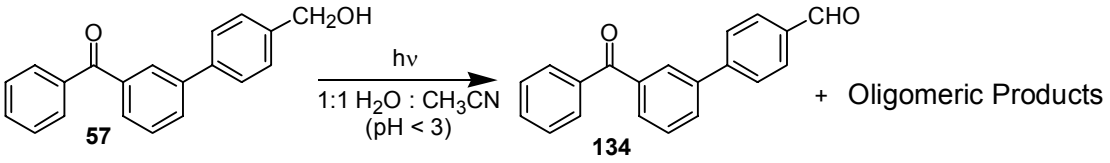

57 134 [4.8]

No photoredox product **135** was observed.

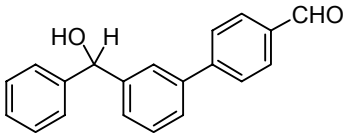

135

Extensive photoproduct studies were not conducted as the photoreaction observed does not seem to result in any photoredox reaction. The summary of the abbreviated photoproduct studies is given in Table 4.3

Following the photolysis of **57** in 1:1 H_2O : CH_3CN (pH 2) by UV-vis spectroscopy resulted in the UV-vis spectral trace shown in Figure 4.7. Loss of the primary band at 256 nm is accompanied with a concomitant increase at higher and lower wavelengths. The spectral traces pass through a couple of isosbestic points with the exception of the peak before irradiation. It is possible that the initial photolysis reaction is more complex and then becomes simpler upon subsequent photolysis (possibly the formation of oligomeric products). The subsequent simplification of the UV-vis spectral trace may arise from the fact that **131** has a much greater extinction coefficient than **57** and may promote additional photochemical reactions.

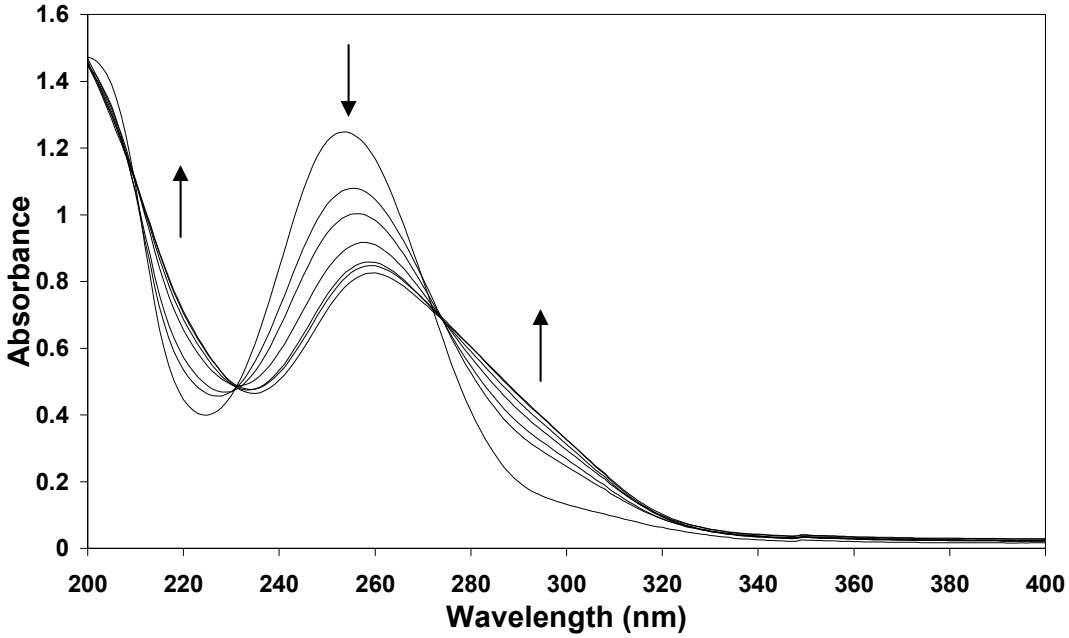

Figure 0.8 UV-vis spectral traces observed on photolysis of **57** in 1:1 H_2O : CH_3CN (pH 2). Each trace is taken after increasing (successive 1 minute intervals until 4 minutes and then successive 2 minute intervals) irradiation time at 300 nm using two lamps at 6.5 x 10^{-5} M.

Table 4.3 Comparison of Product Mixture Ratios from Photolysis of **57** at Varying pHs[b]

Photolysis time 300 nm lamps	**pH[a]**	**% 57**	**%135**	**%134**	**%OP[c]**
2 lamps, 2 minutes	2	75	0	7	18
2 lamps, 5 minutes	2	60	0	11	29
4 lamps, 5 minutes	2	29	0	17	54

[a]Using 14.1 mg of **57** in 300 mL (1.63 x 10^{-4} M) 1:1 H_2O : CH_3CN, pH adjusted with H_2SO_4.
[b]Product mixture ratio determined by integration via ^{1}H-NMR($CDCl_3$).
[c]Oligomeric side product (**OP**) approximate, estimated from integration via ^{1}H-NMR($CDCl_3$).

3.7.2.4 Comparison of Photoproduct Studies of 55, 56 and 57

To facilitate comparison of the photoproduct studies, the three biphenyls' (**55**, **56** and **57**) photoproduct mixture ratios are summarized together under equivalent photolysis times in Table 4.4. The identity of the primary product differs for each biphenyl. All three biphenyls (**55**, **56** and **57**) form the oxidation product (**130**, **133** and **134** respectively) but the amount varies widely. The *ortho* compound **55** favours the formation of the cyclized product **131** as its primary photoproduct. The *meta* compound **56** favours the oxidized product **133** but also forms small amounts of the expected redox product **132** at higher conversions. The *para* compound **57** produces the most oligomeric product, a little oxidized product **134,** and no observable photoredox product **135**. Similarities exist between **55** and **56** in the UV-vis spectral traces performed under neutral conditions. Both seem to be of similar efficiency whereas **57** seems relatively unreactive under neutral conditions (Figure 4.5). Although photolysis of **55** and **56** lead to very different photolysis products, both photoreactions proceed to photoredox products. This is consistent with the concept of the *ortho-meta* effect mentioned previously.[61] The *ortho* and *meta* positions should see much greater activity than the *para* position in the excited states. As the *para* compound seems to primarily form the oligomeric products and does not seem to form the redox product it likely proceeds through a different mechanistic pathway.

The observed photoproduct trend is also consistent with the relative conversions for the different biphenyls. The most reactive is actually **57** but as it is mostly reactive

towards oligomeric products the photoconversion is considered to progress via an alternative pathway. This is likely a similar pathway to that which leads to the oligomeric side-products of all of the compounds explored in this Thesis. Compound **55** is significantly more reactive than **56** and proceeds towards the cyclized product **131** in preference to the oxidation product **130**. Contrastingly, **56** primarily forms the oxidized product **133** and only forms a small amount of the redox product **132** (mostly at pH 1).

Table 4.4 Photoproduct ratio comparison between **55**, **56** and **57** under equivalent conditions[b]

	Photolysis time 300 nm lamps	**pH[a]**	**% 55**	**%131**	**%130**	**%OP[c]**
55	2 lamps, 2 minutes	2	84	10	5	1
55	2 lamps, 5 minutes	2	71	21	5	3
55	4 lamps, 5 minutes	2	42	48	2	8
	Photolysis time 300 nm lamps	**pH[a]**	**% 56**	**%132**	**%133**	**%OP[c]**
56	2 lamps, 2 minutes	2	89	0	7	3
56	2 lamps, 5 minutes	2	88	0	9	3
56	2 lamps, 10 minutes	2	85	1	9	5
	Photolysis time 300 nm lamps	**pH[a]**	**% 57**	**%135**	**%134**	**%OP[c]**
57	2 lamps, 2 minutes	2	75	0	7	18
57	2 lamps, 5 minutes	2	60	0	11	29
57	4 lamps, 5 minutes	2	29	0	17	54

[a]Using (~1.6 x 10^{-4} M of **55**, **56** or **57**) 1:1 H_2O : CH_3CN, pH adjusted with H_2SO_4.
[b]Product mixture ratio determined by integration via ^{1}H-NMR($CDCl_3$).
[c]Oligomeric side product (**OP**)approximate, estimated from integration via ^{1}H-NMR($CDCl_3$).

3.7.3 Nanosecond Laser Flash Photolysis (LFP)

The compounds of this chapter (**55**, **56** and **57**) are unique within this Thesis as they are the only bichromophoric compounds examined. This bichromophoric system is unusual because the biphenyl and the benzophenone share an aromatic ring and may be amalgamated into one larger chromophore with both benzophenone and biphenyl character. In order for photoredox behaviour to be observed, the lowest energy excited state requires the carbonyl and the alcohol to be conjugated to one another electronically. Although the photophysics of **55**, **56** and **57** are unknown, the evidence presented by Xu[129] on the decarboxylation of (3-benzoyl)biphenylacetic acid and the findings by Tahara[127] with regards to 4-phenylbenzophenone **116**, support the assertion that this extended conjugation is possible.

LFP was performed on **55** in 1:1 H_2O : CH_3CN at two different proton concentrations (pH 2 and pH 7) in an attempt to obtain energy on the lowest energy electronically excited triplet state. The transient absorption spectrum obtained in 1:1 H_2O : CH_3CN (pH 7) is presented in Figure 4.9. Two major peaks are visible at 520 nm and 360 nm. These peaks are both quite broad with the band at 520 nm extending from less than 400 nm all the way to 700 nm. This leads to absorption over almost all of the range of the spectrum. As these two bands decay, a longer lived species present at 320 nm appears. This longer lived species may be correlated with the longer lived species observable during the LFP of the parent benzophenone **47**.

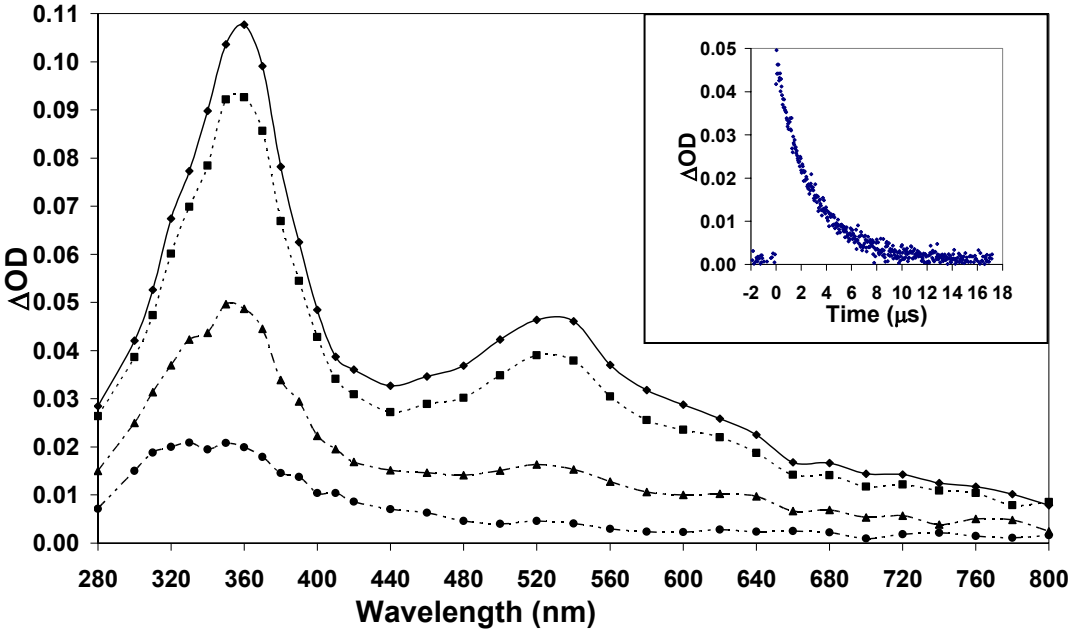

Figure 0.9 Triplet-triplet absorption spectrum observed on LFP (λ_{ex} 266 nm) of **55** in 1:1 H_2O : CH_3CN (pH 7), using a flow cell with continuous N_2 purging. The four spectra are taken at the following intervals: immediately after the laser pulse, after 0.6 μs, after 3 μs and after 8 μs. Inset is decay trace taken at 540 nm.

Direct assignment of the bands from previous literature is not possible as no papers were found to involve the 3-phenylbenzophenone (**115**) chromophoric base. However as photostudies have been performed on both 4-phenylbenzophenone[130] (**116**) and 2-phenylbenzophenone[128] (**117**) some conclusions may be made.

The triplet-triplet absorption spectrum for **117** has a single peak at 360 nm with no other significant peaks at higher wavelengths. This absorption band corresponds closely with the triplet-triplet absorption observed previously for biphenyl[131] and it is likely in the case of **117** that biphenyl is the lowest triplet state that forms after initial excitation of the benzophenone. Similarly **116** also has the lowest triplet state being biphenyl-like in character (π,π^*).[36] However unlike **117**, **116** also has a peak at 525 nm that corresponds well with the benzophenone triplet. Compound **117** is thought to behave

differently because steric hinderance prevents the formation of an “all planar” configuration and must instead interconvert via ring rotation between two different conformers, one with the benzophenone twisted and one with the biphenyl twisted. It is reasonable to conclude that the 3-phenylbenzophenones presented in this chapter would be able to planarize as they do not have the steric hinderance observed for **117**.

The triplet-triplet absorption spectrum of **55** is consistent with this conclusion as the triplet has two peaks, one at 360 nm which corresponds well with biphenyl and one at 525 nm which corresponds well with the benzophenone moiety. Additionally, the longer lived species at 320 nm also corresponds with a transient previously observed during the LFP for **47**. The assignment of the lowest electronically excited triplet state of **55** as an extended biphenyl plus carbonyl conjugated system is consistent with the triplet-triplet absorption spectrum exhibited by **47**.

The triplet-triplet absorption spectrum of **55** in 1:1 H_2O : CH_3CN (pH 2) (shown in Figure 4.10) was taken to compare with the spectrum obtained under neutral conditions. The spectrum retains the peaks at 360 nm and 520 nm observable in the spectrum taken under neutral conditions with an additional broad band centered at 700 nm. Decay traces were taken for all three peaks and lifetimes derived from monoexponential fits. At pH 2 the band at 360 nm is biexponential. This is consistent with the fact that the band at 330 nm does not decay to baseline while the other bands do. The lifetimes derived from fitting the decay traces are tabulated in Table 4.5 for both pH 2 and pH 7 solvent solutions. Considerable proton quenching is observed as the lifetimes shorten for all bands.

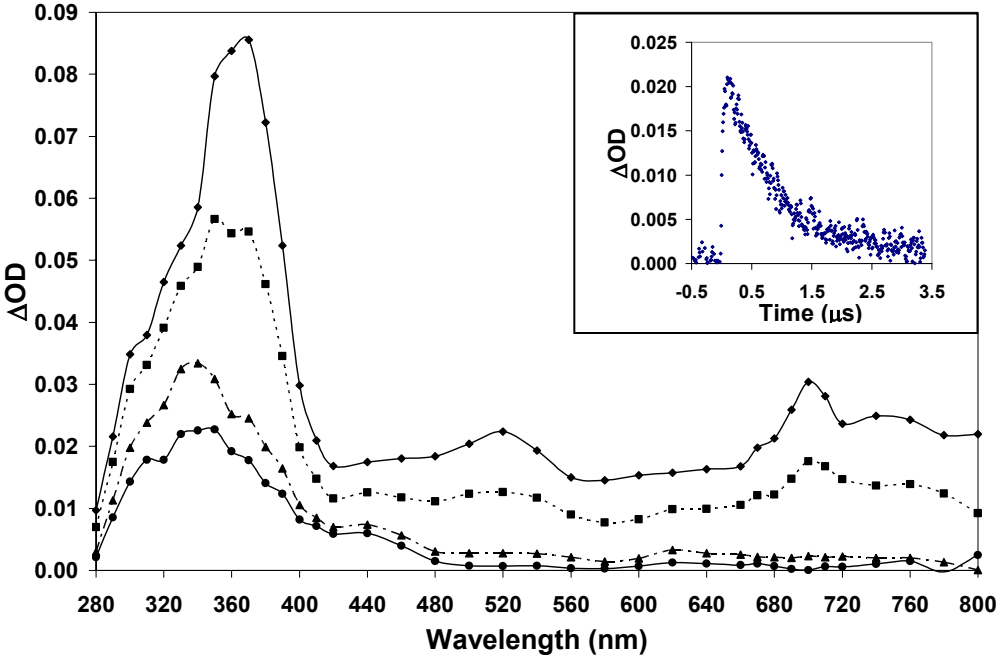

Figure 0.10 Triplet-triplet absorption spectrum observed on LFP (λ_{ex} 266nm) of **55** in 1:1 H_2O : CH_3CN (pH 2), using a flow cell with continuous N_2 purging. The four spectra are taken at the following intervals: immediately after the laser pulse, after 0.7 μs, after 2 μs and after 7 μs. Inset decay trace taken at 700 nm.

Lifetimes of transients for both pH 7 and pH 2 are quenched by oxygen in addition to the quenching observed due to proton concentration. This supports the assertion that the transient observed is most likely the triplet.

Table 4.5 Lifetime comparison of **55** in solvent media of different proton concentrations[a]

pH 7			**pH 2**			
λ_{max}	**360 nm (μs)**	**520 nm (μs)**	**λ_{max}**	**360 nm (μs)**	**520 nm (μs)**	**700 nm (μs)**
N_2	2.2	2.6	**N_2**	0.76	0.98	0.87
Long component	---	3.8	**Long component**	2.7	---	---
O_2	0.12	0.11	**O_2**	0.12	0.12	0.12

[a] Lifetimes were obtained by exponential fitting of decay traces in 1:1 H_2O : CH_3CN, (pH 7 or pH 2), N_2 or O_2 purged; fitting was monoexponential unless otherwise indicated. $[O_2]_{acetonitrile} = 9.1 \times 10^{-3}$ M; $[O_2]_{water} = 1.27 \times 10^{-3}$ M

3.7.4 Proposed Mechanism

The reaction shown in Eqn [4.6] is proposed to proceed through a mechanism similar to that first introduced in Chapter 2 Section 2.2.5. In Section 3.7.3 the LFP spectrum for **55** was analyzed and compared with the spectra for **116** and **117** that were described in the literature. In that section the argument was made that **115** had a lowest triplet state that was a π,π* state primarily biphenyl in character but also containing some benzophenone character due to the inclusion of bands associated with both the benzophenone (520 nm) and the biphenyl (360 nm) chromophores. As the lowest triplet appears to contain both chromophores, the structure of the triplet may be thought of involving both the carbonyl and the aromatic π bonds in a π,π* triplet state. This is consistent with the research presented by Tahara and coworkers on **116**.[127] The presence of the lowest triplet state being a π,π* state is consistent with the observed reaction because a π,π* state is required for the photoredox reaction to occur.

Section 3.7.3 also presented data that showed that the triplet lifetime was quenched by protons which is consistent with the first step in the mechanism being the protonation of the ketone oxygen to give **136a**. As for **47** the ketone for **55** should be basic in the excited state. The acid catalysis is observed in the product studies as well, where **131** was found to be preferentially favoured over **130** as the pH was lowered from pH 7 to pH 2 to pH 1.

Because the triplet state is thought to be an amalgamation of the carbonyl and the biphenyl moieties, planarization should occur to give the structure **136b** which should

promote the deprotonation of a benzylic proton to form the dienol **137a**. The oxidized product **130** may derive from the residual oxidation by atmospheric oxygen of **137b**. The zwitterion **138** is an analogue of the zwitterion introduced in Chapter 2 but instead of resulting in the oxidation of the benzylic position and reduction of the benzophenone carbonyl, cyclization occurs to form the photoredox product **139** which upon workup is oxidized to the cyclized product **131**. This mechanism is shown in Scheme 4.1.

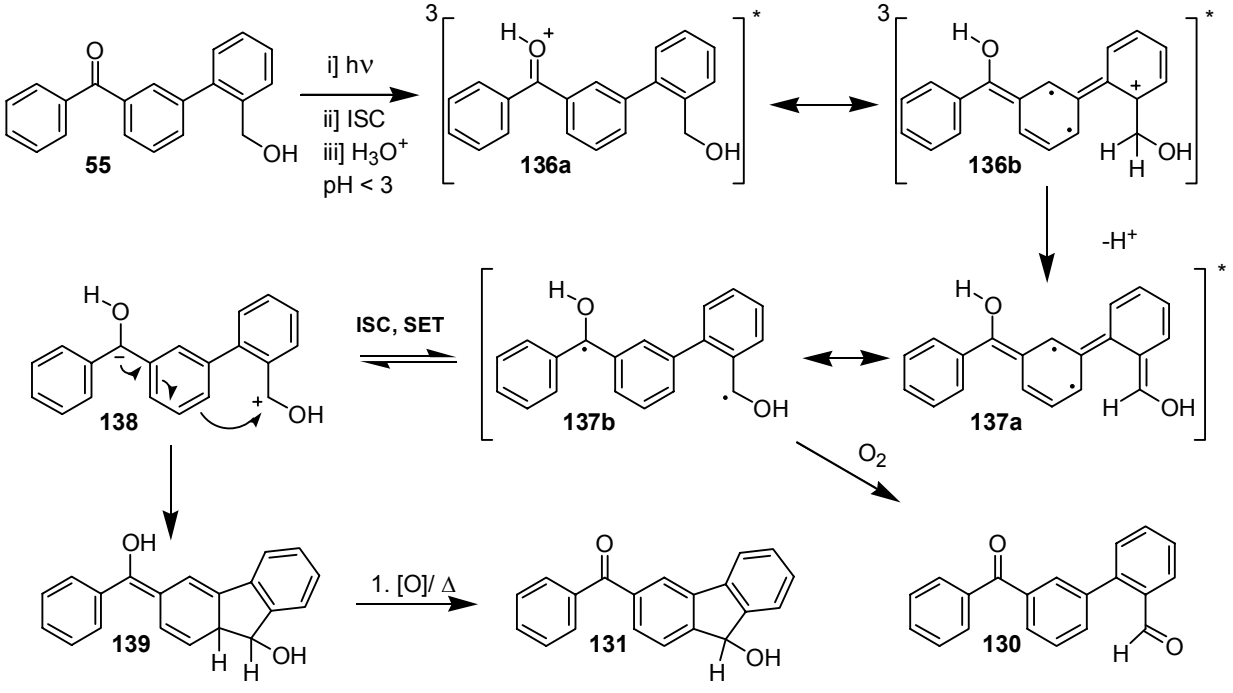

Scheme 0.1

Cyclization of *ortho*-substituted biphenyl has been previously shown to occur photochemically.[132] Although many previous studies presented electrocyclic ring closures,[133,134] the ring closure presented in this Chapter appears to be a nucleophilic attack on the positive charge of the zwitterion by the aromatic ring. Nucleophilic

cyclization via a cation has previously been observed by 2-amino-2'-methylbiphenyl to form fluorene following diazotization.[135]

The oxidation of **139** to **131** must proceed directly rather than first protonating the aromatic ring because photolysis in deuterated aqueous solvent mixture (1:1 D_2O : CH_3CN, (pD 2)) did not result in any incorporation of deuterium into either **131** or **130** according to the integration of the aromatic peaks in the ^{1}H-NMR spectrum or by MS.

The photobehaviour of **56** and **57** differ significantly from **55** so must be dealt with separately. Unlike the case for **55,** the zwitterion (**140**)(analogous to **138**) may not be trapped via cyclization and consequently the majority product of the photolysis of **56** and **57** is the oxidized product rather than the redox product. A proposed mechanism for the photoreaction of **56** is shown in Scheme 4.2. As the mechanism for **57** is expected to be essentially the same it has not been presented in detail.

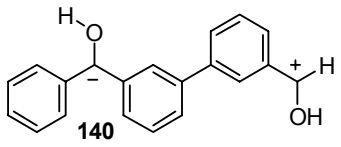

140

Like **55**, the photoreactions of **56** and **57** are also acid-catalysed. This is clearly shown in the differences in the UV-vis spectral traces between the pH 2 and the pH 7 runs. Thus, it is likely that the initial protonation of the triplet to form **138a** is the initial step. As the chromophore for **56** and **57** should be the same as for **55**, the carbonyl and the biphenyl are conjugated to one another and the positive charge will be localized at the carbon attached to the benzylic carbon (**138b**). This promotes the deprotonation to form the dienol **139**. Through product studies and UV-vis spectral traces it became evident that **57** is not as reactive towards this reaction pathway as **55** and **56.** This is not unreasonable because of the *ortho-meta* effect mentioned by Zimmerman.[61] Because this

pathway is not as favourable the oligomeric product pathway competes effectively and **57** has the largest proportion of oligomeric product that is produced.

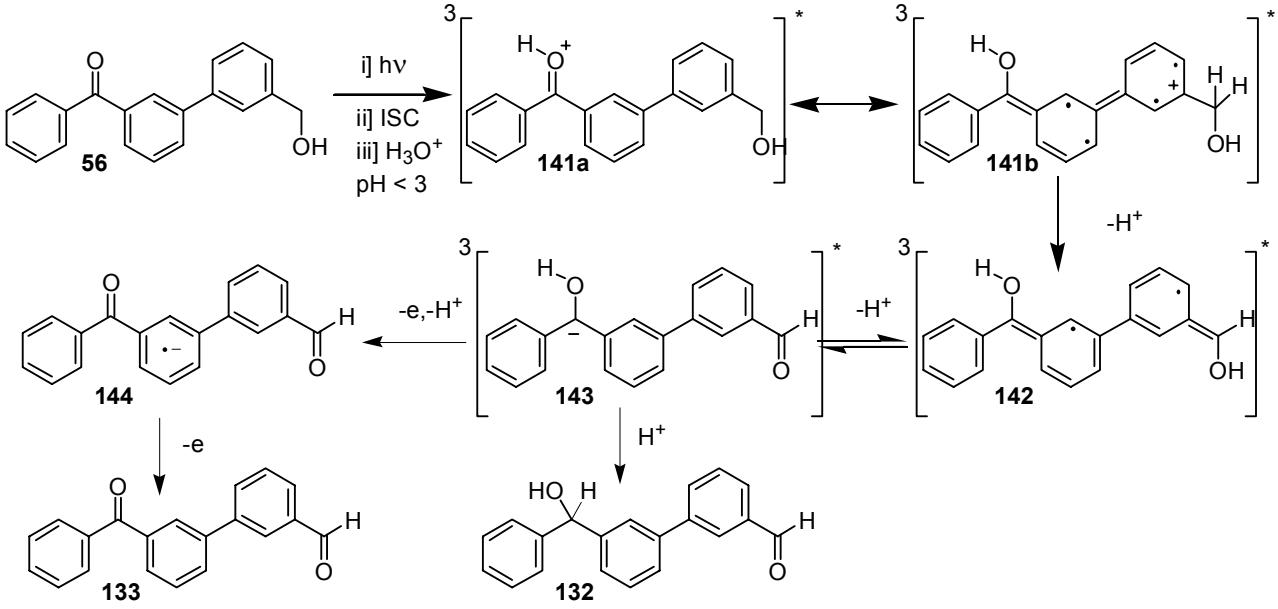

Scheme 0.2

The loss of another proton would result in **143** which, if protonated, would form the redox product **132**. However this only occurred in trace quantities at higher conversions. The main product is the oxidized product **133**. Because this is the majority product, it may be postulated that the anion **143** is not particularly stable. It has previously[136] been shown that the α-hydroxyl proton favours the loss of an electron and a proton (sequentially or via one step loss of a hydrogen atom) to form the radical anion **144**. Subsequent loss of an electron would lead to the oxidized product **133**.

Simple HOMO/LUMO (Chem3D, MOPAC/AM1) representations were produced for **55**, **56** and **57** to provide an estimation of the initial electronic behaviour upon excitation. The similarity between the HOMO/LUMO representations for **55**, **56**, and **57** as compared to **47** is striking. These were presented for **47** in Section 2.2.5. The HOMO/LUMO representations are presented in Figure 4.10, Figure 4.11 and Figure 4.12

for **55**, **56** and **57** respectively. All three compounds contain the same chromophore so all three have identical HOMO/LUMO representations. The HOMO involves the biphenyl chromophore while the LUMO involves the benzophenone chromophore.

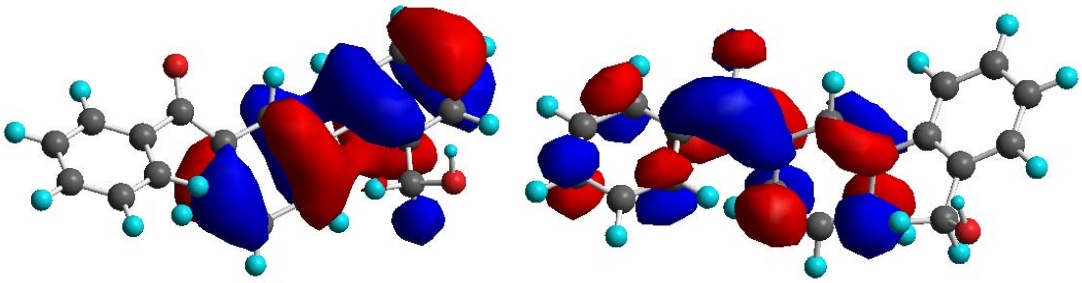

Figure 0.11 HOMO (left) and LUMO (right) of **55** calculated using Chem3D (AM1)

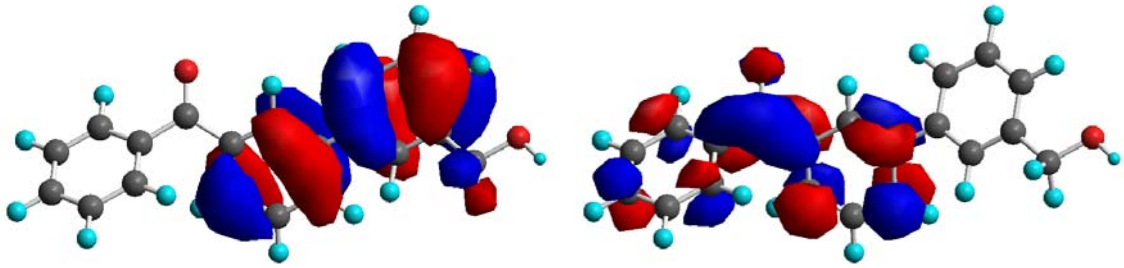

Figure 0.12 HOMO (left) and LUMO (right) of **56** calculated using Chem3D (AM1)

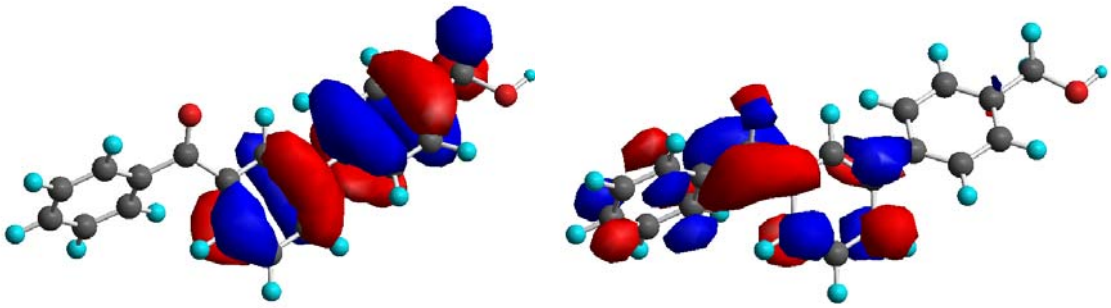

Figure 0.13 HOMO (left) and LUMO (right) of **57** calculated using Chem3D (AM1)

Like **47**, the transition from the HOMO to the LUMO of **55, 56** and **57** involve a decrease in electron density at the *meta* position of the substituted aromatic ring and an increase in the electron density at the carbonyl carbon. Thus it is understandable that **55**,

56 and **57** would behave in a similar manner to **47** and become protonated at the carbonyl oxygen and deprotonated at the benzylic carbon.

3.7.5 Summary

As posited in the introduction, electronic communication across the biphenyl ring is present in the systems presented in this chapter. This electronic communication is a result of the planarization of the biphenyl chromophore to produce an electronically excited triplet state (π,π^*) consisting of the biphenyl chromophore plus the carbonyl group. Although the intramolecular photoredox product is not produced as the major photoproduct in any of the systems (**55**, **56** or **57**), evidence exists that both **55** and **56** undergo intramolecular photoredox reaction. The photoproduct mixture of the *meta*-substituted derivative **56** consists primarily of the oxidized product **133**, with the intramolecular photoredox product **132**, existing as a minor component. The *ortho*-substituted compound **55** undergoes cyclisation to form **131** which is believed to proceed via a redox product which is then oxidized upon workup. Therefore although **55** proceeds to an intramolecular photoredox product, that product is not stable under atmospheric conditions and continues towards a cyclized, oxidation product in a manner reminiscent of the anthraquinone system **42**. Compound **57** does not form significant photoredox product or oxidation product but instead seems to proceed to oligomeric products more efficiently than either **55** or **56**. This difference in photobehaviour once again highlights the recurring theme of the *ortho-meta* effect[61] as the *para*-substituted compound reacts in a completely different manner to the *ortho*- and *meta*-substituted compounds.

3.8 Experimental

3.8.1 General

^{1}H NMR spectra were recorded on either a Bruker AC300 (300 MHz) instrument or a Bruker AVANCE 500 (500 MHz) instrument using chloroform-*d* as the solvent unless otherwise specified. Chemical shifts are reported in ppm and *J*-values are reported in Hz. Splitting patterns are reported as s (singlet), d (doublet), t (triplet), dd (doublet of doublets), dt (doublet of triplets), tt (triplet of triplets) and m (multiplets). Mass spectra and High-resolution-mass spectra (HR-MS) were obtained on a Kratos Concept 1H (EI and HRMS) instrument. UV–vis spectra were recorded on a Varian Cary 1, or 5 spectrometer instrument using baseline correction. Infrared spectra were recorded on a Perkin Elmer FTIR Spectrometer Spectrum 1000 using NaCl plates with neat product or thin film obtained from a solution of dichloromethane. Only strong and medium peaks are reported. Melting point values were obtained using a Gallenkamp Melting Point Apparatus. Measurements of pH(D) values were obtained using a Fisher Accumet 915 pH meter prior to mixing with acetonitrile co-solvent. Transient absorption spectra and kinetic measurements were carried out at the University of Victoria nanosecond LFP facility. Excitation was achieved by a Spectra Physics YAG laser (GCR-11, λ_{ex} 266 nm). Preparative photolysis were performed using a Rayonet RPR 100 photochemical reactor using 300 nm lamps unless otherwise noted.

3.8.2 Common Laboratory Reagents

All solvents used for synthesis (ACS grade) were purchased from Aldrich Chemical Company and used as received unless otherwise noted. THF, diethyl ether, dichloromethane (as reaction mixture solvent) and toluene used in syntheses were either distilled over Na (using benzophenone as and indicator) or used directly from a Solvent Purification System. Acetonitrile (HPLC grade) used for photolyses was checked for impurities by NMR spectroscopy. Organic extracts were dried over anhydrous magnesium sulfate and filtered. Deuterated solvents; D_2O, $CDCl_3$ were purchased from Cambridge Isotope laboratory containing 99.9% D. D_2SO_4 was obtained Aldrich Chemical company and contained 99.9% D. Preparative TLC was carried out on 20 cm x 20 cm silica gel GF Uniplates (Analtech). The following compounds were purchased from Aldrich: 3-hydroxybenzophenone, trifluoromethane sulfonyl anhydride, pyridine, sodium borohydride, magnesium turnings, N-bromosuccinimide, benzoyl peroxide, 2-bromotoluene, 3-bromotoluene, 4-bromotoluene, trimethyl borate, 2-(hydroxymethyl)anthraquinone.

3.8.3 Synthesis

3-Trifluoromethanesulonylbenzophenone (118) [129]

3-Hydroxybenzophenone (**122**) (4.0 g, 20.2 mmol) was placed in a 500 mL 2-necked round bottom flask with 9.8 mL pyridine (120 mmol). The reaction mixture was cooled to 0^oC using an ice-bath. Then trifluoromethane sulfonyl anhydride (10 g, 35 mmol) was added to 50 mL distilled dichloromethane in pressure equalizing dropping funnel and added dropwise to the reaction mixture over 20 minutes. After addition, the

reaction mixture was allowed to warm to room temperature where it was stirred for 4.5 hours. The solution was then poured into 300 mL ice water and the mixture placed in a separatory funnel. The organic fraction was removed and the aqueous fraction extracted three times with 100 mL dichloromethane. The organic fractions were combined and then washed twice with 100 mL 1M HCl to remove any pyridine before drying with anhydrous magnesium sulfate. It was then filtered and the solvent removed under vacuum to yield a crude yield of ~6 g (90%). This was used without further purification. ^{1}H-NMR (300MHz, $CDCl_3$) δ: 7.84 – 7.76 (m, 3H), 7.72 – 7.68 (m, 1H), 7.65 – 7.55 (m, 2H), 7.52 – 7.45 (m, 3H);

General Synthesis of Methylphenyl Boronic Acids (119, 120 and 121)[129]

Magnesium turnings (1.5 molar equivalents) were placed in a flame dried 100 mL round bottom flask and stirred without solvent under nitrogen for 15 minutes. Then 60 mL of distilled THF was added via syringe and the appropriate bromotoluene (1 molar equivalent) (2-bromotoluene (**123**) to produce **119**, 3-bromotoluene (**124**) to produce **120** and 4-bromotoluene (**125**) to produce **121**) was added via syringe. The reaction was initiated by heating with a heat gun. An ice bath was used to control the reaction if the reaction became too vigourous. After the visible reaction had finished the reaction was refluxed for a further 30 minutes under nitrogen. The resulting Grignard reagent was a dark grayish colour but was not viscous. This Grignard mixture was then transferred via syringe to a pressure-equalizing dropping funnel attached to another round bottom flask that had previously been flame-dried and was purged with nitrogen. This other round bottom flask contained a solution of trimethyl borate (1.2 molar equivalents) in 80 mL

distilled THF (under nitrogen). The trimethyl borate and THF were cooled to -78^{o}C using a dry ice/acetone bath prior to the dropwise addition of the Grignard mixture over 30 minutes. After all Grignard solution was added the reaction mixture was allowed to heat up to room temperature and left stirring overnight under a nitrogen atmosphere. The next day (12 hours later) 300 mL 1 M HCl was added for hydrolysis to the reaction mixture along with 100 mL diethyl ether. The mixture was placed in a separatory flask, separated and the aqueous fraction extracted twice more with 100 mL diethyl ether. The organic fractions were then dried with anhydrous magnesium sulfate and the solvent removed under vacuum to yield the crude product which was subsequently recrystallized from hot toluene.

2-Methylphenylboronic acid (119)

A Grignard reagent was produced according to the general procedure using magnesium turnings (1.83 g, 75.3 mmol), and 6.0 mL (50 mmol) 2-bromotoluene (**123**) in 20 mL dry THF. This was then added dropwise over 30 minutes to 12.0 mL of trimethyl borate (0.106 mol) in 100 mL dry THF to produce 5.96 g of crude **119** (88% crude). Recrystallization from hot toluene yields the pure white crystals (**119**) with a yield of 2.29g (34%).

mp. 59-61 ^{o}C (lit. 61-62 ^{o}C)[137]; ^{1}H-NMR (300MHz, $CDCl_3$) δ: 8.20 (d, 7.1 Hz, 1H), 7.44 (dd, 7.4 Hz, 7.4 Hz, 1H), 7.33-7.26 (m, 2H) 2.80 (s, 3H); ^{13}C-NMR (125 MHz, $CDCl_3$) δ: 146.23, 137.21, 132.18, 130.56, 125.16, 23.06 (s)

3-Methylphenylboronic acid (120)

A Grignard reagent was produced according to the general procedure using magnesium turnings (7.50 g, 0.30 mol), and 25 mL (0.20 mol) 3-bromotoluene (**124**) in 60 mL dry THF. This was then added dropwise over 30 minutes to 28 mL of trimethyl borate (0.25 mol) to produce 14.67 g (53% crude) of crude **117**. Recrystallization from hot toluene yields the pure white crystals (**117**) with a yield of 12.13 g (44%).
mp. 72-75 ^{o}C (lit. 74-76 ^{o}C)[138] ^{1}H-NMR (300MHz, $CDCl_3$) δ: 8.08 – 8.01 (m, 2H), 7.40 (d, 4.5 Hz, 2H), 2.47 (s, 3H); ^{13}C-NMR (125 MHz, $CDCl_3$) δ: 137.58, 136.38, 133.68, 133.00, 128.13, 21.70 (s)

4-Methylphenylboronic acid (121)

A Grignard reagent was produced according to the general procedure using magnesium turnings (7.50 g, 0.30 mol), and 25 mL (0.203 mol) 4-bromotoluene (**125**) in 60 mL dry THF. This was then added dropwise over 30 minutes to 28 mL of trimethyl borate (0.247 mol) to produce 21.80 g of crude **121**. Recrystallization from hot toluene yields the pure white crystals (**121)** with a yield of 15.30 g (55%).
mp. 76-77 (lit. 79 ^{o}C)[139] ^{1}H-NMR (300MHz, $CDCl_3$) δ: 8.11 (d, 7.7 Hz, 2H), 7.30 (d, 7.7 Hz, 2H), 2.43 (s, 3H); ^{13}C-NMR (125 MHz, $CDCl_3$) δ: 143.16, 135.93, 129.00, 22.15 (s)

General Synthesis for Suzuki Coupling[129]

The appropriate boronic acid (**119** for **126**, **120** for **127** or **121** for **128**) was dissolved in deoxygenated toluene with K_2CO_3 and **118** (used directly without further purification) in a 2 necked round bottom flask. The reaction apparatus was flushed with nitrogen for 10 minutes before adding $Pd(PPh_3)_4$ through a sidearm and then purging again with nitrogen for 10 minutes before starting to heat. The mixture was refluxed overnight (17 hours) and left to cool. After cooling the mixture was passed through a celite plug before removing solvent under vacuum. The crude residue was column purified using 1:1 ether : hexanes. Recrystallization, if necessary was accomplished from toluene.

3-(2'-(Methyl)phenyl)benzophenone (126)

The coupled product was formed using the general procedure from 2-methylphenylboronic acid (**119**) (2.95 g, 22 mmol) in 55 mL deoxygenated toluene with 4.54 g (32.8 mmol) K_2CO_3 and **118** (4.17 g, 13.1 mmol). $Pd(PPh_3)_4$ (0.37 g, 0.32 mmol) was added as the catalyst through the sidearm before refluxing. This mixture resulted in a crude product yield of 2.33 g (65% yield). After recrystallization 0.85 g (3.1 mmol) of pure product (off-white solid) was formed (24% yield).

^{1}H-NMR (300MHz, $CDCl_3$) δ: 7.87-7.72 (m, 4H), 7.61-7.43 (m, 5H), 7.31-7.21 (m, 4H), 2.28 (s, 3H)

3-(3'-(Methyl)phenyl)benzophenone (127)

The coupled product was formed using the general procedure from 3-methylphenylboronic acid (**120**) (4.13 g, 30.4 mmol) in 200 mL deoxygenated toluene with 5.01 g (36.2 mmol) K_2CO_3 and **118** (~3 g, ~9 mmol). $Pd(PPh_3)_4$ (0.58 g, 0.5mmol) was added as the catalyst through the sidearm before refluxing. This mixture resulted in a crude product yield of 0.054 g (2 % yield) after column purification.(2:3 ether : hexanes eluent).

^{1}H-NMR (300MHz, $CDCl_3$) δ: 8.03 -8.00 (m, 1H), 7.87-7.72 (m, 4H), 7.63-7.30 (m, 7H), 7.22-7.16 (m, 1H), 2.42 (s, 3H)

3-(4'-(Methyl)phenyl)benzophenone (128)

The coupled product was formed using the general procedure from 4-methylphenylboronic acid (**121**) (8.20 g, 60.3 mmol) in 200 mL deoxygenated toluene with 10.00 g (72.4 mmol) K_2CO_3 and **118** (~6 g, ~19 mmol). $Pd(PPh_3)_4$ (0.58 g, 0.5 mmol) was added as the catalyst through the sidearm before refluxing. This mixture resulted in a crude product yield of 4.03 g (25 % yield). After recrystallization 0.50 g (1.8 mmol) of pure product was formed (7.4 % yield).

^{1}H-NMR (300MHz, $CDCl_3$) δ: 8.00 (s, 1H), 7.86-7.68 (m, 4H), 7.63-7.43 (m, 7H), 7.28-7.25 (m, 1H), 2.39 (s, 3H)

General Synthesis for the Bromination and Hydrolysis

The appropriate 3-(methylphenyl)benzophenone (**126** for **55**, **127** for **56**, **128** for **57**) was combined in a round bottom flask with 1.3 molar equivalents of N-bromosuccinimide and catalytic amounts of benzoyl peroxide in benzene and refluxed under nitrogen overnight (17-19 hours). After the reaction mixture had cooled to room temperature, the solution was washed twice with 50 mL distilled water to remove any remaining succinimide side product. The organic layer was then dried with anhydrous magnesium sulfate before filtering and removing the solvent under vacuum. The crude brominated compound was used directly by dissolving the residue in dioxane and adding the equivalent amount of water plus 5 molar equivalents of $CaCO_3$. This mixture was then refluxed for 20 hours and allowed to cool to room temperature. The solvent was removed under vacuum and enough dichloromethane and 1 M HCl was added until all of the solid residue had dissolved. The organic layer was collected and the aqueous layer extracted twice with dichloromethane before combining the organic layers. The combined organic layers were then washed twice with saturated sodium bicarbonate solution before drying with anhydrous magnesium sulfate. The mixture was then filtered and the solvent removed under vacuum. The resulting crude product was purified on a silica column using 1:1 ether : hexanes as the eluent.

3-(2'-(Hydroxymethyl)phenyl)benzophenone (55)

In a round bottom flask, 3-(2'-methylphenyl)benzophenone (**126**) (0.85 g, 3.1 mmol), N-bromosuccinimide (0.81 g, 4.6 mmol), benzoyl peroxide (0.012 g, 0.087 mmol) and 25 mL benzene were combined together according to the general synthesis (see

above) to produce the brominated compound (1.01 g crude yield). This was used directly in the hydrolysis reaction by combining the crude brominated compound with 25 mL dioxane, 25 mL distilled water and 1.54 g (15.4 mmol) $CaCO_3$ and refluxing for 17 hours. After workup a crude yield of 0.419 g (47% yield) was obtained. After column purification 0.179 g (20% yield) was obtained.

^{1}H-NMR (500MHz, $CDCl_3$) δ: 7.84-7.78 (m, 4H), 7.63-7.58 (m,1H), 7.58-7.52 (m, 3H), 7.49-7.45 (m, 2H), 7.40 (ddd, 7.4 Hz, 7.4 Hz, 1.5 Hz, 1H), 7.36 (ddd, 7.4 Hz, 7.4 Hz, 1.5 Hz, 1H), 7.29 (dd, 7.4 Hz, 1.5 Hz, 1H) 4.62 (s, 2H) ; ^{13}C-NMR (125 MHz, $CDCl_3$) δ: 196.79, 141.06, 140.54, 138.23, 137.91, 137.74, 133..37, 132.75, 130.87, 130.33, 130.29, 129.17, 128.83, 128.57, 128.51, 128.51, 128.42, 128.10, 63.32; IR (thin film from CH_2Cl_2 solution, NaCl plates): ν = 3433, 3059, 3027, 2928, 2877, 1660, 1644, 1596, 1574, 1470, 1446, 1417, 1319, 1193, 1179, 1026, 948, 914, 820, 646 cm^{-1}; UV-Vis(1:1 pH 2 H_2SO_4 - CH_3CN): λ_{max} = 253 nm, (ε = 210,000); MS (EI) *m/z*; 288 (30,M+), 279 (30), 181 (20), 167 (40), 149 (100), 105 (85); Calculated for $C_{20}H_{16}O_2$ 288.1150; observed 288.1158

3-(3'-(Hydroxymethyl)phenyl)benzophenone (56)

In a round bottom flask, 3-(3'-methylphenyl)benzophenone (**127**) (0.0540 g, 0.198 mmol), N-bromosuccinimide (1.88 g, 11 mmol), benzoyl peroxide (0.013 g, 0.094 mmol) and 40 mL benzene were combined together according to the general synthesis (see above) to produce the brominated compound (2.22 g crude yield). This was then used directly in the hydrolysis reaction by combining the crude brominated compound with 70 mL dioxane, 70 mL distilled water and 3.11 g (31 mmol) $CaCO_3$ and refluxing

for 17 hours. After workup a crude yield of 0.0238 g (40% yield) was obtained. After column purification 0.0076 g (14% yield) was obtained.

^{1}H-NMR (300MHz, $CDCl_3$) δ: 8.00 (s, 1H), 7.87-7.72 (m, 4H), 7.63-7.33 (m, 8H), 4.75 (s, 2H), 1.93 (s, 1H); ^{13}C-NMR (125 MHz, $CDCl_3$) δ: 196.95, 141.82, 141.43, 140.71, 138.42, 137.75, 132.80, 131.30, 130.34, 129.40, 129.28, 128.97, 128.79, 128.59, 126.74, 126.58, 126.03, 65.47; IR (thin film from CH_2Cl_2 solution, NaCl plates): ν = 3412, 3059, 3028, 2920, 2871, 1655, 1595, 1576, 1446, 1405, 1320, 1263, 1178, 1026, 1000, 964, 781, 720, 698, 667, 647 cm^{-1}; UV: λ_{max} =202 nm (ε = 45,000), 249 nm (ε = 180,000) (1:1 pH 2 H_2SO_4 - CH_3CN); MS (EI) *m/z*; 288 (100,M+), 211 (60), 182 (10), 165 (10), 152 (25), 105 (70), 77 (45), 51 (10); Calculated for $C_{20}H_{16}O_2$ 288.1150; observed 288.1159

3-(4'-(Hydroxymethyl)phenyl)benzophenone (57)

In a round bottom flask, 3-(4'-methylphenyl)benzophenone (**128**) (0.50 g, 1.8 mmol), N-bromosuccinimide (0.43 g, 2.4 mmol), benzoyl peroxide (0.02 g, 0.14 mmol) and 40 mL benzene were combined together according to the general synthesis (see above) to produce the crude brominated compound (0.50 g (1.4 mmol) crude yield). This was used directly in the hydrolysis reaction by combining the crude brominated compound with 30 mL dioxane, 30 mL distilled water and 0.72 g (7.2 mmol) $CaCO_3$ and refluxed for 20 hours. After workup a crude yield of 0.28 g (55% yield) was obtained. After column purification a colourless oil in a yield of 0.16 g (32% yield) was obtained.

^{1}H-NMR (300MHz, $CDCl_3$) δ: 8.01-7.99 (m, 1H), 7.85-7.71 (m, 4H), 7.62-7.39 (m, 8H), 4.72 (s, 2H); ^{13}C-NMR (125 MHz, $CDCl_3$) δ: 196.95, 141.25, 140.72, 139.71, 138.41, 137.74, 132.79, 131.20, 130.34, 129.21, 128.98, 128.73, 128.58, 127.77, 127.60, 65.21; IR (thin film from CH_2Cl_2 solution, NaCl plates): ν = 3400, 3059, 3027, 2920, 2871, 1656, 1651, 1595, 1579, 1446, 1434, 1319, 1253, 1014, 955, 813, 786, 761, 716, 693, 647 cm^{-1}; UV-Vis (1:1 pH 2 H_2SO_4 - CH_3CN): λ_{max} = 253 nm (ε = 200,000); MS (EI) *m/z*; 288 (85, M+), 211 (40), 182 (10), 165 (10), 152 (45), 105 (100), 77 (65), 55 (20); Calculated for $C_{20}H_{16}O_2$ 288.1150; observed 288.1152

3.8.4 Product Studies

3.8.4.1 General

All photolysis reactions were performed using a Rayonet RPR 100 photochemical reactor with 300 nm lamps varying from one lamp to sixteen lamps, and a water-cooled cold finger. Solutions of substrate (~10^{-4} to 10^{-3} M, 100 mL to 300 mL total) were photolysed for times ranging from 1 minute to 10 minutes. The quartz photolysis tubes were purged with argon for 15 minutes prior to photolysis and then purged continuously with argon (unless otherwise noted) during photolysis, both to remove oxygen from the solution and to provide continuous mixing during photolysis.

After photolysis of aqueous samples, the photolysis mixture was placed in a separatory funnel and extracted twice with dichloromethane (100 mL). The organic fractions were combined and dried over anhydrous magnesium sulfate before filtering

and removing the solvent under vacuum. The residue was placed on a vacuum line for 30 minutes to remove any remaining solvent before characterization of the product mixture via NMR spectroscopy. Samples consisting entirely of organic solvents (acetonitrile) were directly evaporated under vacuum. The progress of reaction was followed by ^{1}H-NMR spectroscopy and the product ratio of the product mixture determined by integration when possible. If separation of the product mixture was warranted, the separation was accomplished using preparatory scale TLC. A maximum of 100 mg was placed on any one plate. The individual separated bands were scraped off into beakers and extracted several times with the appropriate solvent (usually CH_2Cl_2 or diethyl ether) and the solvent removed to yield the purified photoproducts. For aqueous solutions at pH values other than 7, the pH of the aqueous portion was adjusted before combination with acetonitrile. For acidic solutions the pH was adjusted with H_2SO_4 (or D_2SO_4) and for basic solutions the pH was adjusted with NaOH (or NaOD).

3.8.4.2 Individual Product Study Details

Photolysis of 55

Using a 500 mL quartz photolysis tube, **55** (14.1 mg) was dissolved in 150 mL CH_3CN and then 150 mL pH 2 H_2O was added to give a concentration of 1.6 x 10^{-4} M. This was purged with Ar for 15 minutes prior to photolysis with two 300 nm lamps for 5 minutes. The photolysis tube contents were placed in a separatory flask after photolysis and extracted twice with 50 mL CH_2Cl_2. The organic layer was then dried with anhydrous $MgSO_4$ and gravity filtered. The solvent was then removed *in vacuo* and the flask placed on a vacuum line for 20 minutes to remove any remaining solvent. The

reaction was then characterized via ^{1}H-NMR spectroscopy and yielded a conversion of 21% of **131** with 5% **130** and 3% oligomeric product. Photolysis for 5 minutes with 4 lamps using the same concentration yields a conversion of 58% via ^{1}H-NMR spectroscopy. (42% **55**; 48% **131**; 2% **130)**. Separation of the product mixture by preparative TLC yielded **131** and **130**.

131 : ^{1}H-NMR (500MHz, $CDCl_3$) δ: 8.08 (s, 1H), 7.84-7.81 (m, 2H), 7.75-7.71 (m, 2H), 7.70- 7.66 (m, 2H), 7.62-7.59 (m, 1H), 7.52-7.48 (m, 2H), 7.41 (ddd, 7.4 Hz, 7.7 Hz, 1.1 Hz, 1H), 7.36 (ddd, 7.4 Hz, 7.3 Hz, 1.2 Hz, 1H), 5.66 (s, 1H) ;^{13}C NMR ($CDCl_3$, 125 MHz) δ: 196.84, 150.01, 145.87, 140.67, 139.33, 138.91, 137.91, 132.79, 130.33, 130.30, 129.66, 128.75, 128.60, 125.47, 125.07, 121.55, 120.75, 75.35 (s) ; MS (EI) *m/z*; 286 (85, M+), 207 (25), 181 (100), 152 (30), 105 (100);

130 : ^{1}H-NMR (500MHz, $CDCl_3$) δ: 10.01 (s, 1H), 8.02 (dd, 7.7 Hz, 1.4 Hz, 1H), 7.86 (ddd, 4.5 Hz, 4.4 Hz, 1.8 Hz, 1H), 7.84-7.80 (m, 3H), 7.65 (ddd, 7.6 Hz, 7.4 Hz, 1.4 Hz, 1H), 7.61-7.57 (m, 3H), 7.54-7.43 (m, 4H); ^{13}C NMR ($CDCl_3$, 125 MHz) δ: 196.40, 191.96, 144.90, 138.37, 138.16, 137.49, 134.04, 133.96, 132.94, 131.40, 131.10, 130.27, 129.92, 128.66, 128.53, 128.31; Photolysis of **55** in pH 7 (two 300 nm lamps for 5 minutes) results in a product ratio of 69% **55**; 0% **131**; 19% **130**; 10% oligomeric products.

Photolysis of **55** in pH 1 (two 300 nm lamps for 5 minutes) results in a product ratio of 72% **55**; 22% **131**; 1% **130**; 3% oligomeric products.

Photolysis of **55** was accomplished at different irradiation times and conditions. This data on the photolyses of **55** is summarized in Table 4.1.

Photolysis of 56

Using a 500 mL quartz photolysis tube, **56** (13.7 mg) was dissolved in 150 mL CH_3CN and then 150 mL pH 2 H_2O was added to give a concentration of 1.6 x 10^{-4} M. This was purged with Ar for 15 minutes prior to photolysis with two 300 nm lamps for 5 minutes. The photolysis tube contents were placed in a separatory flask after photolysis and extracted twice with 50 mL CH_2Cl_2. The organic layer was then dried with anhydrous $MgSO_4$ and gravity filtered. The solvent was then removed *in vacuo* and the flask placed on a vacuum line for 20 minutes to remove any remaining solvent. The reaction was then characterized via ^{1}H-NMR spectroscopy and yielded a conversion of 1% of **132** with 9% **133** and 3% oligomeric product. Photolysis for 10 minutes with 2 lamps using the same concentration yields a conversion of 15% via ^{1}H-NMR spectroscopy. (85% **56**; 1% **132**; 9% **133**; 5% oligomeric**)**. Separation of the product mixture by preparative TLC yielded **133**.

Photolysis of **56** in pH 7 (two 300 nm lamps for 10 minutes) results in a product ratio of 97% **56**; 0% **132**; 3% **133**; 1% oligomeric products.

Photolysis of **56** in pH 1 (two 300 nm lamps for 10 minutes) results in a product ratio of 51% **56**; 2% **132**; 15% **133**; 31% oligomeric products.

Photolysis of **56** was accomplished at different irradiation times and conditions. This data on the photolyses of **56** is summarized in Table 4.2.

Photolysis of 57

Using a 500 mL quartz photolysis tube, **57** (14.1 mg) was dissolved in 150 mL CH_3CN and then 150 mL pH 2 H_2O was added to give a concentration of 1.6 x 10^{-4} M. This was purged with Ar for 15 minutes prior to photolysis with two 300 nm lamps for 2 minutes. The photolysis tube contents were placed in a separatory flask after photolysis and extracted twice with 50 mL CH_2Cl_2. The organic layer was then dried with anhydrous $MgSO_4$ and gravity filtered. The solvent was then removed *in vacuo* and the flask placed on a vacuum line for 20 minutes to remove any remaining solvent. The reaction was then characterized via ^{1}H-NMR($CDCl_3$) and yielded a conversion of 0% of **135** with 7% **134** and 18% oligomeric product. Photolysis for 5 minutes with 4 lamps using the same concentration yields a conversion of 71% via ^{1}H-NMR ($CDCl_3$). (29% **56**; 0% **135**; 17% **134**; 54% oligomeric**)**.

Photolysis of **57** was accomplished at different irradiation times and conditions. This data on the photolyses of **57** is summarized in Table 4.3.

3.8.4.3 UV-Vis Studies

Using 1 cm quartz cuvettes or quartz fluorescence cells, solutions were prepared by filling with 3 mL of the appropriate solvent mixture and spiking with 1-30 μL of concentrated solution of substrate in acetonitrile to get the desired OD. Final concentrations are ~10^{-6} to 10^{-5} M. Cuvettes were then bubbled using fine needles through septa with argon or nitrogen for 15 minutes to remove any dissolved oxygen. Parafilm was then placed over the septa before the UV-vis spectral traces were performed.

3.8.4.4 Laser Flash Photolysis (LFP)

LFP was performed in the University of Victoria LFP facility using an excitation wavelength of 266 nm (pulse width $\approx$ 20 ns) using a Nd-YAG Spectra Physics laser (GCR-11), power kept under 25 mJ / pulse using attenuation of power.

The LFP spectra were collected using a flow cell containing 1:1 H_2O : CH_3CN purged with N_2 prior to excitation for 15 minutes. The flow cell consisted of a chamber with ~100 mL of solution containing substrate of ~10^{-5} M with an OD = 0.4 at 266 nm determined by UV-vis spectroscopy. From the flow chamber the solution was pumped continuously into a 7 mm x 7 mm quartz cell at flow rates of ~1.5 mL / min.

Spectra were obtained by plotting the absorbance value at a fixed time after laser excitation for a given wavelength and repeating for other wavelengths at 10 or 20 nm increments across the UV-vis region (280 nm – 700 nm). Multiple shots (4 to 10) were taken and averaged before plotting. Four different windows were examined to yield data at various times after excitation. This allowed simultaneous generation of spectra at four different times. Windows were selected to illustrate important points in the decay of the transient.

Decay data was obtained by measuring 500 absorbance points at equivalent time intervals within a chosen time scale. Time scales used varied between 50 ns and 1 ms. Lifetimes were determined from fitting of the exponential decay. Polyexponential decays were estimated by fitting different regions of the decay with monoexponential fitting.

Chapter 5
Summary and Future Directions

4.1 Summary

A new class of photochemical reactions of benzophenones and related compounds has been documented and studied in detail in this Thesis. This reaction involves a formal intramolecular photoredox reaction in which the aromatic ketone is reduced to an alcohol and an appropriately located hydroxymethyl substituent is oxidized to the aldehyde or ketone. This transformation cannot be readily achieved using known thermal chemistry.

The mechanistic details explored in this Thesis share the following characteristics: (a) The reactions require water and are acid-catalyzed, (b) exhibit a profound *meta* effect that results in (c) the deprotonation of the benzylic C-H proton as a key step. This deprotonation forms a unique double enolic intermediate which ketonizes to give the photoredox product.

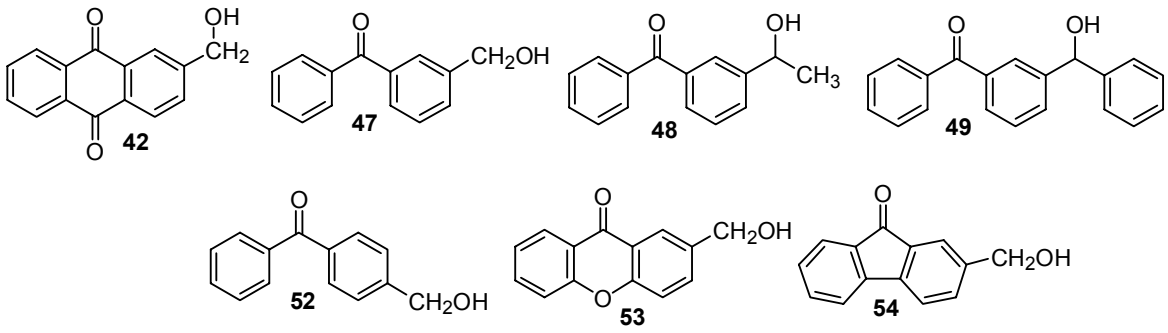

The acid catalysis has been determined via both photoproduct studies and LFP lifetime measurements. Reaction efficiencies vary dramatically; however, depending on the chromophoric substrate (**42** and **53** are reactive at pH 7 while **47**, **48** and **49** are only significantly reactive under acidic conditions). Despite these variations, all reactive

substrates showed an increase in photochemical efficiency towards photoredox behaviour upon an increase in acidity. This is also related to the reaction dependence on the presence of water. When the reactive substrates were photolysed in pure acetonitrile, no photoredox reaction was observed and only hydrogen abstraction type oligomeric products were produced.

The *para*- compounds explored in this Thesis (**52** and **57**) exhibited essentially no photoredox reaction and resulted primarily in hydrogen abstraction type oligomeric side products. When compared to the analogous *meta*- compounds (**47** and **56**) the *meta* effect[61] is clearly a factor in this reaction. This is unsurprising as the photoredox reaction is expected to proceed via electronic communication through the aromatic chromophore.

The activation of the benzylic carbon through the electronic transmission resulted in the deprotonation of a benzylic proton. This deprotonation was explored briefly via competitive studies of **47-αD** where it was discovered that a marked preference was observed for the deprotonation of the proton over the deuteron on the monodeuterated benzylic carbon. When deprotonation is hindered there is a marked decrease in the efficiency of the reaction. This was observed from the photoinertness of the *meta*-methoxy compound **78**.

The last step in the proposed mechanism is the protonation of the carbanion of the intermediate to form the photoredox product. The origin of the benzylic proton was determined to arise from the aqueous solvent rather than another source. Thus, although the photoredox product is formally intramolecular, the photoredox reaction is water mediated.

The oligomeric side products previously mentioned appear to arise via hydrogen abstraction by the benzophenone carbonyl and subsequent bimolecular reactions. Because of this, concentration of substrate plays a role in the photochemistry. This side reaction is favoured by the n,π* state. By contrast the π,π* state is required for the intramolecular photoredox reaction as the aromatic π system needs to be involved to conjugate the carbonyl with the benzylic alcohol. This requirement is observed numerous times throughout this Thesis. Increasing solvent polarity has the effect of increasing the photoredox reaction efficiency which is consistent with the increased stability of the π,π* triplet excited state in more polar solvent media. Protonation of the carbonyl also stabilizes the π,π* triplet excited state and reinforces the need for acid catalysis.

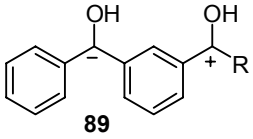

89

leads to photoredox product

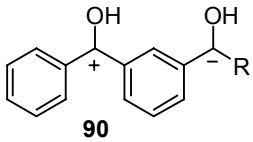

90

photoinert towards photoredox

The presence of a specific zwitterion resonance contributor was postulated to be critical in the progression towards the photoredox product. If the resonance contributor was stabilized towards favouring a cation at the benzylic methylene or an anion at the benzophenone carbonyl carbon (zwitterion **89**) the photoredox reaction was favoured. When the opposite resonance contributor (zwitterion **90**) is favoured the compound is observed to be photoinert, such as for **28**, **78** and **80**. This may explain the irreversibility of the reaction for most substrates that undergo the photoredox reaction.

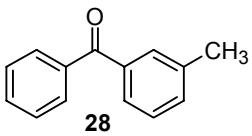

28

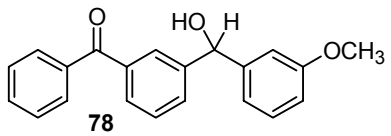

78

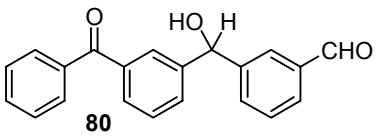

80

The photoredox reaction was determined to be general enough that even the

presence of alternative chromophores such as xanthone, in **53**, and fluorenone, in **54**, exhibited photoredox behaviour if the conditions were appropriate. The reaction appears to progress via the triplet excited state and this is supported in part by the relative photoinertness of **54** which exhibits significantly lower ISC. This is in addition to the evidence presented via LFP spectra and lifetimes data.

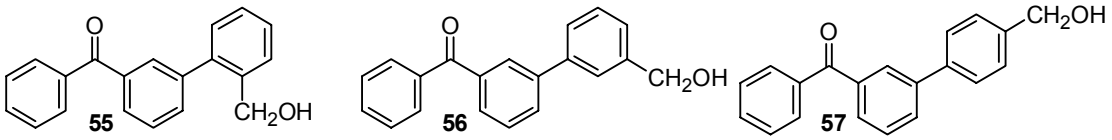

Another chromophore was also explored via the bichromophoric system of Chapter 4. This system was interesting because although the photoredox reaction continues to arise via the excited benzophenone chromophore, electronic transmission via the phenyl spacer resulted in conjugation across nearly the entire molecule. The photoredox reaction did not progress via the same pathway for **55** as for **56** however as **55** undergoes cyclization to form a redox product that is oxidized upon workup while **56** forms a small amount of the redox product directly. This system was also interesting because the *ortho-meta* effects[61] were also clearly present because **55** and **56** showed some photoredox reaction while **57** showed only oligomeric side products.

4.2 Future Directions

Since this Thesis explores a previously undiscovered class of photochemical reactions, it provides a good framework for future studies. Aside from continuing to explore compounds of this Thesis in more detail, some additional compounds would be useful to explore. The photochemical and photophysical studies on the photoredox reaction of **53** and **54** are still only at the preliminary stage and there still remains much to

be done. Unlike the meta-substituted benzophenone, **47**, the *para*-substituted benzophenone, **52**, is not active enough to compete with the hydrogen abstraction pathway that leads to oligomeric side-products. However because **53** is active even under neutral conditions, the enhancement due to the *meta*-effect may not be needed. Consequently it would be interesting to explore the *para*- analogue of **53**, **136**.

An additional factor that could promote the photoredox reaction lies in the oxygen at the *meta*- position. This should inductively withdraw electron density from the benzylic position enhancing the possibility of deprotonation of the benzylic carbon. Normally the *ortho*-substituted analogues undergo intramolecular hydrogen abstraction and do not proceed via the same mechanism as the different substrates presented in this Thesis but 1-(hydroxymethyl)fluoroenone (**137**) may behave differently because 9-fluorenones have a π,π^* lowest energy excited state and, as observed for **54**, are not prone to hydrogen-abstraction side products.

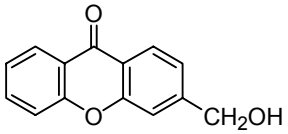

136

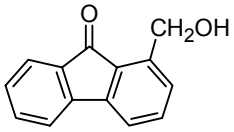

137

In addition to those extensions of the fluorenone and xanthone analogues, other alternative chromophoric analogues may be explored. Compound **138** would be a logical choice as it extends the conjugation from **54** and would have the same central ring aromaticity profile as **53**. It would be interesting to discover whether the dehydroxylation observed for **53** is also observed for **138**. Compound **139** and compound **140** would break the conjugation while retaining the rigid attachment of the two phenyl rings and would also provide an interesting addition to the study of **47**.

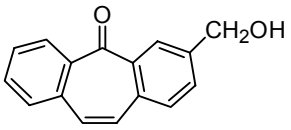

138

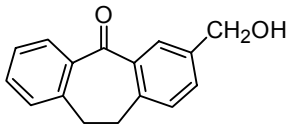

139

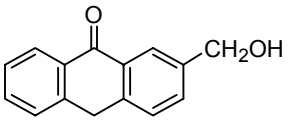

140

The bichromophoric compounds **55**, **56** and **57** are likewise only partially studied. The cyclization of **55** was particularly interesting as relatively few examples of cyclization of aromatic systems exist that do not proceed through electrocyclic mechanisms. The mechanism of cyclization still requires significant study and additional photochemical and photophysical studies are required. Further exploration of that system could examine the photochemistry of the cyclized product **131** or the redox analogue **141**.

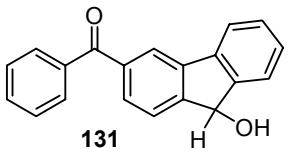

131

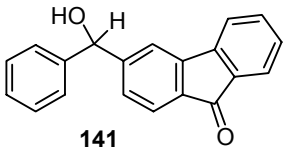

141

This Thesis has presented a new class of photochemical reactions of aromatic ketones. This makes a significant addition to the understanding of the photochemical redox reactions of aromatic ketones and sheds light on a previously unexplored area of photochemistry.

References

[1] Julliard, M.; Chanon, M. *Chem. Rev.,* **1983**, 83, 425-506

[2] Ciamician G.; Silber, P., *Ber. Detsch. Chem. Ges.,* **1886**, *19*, 2899-2900

[3] Döpp., D. In *Photochemical Reactivity of the Nitro Group, CRC Handbook of Organic Photochemistry and Photobiology*, Horspool, W. M., Song, P.-S. Eds.; CRC Press: Boca Raton, 1995; p 1019-1062

[4] Ishii, Y.; Tukada, H.; Nakagaki, R.; Mutai, K. *Chem. Lett.,* **1990**, 1559-1562

[5] Nakagai, R.; Mutai, K.; Nagakura, S. *Chem. Phys. Lett.,* **1990**, 167, 439-444

[6] Chow, Y. L., *The Chemistry of Functional Groups, Supplement F (The Chemistry of Amino, Nitroso and Nitro Compounds and Their Derivatives),* Patai, S., Ed., John Wiley & Sons, Chichester, 1982, Chapter 6

[7] Döpp, D. *Top. Curr. Chem.,* **1975**, 55, 49-85

[8] Yip, R. W.; Sharma, D. K.; Giasson, R.; Gravel, D. *J. Phys. Chem.,* **1985**, 89, 5328-5330

[9] Yip, R. W.; Sharma, D. K.; Giasson, R.; Gravel, D. *J. Phys. Chem.,* **1991**, 95, 6078-6081

[10] Wan, P.; Yates, K. *Can. J. Chem.,* **1986**, 64, 2076-2086

[11] Morrison, J.; Osthoff, H.; Wan, P. *Photochem. Photobiol. Sci.*, **2002**, 1, 384-394

[12] Pitts, J. N. Jr.; Wan, J. K.S. In *The Chemistry of The Carbonyl Group*; Patai, S. Ed.; Interscience Publishers, London, **1966**

[13] Paul, H.; Small, R.D.; Scaiano, J.C. *J. Am. Chem. Soc.,* **1978**, 100, 4520-4527

[14] Dorigo, A. E.; McCarrick, M.A.; Loncharich, R.J.; Houk, K.N. *J. Am. Chem. Soc.,* **1990**, 112, 7508-7514

[15] Scaiano, J.C. *J. Am. Chem. Soc.,* **1980**, 102, 5399-5400

[16] Griller, D.; Howard, J. A.; Marriott, P.R., Scaiano, J.C. *J. Am. Chem. Soc.,* **1981**, 103, 619-623

[17] Padwa, A. *Tetrahedron Lett.,* **1964**, 5, 3465-3469

[18] Walling, C.; Gibian, M.J. *J. Am. Chem. Soc.,* **1965**, 87, 3361-3364

[19] Wagner, P.J. *Acc. Chem. Res.,* **1971**, 4, 168-177

[20] Scaiano, J. C. *J. Photochem.,* **1973**, 2, 81-118

[21] Wagner, P.J. *Top. Curr. Chem.,* **1976**, *66*, 1-52

[22] Charney, D. R.; Dalton, J. C.; Hautala, R.R.; Snyder, J.J.; Turro, N.J. *J. Am. Chem. Soc.,* **1974**, *96*, 1407-1410

[23] Nau, W.M.; Cozens, F.L.; Scaiano, J.C. *J. Am. Chem. Soc.,* **1996**, *118*, 2275-2282

[24] Ciamician, G.; Silber, P. *Ber*., **1900**, *33*, 2911-2913

[25] Cohen, S.G.; Baumgarten,R.J. *J. Am. Chem. Soc.,* **1965**, *87*, 2996-2997

[26] Backstrom, H. J.L.; Sandros, K. *Acta. Chim. Scand.,* **1960**, *14*, 48-62

[27] Walling, C.; Wagner, P.J. *J. Am. Chem. Soc.,* **1964**, *86*, 3368-3375

[28] Yang, N.C.; Yang, D. –H. *J. Am. Chem. Soc.,* **1958**, *80*, 2913-2914

[29] Förster, T. *Naturwissenschaften,* **1949**, *36*, 186-187

[30] Weller, A. *Prog. React. Kinet.,* **1961**, *1*, 189-214

[31] Ireland, J.F.; Wyatt, P.A.H. *Adv. Phys. Org. Chem.,* **1976**, *12*, 131-221

[32] Wan, P.; Shukla, D. *Chem. Rev.,* **1993**, *93*, 571-584

[33] Tolbert, L. M.; Solntsev, K.M. *Acc. Chem. Res.,* **2002**, *35*, 19-27

[34] Wan, P.; Krogh, E.; Chak, B. *J. Am. Chem. Soc.,* **1988**, *110*, 4073-4074

[35] Ireland, J. F.; Wyatt, P.A.H. *J. Chem. Soc., Faraday Trans. 1,* **1973**, *69*, 161-168

[36] Turro, N. J. *Modern Molecular Photochemistry*; University Science Books: Mill Valley, CA, **1991**.

[37] Garcia-Garibay, M. A.; Campos, L. M. In *CRC Handbook of Organic Photochemistry and Photobiology*, 2nd ed.; Horspool, W. M., Lenci, F. Eds.; CRC Press: Boca Raton, FL, **2004**; Chapter 48.

[38] Wagner, P. J.; Klan, P. In *CRC Handbook of Organic Photochemistry and Photobiology*, 2nd ed.; Horspool, W. M., Lenci, F. Eds.; CRC Press: Boca Raton, FL, **2004**; Chapter 52.

[39] Zimmerman, H. E.; Schuster, D. I. *J. Am. Chem. Soc.,* **1962**, *84*, 4527-4540

[40] Hammond, G.S.; Moore, W.M.; *J. Am. Chem. Soc.,* **1959**, *81*, 6334-6334

[41] Moore, W.M.; Hammond, G.S.; Foss, R.P. *J. Am. Chem. Soc.,* **1962**, *83*, 2789-2794

[42] Horspool, W.; Armesto, D. *Organic Photochemistry, A Comprehensive Treatment*; Ellis Horwood Limited: Chichester, England, **1992**, Chapter 3

[43] Brown, R. E.; Singer, L.A.; Parks, J.H. *Chem. Phys. Lett.*, **1972**, *14*, 193-195

[44] Herkstroeter, W.G.; Lamola, A.A.; Hammond, G.S. *J. Am. Chem. Soc.,* **1964**, *86*, 4537-4540

[45] Filipescu, N.; Minn, F. L. *J. Am. Chem. Soc.,* **1968**, *90*, 1544-1547

[46] Nagulb, Y. M. A.; Steel, C.; Cohen, S. G. *J. Phys. Chem.,* **1987**, *91*, 3033-3036

[47] Schuster, D.M.; Weil, T.M. *J. Am. Chem. Soc.,* **1973**, *95*(12),4091-4092

[48] Yang, N.C.; Rivas, C. *J. Am. Chem. Soc.*, **1961**, *83*, 2213-2213

[49] Porter, G.; Suppan, P.; *Trans. Faraday Soc.,* **1965**, *61*, 1664-1673

[50] Pitts, J.N., Jr.; Johnson, H.W. Jr.; Kuwana, T. *J. Phys. Chem.*, **1962**, *66*, 2456-2461

[51] Piette L. H.; Sharp, J.H.; Kuwana, T. *J. Chem. Phys.*, **1962**, *36*, 3094-3095

[52] Wagner, P. J.; Hammond, G.S. *Properties and Reactions of Organic Molecules in their Triplet States* In *Advances in Photochemistry*, Noyes, W. A. Jr.; Hammond, G.S.; Pitts, J. N. Jr. Eds., Vol 5 Interscience Publishers, New York, **1968**

[53] Porter, G.; Suppan, P.; *Pure Appl. Chem.*, **1964**, *9*, 499-505

[54] Bosca, F.; Cosa, G.; Miranda, M. A.; Scaiano, J.C. *Photochem. Photobiol. Sci.*, **2002**, *1*, 704-708

[55] Reichardt, C. *Solvents and Solvent Effects in Organic Chemistry*, Wiley-VCH: Weinheim, **2003**

[56] Hashimoto, S.; Yasuka, M.; Mouri, M. *Nippon Kagaku Kaishi,* **1978**, *1*, 79-81

[57] Ledger, M. B.; Porter, G. *J. Chem. Soc., Faraday Trans. 1,* **1972**, *68*, 539-553

[58] Rayner, D. M.; Wyatt, P. A. H. *J. Chem. Soc., Faraday Trans. 2,* **1974**, *70*, 945-954

[59] Ramseier, M.; Senn, P.; Wirz, J. *J. Phys. Chem. A,* **2003**, 107, 3305-3315

[60] Shizuka, H.; Kimura, E. *Can. J. Chem.,* **1984**, *62*, 2041-2046

[61] (a) Zimmerman, H. E. *J. Am. Chem. Soc.,* **1995**, *117*, 8988-8991; (b) Zimmerman, H. E. *J. Phys. Chem. A*, **1998**, *102*, 5616-5621

[62] Bosca, F.; Miranda, M.A.; Carganico, G.; Mauleon, D. *Photochem. Photobiol.,* **1994**, *60*, 96-101

[63] Constanzo, L. L.; De Guidi, G.; Condorelli, G.; Cambria, A.; Famax M. *Photochem. Photobiol.,* **1989**, *50*, 359-365

[64] Chignell C.; Sik, R.H. *Photochem. Photobiol.,* **1995**, *62*, 205-207

[65] Budac, D.; Wan, P. *J. Photochem. Photobiol. A: Chem,* **1992**, *67*, 135-166

[66] Martinez, L.J.; Scaiano, J.C. *J. Am. Chem. Soc.,* **1997**, *119*, 11066-11070

[67] Cosa, G.; Martinez, L.J.; Scaiano, J.C. *Phys. Chem. Chem. Phys.*, **1999**, *1*, 3533-3537

[68] Margerum, J.D.; Petrusis, C.T. *J. Am. Chem. Soc.,* **1969**, *91*, 2467-2472

[69] Huck, L.A.; Wan, P. *Org. Lett.*, **2004**, *6*, 1797-1799

[70] Huck, L. A.; Xu, M.; Forest, K.; Wan, P. *Can. J. Chem.,* **2004**, *82*,1760-1768

[71] Hearst, J. E. *Science,* **1995**, *268*, 1858-1859

[72] Galland, P.; Senger, H. *Photochem. Photobiol.,* **1988**, *48*, 811-820

[73] Fuller, R. C.; Kidder, G. W.; Nugent, N.A.; Dewey, V.C.; *Photochem. Photobiol.,* **1971**, *14*, 359-371

[74] Lorente C.; Thomas, A.H. *Acc. Chem. Res.,* **2006** *39*, 395-402

[75] Thomas, A.H.; Lorene, C.; Capparelli, A.L.; Pokherel, M. R.; Braun, A. M.; Oliveros, E. *Photochem. Photobiol. Sci.,* **2002**, *1*, 421-426

[76] Cabrerizo, F.M.; Petroselli, G.; Lorente, C.; Capparelli, S. L.; Thomas, A. H.; Braun, A. M.; Oliveros, E. *Photochem. Photobiol.,* **2005**, *81*, 1234-1240

[77] Albert, A. *Biochem. J.,* **1953**, 54, 646-654

[78] Lorente, C.; Capparelli, A.L.; Thomas, A.H.; Braun, A.M.; Oliveros, E.; *Photochem. Photobiol. Sci.,* **2004**, *3*, 167-173

[79] Baur, R.; Kappel, M.; Mengel, R.; Pfleiderer, W. "Photochemistry of pteridines" In *Chemistry and Biology of Pteridines*; Kisliuk, R. L.; Brown, G.M., Eds.; Elsevier/North Hollond: New York, **1979**; pp13-18

[80] Thomas, A. H.; Cabrerizo, R.; Vignoni, M.; Erra-Balsells, R.; Cabrerizo, F. M.; Capparelli, A. L. *Helv. Chim. Acta.,* **2006**, *89*, 1090-1104

[81] Gorner, H. *Photochem. Photobiol.,* **2003**, *77*, 171-179

[82] Fuchs, B.; Mayer, W.J.W.; Abramson S. *J. Chem. Soc., Chem. Commun.,* **1985**, 1711-1713

[83] Lukeman, M.; Xu, M.; Wan, P. *Chem. Commun.,* **2002**, 136-137

[84] Dever, D.F.; Calvert, J.G. *J. Am. Chem. Soc.,* **1962**, 84, 1362-1368

[85] Sammes, P.G. *Tetrahedron*, **1976**, 32, 405-422

[86] Cai, X.; Sakamoto, M.; Yamaji, M.; Fujitsuka, M.; Majima, T. *J. Phys. Chem. A,* **2005**, *105*, 5989-5994

[87] Görner, H.; Kuhn, H. J. *J. Phys. Chem.,* **1986**, *90*, 5946-5955

[88] Basarić, N.; Mitchell, D.; Wan, P. *Can. J. Chem.,* **2007**, *85*, 561-571

[89] Smith, M.B.; March, J. *March's Advanced Organic Chemistry*, *5th Ed.*, John Wiley & Sons, Inc. New York, NY, **2001**

[90] Takeda, K.; Kajii, Y.; Shibuya, K.; Obi, K. *J. Photochem. Photobiol. A.,* **1998**, *115*, 109-115

[91] Oatis, J. E. Jr.; Knapp, D.R. *Tetrahedron Lett*., **1998**, *39*, 1665-1668

[92] Nutaitis, C.F.; Gribble, G.W. *Tetrahedron Lett.,* **1983**, *24*, 4287-4290

[93] Miziak, P.; Zon, J.; Amrhein, N.; Gancarz, R. *Phytochemistry*, **2007**, *68*(4), 407-415

[94] Gemal, A.L.; Luche, J.-L. *J. Org. Chem*., **1979**, *44*, 4187-4188

[95] Sakaguchi, Y.; Hayashi, H. *J. Photochem. Photobiol. A.,* **1992**, *65*, 183-190

[96] Pownall, J. J.; Huber, J. R. *J. Am. Chem. Soc.,* **1971**, *93*, 6429-6436

[97] Murphy, R. S.; Barros T. C., Barnes, J.; Mayer, B.; Marconi, G.; Bohne, C. *J. Phys. Chem.,* **1999**, *103*, 137-146

[98] Scaiano, J. C. *J. Am. Chem. Soc.,* **1980**, *102*, 7747-7753

[99] Connors, R.E.; Christian, W.R. *J. Phys. Chem.,* **1982**, 86, 1524-1528

[100] Kobayashi, T.; Nagakura, S. *Chem. Phys. Lett.,* **1976**, *43*, 429-434

[101] Andrews, L. J..; Deroulede, A.; Linschitz, H. *J. Phys. Chem.,* **1978**, *82*, 2304-2309

[102] Biczók L.; Bérces T.; Linshitz, H. *J. Am. Chem. Soc.,* **1997**, *119*, 11071-11077

[103] Eckstein M.; Marona, H. *Polish J. Chem.*, **1980**, *54*, 1281-1285

[104] Garner, A.; Wilkinson, F. *J. Chem. Soc., Faraday Trans. 2,* **1976**, *72*, 1010-1020

[105] Wilkinson, F.; Garner, A. *J. Chem. Soc., Faraday Trans. 2,* **1977**, *73*, 222-223

[106] Wilkinson, F.; Garner, A. *Photochem. Photobiol.,* **1978**, *27*, 659-670

[107] Kasha, M. *Light and Life*, John Hopkins University Press, Baltimore MD, **1955**

[108] Blake, J. S.; Gagnon, E.; Lukeman, M.; Scaiano, J.C. *Org. Lett.,* **2006**, *8*, 1057-1060

[109] Montalti, M.; Credi A.; Prodi L.; Gandolfi, M. T. *Handbook of Photochemistry, 3rd Ed.*, CRC Press, Talor & Francis Group, Boca Ratan, FL, **2006**

[110] Wan, P.; Yates, K.; Boyd, M.K. *J. Org. Chem.,* **1985**, *50*, 2881-2886

[111] Murphy, R.S.; Moorlag, C.P.; Green, W.H.; Bohne, C. *J. Photochem. Photobiol. A. Chem.,* **1997**, *110*, 123-129

[112] Nakajima, A. *Mol. Photochem.*, **1976**, *72(2)*, 251-262

[113] Yoon, N. M.; Pak, C.S.; Brown, H.C.; Krishnamurthy, S.; Stocky, T.P. *J. Org. Chem.*, **1973**, *38*(16) 2786-2792

[114] Robertson, G. B. *Nature,* **1961**, *191*, 593-594

[115] Trotter J. *Acta Cryst.,* **1961**, *14*, 1135-1140

[116] Suzuki K. *Bull. Chem. Soc. Jpn.,* **1959***, 32*, 1340-1350

[117] Uchimura H.; Tajiri, A.; Hatano, M. *Bull. Chem. Soc. Jpn.,* **1981**, *54*, 3279-3285

[118] Lim, E.C.; Li, Y. *J. Chem. Phys.,* **1970**, *52*, 6416-6422

[119] Venkataraman, L.; Klare, J.E.; Nuckolls, C.; Hybertsen M.S.; Steigerwald, M.L *Nature*, **2006**, 442, 904-907

[120] Imamura, A.; Hoffman, R. *J. Am. Chem. Soc.,* **1968**, *90*, 5379-5384

[121] T. C. Werner, In *Modern Fluorescence Spectroscopy*, Vol. 2, E. Wehry (ed.), Plenum Press, New York, **1976**.

[122] Berlman, I. *J. Chem. Phys*., **1970**, *52*, 5616-5621

[123] Wagner, P. J. *J. Am. Chem. Soc.,* **1967**, *89*, 2820-2825

[124] Zimmerman, H.E.; Crumrine, D.S. *J. Am. Chem. Soc.,* **1972** *94*, 498-506

[125] Mislow, K.; Gordon, A. J. *J. Am. Chem. Soc.,* **1963**, *85*, 3521-3521

[126] Maus, M.; Rettig, W.; Bonafoux, D.; Lapouyade, R. *J. Phys. Chem. A,* **1999**, *103*, 3388-3401

[127] Tahara, T.; Hamaguchi, H.; Tasumi, M. *J. Phys. Chem.,* **1990***, 94*, 170-178

[128] Scaiano, J. C.; Nicodem, D.E. *Can. J. Chem.,* **1984**, *62*, 2346-2350

[129] Xu, Musheng. PhD Thesis, **2003**, University of Victoria

[130] Prater, K.; Freund W.L.; Bowman, R.M. *Chem. Phys. Lett.,* **1998**, *295*, 82-88

[131] Leigh, W.J.; Scaiano, J.C. *J. Am. Chem. Soc.,* **1983**, *105*, 5652-5657

[132] Huang, C.-G.; Beveridge, K.A.; Wan P. *J. Am. Chem. Soc.,* **1991**, *113*, 7676-7684

[133] Padwa, A.; Doubleday, C.; Mazzu, A. *J. Org. Chem.,* **1977**, *42*, 3271-3279

[134] Buntrock, R. E.; Taylor, E. C. *Chem. Rev.,* **1968**, *68*, 209-227

[135] Taylor, E. C.; Strojny, E. J. *J. Am. Chem. Soc.,* **1960**, *82,* 5198-5202

[136] Morrison, J.; Wan, P.; Corrie, J.E.T.; Munasinghe, V.R.N. *Can. J. Chem.,* **2003**, *81*, 586-597

[137] Moessner, C.; *Org. Lett.*, **2005**, *7*, 2667-2669

[138] Loyd, D.; *J. Med. Chem.*, **2004**, *47*, 5612-5615

[139] Tsang, W.C.P.; *J. Am. Chem. Soc.*, **2005**, *127*, 14560-14561